Mechanisms Regulating Macrophage Activation and Function during Bacterial Infection and Carcinogenesis

By

Dana Michelle Hardbower

Dissertation
Submitted to the Faculty of the
Graduate School of Vanderbilt University
in partial fulfillment of the requirements
for the degree of

DOCTOR OF PHILOSOPHY

in

Microbiology and Immunology

May 12, 2017
Nashville, Tennessee

Approved by:
Eric P. Skaar, MPH, PhD
Luc Van Kaer, PhD
Timothy L. Cover, MD
James R. Goldenring, MD, PhD
Keith T. Wilson, MD

To my family, for their unending love and encouragement

and

To Zachary, my rock, my inspiration, my best friend

ACKNOWLEDGEMENTS

When I began my graduate training in 2011, I was completely unaware of exactly what I was getting myself into. I now understand how challenging, frustrating, and utterly rewarding scientific research can be. And, I have many people to thank for getting me where I am today.

Keith has worn many hats during my training. He has been a teacher, providing immeasurable guidance in taking data and crafting a compelling story. He has been a mentor, guiding me through these early years of a scientific career by example. He has been a challenger, pushing me to do better and better. Keith has been a devil's advocate, my harshest critic when needed and my strongest supporter. And, I cannot thank him enough. Many people in the lab have greatly enriched my graduate training. Kshipra and Asim were always available to teach me new techniques and provide assistance with experiments when needed. I could not have published my papers without them. Dan and Margaret – the mouse gurus. How could I have done my experiments without the countless hours they spend weaning and genotyping mice? And, of course, our daily crossword puzzle-filled lunches never failed to put a smile on my face, even on the worst of days. Lori has been my much relied upon professional mentor. Her advice was invaluable. To all the members of Keith's lab, thank you from the bottom of my heart.

My mother, Dianne, and father, Byron have always provided me with a supportive environment in which to pursue my goals. That did not end when I moved to Nashville six years ago. They have encouraged me every step of the way, from fielding countless phone calls from a very frustrated daughter to sending me O'Charley's gift cards to celebrate my success. I hope that in everything I have and will accomplish, I make them proud. My brother, Mitchell, my sister, Beth, and my brother-in-law, Danny, have always made me smile and been a source of support and advice when needed. Finally, I could not have finished my graduate training without the love and support of my boyfriend, Zac. A graduate student at Vanderbilt himself, Zac has provided advice, acted as a sounding board for ideas, and pushed me to constantly improve as a scientist. He has inspired me in so many ways – scientific and beyond – and I look forward to spending each day of my life working side by side with him.

During my training I was supported by NIH grants R01DK053620, R01AT004821, R01CA190612, P01CA116087, and P01CA028842, a Department of Veterans Affairs Merit Review grant I01BX001453, the Thomas F. Frist Sr. Endowment, and the Vanderbilt Center for Mucosal Inflammation and Cancer, all of which were obtained by Keith Wilson. I was also supported by the Cellular, Biochemical, and Molecular Training grant (T32GM008554) and a Ruth L. Kirschstein pre-doctoral fellowship (F31DK10715).

As I take my next career steps, I have reflected upon my time here at Vanderbilt and I have come to realize that science is truly a team effort and progress cannot be made without the contributions, both big and small, of many people. I will hold dear the lessons that countless people have taught me and carry with me a great sense of appreciation for the time and effort spend by many to shape me into the scientist that I have become.

TABLE OF CONTENTS

LIST OF FIGURES

Figure **Page**

LIST OF ABBREVIATIONS

Term	Abbreviation
Acetylation	Ac
American Type Culture Collection	ATCC
Amphiregulin	AREG
Arginase 1	ARG1
Arginase 2	ARG2
Avian erythroblastosis oncogene B	ERBB
Azoxymethane	AOM
Betacellulin	BTC
Bone marrow-derived dendritic cells	BMDCs
Bone marrow-derived macrophages	BMmacs
cAMP response element-binding protein	CREB
Caspase 1	CASP1
C-C motif ligand	CCL
Chitinase-like 3	CHIL3
Chromatin immunoprecipitation	ChIP
Colitis-associated carcinogenesis	CAC
Colony forming units	CFUs
Colonic epithelial cells	CECs
Colony stimulating factor 1	CSF1
C-X-C motif ligand	CXCL
Cytotoxin-associated gene A	CagA
Di-/Tri-methylation	me2/3
Difluoromethylornithine	DFMO
Dextran sodium sulfate	DSS
Dulbecco's modified Eagle's medium	DMEM

Term	Abbreviation
Epidermal growth factor	EGF
Epidermal growth factor receptor	EGFR
Epigen	EPGN
Epiregulin	EPR
Euchromatic histone lysine methyltransferase 2	EHMT2
Extracellular signal-regulated kinases	ERK
Fetal bovine serum	FBS
Forkhead box A3	FOXA3
Forkhead box P3	FOXP3
Gastric epithelial cells	GECs
Gastric lymph node	GLN
Gastric macrophages	Gmacs
Glyceraldehyde 3-phosphate dehydrogenase	GAPDH
Granulocyte/macrophage colony stimulating factor	GM-CSF
Growth factor receptor bound protein 2	GRB2
Hematoxylin and eosin	H&E
Heme oxygenase 1	HMOX1
Heparin-binding epidermal growth factor	HB-EGF
Histone 3, Lysine 4	H3K4
Histone 3, Lysine 9	H3K9
Hours	h
Human epidermal growth factor receptor	HER
Inflammatory bowel disease	IBD
Inhibitor of apoptosis	IAP
Inhibitor of kappa light polypeptide gene enhancer in B cells, kinase	IKBK
Inhibitor of kappa light polypeptide gene enhancer in B cells, inhibitor a	NFKBIA

Term	Abbreviation
Insulin-gastrin	INS-GAS
Interferon regulatory factor	IRF
Institutional Animal Care and Use Committee	IACUC
Interferon gamma	IFN
Interleukin	IL
Janus kinase	JAK
Leukemia inhibitory factor	LIF
Lipopolysaccharide	LPS
Liquid chromatography-mass spectrometry	LC-MS
Lysine acetyltransferase 2A	KAT2A
Kilodalton	kD
Lysozyme 2	LYZ2
Macrophage-colony stimulating factor	M-CSF
Macrophage-stimulating protein receptor	MSTR1
Mitogen-activated protein kinase	MAPK
Monomethylation	me1
Months	mo
Multiplicity of infection	MOI
Myeloid differentiation primary response 88	MYD88
Myeloperoxidase	MPO
Myogenic Differentiation 1	MYOD1
Neutrophil activating protein A	NapA
Nitric Oxide	NO
Nitric oxide synthase 2	NOS2
NLR family, pyrin domain containing	NLRP
Nuclear factor kappa-light-chain enhancer of activated B cells	NF-κB

Term	Abbreviation
Ornithine decarboxylase	ODC
Phorbol-12-myristate-13-acetate	PMA
Phosphatidylinositol 3 kinase	PI3K
Polymorphonuclear cell	PMN
Phospho-EGFR	pEGFR
Phospho-inhibitor of kappa light polypeptide gene enhancer in B cells, kinase	pIKBK
Phospho-inhibitor of kappa light polypeptide gene enhancer in B cells, inhibitor a	pNFKBIA
Phospho-mitogen-activated protein kinase	pMAPK
Phospho-signal transducer and activator of transcription	pSTAT6
Phospho-v-rel avian reticuloendotheliosis viral oncogene homolog A	pRELA
Polyamine oxidase	PAOX
Post-infection	p.i.
Pre-mouse Sydney Strain 1	PMSS1
Protein kinase B	PKB
Protein kinase C	PKC
RAR-related orphan receptor C	RORC
Reactive nitrogen species	RNS
Reactive oxygen species	ROS
Real time	RT
Regulatory macrophage	Mreg
Regulatory T cell	Treg
Resistin like A	RETNLA
Ribosomal protein S6	RPS6
Roswell Park Memorial Institute medium	RPMI
Serine	S
Signal transducer and activator of transcription	STAT

Term	Abbreviation
Solute carrier family 7, member 1	SLC7A1
Solute carrier family 7, member 2	SLC7A2
Spermidine/spermine N(1)-acetyltransferase	SAT1
Spermidine synthase	SRM
Spermine oxidase	SMOX
Spermine synthase	SMS
Stable isotope labeling with amino acids in cell culture	SILAC
Standard error of the mean	S.E.M.
Stathmin	STMN1
Stem cell-derived tyrosine kinase receptor	STK
Superoxide dismutase	SOD
Sydney Strain 1	SS1
T box 21	TBX21
Transforming growth factor beta activated kinase 1	TAK1
Tissue microarray	TMA
total EGFR	tEGFR
Transforming growth factor	TGF
Tripartite motif containing 28	TRIM28
Tumor necrosis factor	TNF
Tumor necrosis factor (ligand) superfamily member 14	TNFSF14
Type four secretion system	T4SS
Tyrosine	Y
Tyrosine-protein kinase receptor 3	TYRO3
Vacuolating cytotoxin A	VacA
C-V-Myc Avian Myelocytomatosis Viral Oncogene Homolog	C-MYC
v-rel avian reticuloendotheliosis viral oncogene homolog A	RELA

Term	Abbreviation
Vascular endothelial growth factor A	VEGFA
Wildtype	WT

ORIGINAL PUBLICATIONS

Research Manuscripts

Hardbower, D.M., Coburn, L.A., Asim, M., Sierra, J.C., Singh, K., Barry, D.P., Piazuelo, M.B., Gobert, A.P., Washington, M.K., and Wilson, K.T. EGFR-mediated macrophage activation promotes colitis-associated tumorigenesis. ***Oncogene.*** Epub ahead of print. PMID: 28263971.

Hardbower, D.M., Asim, M., Luis, P.B., Singh, K., Barry, D.P., Yang, C., Steeves, M.A., Cleveland, J.L., Schneider, C., Piazuelo, M.B., Gobert, A.P., and Wilson, K.T. Ornithine decarboxylase regulates M1 macrophage activation and mucosal inflammation via histone modifications. (2017) ***Proc Natl Acad Sci USA***. 114(5): E761-E760. PMID: 28096401.

Singh, K., Al-Green, N.T., Verriere, T.G., Coburn, L.A., Asim, M., Barry, D.P., Allaman, M.M., Hardbower, D.M., Delgado, A.G., Piazuelo, M.B., Vallance, B.A., Gobert, A.P., and Wilson, K.T. The L-Arginine transporter solute carrier family 7 member 2 mediates the immunopathogenesis of attaching and effacing bacteria. (2016) ***PloS Pathog.*** 12(10):e1005984. PMID: 27783672

Hardbower, D.M., Singh, K., Asim, M., Verriere, T.G., Olivares-Villagómez, D., Barry, D.P., Allaman, M.M., Washington, M.K., Peek, R.M. Jr., Piazuelo, M.B., and Wilson, K.T. EGFR regulates macrophage activation and function in bacterial infection. (2016) ***J Clin Invest***. 126(9): 3296-3312. PMID: 27482886.

Hardbower, D.M., Verriere, T., Asim, M., Barry, D.P., Murray-Stewart, T., Lewis, N.D. Chaturvedi, R., Casero, R.A. Jr., Piazuelo, M.B., and Wilson, K.T. Arginase 2 deletion leads to enhanced M1 macrophage activation and upregulated polyamine metabolism in response to *Helicobacter pylori* infection. (2016) ***Amino Acids.*** 48(10): 2375-2388. PMID: 27074721

Chaturvedi, R., de Sablet, T., Asim, M., Piazuelo, M.B., Barry, D.P., Verriere, T.G., Sierra, J.C., Hardbower, D.M., Delgado, A.G., Schneider, B.G., Israel, D.A., Romero-Gallo, J., Nagy, T., Morgan, D.R., Murray-Stewart, T., Bravo, L.E., Peek, R.M. Jr, Fox, J.G., Woster, P.M., Casero, R.A., Jr, Correa, P., and Wilson, K.T. Increased *Helicobacter pylori*-associated gastric cancer risk in the Andean region of Colombia is mediated by spermine oxidase. (2015) ***Oncogene***. 34(26): 3429-3440. PMC4345146.

Krakowiak, M., Noto J., Piazuelo, M., Hardbower, D.M., Romero-Gallo, J., Delgado, A., Chaturvedi, R., Correa, P., Wilson, K.T. and Peek R.M. Jr. Matrix metalloproteinase 7 restrains *Helicobacter pylori*-induced gastric inflammation and premalignant lesions in the stomach by altering macrophage polarization. (2014) ***Oncogene***. 34(14): 1865-1871. PMC4237684.

Reviews

Hardbower, D.M., Peek, R.M. Jr and Wilson, K.T. At the Bench: *Helicobacter pylori*, dysregulated host responses, DNA damage and gastric cancer. (2014) ***J Leukoc Biol***. 96: 201-212. PMC4101087.

Hardbower, D.M., de Sablet, T., Chaturvedi, R and Wilson, K.T. Chronic inflammation and oxidative stress: The smoking gun for *Helicobacter pylori*-induced gastric cancer? (2013) ***Gut Microbes***. 4(6): 475-481. PMC4101087.

CHAPTER 1

INTRODUCTION

1.1 Macrophage Activation and Function

Macrophages are a dynamic and highly plastic subset of innate immune cells[1-4]. Derived from myeloid progenitor cells in the bone marrow, macrophages have the capacity to take on a broad range of roles within many different contexts[1-4]. Macrophages can become highly specialized resident macrophages within various tissues, such as alveolar macrophages in the lung, osteoclasts with bone, microglial cells in the central nervous system, and Kupffer cells within the liver[3]. Macrophages are also highly efficient, professional phagocytes, which is an essential role in both embryogenesis and in the maintenance of blood and tissue homeostasis[2,3]. Moreover, macrophages are highly adapted for immune surveillance, antigen presentation, and pathogen clearance[2,3]. The fate of a macrophage is highly dependent on the cytokine milieu and other environmental cues within the niche a macrophage occupies[2-5]. The role of macrophages in the context of immune response to pathogens and tumorigenesis will be the focus of this dissertation.

An essential step in macrophage function is macrophage activation, sometimes referred to as macrophage polarization[2,3,6], which is outlined in Figure 1. Classically activated M1 macrophages are highly pro-inflammatory and anti-microbial[2-4,6]. M1 macrophages are activated in response to pathogen associated molecular patterns, and cytokines that include interferon (IFN)-γ, and tumor necrosis factor (TNF)-α[1-3]. Common markers of M1 macrophages are nitric oxide synthase 2 (NOS2), interleukin (IL)-1β, TNF-α, IL-6, and IL-12[2-4,6]. M1 macrophages are essential for the clearance of bacterial pathogens and for the initiation of adaptive immune responses[1,4]. M1 macrophages are associated with Th1 and Th17 responses because they produce IL-1β, IL-6, IL-12, and IL-23, cytokines known to induce said T cell subsets[3,6]. M1 macrophages have traditionally been associated with anti-tumorigenic responses, as well[4,6,7]. However, recent studies have called this into question, citing the potential for DNA damage caused by high levels of reactive oxygen species (ROS) and reactive nitrogen species (RNS) produced by activated macrophages[8-10].

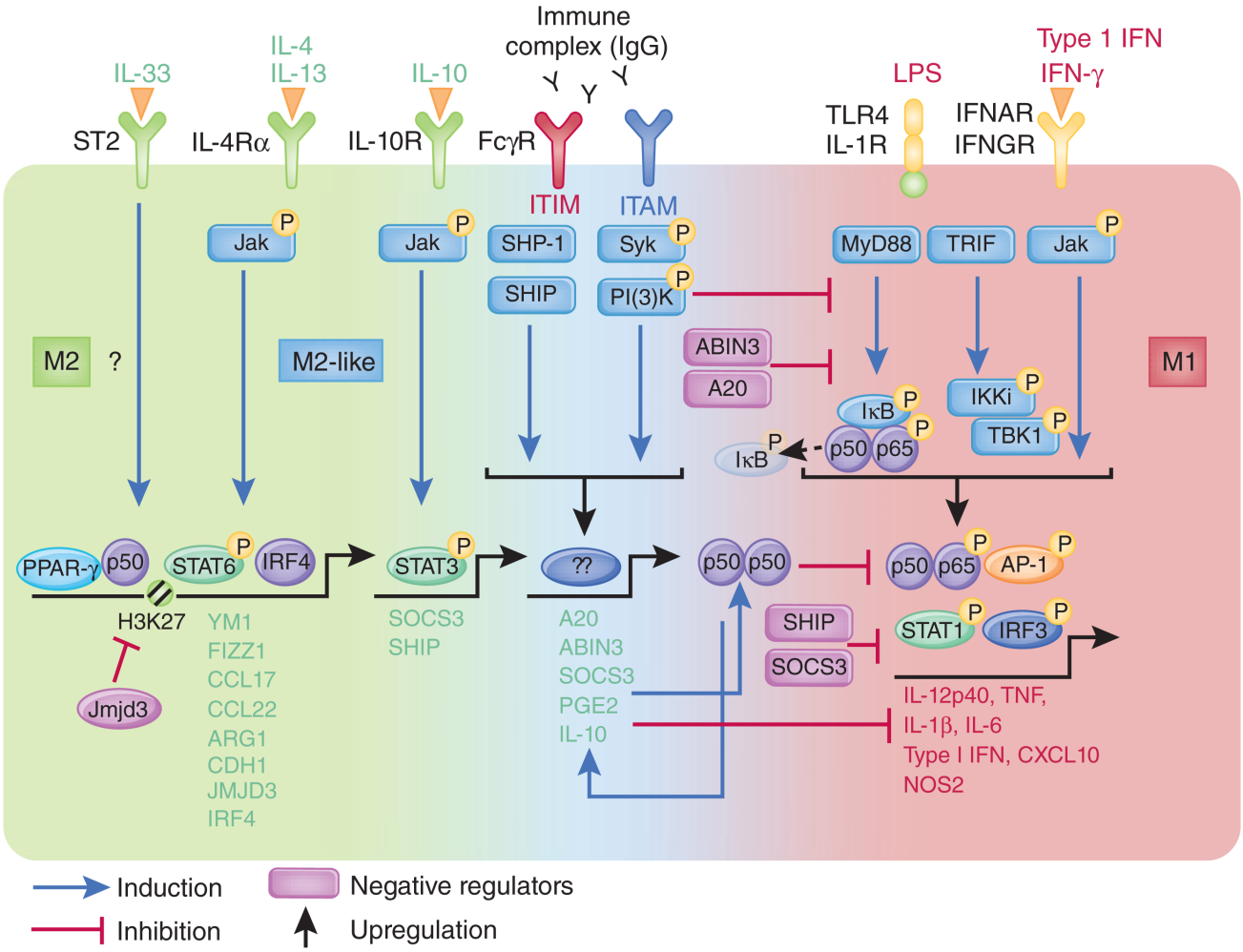

Figure 1. Molecular pathways of macrophage activation. M1 stimuli such as lipopolysaccharide (LPS) and interferon (IFN)-γ signal through the toll-like receptor (TLR) 4, IFN-α, or IFN-β receptor (IFNAR) and IFN-γ receptor (IFNGR) pathways, inducing activation of the transcription factors nuclear factor kappa-light-chain-enhancer of activated B cells (NF-κB; p65 and p50), activator protein 1 (AP-1), interferon regulatory factor (IRF) 3 and signal transducer and activator of transcription (STAT) 1, which leads to the transcription of M1 genes (red lettering indicates molecules encoded). In contrast, M2 stimuli such as interleukin (IL)-4 and IL-13 signal through IL-4 receptor alpha (IL-4Rα) to activate STAT6, which regulates the expression of M2 genes (green lettering indicates molecules encoded). The regulation of these genes also involves jumonji domain-containing protein 3 (JMJD3), IRF4, peroxisome proliferator-activated receptor (PPAR)-γ and p50. IL-10 and immune complexes, plus LPS and IL-1, trigger M2-like macrophage polarization. IL-10 signals through its receptor (IL-10R), activating STAT3. Immune complexes trigger Fcγ receptor (FcγR) signaling, leading to the expression of molecules such as A20, ABIN3, SOCS3, prostaglandin E2 and IL-10, which negatively regulate the TLR4 and IL-1R and interferon-signaling pathway. Activatory and inhibitory FcγR signaling is initiated by activation of Syk–phosphatidylinositol-3-OH kinase (PI(3)K) and tyrosine phosphatase SHP-1–inositol phosphatase SHIP, respectively. Methylation of histone H3K27 is a post-translational modification linked to gene silencing. A20, deubiquitinating enzyme; ABIN3, A20-binding NF-κB inhibitor; IgG, immunoglobulin G; IκB, NF-κB inhibitor; IKKi, inducible IκB kinase; ITAM, intracellular tyrosine-based activatory motif; ITIM, intracellular tyrosine-based inhibitory motif; Jak, Janus kinase; TBK1, NF-κB activator; TRIF, adaptor protein. Adapted from Reference 6.

M2 macrophages, also known as type 2 or alternatively activated macrophages, are commonly associated with wound healing and anti-fungal responses[2,3,11]. High levels of IL-4, IL-10, and IL-13 are responsible for M2 macrophage activation[3,11]. M2 macrophages produce low levels of pro-inflammatory cytokines and high levels of arginase 1 (ARG1), chitinase-like 3 (CHIL3), and resistin like A (RETNLA)[2,3,11]. M2 macrophages are also known as tumor-associated macrophages because of their pro-tumorigenic properties[2,3,5,7,11-13]. M2 macrophages promote cellular growth and proliferation, and angiogenesis, all of which are hallmarks of carcinogenesis[2,3,5,7,11-13].

While there is much disagreement within the field of macrophage research, some investigators posit that a third subset of macrophage exists – the regulatory macrophage (Mreg)[3,14]. The hallmark of Mreg activation is the production of extremely high levels of IL-10[3,14]. Thus, Mreg macrophages serve as a counterbalance to M1 macrophages in that they limit tissue damage and the extent of inflammation[3,14]. Mreg macrophages are also associated with higher levels of regulatory T cell (Treg) activation in order to prevent autoimmunity[3,14]. Further studies are necessary to confirm the existence of Mreg macrophages. However, this paradigm adequately illustrates the highly plastic nature of macrophage activation, indicating a spectrum of activation rather than distinct subtypes[2,3,6,14].

Macrophage activation is a highly regulated process (Figure 1), marked by the involvement of many different signaling pathways[6,12,15,16]. The balance between M1 and M2 macrophage activation is determined by environmental cues recognized by macrophages[5,17], leading to the activation of different programs of transcriptional regulation[6,12,15,16,18]. M1 macrophages are typically marked by nuclear factor kappa-light-chain enhancer of activated B cells (NF-κB) signaling and interferon regulatory factor (IRF) 5 activation, while M2 macrophages are associated with increased signal transducer and activator of transcription (STAT) 3/6 signaling and IRF4 activation[6,12,15,16,19]. However, many questions remain related to the initiation and regulation of macrophage activation.

A recent study demonstrated that macrophages are essential to the pathogenesis of *Helicobacter pylori*, a highly prolific human pathogen[20]. As will be discussed in Section 1.2, *H. pylori* infection is the single greatest risk factor in the development of gastric cancer[21,22]. Thus, the *H. pylori* model allows for the study of macrophage activation and function within the context of both bacterial

infection *and* carcinogenesis, which encompassed both goals of this dissertation. We also performed studies with *Citrobacter rodentium*, an additional gastrointestinal pathogen that causes colitis in mice, and with known macrophage stimuli, including IFN-γ, lipopolysaccharide (LPS), IL-4, and IL-10. However, *H. pylori* infection is the primary model utilized in the studies outlined in this dissertation.

1.2 *Helicobacter pylori*

H. pylori is a Gram-negative, microaerophilic bacterium that infects up to 50% of the global human population[21-24]. *H. pylori* selectively colonizes the human gastric mucosa and is directly responsible for gastroduodenal pathologies that include chronic gastritis, peptic ulcers, mucosa-associated lymphoid tissue lymphoma, and gastric adenocarcinoma[21-24]. Because *H. pylori* confers an attributable risk of 75% for gastric carcinogenesis, the World Health Organization has classified this organism as a type I carcinogen[25]. As gastric cancer is the third leading cause of cancer death[26], *H. pylori* infection remains a significant public health threat.

Risk factors for the development of gastric cancer include several bacterial factors. Cytotoxin associated gene A (CagA) is one of the most potent virulence factors expressed by *H. pylori*, with pleiotropic effects on both epithelial and immune cells within the stomach[27]. Individuals infected with strains of *H. pylori* that possess the *cagA* gene harbor an increased risk of developing gastric cancer (odds ratio = 1.9, 0.9-4.0 95% confidence interval) over persons infected with a *cagA*$^-$ strain[27]. CagA is translocated into host cells via a type IV secretion system (T4SS) that is encoded on the same pathogenicity island as the *cagA* gene. Once in the cell, host kinases phosphorylate CagA, which initiates a variety of CagA functions, including activation of mitogen activated protein kinases (MAPK), inhibition of apoptosis, disruption of cell growth, and dysregulation of cell motility[28,29]. Intriguingly, the mechanism by which CagA increases an individual's risk for gastric cancer has not been fully elucidated.

Another *H. pylori* virulence factor linked to gastric cancer is the vacuolating cytotoxin A (VacA). VacA enhances the ability of *H. pylori* to successfully and persistently colonize human gastric mucosa[30]. Moreover, strains harboring the *vacA* s1m1 allele are associated with increased severity of

gastric inflammation and cancer risk[30]. VacA increases intracellular concentrations of ROS and augments oxidative stress in both epithelial and immune cells[28,31,32]. Additional risk factors for gastric cancer include the phylogeographic origin of the infecting strain[33]; several host genetic factors, including polymorphisms in genes encoding *IL1B*, *IL8*, *IL10*, *TNFA* and *IFNG*[34]; lifestyle choices[9,35], such as smoking; the microbiome[9,35]; and other environmental factors[9,35]. Thus, both bacterial and host risk factors are important, but the ability to predict gastric cancer risk remains elusive.

It is still unclear why only 1-3% of the *H. pylori*-infected population will progress to cancer. Despite this low rate of progression from *H. pylori* infection to cancer, the global incidence of gastric cancer is still incredibly high (Figure 2), with nearly one million new cases reported since 2012[36]. Based on decades of research, gastric cancer in *H. pylori*-infected individuals is a result of synergism between host factors, bacterial factors, and environmental factors[21,27,35,37-39]. Thus, more research is necessary to better understand which factors that are most critical for progression from *H. pylori* infection to gastric cancer. In particular, more studies related to the relationship between *H. pylori* and the human immune system are necessary, especially considering the ability of the pathogen to evade nearly all immune responses. Thus, we chose to focus this dissertation on the relationship between *H. pylori* and the immune system – particularly macrophages – to better understand the role of inflammation in the promotion of gastric cancer.

1.3 The Immune System and *H. pylori*: A Dynamic Relationship

H. pylori is one of the more prolific and highly successful human pathogens. Its success is centered on the ability of the bacterium to establish a persistent infection, while resisting the chronic inflammatory responses designed to clear the infection[9,40-42]. The host immune system mounts a robust response that integrates innate and adaptive constituents (Figure 3), as well as the generation of a humoral response[40,42].

The innate immune response includes macrophage, neutrophil, and dendritic cell functions. Indeed, macrophages in particular are essential for *H. pylori*-induced gastritis in murine models of infection[20]. The oxidative burst from phagocytes – primarily neutrophils and macrophages – comprises a major component of the initial immune response to *H. pylori*[43]. As previously discussed, *H. pylori* is

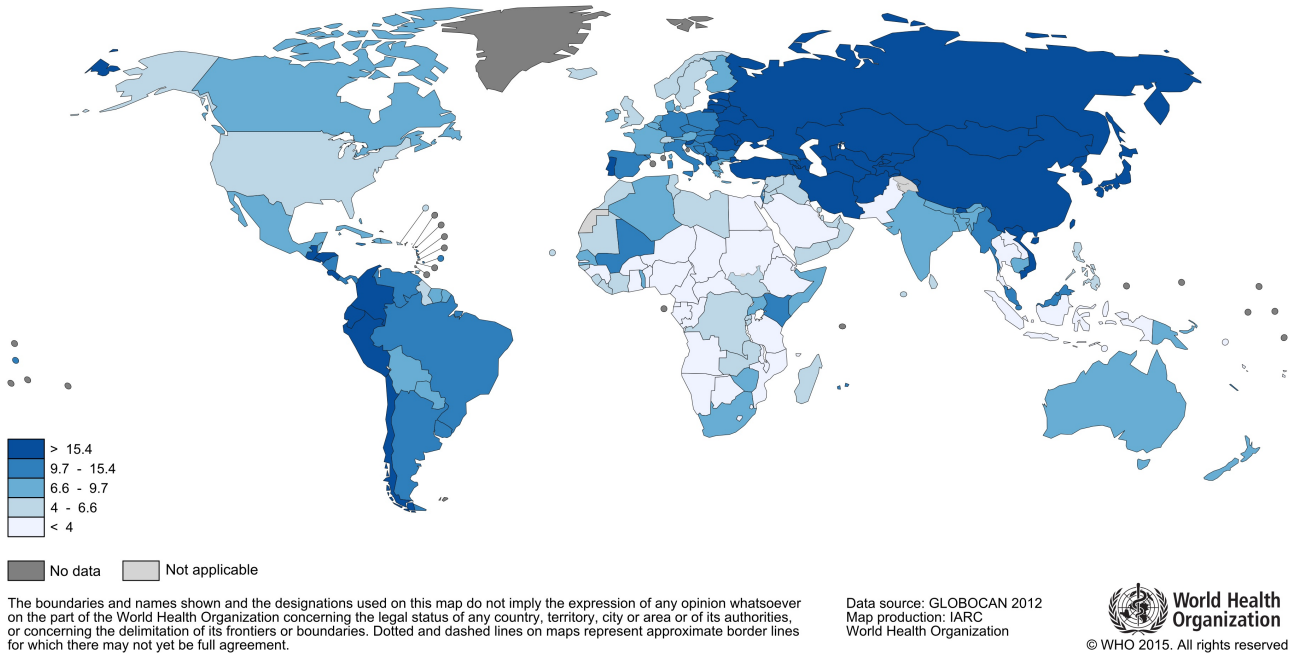

Figure 2. Global gastric cancer incidence rates among males. Gastric cancer is the third leading cause of cancer-related death. Nearly one million new cases of gastric cancer were diagnosed since 2012. *H. pylori* infection is the leading risk factor for gastric carcinogenesis. As such, high infection rates and increased prevalence of highly virulent *H. pylori* strains in Latin America and Eastern Asia account for the high incidence rates in these regions. Adapted from Reference 36.

capable of inducing oxidative bursts, which release significant amounts of oxyradicals into the infected microenvironment[44,45]. Unlike many other human pathogens, *H. pylori* has the ability to survive the oxidative burst. Neutrophil activating protein A (NapA), catalase, and superoxide dismutase (SOD) work in concert to alleviate the stress of this response[44]. Furthermore, *H. pylori* can survive oxidative damage by subverting phagolysome-mediated killing in a VacA-dependent manner, the details of which remain to be determined[46]. The ability of *H. pylori* to evade the innate immune response creates a cycle of consistent immunocyte infiltration, oxidative burst, and DNA damage that contributes to gastric carcinogenesis.

Another key aspect of the insufficient immune response is incomplete polarization of macrophages to the antibacterial, classically activated, M1 phenotype. Our laboratory has reported that oral administration of α-difluoromethylornithine (DFMO), an irreversible inhibitor of ornithine decarboxylase (ODC), reduces *H. pylori* colonization in mice, and this was associated with increased NOS2 protein expression and nitric oxide (NO) production by gastric macrophages[47]. While ODC is not a prototypical marker of alternatively activated, M2 macrophages, it may function in much the same way by reducing antimicrobial NO production and thus an M1 response. Additionally, *H. pylori* subverts M1 macrophage activation through the induction of heme oxygenase 1 (HMOX1) via a CagA-dependent mechanism[48]. And, the induction of HMOX1 in macrophages enhances anti-inflammatory, Mreg activation to promote *H. pylori* survival[48].

Moreover, we have found that gastric macrophages from *H. pylori*-infected mice can express IL-10 and transforming growth factor (TGF)-β, which also can act to impair M1 response. By failing to eradicate the bacteria, the innate immune system continually mounts a response to *H. pylori*, further contributing to the malicious cycle of immune cell ROS production, oxidative stress, and DNA damage.

Dendritic cell activation by *H. pylori* has also been demonstrated in a number of studies[40,49]. Intriguingly, it appears that as in the intestine, dendritic cells send dendrites into the gastric lumen to sample lumen antigens[50]. It is established that signaling through dendritic cells can have potent effects on activating Th1 and Th17 responses[50]. However, in the case of *H. pylori* infection, dendritic cells can also contribute to the bacterial persistence by inducing immune tolerance. Despite such a vigorous

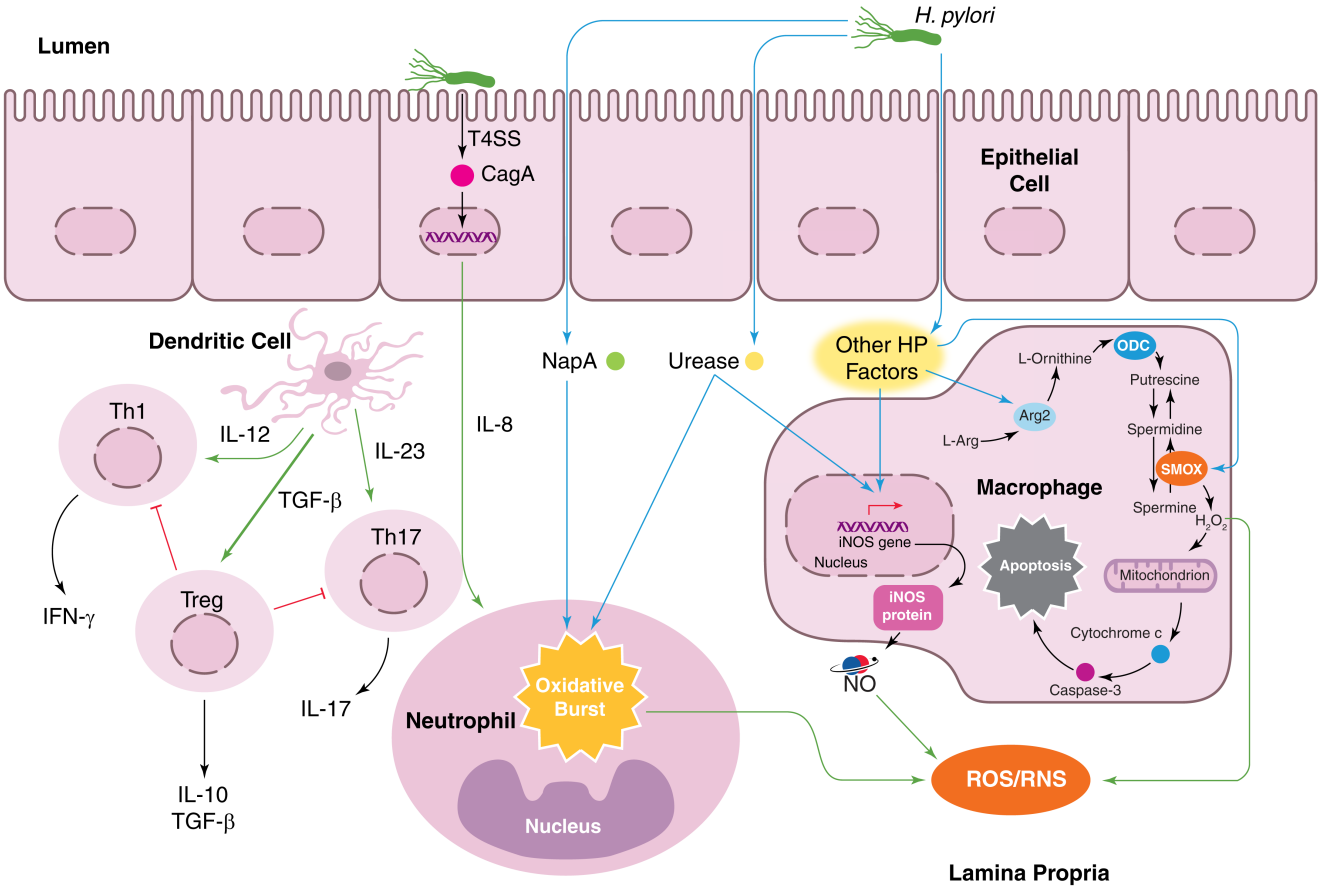

Figure 3. Schematic summary of the interactions between *H. pylori* and innate and adaptive immune cells in the stomach. *H. pylori* infection leads to Interleukin (IL)-8 production, which may be dependent on cytotoxin gene A (CagA) translocation. IL-8 is a chemoattractant that recruits neutrophils. *H. pylori* neutrophil activating protein A (NapA) and urease cause neutrophils to undergo an oxidative burst, exuding substantial amounts of reactive oxygen species (ROS) into the infected microenvironment. Moreover, NapA leads to increased *H. pylori* survival in neutrophils, compounding their effects on oxidative stress. Macrophage inducible nitric oxide synthase (iNOS) is induced by urease during infection, leading to the production of nitric oxide (NO), a reactive nitrogen species (RNS). As yet, undetermined *H. pylori* (HP) factors induce arginase 2 (ARG2) activation in macrophages, resulting in apoptosis. Ornithine decarboxylase (ODC) is also induced in macrophages during infection. This leads to downstream H_2O_2 production by spermine oxidase (SMOX) and apoptosis. Moreover, *H. pylori* infection alters the cytokine milieu produced by dendritic cells in favor of an increased Treg response and a decreased Th1/Th17 response. Such alterations promote immune tolerance and persistence of the pathogen. Image adapted from Reference 35.

response, eradication of this pathogen is rarely achieved in the absence of antibiotics, leading to sustained inflammation over the lifetime of the infected host. Chronic inflammation leads to tissue injury, oxidative stress, and DNA damage[9,35,40,42].

The adaptive branch of the immune system, specifically T helper cells, has also been implicated as contributory to *H. pylori*-induced chronic inflammation[51]. Th1 and Th17 T cell subsets primarily mediate chronic gastritis[52,53]. Th1 cells secrete high levels of pro-inflammatory IFN-γ, and IL-17 produced by Th17 cells has been shown to enhance the production of the chemokine, IL-8[51-53]. These pro-inflammatory cytokines enhance recruitment of immunocytes to the site of infection and perpetuate the chronic inflammatory state of an infected host. Moreover, the influx of Th1 and Th17 cells into the gastric mucosa has been associated with increased epithelial damage, increased epithelial proliferation and metaplastic responses[54].

Numerous studies have also found that Tregs are present within the gastric mucosa during infection[50,55-57]. *H. pylori*, acting through dendritic cells, can preferentially induce a Treg response instead of Th1/Th17 responses[50,58]. This is in marked contrast to findings in models of colitis, where dendritic cells and macrophages are linked to activation of Th1/Th17 responses. Moreover, IL-10 produced by Tregs results in decreased IL-8 production[57]. This facilitates bacterial persistence within the host and promotes immune tolerance.

Taken together, these data demonstrate a dynamic and prolonged interaction between *H. pylori* and the host immune system. The inability of the immune system to clear *H. pylori* infection results in a vicious cycle of inflammatory events, which result in tissue and DNA damage. This promotes gastric carcinogenesis. A better understanding of the immune response to *H. pylori* is necessary to identify therapeutic targets for intervention in *H. pylori*-mediated carcinogenesis. Additionally, the findings made within the *H. pylori* model can be applied to other disease states marked by chronic inflammation.

The macrophage response to *H. pylori* infection, as well as macrophage responses during carcinogenesis, is the central theme of this dissertation. The studies presented herein aimed to better understand macrophage activation, specifically focusing on two pathways that are essential for life and

have ubiquitous roles in cellular function – epidermal growth factor receptor (EGFR) signaling and ODC-mediated polyamine metabolism.

1.4 Epidermal Growth Factor Receptor: An Overview

EGFR (also known as ERBB1) is a 170 kilodalton (kD) receptor tyrosine kinase[59-61]. EGFR contains multiple domains, including an extracellular ligand binding domain, a transmembrane domain, a kinase domain, and a regulatory domain[59-61]. There are at least seven ligands that can activate EGFR signaling. The canonical ligand is epidermal growth factor (EGF) and non-canonical ligands include amphiregulin (AREG), TGF-α, betacellulin (BTC), epiregulin (EPR), epigen (EPGN), and macrophage-produced heparin-binding EGF (HB-EGF)[60-63]. Upon ligand binding, EGFR can form a homodimer or a heterodimer with any member of the avian erythroblastosis oncogene B (ERB)/human epidermal growth factor receptor (HER) family of proteins[59-61,64]. In the event of heterodimerization, EGFR most often forms a dimer with ERBB2[60]. Canonically, dimerization as a result of ligand binding upregulates the kinase activity of EGFR, such that autophosphorylation occurs at one of a least six known tyrosine residues (Figure 4), the most common of which is tyrosine (Y) 1068[59-61]. It should be noted, however, that non-canonical phosphorylation can occur at serines and threonines in the intracellular domain, and that non-canonical phosphorylation can be ligand independent[65-67] (Figure 4).

Following phosphorylation, EGFR transactivation leads to downstream signaling. EGFR signaling is one of the most important and ubiquitous signaling pathways in mammalian cells (Figure 4), as EGFR has been shown to interact with at least 219 downstream modulators[68]. Common EGFR signaling targets include protein kinase B (PKB, also known as AKT), MAPK proteins, Janus kinase (JAK)/STAT proteins, and protein kinase C (PKC)[59,60,68]. As such, EGFR signaling has broad effects on cellular proliferation, growth, differentiation, transcriptional regulation, angiogenesis, and survival[59,60,68].

EGFR signaling has been associated with several diseases, including Alzheimer's disease, polycystic kidney disease, and inflammatory bowel disease[61]. However, EGFR signaling has received the most attention in carcinogenesis[69-73]. EGFR mutations, leading to aberrant signaling, has been linked to increased risk for lung, breast, liver, colorectal, and gastric cancers[69]. In fact, high levels of

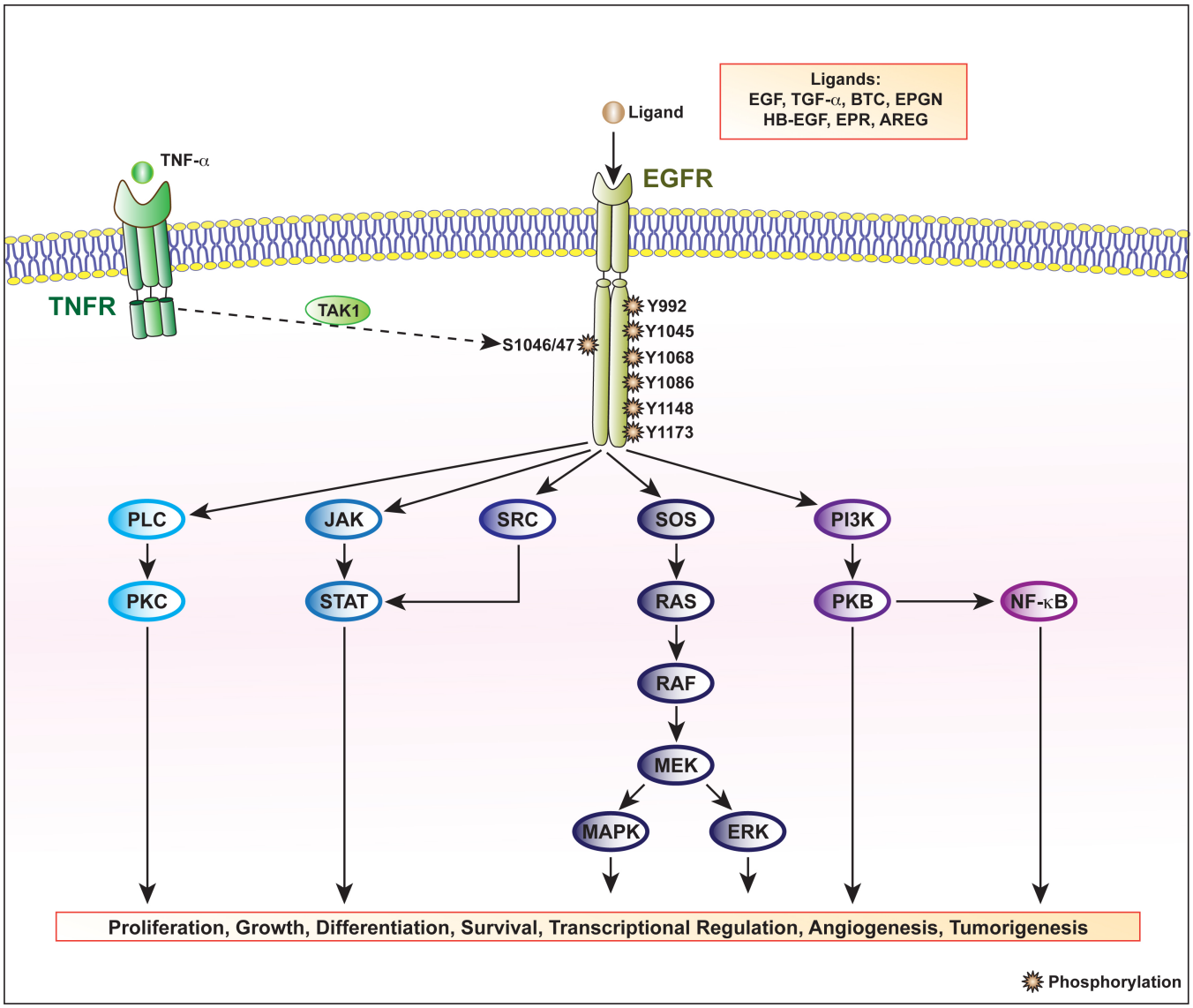

Figure 4. An overview of epidermal growth factor receptor (EGFR) signaling. EGFR signaling can be induced in a ligand-dependent manner. Known EGFR ligands include epidermal growth factor (EGF), transforming growth factor (TGF)-α, betacellulin (BTC), epigen (EPGN), heparin-binding-EGF (HB-EGF), epiregulin (EPR), and amphiregulin (AREG). Ligands bind to the extracellular ligand binding domain. Upon binding, EGFR forms a homodimer or a heterodimer with (ERBB) 2 (not depicted here). Dimerization increases the kinase activity of the intracellular kinase domain that then autophosphorylates the autophosphorylation domain at the listed tyrosines (Y). Ligand-independent activation can occur through tumor necrosis factor (TNF)-α binding to TNF receptor (TNFR), which then leads to transforming growth factor beta-activated kinase 1 (TAK1)-mediated phosphorylation at serine (S) 1046/47. Phosphorylation of a tyrosine leads to the activation of many downstream pathways, including i) phospholipase C (PLC) and protein kinase C (PKC) signaling, ii) Janus kinase (JAK)/signal transducer and activator of transcription (STAT) signaling, iii) v-src avian sarcoma (Schmidt-Ruppin A-2) viral oncogene homolog (SRC) signaling, iv) mitogen-activated protein kinase (MAPK) signaling [Constituents: son of sevenless (SOS), rat sarcoma viral oncogene homolog (RAS), rapidly accelerated fibrosarcoma (RAF), mitogen-activated protein kinase kinase (MEK), and extracellular signal-regulated kinase (ERK)], v) phosphatidylinositol-3-kinases (PI3K) and protein kinase B (PKB; also known as AKT) signaling, and vi) nuclear factor kappa-light-chain-enhancer of activated B cells (NF-κB) signaling. EGFR signaling has pleiotropic effects on a multitude of cellular processes.

EGFR overexpression have been linked to decreased survival in both gastric and colorectal cancers[69], which are of particular relevance in this dissertation. The exact nature of the role of EGFR signaling in the aforementioned diseases remains unclear[8,73] and further studies are needed to identify additional points of therapeutic intervention within this pathway.

EGFR and Macrophages: A Limited History

To date, the role of EGFR signaling has primarily been studied in epithelial cells[60,67,71,74-77] and there is a lack of literature related to the role of EGFR signaling in macrophages. Tyrosine kinase phosphorylation in the regulation of macrophage activation is not a novel concept[78]. The receptor tyrosine kinases, macrophage stimulating protein receptor 1 (MSTR1; known as stem cell-derived tyrosine kinase receptor (STK) in mice) and tyrosine-protein kinase receptor 3 (TYRO3), have been shown to extensively modulate macrophage activation[78]. MSTR1 and TYRO3 recruit downstream mediators, such as growth factor receptor bound protein 2 (GRB2) and phosphatidylinositol 3 kinase (PI3K), in order to alter gene expression toward either M1 or M2 macrophage activation[78]. GRB2 and PI3K are also known downstream mediators of EGFR signaling, setting a precedent for the study of EGFR signaling in macrophages[61].

Indeed, previous studies have begun to assess the presence and role of EGFR in macrophages. EGFR was first identified in macrophages in cases of uveal melanoma[79]. Further studies revealed that monocytes, macrophage precursors located in blood, also express EGFR and that the expression of EGFR was necessary for human cytomegalovirus entry[80]. EGFR signaling was shown to be indirectly activated in macrophages during meprin-α-mediated oxidized low-density lipoprotein release in models of atherosclerosis in the heart[81]. Importantly, this study revealed a function for EGFR signaling – the regulation of ROS production[81].

Prior to the studies outlined in Chapters 2-4, only two studies had established relevance for EGFR signaling in macrophages in human disease. EGFR signaling in Kupffer cells (resident liver macrophages) was shown to promote liver tumorigenesis through enhanced IL-6 expression[82]. IL-6 is an M1-associated cytokine with known roles in epithelial cell proliferation[82]. Additionally, EGFR

signaling in macrophages was shown to regulate cytokine production during experimental colitis in mice[83]. However, there are no studies assessing the role of EGFR signaling in macrophages specifically during either bacterial infection or colon carcinogenesis, providing impetus for the studies outlined in Chapters 2-4.

1.5 Ornithine Decarboxylase and Polyamines: An Overview

Polyamine metabolism is responsible for the synthesis of the three main polyamines – putrescine, spermidine, and spermine[84,85]. The semi-essential amino acid, L-arginine, is transported into cells by either solute carrier family 7, member 1 (SLC7A1) or solute carrier family 7, member 1 (SLC7A2)[86-88]. Once in cells, L-arginine is converted into L-ornithine and urea by ARG1 or arginase 2 (ARG2)[86,87]. It should be noted that L-arginine is also the substrate for NOS2, and competition for L-arginine is important in macrophage activation[89]. L-ornithine is the substrate for ODC, which is the rate-limiting enzyme in polyamine metabolism[84,86,87]. The enzymatic activity of ODC results in the decarboxylation of L-ornithine to produce putrescine[84,86,87]. Putrescine is then converted into spermidine by spermidine synthase (SRM) and spermine by spermine synthase (SMS)[86,87]. Polyamines are constantly in flux such that spermine can be converted into spermidine by spermine oxidase (SMOX) and spermidine can be converted into putrescine by the combined activity of spermidine/spermine N-1 acetyl transferase (SAT1) and polyamine oxidase (PAOX)[86,87]. As ODC is the rate-limiting enzyme in this process, Chapter 5 will focus on ODC. Polyamine metabolism is outlined in Figure 5.

ODC is essential for life and is intensively regulated from transcription to post-translational modifications to direct inhibition by ODC modifying enzymes, like antizyme[87]. ODC has been implicated as having a role in many different cancers because of the global control exerted by polyamines on cellular survival, growth and proliferation, DNA synthesis, transcription, and translation[84,85,87,90-93]. As such, ODC is a common target for therapeutic intervention[87,91,94], and one such inhibitor, DFMO, is routinely used as a chemotherapeutic in various cancers[87,91,94].

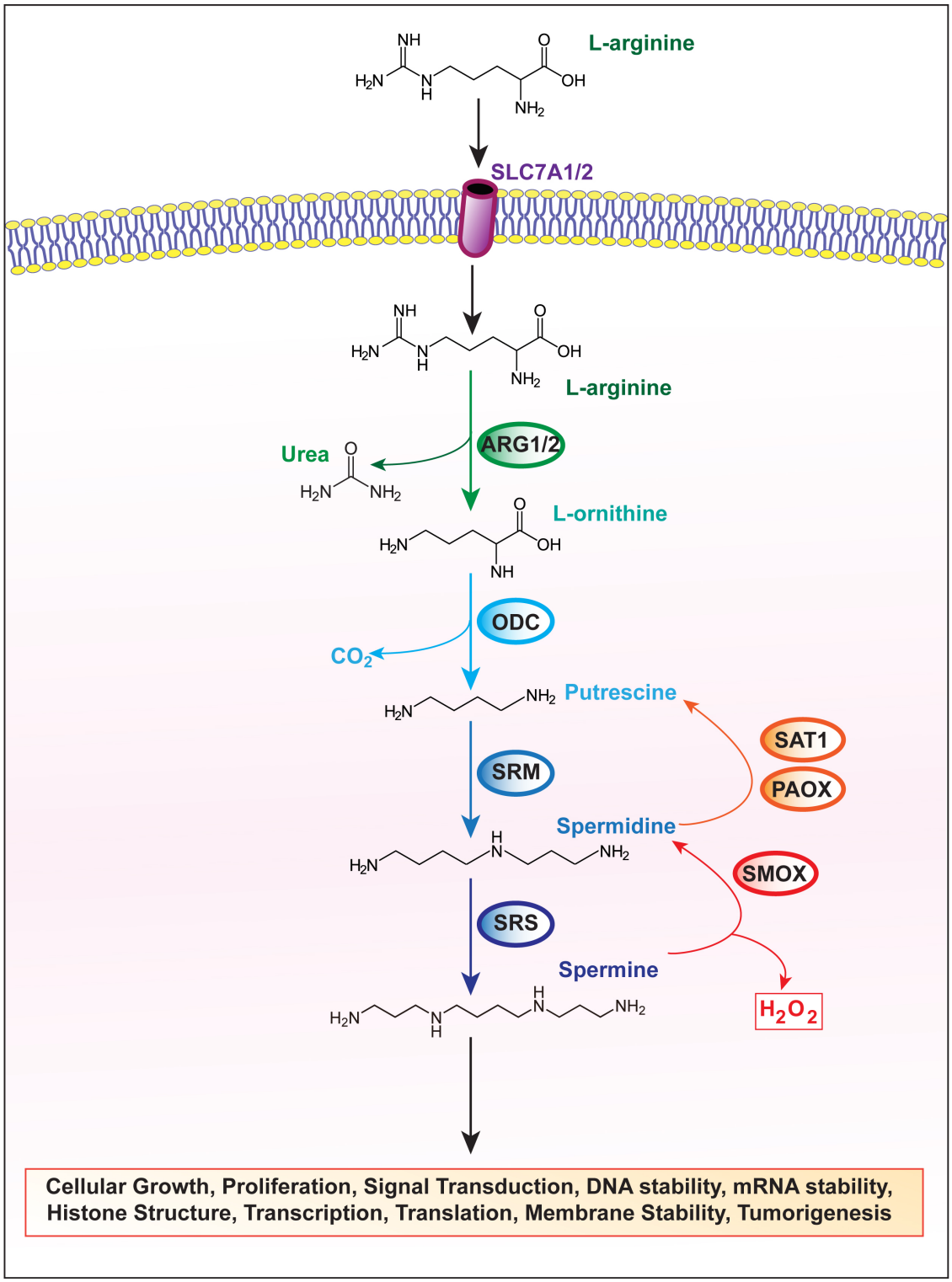

Figure 5. Polyamine metabolism. L-arginine is transported into cells via solute carrier transport protein, family 7, member 1 (SLC7A1) or SLC7A2. Once in cells, L-arginine is converted into L-ornithine by arginase 1 (ARG1) or ARG2, producing urea as a by-product. L-ornithine is converted into putrescine by ornithine decarboxylase (ODC), producing carbon dioxide (CO_2) as a by-product. Putrescine is converted into spermidine by spermidine synthase (SRM) and into spermine by spermine synthase (SMS). Spermine is converted back into spermidine by spermine oxidase (SMOX), producing hydrogen peroxide (H_2O_2) as a by-product. Spermidine is converted into putrescine by polyamine oxidase 1 (PAOX) and spermidine/spermine N-1 acetyl transferase (SAT1). Putrescine, spermidine, and spermine affect many cellular processes.

ODC, Macrophages, and *H. pylori*

The Wilson laboratory has been particularly interested in the role of ODC in macrophages during *H. pylori* infection for many years. Previous studies from the Wilson laboratory have made several key advances in our understanding of the role of ODC in macrophages during infection.

Firstly, ODC is induced in both murine[95,96] and human[47] macrophages during *H. pylori* infection *in vitro* and *in vivo*. This was the first direct evidence that ODC may have a role in macrophage function during *H. pylori* infection. Induction of ODC expression in macrophages is dependent upon the activity of C-v-myc avian myelocytomatosis viral oncogene homolog (C-MYC) as a transcriptional enhancer[95]. Moreover, MAPK1/3 (also known as extracellular signal-regulated kinase [ERK1/2]) signaling in macrophages is critical for ODC expression and activity during *H. pylori* infection[97]. MAPK1/3 signaling is also downstream of EGFR signaling, representing a potential link between EGFR and ODC in macrophages.

From a functional perspective, ODC appears to play a role in the regulation of inflammation during *H. pylori* infection. The induction of ODC has been linked to increased macrophage apoptosis during *H. pylori* infection[95,96]. Moreover, knockout or inhibition of ODC in macrophages increases NOS2 expression and NO production during *H. pylori* infection[47,96]. The increase in NO production was seen in both the macrophage cell line, RAW 246.7, and in isolated gastric macrophages (Gmacs) following acute *H. pylori* infection[47,96]. Treatment of Mongolian gerbils with DFMO attenuated *H. pylori*-mediated gastric cancer in gerbils, in part, by decreasing inflammation[37]. While the gerbil model allows for the study of *H. pylori*-mediated gastric carcinogenesis, no experiments can be performed on macrophages specifically, due to lack of available reagents for gerbil studies, leaving lingering questions about the role of ODC in macrophage function *in vivo*.

As such, to date, we have no mechanism by which ODC in macrophages regulates the response to *H. pylori* infection. The study outlined in Chapter 5 was designed to specifically address the role of ODC in macrophages in the regulation of macrophage activation and in the modulation of the pathogenesis of gastrointestinal pathogens *in vivo*. The cell-specific knockout mouse model is a critical tool that has allowed for the studies in Chapter 5 to take place.

1.6 Thesis Aims and Significance

The overarching goal of this dissertation is to identify proteins that significantly modulate macrophage activation and function during bacterial infection and carcinogenesis. Macrophage activation along the M1 to M2 paradigm is not a new concept, and much is known about the regulation of macrophage activation. However, what is known about macrophage activation is mostly limited to reductionist experiments performed *in vitro* with known stimuli; relatively fewer studies have focused on macrophage activation and function in disease models *in vivo*, especially in bacterial infection models. The studies outlined in this dissertation have identified two proteins – EGFR and ODC – as regulators of macrophage activation during bacterial infection and carcinogenesis.

Prior to this dissertation, relatively little was known about the function of either EGFR or ODC in regulating macrophage activation and function. The concept of EGFR signaling occurring in macrophages had been minimally addressed prior to this work, and no mechanisms by which EGFR may regulate macrophage function had been determined. Similarly, the Wilson laboratory had studied the role of ODC in macrophages for several years, but only within the context of macrophage apoptosis. No studies had been performed to determine the role of ODC in the regulation of macrophage activation along the M1 to M2 paradigm. This dissertation provides the first comprehensive studies related to the roles of EGFR and ODC in macrophage activation by addressing four specific aims. The aims of this dissertation are outlined in Figure 6.

EGFR signaling robustly occurs in macrophages, but the function of EGFR signaling in macrophages remains poorly understood. Chapters 2-4 address three aims designed to determine the role of EGFR signaling in macrophages during both *H. pylori* and *C. rodentium* infection and during carcinogenesis. Chapter 2 focuses on the role of EGFR signaling in macrophages during bacterial infection. The presence of EGFR in macrophages was confirmed in both murine and macrophage cells lines. Moreover, since there is a notably higher gastric cancer incidence in Latin America (Figure 2), we obtained samples from *H. pylori*-infected individuals and determined that EGFR signaling also occurs in humans during active *H. pylori* infection. In addition to human samples, we assessed the levels of EGFR signaling in macrophages using a human tissue microarray (TMA). This TMA contains samples

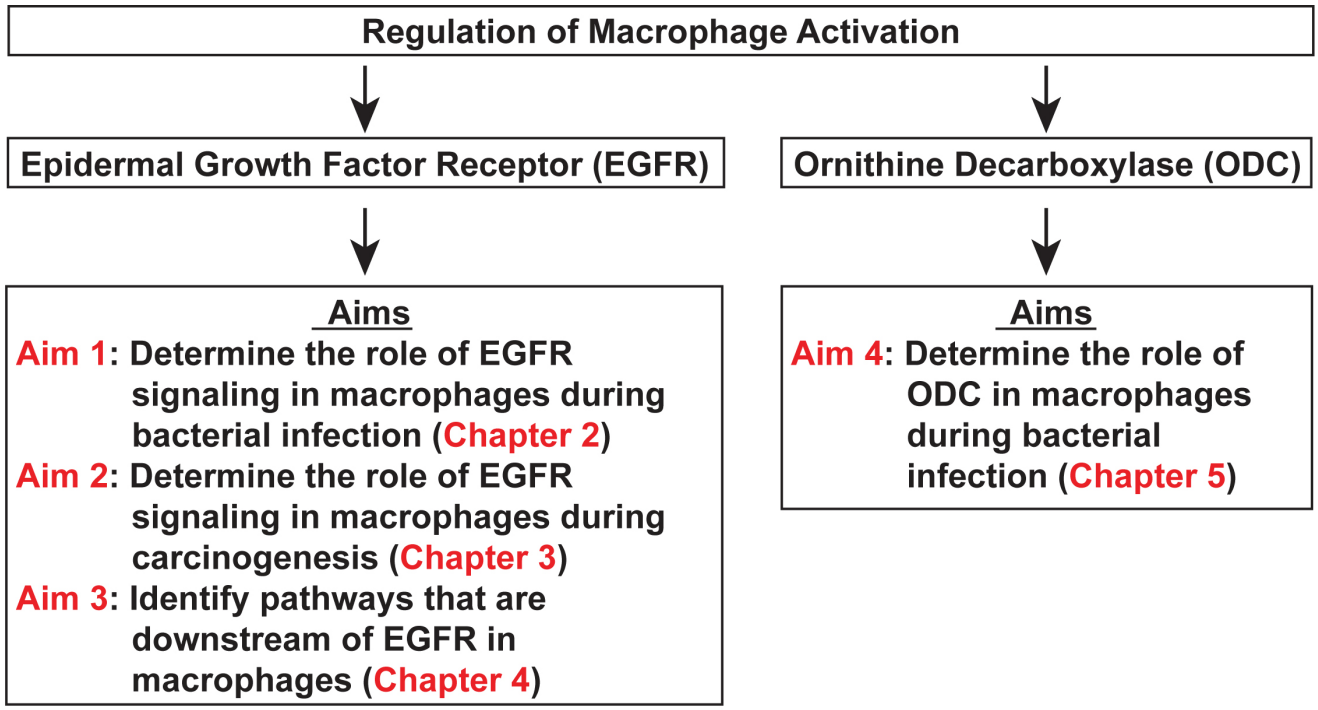

Figure 6. Outline of the aims of this dissertation. The overarching theme of this dissertation is to determine mechanisms by which macrophage activation is regulated. Chapters 2-4 will determine the role of epidermal growth factor receptor (EGFR) signaling in the regulation of macrophage activation and function during bacterial infection and carcinogenesis. Chapter 5 will assess the role of ornithine decarboxylase (ODC) in the regulation of macrophage activation and function during bacterial infections.

that spanned the entire Correa Cascade of gastric carcinogenesis – normal tissue to gastritis and metaplasia to gastric adenocarcinoma. Importantly, we demonstrated that EGFR signaling is detectable from gastritis to gastric adenocarcinoma, and the level of signaling increases in cancer. This is the first time that active EGFR signaling in macrophages was demonstrated in human cancer cases and is indicative of the potential importance of macrophage-specific EGFR signaling in carcinogenesis, providing the impetus for the studies outlined in Chapter 3.

Moreover, by leveraging a myeloid-specific EGFR knockout mouse model and primary bone marrow-derived macrophages (BMmacs), we were able to examine *H. pylori* and *C. rodentium* pathogenesis *in vivo* and macrophage activation *in vitro* in Chapter 2. This chapter outlines the central role that EGFR signaling has in regulating M1, M2, and Mreg activation across a variety of stimuli. EGFR deficiency in macrophages had a marked effect on the adaptive immune response, as it resulted in a diminished Th17 and enhanced Treg response to chronic *H. pylori* infection, leading to decreased histologic gastritis and increased bacterial persistence. Similarly, myeloid-specific deletion of EGFR also attenuated the immune response to *C. rodentium* infection in the colon. Thus, these data indicate that EGFR signaling promotes M1 macrophage activation and is pro-inflammatory during enteric bacterial infections. The findings in Chapter 2 represent a critical advancement in our understanding of EGFR signaling in the regulation of macrophage function during bacterial infection.

Building upon the findings in Chapter 2, the aim of Chapter 3 is to explore the role of EGFR signaling in macrophages during colon carcinogenesis. Obviously, *H. pylori* is the leading risk factor for gastric cancer, but a mouse model necessary for studying the role of EGFR signaling in macrophages during gastric cancer is not yet available. However, the azoxymethane (AOM)-dextran sodium sulfate (DSS) model of colon carcinogenesis can be readily utilized in our myeloid-specific EGFR knockout mouse model. Chapter 3 demonstrates that EGFR signaling in macrophages – not epithelial cells – is a key factor in colitis-associated carcinogenesis (CAC). These results of these studies were surprising in that i) macrophage EGFR, and *not* epithelial EGFR, was pro-tumorigenic, and ii) both pro-tumorigenic M2 activation and M1 activation, typically thought to be anti-tumorigenic, were necessary for CAC. The

studies in Chapter 3 provide the impetus for further studies related to the role of EGFR signaling in macrophages during colon carcinogenesis, given that these were the first observations of their kind.

EGFR signaling in macrophages is an extremely understudied subject. Within the context of epithelial cells, the downstream targets of EGFR signaling are well understood[59,60], but it does not necessarily follow that the pathways that are downstream of EGFR in epithelial cells must be the same pathways that are downstream of EGFR in macrophages. Thus, the aim of Chapter 4 is to utilize unbiased proteomic techniques to elucidate pathways that are downstream of EGFR in macrophages. Many pathways are known to be downstream targets of EGFR signaling (Figure 4), but pathways specific to EGFR signaling in macrophages remain unknown. Chapter 4 outlines the use of stable isotope labeling with amino acids in cell culture (SILAC), an unbiased technique, to identify phospho-proteins that are modified by EGFR signaling during *H. pylori* infection in macrophages. While this aim is not yet fully developed, the goal is to identify factors specific to macrophages that may represent targets for chemotherapeutics. Indeed, SILAC analysis thus far has identified tripartite motif containing 28 (TRIM28) as a potential downstream target of EGFR signaling in macrophages. Further studies are planned.

Finally, Chapter 5 assesses a second protein, ODC, which is the rate-limiting enzyme in polyamine metabolism. Like EGFR, ODC is essential for life and its role in regulating polyamine metabolism has effects on many different cellular processes. Myeloid-specific ODC knockout mice had exacerbated histologic gastritis, coupled with decreased *H. pylori* burden following chronic infection. Similarly, in the *C. rodentium* infection model, the mice with myeloid-specific ODC knockout exhibited increased colitis. Moreover, M1 macrophage activation was significantly enhanced due to alterations in histone modifications that increased transcription of pro-inflammatory cytokines. While the studies outlined in Chapter 2 and Chapter 3 demonstrated that EGFR is a pro-inflammatory mediator, Chapter 5 determined that ODC was an anti-inflammatory mediator.

Overall, this dissertation is focused on the regulation of macrophage activation under various conditions. The studies outlined in the subsequent chapters reveal roles for EGFR and ODC, two proteins critical for life, in controlling macrophage responses during both bacterial infection and

carcinogenesis. Taken together, the data underscore that while many studies have been performed, much remains to be learned about the proteins and pathways that regulate macrophage activation. Moreover, EGFR and ODC are classically studied in the context of epithelial cell function. The coming chapters demonstrate the importance of challenging existing norms, as such studies can reveal critical new information about biology.

CHAPTER 2

EGFR SIGNALING IN MACROPHAGES DURING BACTERIAL INFECTION

2.1 Introduction

Macrophages represent a dynamic subset of innate immune cells, with functions in immune surveillance, immunity to pathogens, wound healing, antigen presentation, and cytokine/chemokine production[1,3,4]. A critical step in macrophage function is macrophage activation[2]. Classically-activated, M1 macrophages are generated in response to pathogens and pro-inflammatory cytokines[1-3,98]. M1 macrophages mediate the anti-microbial response to pathogens[1-3]. Alternatively-activated, M2 macrophages are generated in response to IL-4 and are associated with wound healing[2,3,11,98] and promotion of tumorigenesis[7,13]. Thirdly, Mregs are anti-inflammatory, secreting high concentrations of IL-10 to counter-regulate the M1 response[2,14].

Many studies have focused on signaling pathways that regulate macrophage activation, including JAK/STAT, NF-κB, IRF, and cAMP response element-binding protein (CREB)[12,15,16,18,19,99]. Recent evidence suggests that tyrosine kinase signaling also regulates macrophage activation[78]. Specifically, EGFR signaling has been implicated in macrophage function in mouse models of glaucoma, colitis, and cancer[79,82,83,100]. Mice lacking EGFR in resident liver macrophages (Kupffer cells) developed less hepatocellular carcinoma, as a direct result of decreased cytokine production by Kupffer cells[82]. However, the role of macrophage EGFR signaling in bacterial infections has not been studied.

To investigate this, we chose a highly prolific human pathogen, *Helicobacter pylori*[21]. *H. pylori* is a Gram-negative, microaerophilic bacterium that infects approximately 50% of the global population[24,101]. Infection with *H. pylori* is the single greatest risk factor for the development of gastric cancer, which is the third leading cause of cancer death worldwide[22,24,102]. The combination of *H. pylori*-produced oncoproteins, such as CagA, and infection-induced chronic inflammation, which fails to eradicate the infection, creates a vicious cycle of tissue and DNA damage[9,35,37,40,41]. Importantly, macrophages play a critical role in *H. pylori*-mediated gastritis[20,47,103]. Thus, enhanced understanding of the regulation of macrophage responses to *H. pylori* could prove very useful in devising new strategies

for chemoprevention of gastric cancer, as antibiotic treatment is often ineffective in eradicating the pathogen, especially in high-risk regions[9,23,35,40].

To gain further insights into the role of macrophage EGFR signaling in mucosal inflammation driven by bacterial infection, we also utilized the murine pathogen, *Citrobacter rodentium*, an attaching and effacing enteric bacterial pathogen that mimics enteropathogenic and enterohemorrhagic *Escherichia coli*[104]. *C. rodentium* infection leads to acute colon inflammation, marked by significant macrophage infiltration[105,106] and has been used as a mouse model of inflammatory bowel disease. Here, we demonstrate that EGFR signaling i) is activated in macrophages in response to the bacterial pathogens *H. pylori* and *C. rodentium*, ii) plays a critical role in macrophage activation and function, and iii) is involved in human macrophages during *H. pylori*-induced disease progression.

2.2 Results

EGFR phosphorylation in macrophages occurs during human *H. pylori* infection

In previous studies, we determined that phosphorylated EGFR (pEGFR) in epithelial cells is correlated with early stages of gastric carcinogenesis in humans[74]. We also observed that mononuclear cells in the lamina propria of stomach tissues contained pEGFR (Appendix A, Figure 1). To determine if pEGFR localized to macrophages, we utilized human tissues from Colombia, a region with a high prevalence of gastric cancer[33,37,107]. These gastric biopsies were from patients with *cagA*$^+$ *H. pylori* infection and chronic, active gastritis. Using CD68 as a macrophage marker, we found high levels of CD68$^+$pEGFR$^+$ macrophages in gastritis tissues, which were significantly increased versus uninfected, control patients (Figure 7A and 7B). These data indicate that pEGFR is upregulated in human gastric macrophages during *H. pylori*-induced inflammation.

To examine these findings in a larger number of cases, we utilized a human TMA[74] from Vanderbilt University Medical Center that included gastric tissues from patients spanning the histological range from normal to gastric cancer. We stained the TMA for CD68 and pEGFR (Figure 7C) and utilized CellProfiler to quantify CD68$^+$pEGFR$^+$ cells. The percentage of CD68$^+$pEGFR$^+$ macrophages was significantly increased in gastritis and in intestinal metaplasia (Figure 7D). Further,

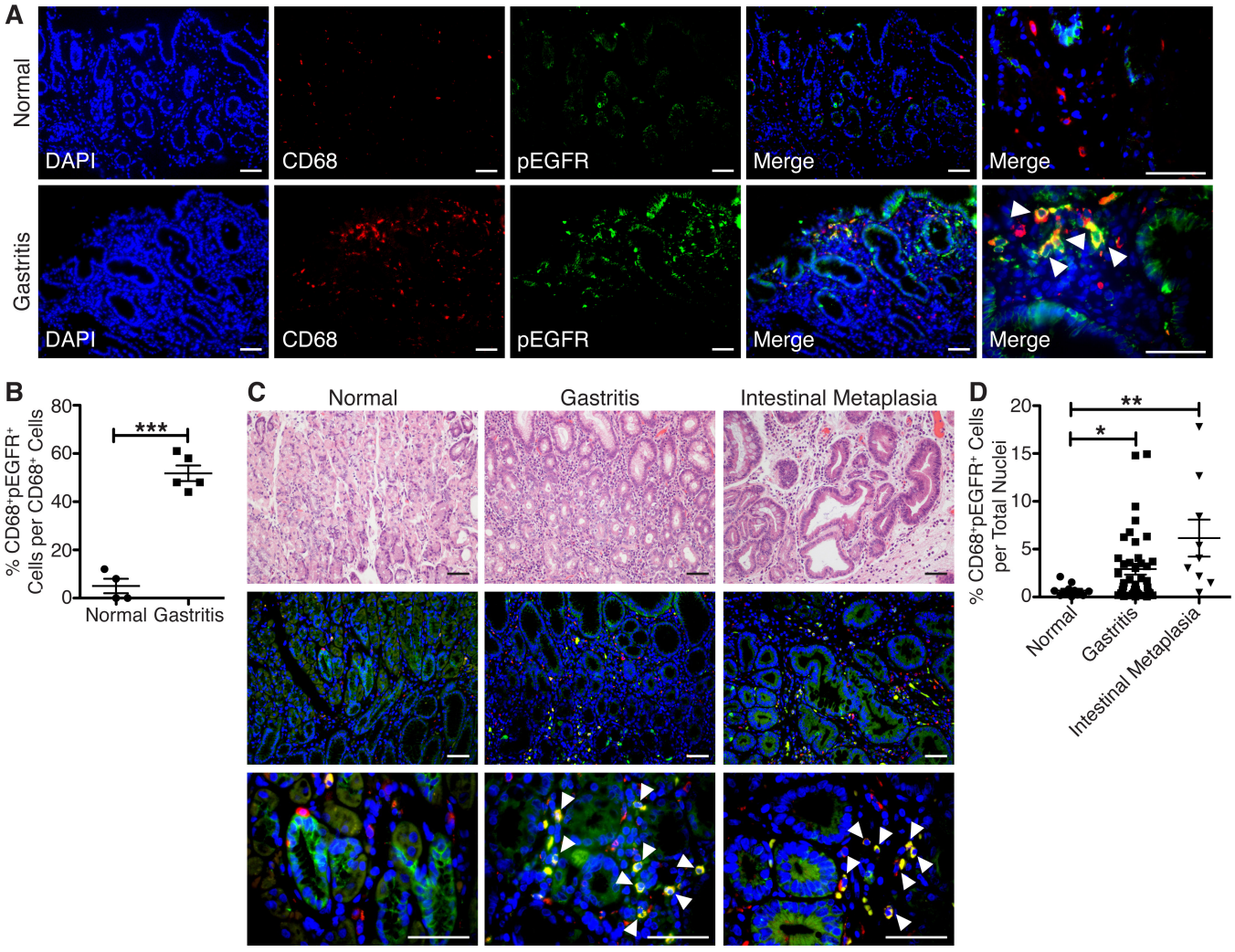

Figure 7. Increased pEGFR levels in human gastric macrophages in *H. pylori*-induced gastritis and precancerous intestinal metaplasia. (A) Representative immunofluorescence images of human gastric biopsies with normal histology and active, non-atrophic gastritis. CD68 = red, pEGFR Y1068 = green, Yellow = merge, Blue = DAPI. Scale bar = 50 μM. *n* = 4 normal samples and 5 gastritis samples. (B) Quantification of the percentage of $CD68^+pEGFR^+$ macrophages per the total number of $CD68^+$ cells in 10 fields per slide from (A). Slides were analyzed in a blinded manner. ***$P < 0.001$. *n* = 4 normal samples and 5 gastritis samples. Statistical significance was calculated by the Student's *t* test. (C) Representative hematoxylin and eosin (H&E) images and immunofluorescence images of gastric tissues from the Vanderbilt University TMA. Red = CD68, Green = EGFR pY1068, Yellow = merge, Blue = DAPI. Scale bar = 100 μM. *n* = 12 normal samples, 41 gastritis samples, and 9 intestinal metaplasia samples. (D) Quantification of the percentage of $CD68^+pEGFR^+$ cells per the total number of cells in each individual core in the TMA, as determined by CellProfiler. *$P < 0.05$. **$P < 0.01$. *n* = 12 normal samples, 41 gastritis samples, and 9 intestinal metaplasia samples. Statistical significance was calculated by one-way ANOVA with the Kruskal-Wallis test, followed by the Mann-Whitney *U* test.

the percentage of $CD68^{+}pEGFR^{+}$ macrophages was also increased in both intestinal-type and diffuse-type gastric cancer (Appendix A, Figure 2A and 2B). Importantly, a significant percentage of the total $CD68^{+}$ macrophages were $pEGFR^{+}$ in intestinal metaplasia, and in intestinal-type and diffuse-type gastric cancer, indicating that EGFR signaling in macrophages has a critical role in gastric carcinogenesis (Appendix A, Figure 2C). The percentage of $CD68^{-}pEGFR^{+}$ cells, the majority of which are epithelial cells, decreased in both types of gastric cancer (Appendix A, Figure 3A). These data are consistent with our previous report in which we demonstrated diminished pEGFR levels in gastric epithelial cells by immunoperoxidase staining in cases of gastric cancer compared to earlier stages of disease[74]. While there was an overall positive correlation between the percentage of $CD68^{+}pEGFR^{+}$ and the percentage of $CD68^{-}pEGFR^{+}$ cells (Appendix A, Figure 3B), this was driven primarily by cases of active gastritis (Appendix A, Figure 3C), suggesting a potential interaction between macrophages and non-macrophages in induction of EGFR signaling during gastric inflammation. Importantly, the correlation between macrophage and non-macrophage/epithelial pEGFR levels was lost in intestinal-type and diffuse-type gastric cancer (Appendix A, Figure 3C), indicating that macrophage EGFR signaling is independent of epithelial EGFR signaling at the end stages of the histologic cascade. These data demonstrate that EGFR signaling plays an important role in macrophage function during chronic inflammation and carcinogenesis in the human stomach.

H. pylori infection induces EGFR phosphorylation in macrophages

To extend these observations, we determined whether *H. pylori* infection is sufficient to induce EGFR phosphorylation in macrophages *in vitro*. In murine RAW 264.7 cells, pEGFR levels peaked at 30 minutes post infection (p.i.) (Figure 8A). Phosphorylation was detectable at two residues, Y1068 and serine (S) 1046/7 (Figure 8A). Densitometric analysis confirmed the induction of EGFR phosphorylation at both residues, and determined that the induction at 30 min p.i. was significantly greater than the induction at 15 min p.i. at pY1068 and pS1046/7 (Figure 8B and 8C). Additionally, phosphorylation of differentiation into macrophages (Figure 8D). The clinically-available, EGFR-specific tyrosine kinase inhibitor, gefitinib, effectively diminished EGFR phosphorylation (Figure 8E). Similarly, in primary

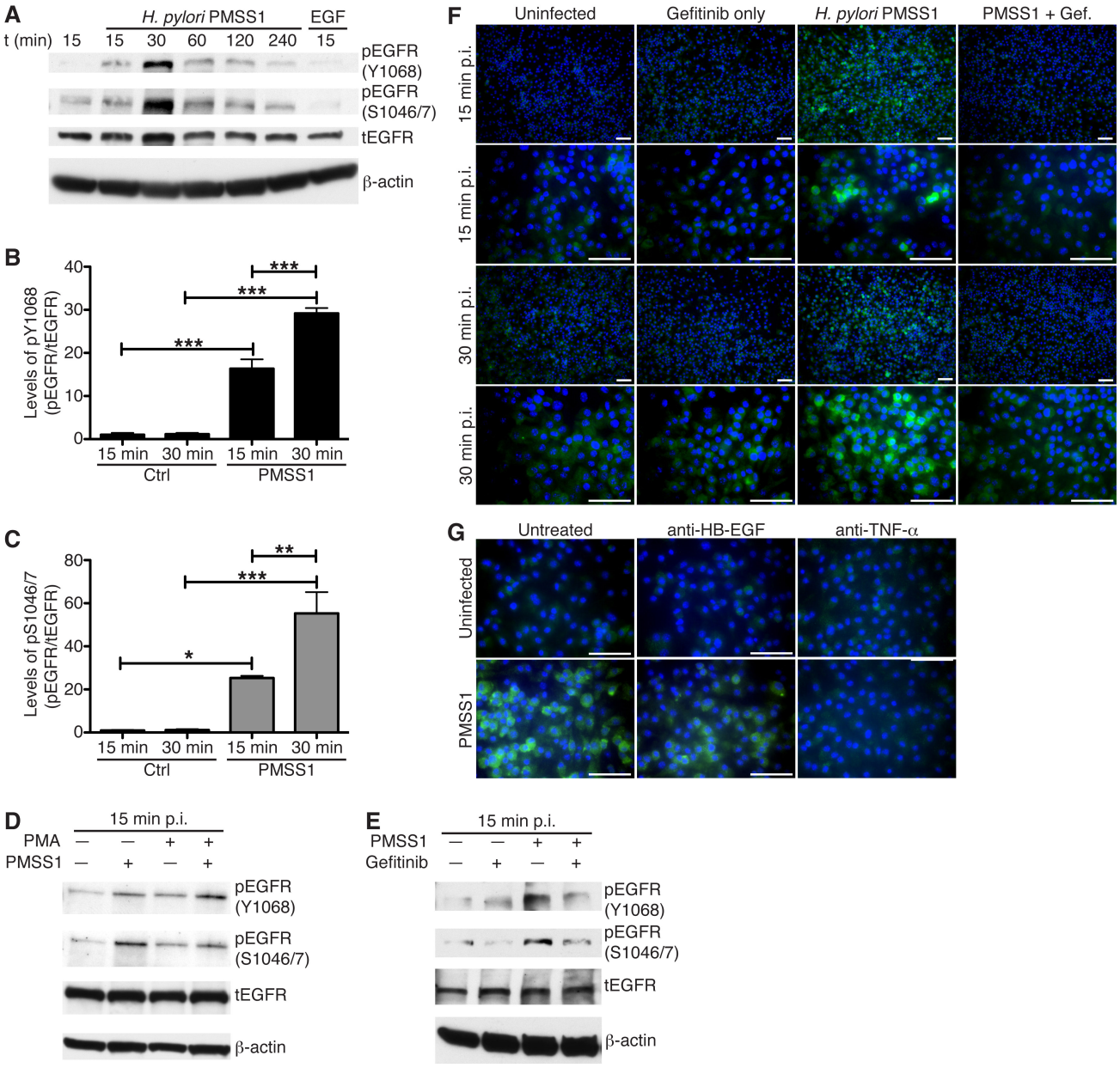

Figure 8. EGFR signaling in macrophages is induced by *H. pylori* infection in murine and human macrophages. (A) Representative western blot of EGFR pY1068 and pS1046/7 in RAW 264.7 cells at various time points post-infection (p.i.) with *H. pylori* PMSS1 or stimulation with EGF (5 ng/mL). *n* = 3 biological replicates. (B) Densitometric analysis of the levels of pY1068 compared to levels of tEGFR at 15 and 30 min p.i. *** $P < 0.001$. *n* = 3 biological replicates. (C) Densitometric analysis of the levels of pS1046/7 compared to levels of tEGFR at 15 and 30 min p.i. * $P < 0.05$, ** $P < 0.01$, *** $P < 0.001$. *n* = 3 biological replicates. Statistical significance in (B) and (C) was calculated by one-way ANOVA with Newman-Keuls post-test. (D) Representative western blot of EGFR at pY1068 and pS1046/7 in THP-1 cells at 15 min p.i. with *H. pylori* PMSS1. Monocytes [− phorbol-12-myristate-13-acetate (PMA)] and macrophages (+ PMA) are represented in this blot. *n* = 3 biological replicates. (E) Representative western blot of EGFR at pY1068 and pS1046/7 in RAW 264.7 cells at 15 min p.i. with *H. pylori* PMSS1 ± 10 μM gefitinib. *n* = 3 biological replicates. (F) Representative immunofluorescence images of WT BMmacs infected with *H. pylori* PMSS1 ± 10 μM gefitinib at times indicated. Green = EGFR pY1068, Blue = DAPI. Scale bar = 50 mM. *n* = 5 biological replicates. (G) Representative immunofluorescence images of WT BMmacs infected with *H. pylori* PMSS1 ± 10 ng/mL anti-TNF-α or ± 25 ng/mL anti-HB-EGF at 30 min p.i. Green = pEGFR Y1068, Blue = DAPI. Scale bar = 50 μM. *n* = 3 biological replicates.

BMmacs from naive C57BL/6 wild-type mice, *H. pylori* infection was sufficient to induce EGFR phosphorylation, which was attenuated by gefitinib (Figure 8F). Thus, EGFR transactivation is upregulated in macrophages in response to a bacterial pathogen, and it is a conserved feature of macrophage immune responses, as it is present in both mouse and human systems.

EGFR activation can occur in either a ligand-dependent or ligand-independent manner[66,108]. Previous studies in epithelial cells have revealed that pY1068 is a marker of ligand-dependent activation and pS1046/47 is a marker of ligand-independent activation[66,108]. Since our data indicate that *H. pylori* infection leads to the phosphorylation of both residues, we investigated activation mechanisms in macrophages. HB-EGF is primarily produced by macrophages and is an EGFR ligand[63]. TNF-α is a known inducer of ligand-independent EGFR activation[66,67]. Treatment of wildtype (WT) BMmacs with an anti-HB-EGF neutralizing antibody resulted in a modest inhibition of *H. pylori*-induced EGFR phosphorylation (Figure 8G). However, treatment of macrophages with anti-TNF-α neutralizing antibody ablated EGFR activation at pY1068 and pS1046/47 (Figure 8G and Appendix A, Figure 4). Moreover, treatment with recombinant TNF-α also stimulated phosphorylation at S1046/47 (Appendix A, Figure 4). These data suggest that EGFR can be activated in a ligand-independent, TNF-α-dependent mechanism in macrophages during *H. pylori* infection.

Macrophage EGFR signaling is critical for controlling bacterial burden and mounting an adequate immune response to infection

To determine the role of EGFR signaling in macrophages *in vivo*, we obtained $Egfr^{fl/fl}$ mice crossed to $LysM^{cre/cre}$ mice, creating the $Egfr^{\Delta mye}$ mouse[83]. The *LysM* driver leads to the excision of the *Egfr* alleles that are flanked by *loxp* sites in myeloid cells[83,109].

We determined knockdown of EGFR in several ways. Firstly, $Egfr^{fl/fl}$ and $Egfr^{\Delta mye}$ BMmacs were isolated and infected with *H. pylori* PMSS1 for 24 hours (h); DNA was isolated and excision of the *Egfr* gene was detected (Appendix A, Figure 5A). Secondly, significant knockdown of total EGFR (tEGFR) protein levels was demonstrated in $Egfr^{\Delta mye}$ versus $Egfr^{fl/fl}$ BMmacs, both before and after infection with *H. pylori* (Appendix A, Figure 5B and 5C).

Thirdly, previous studies have demonstrated that the peak of macrophage infiltration is 48 h p.i. with *H. pylori*[97,110]. Using flow cytometry, and F4/80 and CD11b as macrophage markers, the number of tEGFR$^+$ Gmacs was significantly decreased in *Egfr*$^{\Delta mye}$ versus *Egfr*$^{fl/fl}$ mice at this timepoint (Appendix A, Figure 5D). Further, the number of infiltrating Gmacs was not different between genotypes (Appendix A, Figure 5E). The number of pan-cytokeratin$^+$tEGFR$^+$ gastric epithelial cells was also not different (Appendix A, Figure 5F), indicating the specificity of the LysM-Cre driver. The use of an isotype control antibody verified the specificity of the tEGFR staining (Appendix A, Figure 5G).

Lastly, we determined expression levels of lysozyme 2 (*Lyz2*), the gene on which the Cre recombinase was placed, and of *Cre* itself. Gastric tissues at 4 months (mo) p.i. and BMmacs infected with *H. pylori* demonstrated that while the *Egfr*$^{fl/fl}$ mice expressed *Lyz2*, the *Egfr*$^{\Delta mye}$ mice had no *Lyz2* expression (Appendix A, Figure 6), verifying the durability of the *Lyz2* knockout. Further, there were very high levels of *Cre* mRNA both before and after chronic infection, confirming that there was no loss of *Cre* expression during our experiments (Appendix A, Figure 6).

Having established that EGFR is effectively deleted only in macrophages before and after infection, we utilized our established model of chronic infection with *H. pylori* Sydney Strain 1 (SS1) for 4 mo[47,96,103]. *Egfr*$^{\Delta mye}$ mice demonstrated significantly decreased histologic gastritis after four-month *H. pylori* SS1 infection (Figure 9A and 9B), and decreased acute gastritis after one-month *H. pylori* pre-mouse Sydney Strain 1 (PMSS1) infection (Appendix A, Figure 7A). Previous reports have indicated that gastric inflammation, as a marker of immune response, is associated with control of *H. pylori* load in mouse models[111,112]. As such, there was increased *H. pylori* colonization in *Egfr*$^{\Delta mye}$ mice, compared to *Egfr*$^{fl/fl}$ or *LysM*$^{cre/cre}$ mice (Figure 9C). Increased colonization in *Egfr*$^{\Delta mye}$ mice was also observed in the one-month model of infection with *H. pylori* PMSS1 (Appendix A, Figure 7B).

CD68$^+$ Gmacs from infected gastric tissues in *Egfr*$^{fl/fl}$ and *LysM*$^{cre/cre}$ mice demonstrated a high level of co-localization with pEGFR *in situ*, indicating that *H. pylori* infection induces EGFR signaling in macrophages (Figure 9D). CD68$^+$ Gmacs in infected *Egfr*$^{\Delta mye}$ gastric tissues did not have any detectable pEGFR (Figure 9D). Moreover, CD68$^+$ Gmacs in infected *Egfr*$^{\Delta mye}$ gastric tissues did not have any demonstrable tEGFR, while CD68$^+$ Gmacs from *Egfr*$^{fl/fl}$ and *LysM*$^{cre/cre}$ mice had high levels of

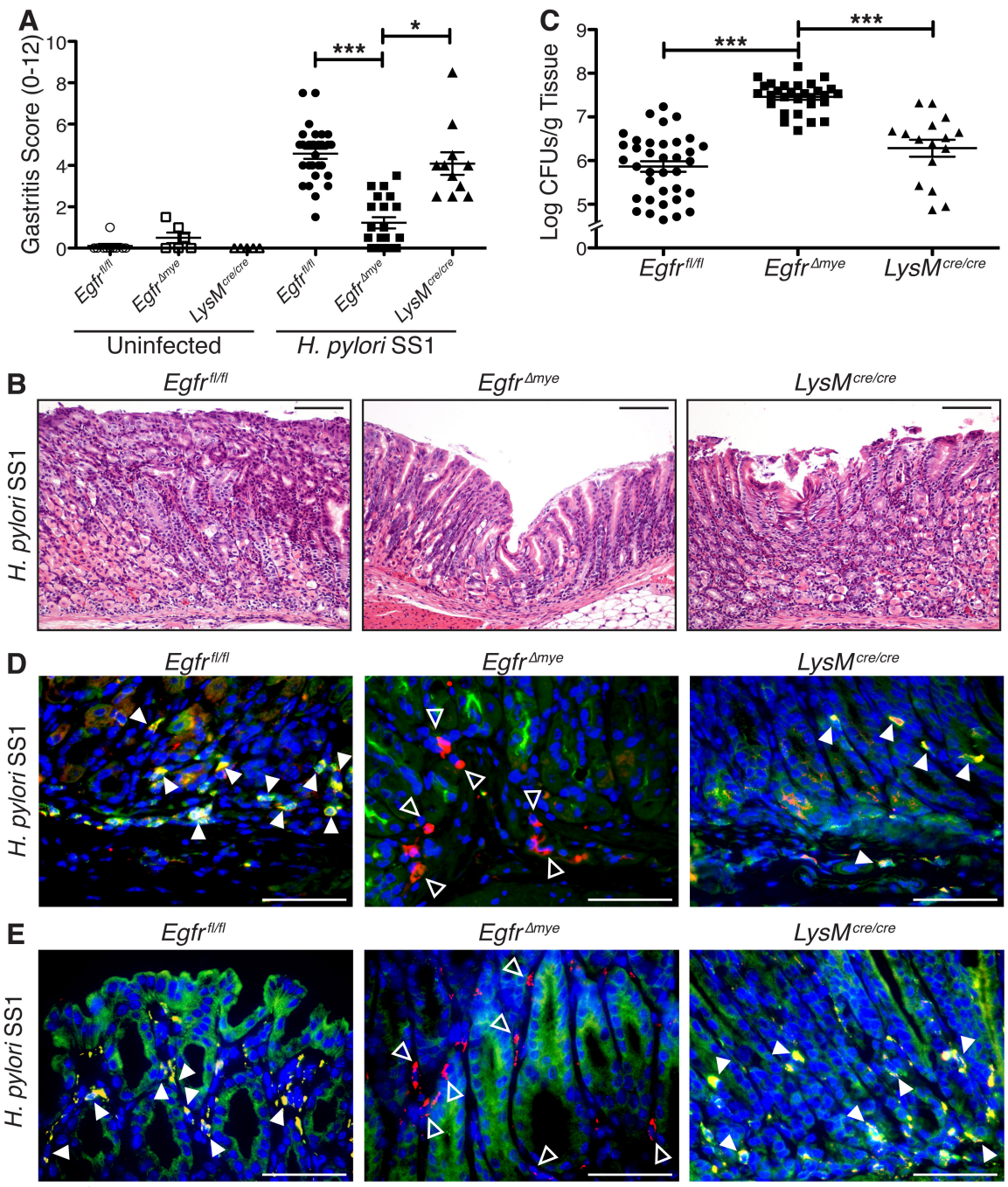

Figure 9. *Egfr*$^{\Delta mye}$ mice have significantly increased *H. pylori* burden, but significantly decreased gastritis after chronic infection. (A) Gastritis scores were assessed 4 mo p.i in by a gastrointestinal pathologist in a blinded manner according to the updated Sydney System. *$P < 0.05$. ***$P < 0.001$. (B) Representative H&E images from infected mice in (A). Scale bars = 100 μM. (C) Colonization of *H. pylori* SS1 was assessed by serial dilution and culture 4 mo post infection (p.i.). ***$P < 0.01$. In (A) and (C), n = 5-10 uninfected and 11-30 *H. pylori* SS1 mice per genotype. Statistical significance in (A) and (C) was calculated by one-way ANOVA with Newman-Keuls post-test. (D) Representative immunofluorescence images of pEGFR from infected mice in (A) and (B). Green = EGFR pY068, Red = CD68, Yellow = merge, Blue = DAPI. Closed arrows indicate CD68$^+$pEGFR$^+$ macrophages. Open arrows indicate CD68$^+$pEGFR$^-$ macrophages. Scale bars = 50 μM. (E) Immunofluorescence images of tEGFR from infected mice in (A) and (B). Green = tEGFR, Red = CD68, Yellow = merge, Blue = DAPI. Closed arrows indicate CD68$^+$tEGFR$^+$ macrophages. Open arrows indicate CD68$^+$tEGFR$^-$ macrophages. Scale bars = 50 μM. In (D) and (E), n = ≥ 3 mice per genotype.

tEGFR (Figure 9E). These data indicate that the deletion of EGFR is maintained throughout chronic *H. pylori* infection.

To determine if our findings were generalizable to another enteric bacterial infection, $Egfr^{fl/fl}$ and $Egfr^{\Delta mye}$ mice were inoculated with *C. rodentium* for 14 days, a model of colitis[113]. $Egfr^{\Delta mye}$ mice exhibited increased *C. rodentium* bacterial burden in colonic tissue (Appendix A, Figure 8A). When compared to $Egfr^{fl/fl}$ mice, $Egfr^{\Delta mye}$ mice were protected from weight loss, indicative of decreased clinical disease severity (Appendix A, Figure 8B). Decreased disease severity, combined with increased colonization, in the *C. rodentium* model is concordant with the findings in the *H. pylori* model above. $CD68^+$ macrophages from infected colonic tissues in $Egfr^{fl/fl}$ mice demonstrated a high level of co-localization with pEGFR, indicating that *C. rodentium* infection also induces EGFR signaling in macrophages (Appendix A, Figure 8C). $CD68^+pEGFR^+$ colonic macrophages were not present in infected $Egfr^{\Delta mye}$ colonic tissues, again confirming effective *Egfr* excision in these mice (Appendix A, Figure 8C). These data further indicate that EGFR signaling in macrophages is important in the host response to enteric infections.

EGFR signaling is critical for pro-inflammatory chemokine production *in vivo*

Based on our *in vivo* findings, we hypothesized that the loss of *Egfr* in myeloid cells diminished the innate immune responses to bacterial pathogens. To assess host immune responses, we utilized a Luminex Multiplex Array to assess 32 chemokines/cytokines. Six analytes were significantly decreased in gastric tissues from *H. pylori*-infected $Egfr^{\Delta mye}$ mice versus $Egfr^{fl/fl}$ or $LysM^{cre/cre}$ mice (Figure 10). Moreover, all of these analytes, C-X-C motif ligand (CXCL) 1 (GRO-α, KC), CXCL9 (MIG), CXCL10 (IP-10), C-C motif ligand, CCL3 (MIP-1α), CCL4 (MIP-1β), and CCL5 (RANTES), were altered at both the mRNA and protein levels (Figure 10), indicating that loss of EGFR in myeloid cells leads to a significant ablation of the innate immune response at the transcriptional level. Alterations in chemokine responses further indicate that macrophage EGFR signaling is necessary for the gastric inflammatory response to *H. pylori*. Cytokines that were either not significantly different between genotypes, not increased by *H. pylori* infection, or not detected are listed in Appendix A, Table 1.

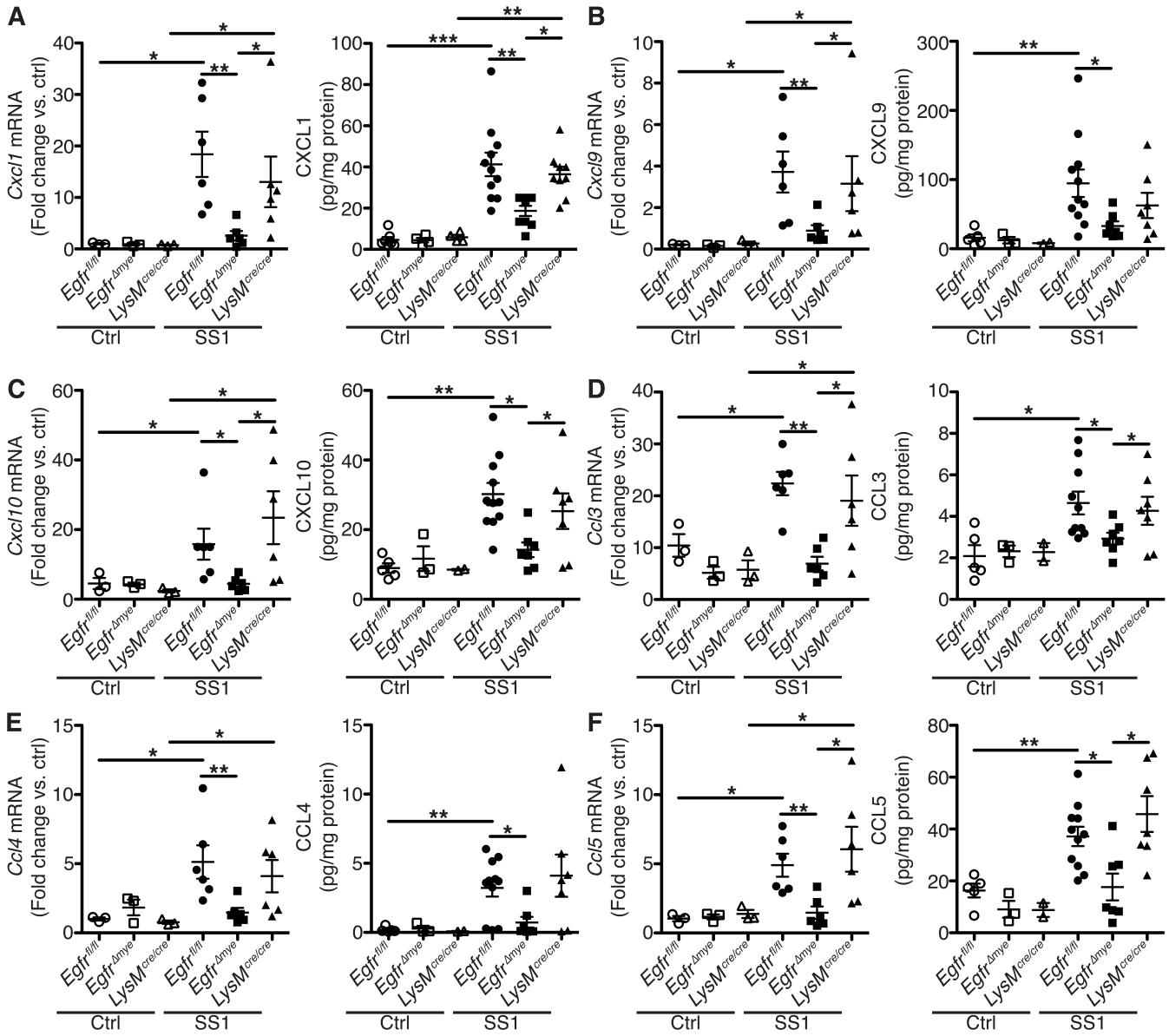

Figure 10. *Egfr*$^{\Delta mye}$ mice have significantly decreased chemokine production in gastric tissue. mRNA and protein levels of cytokines/chemokines, (A) CXCL1 (KC), (B) CXCL10 (IP-10), (C) CXCL9 (MIG), (D) CCL3 (MIP-1α), (E) CCL5 (RANTES), and (F) CCL4 (MIP-1β), were assessed by RT-PCR and Luminex Multiplex Array, respectively, from gastric tissue 4 mo p.i. with *H. pylori* SS1. **P* < 0.05. ***P* < 0.01. Statistical significance was calculated by one-way ANOVA with the Kruskal-Wallis test, followed by the Mann-Whitney *U* test. In all panels, *n* = 2-5 uninfected and 6-11 infected mice per genotype.

EGFR signaling is critical for pro-inflammatory cytokine production and *Nos2* expression by macrophages *in vivo*

Given the high degree of co-localization of pEGFR and $CD68^+$ macrophages in both gastric and colonic tissues during infection and the fact that macrophages are known to be major drivers of *H. pylori*-induced inflammation[20], we next examined genes typically expressed by macrophages. Markers of M1 macrophage activation –*Nos2*, *Tnfa*, and *Il1b* – were all decreased in gastric tissues from *H. pylori*-infected $Egfr^{\Delta mye}$ versus $Egfr^{fl/fl}$ mice (Figure 11A). Markers of Mreg activation – *Il10*, *Tgfb*, and tumor necrosis factor (ligand) superfamily member 14 *(Tnfsf14*; *Light)* – were also decreased in infected $Egfr^{\Delta mye}$ gastric tissues (Figure 11B). Markers of M2 activation – *Arg1* and *Chil3* – were not significantly altered in $Egfr^{\Delta mye}$ mice (Appendix A, Figure 9). IL-1β protein was also significantly decreased in *H. pylori*-infected $Egfr^{\Delta mye}$ gastric tissues (Figure 11C), supporting the mRNA data indicating a role for myeloid EGFR in regulating the M1 response to *H. pylori*. Furthermore, Gmacs from infected $Egfr^{\Delta mye}$ mice expressed less *Nos2* mRNA (Figure 11D) and NOS2 protein (Figure 11E) compared to Gmacs from infected $Egfr^{fl/fl}$ mice. As there was no difference in macrophage infiltration (Appendix A, Figure 4E), these data indicate that the changes in NOS2 levels are specifically due to loss of EGFR rather than alterations in macrophage number.

In the *C. rodentium* model, only M1 markers were significantly induced by infection in colon tissues from $Egfr^{fl/fl}$ mice; as in *H. pylori* infection, expression levels of *Nos2* and *Tnfa* were significantly decreased in the $Egfr^{\Delta mye}$ mice, and *Il1b* showed a similar trend (Appendix A, Figure 10). Thus, macrophage EGFR signaling is an important mediator of pro-inflammatory and anti-inflammatory gene expression during gastrointestinal mucosal infection.

EGFR signaling is a key component in macrophage activation and function

Because limited numbers of Gmacs can be obtained for experimentation, we utilized BMmacs for further studies addressing the role of EGFR in macrophages. We also utilized bone marrow-derived dendritic cells (BMDCs) to assess the role of EGFR signaling in the dendritic cell population. Differentiation of macrophages and dendritic cells is demonstrated in Appendix A, Figure 11. WT

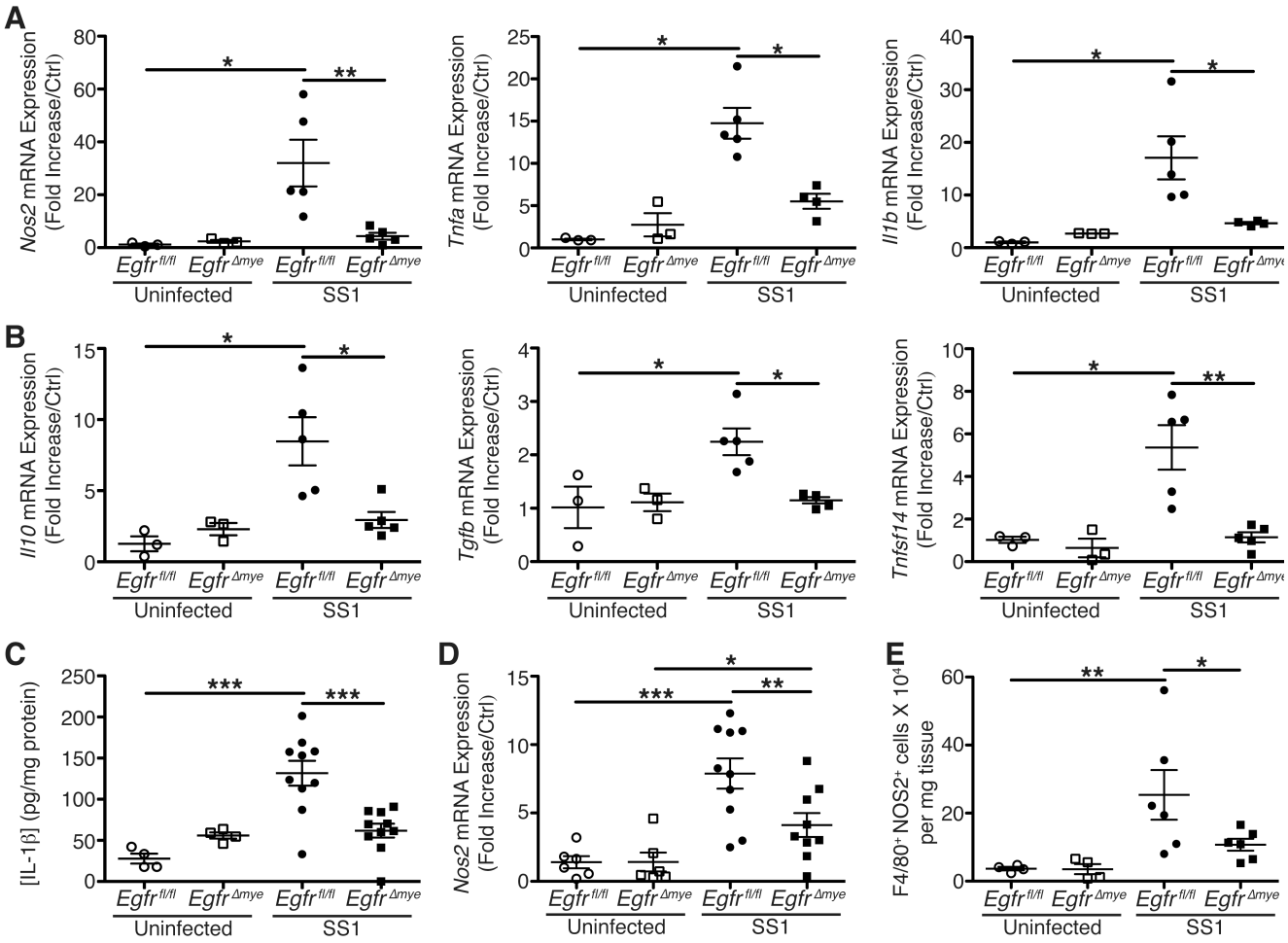

Figure 11. *Egfr*$^{\Delta mye}$ mice have significantly decreased M1 and Mreg cytokine production in gastric tissue and gastric macrophages. (A) mRNA levels of pro-inflammatory cytokines, *Nos2*, *Tnfa*, and *Il1b*, were assessed by RT-PCR from gastric tissue 4 mo p.i. with *H. pylori* SS1. **P* < 0.05. ***P* < 0.01. (B) mRNA levels of anti-inflammatory cytokines, *Il10*, *Tgfb*, and *Tnfsf14* (*Light*), were assessed by RT-PCR from gastric tissue 4 mo p.i. with *H. pylori* SS1. **P* < 0.05. ***P* < 0.01. Statistical significance in (A) and (B) calculated by one-way ANOVA with Kruskal-Wallis test, followed by Mann-Whitney *U* test. In (A) and (B), *n* = 3 uninfected and 5 infected mice per genotype. (C) Measurement of IL-1β by ELISA in gastric tissues 4 mo p.i. with *H. pylori* SS1. ****P* < 0.001. *n* = 4 uninfected and 10 infected mice per genotype. (D) F4/80$^+$ gastric macrophages (Gmacs) were magnetically selected from the lamina propria at 48 h p.i. with *H. pylori* SS1 and mRNA levels of *Nos2* were assessed by RT-PCR. ***P* < 0.01. *n* = 6 uninfected and 9-10 infected mice per genotype. Statistical significance in (C) and (D) was calculated by one-way ANOVA with Newman-Keuls post-test. (E) Protein levels of NOS2 were assessed in F4/80$^+$ Gmacs 48 h p.i. with *H. pylori* SS1. **P* < 0.05. *n* = 4 uninfected and 6 infected mice per genotype. Statistical significance calculated by one-way ANOVA with Kruskal-Wallis test, followed by Mann-Whitney *U* test.

BMmacs treated with gefitinib demonstrated significantly decreased M1 activation in response to *H. pylori*, as determined by decreased expression of *Nos2*, *Tnfa*, and *Il1b* (Figure 12A). BMmacs from $Egfr^{\Delta mye}$ mice also exhibited decreased expression of these M1 genes when compared to $Egfr^{fl/fl}$ BMmacs (Figure 12B). As in gastric tissues, Mreg activation with *H. pylori* infection, denoted by induction of *Il10* and *Tgfb*, was decreased in both WT BMmacs treated with gefitinib and in $Egfr^{\Delta mye}$ BMmacs (Appendix A, Figure 12A and 12B). M2 gene expression was not induced by *H. pylori* infection in BMmacs (Appendix A, Figure 12C and 12D). Similarly, M1 and Mreg markers induced by *C. rodentium* infection were decreased by inhibition of EGFR signaling (Appendix A, Figure 13A and 13B). These BMmac data corroborate our *in vivo* findings and indicate that EGFR is a key regulator of macrophage activation during bacterial infection.

To determine if EGFR has a global role in macrophage activation, we treated $Egfr^{fl/fl}$ and $Egfr^{\Delta mye}$ BMmacs with the prototypical stimuli for M1, M2, and Mreg activation and assessed activation by gene expression. Stimulation of BMmacs with IFN-γ and LPS induces an M1 response[3]. As with *H. pylori* or *C. rodentium* infection, an M1 stimulus induced significantly decreased expression of *Nos2*, *Il1b*, and *Tnfa* in $Egfr^{\Delta mye}$ BMmacs (Appendix A, Figure 14A). Neither *H. pylori* nor *C. rodentium* induce a significant M2 response (Appendix A, Figure 9; Appendix A, Figure 12D and C). However, $Egfr^{\Delta mye}$ BMmacs activated with IL-4, a classical M2 stimulus[3], demonstrated significantly diminished mRNA expression of M2 genes, *Arg1*, *Chil3*, and *Retnla* (*Relma*) when compared with $Egfr^{fl/fl}$ BMmacs (Appendix A, Figure 14B). Moreover, Mreg activation, as evidenced by *Il10* and *Tgfb* expression, was significantly diminished in $Egfr^{\Delta mye}$ BMmacs (Appendix A, Figure 14C). Thus, EGFR has the capacity to regulate all subsets of macrophage activation under various conditions. These data further demonstrate the central role that EGFR plays in regulating macrophage activation.

H. pylori-stimulated NOS2 protein levels were also diminished in RAW 264.7 cells treated with gefitinib or AG1478, a second inhibitor of the EGFR tyrosine kinase domain (Figure 12C), or in WT BMmacs treated with gefitinib (Figure 12D). Both RAW 264.7 cells treated with EGFR inhibitors (Figure 8E) or $Egfr^{\Delta mye}$ BMmacs (Figure 12F) produced decreased NO, an effector we have shown to have anti-microbial effects[47,114,115], in response to *H. pylori*. Thus, when RAW 264.7 cells were treated with

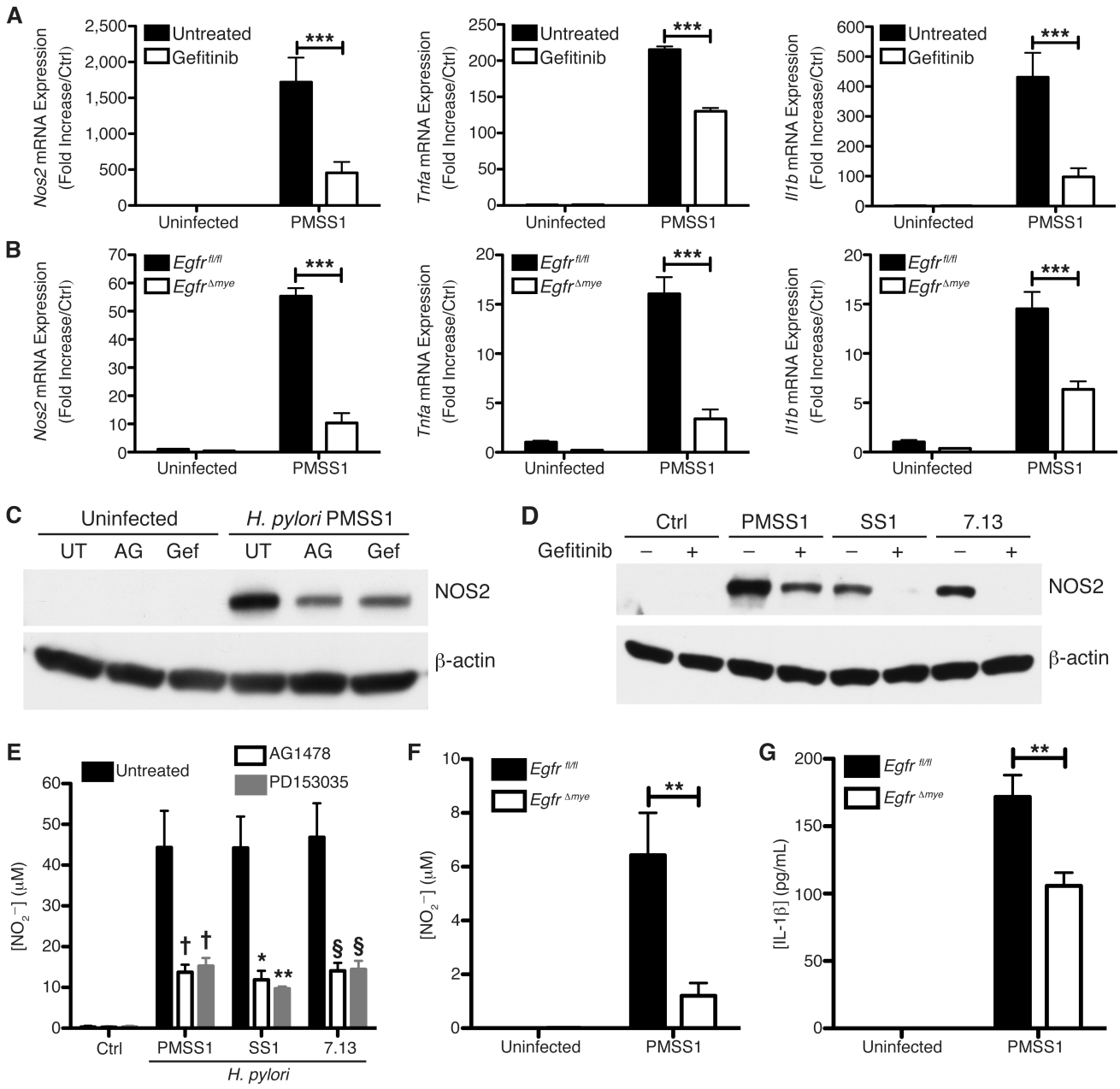

Figure 12. EGFR signaling is critical for macrophage activation and function. (A) mRNA levels of M1 activation markers, *Nos2*, *Tnfa*, and *Il1b*, were assessed by RT-PCR in WT BMmacs 24 p.i. with *H. pylori* PMSS1 ± 10 μM gefitinib. ***P < 0.001. n = 3 biological replicates. (B) mRNA levels of M1 activation markers *Nos2*, *Tnfa*, and *Il1b*, were assessed by RT-PCR in $Egfr^{fl/fl}$ and $Egfr^{\Delta mye}$ BMmacs 24 p.i. with *H. pylori* PMSS1. ***P < 0.001. n = 3 mice per genotype. (C) Representative western blot of NOS2 in RAW 264.7 cells 24 h p.i. with *H. pylori* PMSS1 ± 150 nM AG1478 (AG) or 10 μM gefitinib (Gef). UT = untreated. n = 3 biological replicates. (D) Representative western blot of NOS2 in WT BMmacs 24 h p.i. with *H. pylori* PMSS1, SS1 or 7.13 ± 10 μM gefitinib. n = 3 biological replicates. (E) Measurement of NO_2^- from RAW 264.7 cell supernatants 24 h p.i. with *H. pylori* PMSS1, SS1 or 7.13 ± 150 nM AG1478 or 300 nM PD153035. †P < 0.05 vs. PMSS1 only. *P < 0.05, **P < 0.01 vs. SS1 only. §P < 0.05 vs. 7.13 only. n = 5 biological replicates. (F) Measurement of NO_2^- from $Egfr^{fl/fl}$ and $Egfr^{\Delta mye}$ BMmac supernatants 24 h p.i. with *H. pylori* PMSS1. **P < 0.01. n = 3 mice per genotype. (G) Measurement of IL-1β in $Egfr^{fl/fl}$ and $Egfr^{\Delta mye}$ BMmacs supernatants 24 h p.i. with *H. pylori* PMSS1. **P < 0.01. n = 3 mice per genotype. Statistical significance in all panels was calculated by one-way ANOVA with Newman-Keuls post-test.

gefitinib there was significantly increased *H. pylori* survival when bacteria were separated from macrophages by a Transwell filter support, a model that prevents phagocytosis and allows for direct measurement of the ability of macrophages to kill extracellular *H. pylori* (Appendix A, Figure 15). These data are consistent with the increased bacterial survival in both the *H. pylori* and *C. rodentium* mouse models of infection with myeloid-specific deletion of *Egfr*. Moreover, *H. pylori*-stimulated IL-1β protein secretion was attenuated in $Egfr^{\Delta mye}$ versus $Egfr^{fl/fl}$ BMmacs (Figure 12G). There was no *H. pylori* strain specificity for inducing EGFR-mediated macrophage immune responses, as infection with multiple *H. pylori* strains resulted in similar findings.

Macrophages are also professional phagocytes. Therefore, we assessed the effect of EGFR signaling on macrophage phagocytosis of *H. pylori,* using a gentamicin protection assay[48] and siRNA to ensure effective loss of EGFR (Appendix A, Figure 16A). There was no difference in phagocytosis between *Egfr* knockdown cells and cells transfected with a non-targeting siRNA pool (Appendix A, Figure 16B). Additionally, there was no difference in phagocytosis between untreated and gefitinib-treated cells, confirming the findings with *Egfr* siRNA (Appendix A, Figure 16C). We verified that 200 μg/mL gentamicin effectively killed extracellular *H. pylori*, while 10 μM gefitinib and 0.1% saponin had no effect on *H. pylori* viability (Appendix A, Figure 16C). These findings confirmed the efficacy of this assay. Thus, EGFR signaling does not appear to play a role in bacterial phagocytosis.

EGFR is associated with resistance to apoptosis in epithelial cells[74], raising the possibility that the phenotypic effects observed in macrophages lacking EGFR are due to diminished cell survival. However, there was no difference in *H. pylori*-induced apoptosis in RAW 264.7 cells with *Egfr* knockdown (Appendix A, Figure 17A and 17B) or treated with gefitinib (Appendix A, Figure 17C). Additionally, neither WT BMmacs with our without gefitinib, nor $Egfr^{\Delta mye}$ versus $Egfr^{fl/fl}$ BMmacs had any differences in *H. pylori*-induced apoptosis (Appendix A, Figure 17D and 17E). Similarly, we detected no differences in Annexin-V/7AAD levels in $F4/80^{+}CD11b^{+}$ Gmacs from *H. pylori*-infected $Egfr^{fl/fl}$ and $Egfr^{\Delta mye}$ mice (Appendix A, Figure 17F). Importantly, there were no differences in the number of Gmacs between genotypes, further indicating that the cells are viable with or without EGFR (Appendix A, Figure 17G). Moreover, no differences in cleaved caspase 3 levels were detected in $CD68^{+}$ Gmacs in

tissues from *Egfr*$^{fl/fl}$ and *Egfr*$^{\Delta mye}$ mice 4 mo p.i., when assessed by immunofluorescence (Appendix A, Figure 17H). Taken together, these data indicate that EGFR does not regulate cell viability in macrophages and further confirm that the effects on macrophage phenotype of *Egfr* deletion are due solely to the loss of EGFR.

As our mouse model is a myeloid-specific knockout of EGFR, we also examined expression of dendritic cell cytokines under conditions where EGFR signaling is inhibited. WT BMDCs treated with gefitinib exhibited no differences in *H. pylori*-induced mRNA expression of relevant cytokines, *Tnfa*, *Il6*, *Il12b*, and *Il10* (Appendix A, Figure 18A). Similarly, *Egfr*$^{\Delta mye}$ BMDCs demonstrated no difference in *H. pylori*-stimulated expression of these same cytokines, when compared to *Egfr*$^{fl/fl}$ BMDCs (Appendix A, Figure 18B). Moreover, *Egfr*$^{\Delta mye}$ BMDCs expressed the same level of surface major histocompatibility complex II during *H. pylori* infection as the *Egfr*$^{fl/fl}$ BMDCs (Appendix A, Figure 18C, and 18D). Taken together, these data indicate that EGFR signaling does not regulate dendritic cell cytokine production or antigen presentation.

EGFR signaling and NF-κB signaling form an important link in macrophages that is necessary for cytokine production

To further address downstream effects of EGFR in macrophages, we examined the NF-κB signaling pathway, a key mediator of cytokine production and innate immune responses to pathogens. *H. pylori* infection leads to NF-κB signaling, directly resulting in the production of cytokines and chemokines[116,117]. Because we are studying bacterial pathogens, we examined the classical NF-κB signaling pathway that includes myeloid differentiation primary response 88 (MyD88), inhibitor of kappa light polypeptide gene enhancer in B cells, kinase (IKBK, IKK), and inhibitor of kappa light polypeptide gene enhancer in B cells, inhibitor a (NFKBIA, IκBα).

Based on our findings that *H. pylori*-induced phosphorylation of EGFR was present at 15 min p.i. and abundant at 30 min p.i., downstream NF-κB-related signaling was assessed beginning at the latter timepoint. *H. pylori*-infected *Egfr*$^{\Delta mye}$ BMmacs demonstrated decreased MyD88 protein levels 30 min p.i., as compared to *Egfr*$^{fl/fl}$ BMmacs (Figure 13A). A similar decrease was observed in WT

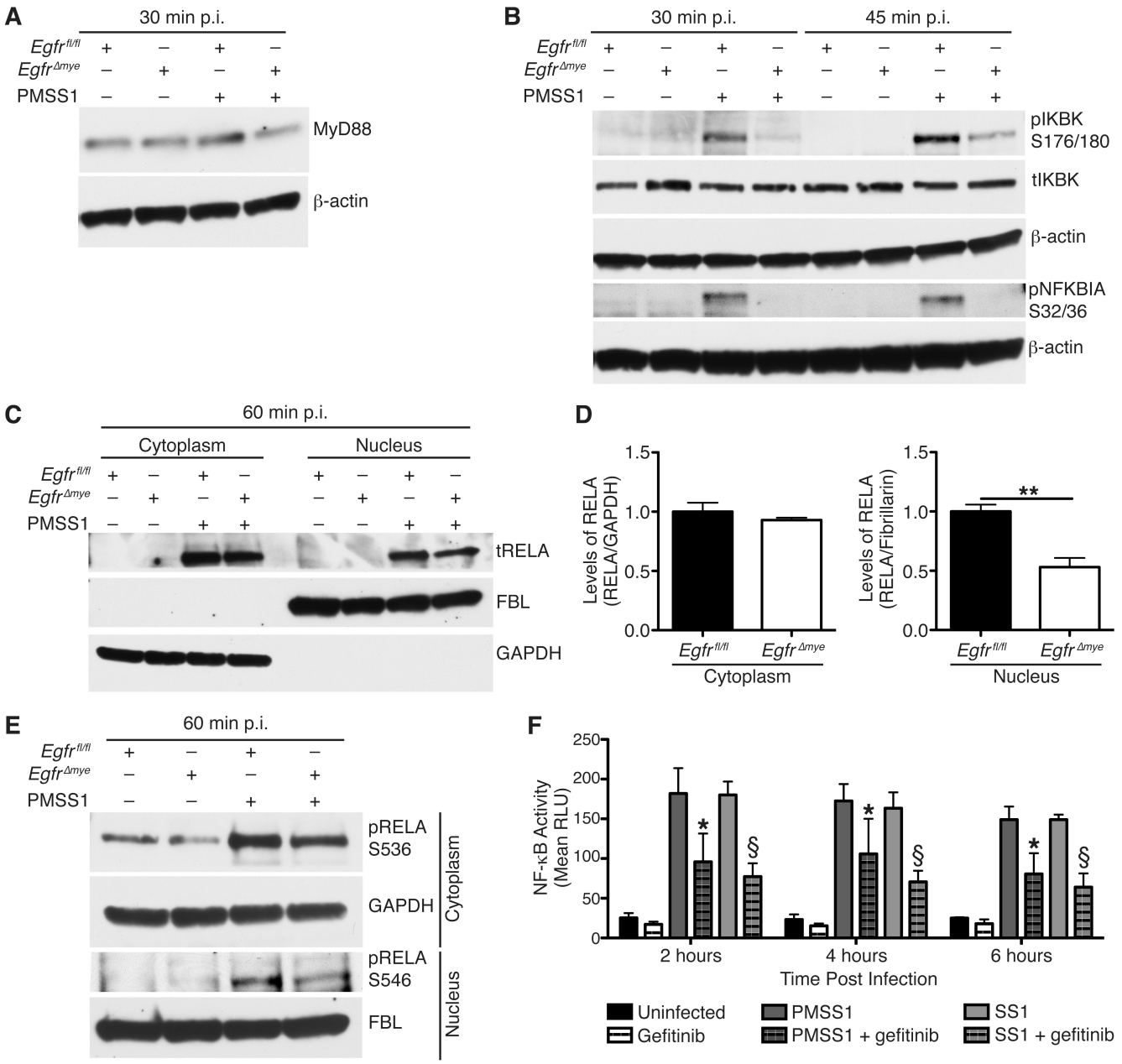

Figure 13. EGFR and NF-κB form a critical link in macrophages in response to *H. pylori*. (A) Representative western blot of MyD88 protein levels in *Egfr*$^{fl/fl}$ and *Egfr*$^{\Delta mye}$ BMmacs 30 min p.i. with *H. pylori* PMSS1. *n* = 3 biological replicates. (B) Representative western blots of pIKBK (pIKK) and pNFKBIA (pIkBa) protein levels in *Egfr*$^{fl/fl}$ and *Egfr*$^{\Delta mye}$ BMmacs 30 min and 45 min p.i. with *H. pylori* PMSS1. *n* = 3 biological replicates. (C) Representative western blot of cytoplasmic and nuclear fractions of tRELA (p65) in *Egfr*$^{fl/fl}$ and *Egfr*$^{\Delta mye}$ BMmacs 60 min p.i. with *H. pylori* PMSS1. *n* = 3 biological replicates. (D) Densitometric analysis of cytoplasmic and nuclear tRELA. *n* = 3 biological replicates. ***P* < 0.01. *n* = 3 biological replicates. Statistical significance was calculated by Student's *t* test. (E) Western blot of cytoplasmic and nuclear fractions of phospho-RELA (pp65) in *Egfr*$^{fl/fl}$ and *Egfr*$^{\Delta mye}$ BMmacs 60 min p.i. with *H. pylori* PMSS1. (F) Measurement of luminescence from NF-κB luciferase reporter in immortalized, bone marrow-derived macrophages (NGL cells), at indicated time points p.i. with *H. pylori* PMSS1 or SS1 ± 10 μM gefitinib. **P* < 0.05 vs. PMSS1 only. §*P* < 0.05 vs. SS1 only. *n* = 4 biological replicates. Statistical significance was calculated by one-way ANOVA with Newman-Keuls post-test.

BMmacs treated with gefitinib (Appendix A, Figure 19A). Moreover, *Egfr*$^{\Delta mye}$ BMmacs exhibited significantly decreased phospho-IKBK (pIKBK) and phospho-NFKBIA (pNFKBIA) levels at 30 and 45 min p.i., versus *Egfr*$^{fl/fl}$ BMmacs (Figure 13B). *H. pylori*-infected WT BMmacs treated with gefitinib also had decreased pIKBK and pNFKBIA, as compared to untreated BMmacs (Appendix A, Figure 19B and 19C).

Consistent with the MyD88, pIKBK, and pNFKBIA data, there was significantly less v-rel avian reticuloendotheliosis viral oncogene homolog A (RELA; p65) translocation to the nucleus 60 min after *H. pylori* infection in *Egfr*$^{\Delta mye}$ BMmacs (Figure 13C). Densitometric analysis confirmed the significant decrease in nuclear RELA levels, with no change in the cytoplasmic levels of RELA (Figure 13D). A similar reduction in nuclear translocation of RELA was observed in WT BMmacs treated with gefitinib (Appendix A, Figure 19D, 19E, and 19F). Nuclear levels of phospho-RELA were also decreased in *Egfr*$^{\Delta mye}$ BMmacs 60 min p.i., as compared to *Egfr*$^{fl/fl}$ BMmacs (Figure 13E). Moreover, BMmacs expressing an NF-κB luciferase reporter (NGL cells[118,119]) demonstrated decreased *H. pylori*-stimulated NF-κB activity when treated with gefitinib (Figure 13F). Taken together, these data indicate that pEGFR is a key enhancer of macrophage NF-κB signaling in response to *H. pylori* infection, potentiating production of inflammatory mediators, including cytokines and NO.

ERK signaling is also linked to EGFR signaling and contributes to macrophage activation

EGFR signaling is known to interact with many signaling pathways, including MAPK signaling[120,121]. Components of the MAPK signaling pathway include MAPK1 and MAPK3 (hereafter referred to as MAPK1/3)[120,121].We have previously demonstrated that MAPK1/3 signaling has a role in regulating macrophage function in response to *H. pylori*, and that *H. pylori* infection induces phosphorylation of MAPK1/3[97].

EGFR inhibition (Figure 14A) or deletion (Figure 14B) resulted in decreased phospho-MAPK1/3 (pMAPK1/3) levels in BMmacs stimulated with *H. pylori* (Figure 14A and 14B). These data suggest that EGFR activation is upstream of MAPK1/3, and that MAPK1/3 signaling is closely linked to EGFR signaling. To determine the role of MAPK1/3 signaling in macrophage activation, we utilized the

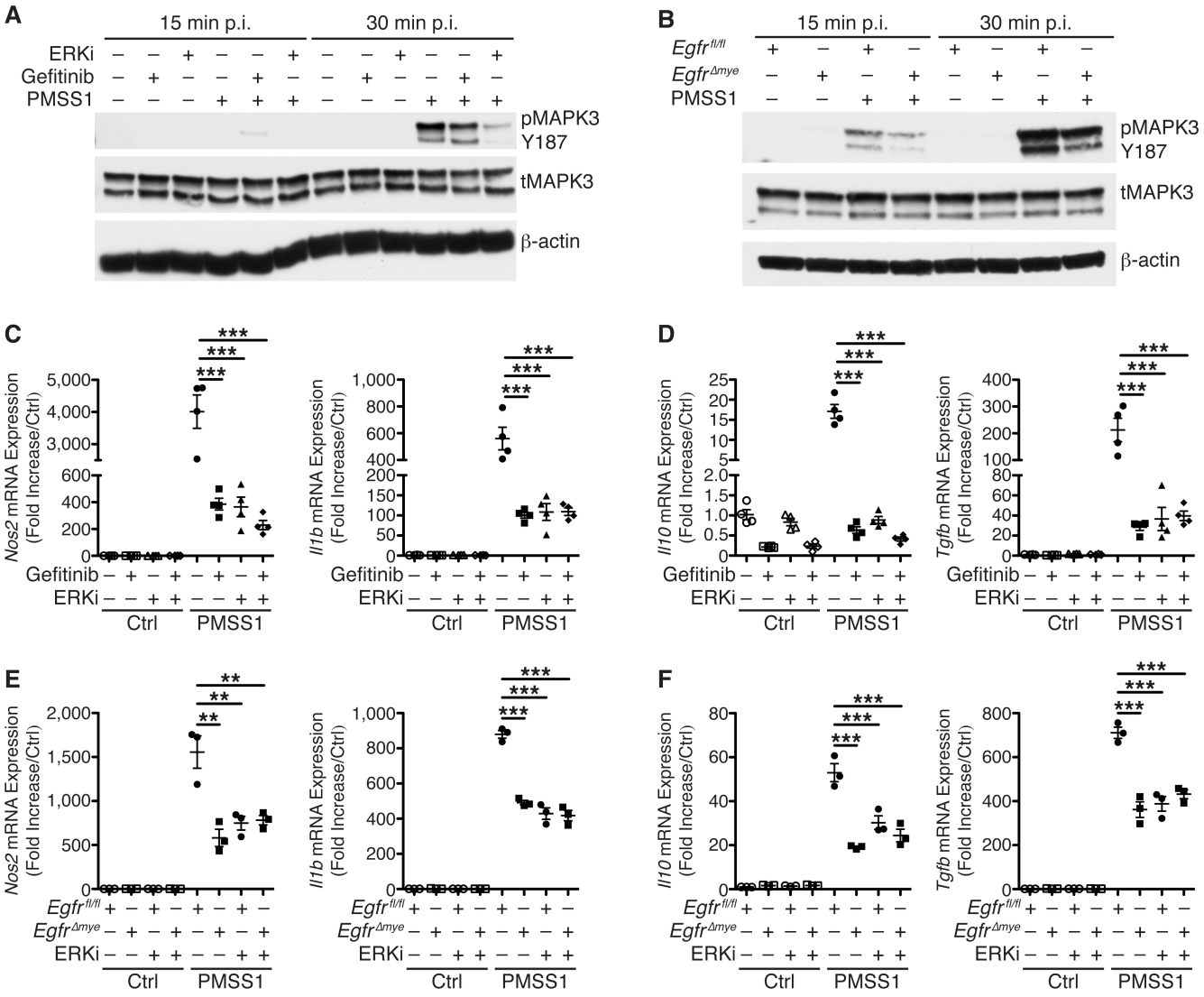

Figure 14. EGFR signaling and MAPK1/3 signaling are linked in regulating macrophage activation in response to *H. pylori*. (A) Representative western blot of pMAPK1/3 levels in WT BMmacs ± 10 μM gefitinib or ± 50 μM ERKi at 15 and 30 min p.i. with *H. pylori* PMSS1. *n* = 3 biological replicates. (B) Representative western blot of pMAPK1/3 levels in $Egfr^{fl/fl}$ and $Egfr^{\Delta mye}$ BMmacs at 15 and 30 min p.i. with *H. pylori* PMSS1. *n* = 3 biological replicates. (C) mRNA levels of M1 activation markers *Nos2* and *Il1b*, were assessed by RT-PCR in WT BMmacs ± 10 μM gefitinib and/or ± 50 μM ERKi 24 p.i. with *H. pylori* PMSS1. ***$P < 0.001$. *n* = 5 mice. (D) mRNA levels of Mreg activation markers *Il10* and *Tgfb*, were assessed by RT-PCR in WT BMmacs ± 10 μM gefitinib and/or ± 50 μM ERKi 24 p.i. with *H. pylori* PMSS1. ***$P < 0.001$. *n* = 5 mice. (E) mRNA levels of M1 activation markers *Nos2* and *Il1b*, were assessed by RT-PCR in $Egfr^{fl/fl}$ and $Egfr^{\Delta mye}$ BMmacs ± 50 μM ERKi 24 p.i. with *H. pylori* PMSS1. **$P < 0.01$, ***$P < 0.001$. *n* = 3 mice per genotype. (F) mRNA levels of Mreg activation markers *Il10* and *Tgfb*, were assessed by RT-PCR in $Egfr^{fl/fl}$ and $Egfr^{\Delta mye}$ BMmacs ± 50 μM ERKi 24 p.i. with *H. pylori* PMSS1. ***$P < 0.001$. *n* = 3 mice per genotype. Statistical significance in (C)-(F) was calculated by one-way ANOVA with Newman-Keuls post-test.

MAPK1/3 inhibitor, ERKi, to prevent MAPK1/3 phosphorylation (Figure 14A). WT BMmacs were treated with gefitinib, ERKi, or both inhibitors in combination prior to infection with *H. pylori*. Gefitinib and ERKi each led to markedly decreased *Nos2* and *Il1b* expression, markers of M1 activation (Figure 14C), and decreased *Il10* and *Tgfb* expression, markers of Mreg activation (Figure 14D). Notably, the combination of gefitinib and ERKi did not further decrease M1 and Mreg gene expression (Figure 14C and 14D). Together, these data suggest that EGFR and MAPK1/3 are in the same pathway, and that EGFR is upstream of MAPK1/3.

Consistent with the data obtained using gefitinib and ERKi, *H. pylori*-infected $Egfr^{fl/fl}$ BMmacs treated with ERKi demonstrated a similar level of reduction of *Nos2*, *Il1b*, *Il10*, and *Tgfb* mRNA expression as the $Egfr^{\Delta mye}$ BMmacs not treated with ERKi (Figure 14E and 14F). As with the combination of gefitinib and ERKi, $Egfr^{\Delta mye}$ BMmacs treated with ERKi did not have any further decrease in M1 and Mreg gene expression (Figure 14E and 14F). These data further support the concept that EGFR and MAPK1/3 are in the same pathway(s), and exert potent effects on macrophage activation in response to *H. pylori* infection.

Macrophage EGFR is necessary for regulating both Th17 and Treg T cell responses during *H. pylori* infection

As macrophages are antigen-presenting cells and play a role in initiating the adaptive immune response during *H. pylori* infection, we sought to determine the nature of the interaction between $Egfr^{\Delta mye}$ macrophages and T cells. Because we detected attenuated chronic inflammation at 4 mo p.i. in $Egfr^{\Delta mye}$ mice, wefocused on this timepoint for detailedanalysis of the adaptive immune response. We utilized two sources of T cells for these studies – magnetically selected $CD4^+$ T cells from the lamina propria of the mouse stomach that were then analyzed by real-time (RT)-PCR and T cells from the perigastric lymph nodes (GLN) that were assayed by flow cytometry.

The Th1 response was detectable, but it was not particularly robust, and there were no significant differences in *Ifng* expression in gastric tissues from infected $Egfr^{fl/fl}$, $Egfr^{\Delta mye}$, and $LysM^{cre/cre}$ mice (Appendix A, Figure 20A). There was a modest, but not statistically significant induction of the

$CD4^+IFN\text{-}\gamma^+$ population in the GLNs from infected $Egfr^{fl/fl}$ mice (Appendix A, Figure 20B). However, the $CD4^+IFN\text{-}\gamma^+$ population was significantly decreased in $Egfr^{\Delta mye}$ GLNs (Appendix A, Figure 20B). The lamina propria T cells exhibited a significant increase in both T box 21 (*Tbx21*, *Tbet*), a transcription factor regulating Th1 differentiation, and *Ifng* expression in $Egfr^{fl/fl}$ mice, but only *Tbx21* expression was significantly decreased in $Egfr^{\Delta mye}$ mice (Appendix A, Figure 20C).

Th17 responses were more robust and more dependent upon macrophage EGFR signaling at 4 mo p.i. *Il17a* mRNA levels were significantly increased in infected $Egfr^{fl/fl}$ and $LysM^{cre/cre}$ gastric tissues, and decreased in infected $Egfr^{\Delta mye}$ gastric tissues (Figure 15A). Similarly, IL-17 protein levels were increased in infected $Egfr^{fl/fl}$ gastric tissues, and significantly decreased in $Egfr^{\Delta mye}$ tissues (Figure 15B). Consistent with these data, the $CD4^+IL\text{-}17^+$ population in the $Egfr^{fl/fl}$ GLNs was significantly increased with infection, and the $CD4^+IL\text{-}17^+$ population in the $Egfr^{\Delta mye}$ GLNs was significantly decreased (Figure 15C). Both RAR-related orphan receptor C (*Rorc*, *Rorγt*), encoding for a transcription factor that mediates Th17 differentiation, and *Il17a* mRNA levels were very highly induced in $CD4^+$ T cells from the lamina propria of $Egfr^{fl/fl}$ mice (Figure 15D). Notably, $Egfr^{\Delta mye}$ mice had significantly less *Rorc* and *Il17a* expression in $CD4^+$ T cells from the lamina propria (Figure 15D).

IL-23, composed of IL-12p19 (IL-23A) and IL-12p40 (IL-12B), and TGF-β are necessary for Th17 differentiation[122]. IL-12B protein (Appendix A, Table 1) and *Tgfb* mRNA levels (Figure 11B) were significantly decreased in $Egfr^{\Delta mye}$ gastric tissue. Moreover, macrophage-derived *Il23a* (Appendix A, Figure 21) and *Tgfb* (Appendix A, Figure 12B) mRNA levels were significantly reduced in $Egfr^{\Delta mye}$ BMmacs. Taken together, these data indicate a diminished potential for Th17 differentiation. These data also indicate that EGFR signaling in macrophages is important for the Th17 response to *H. pylori* infection. The decreased Th17 response in $Egfr^{\Delta mye}$ mice likely contributes to the decreased histologic gastritis.

In contrast to the diminished Th17 response in $Egfr^{\Delta mye}$ mice, the Treg response was significantly increased. mRNA expression of forkhead box P3 (*Foxp3*), a transcription factor specific to Tregs, was not induced in infected $Egfr^{fl/fl}$ gastric tissues, but was significantly upregulated in $Egfr^{\Delta mye}$ tissues (Figure 16A). Similarly, the $CD4^+CD25^+FOXP3^+$ population in the $Egfr^{\Delta mye}$ GLNs was

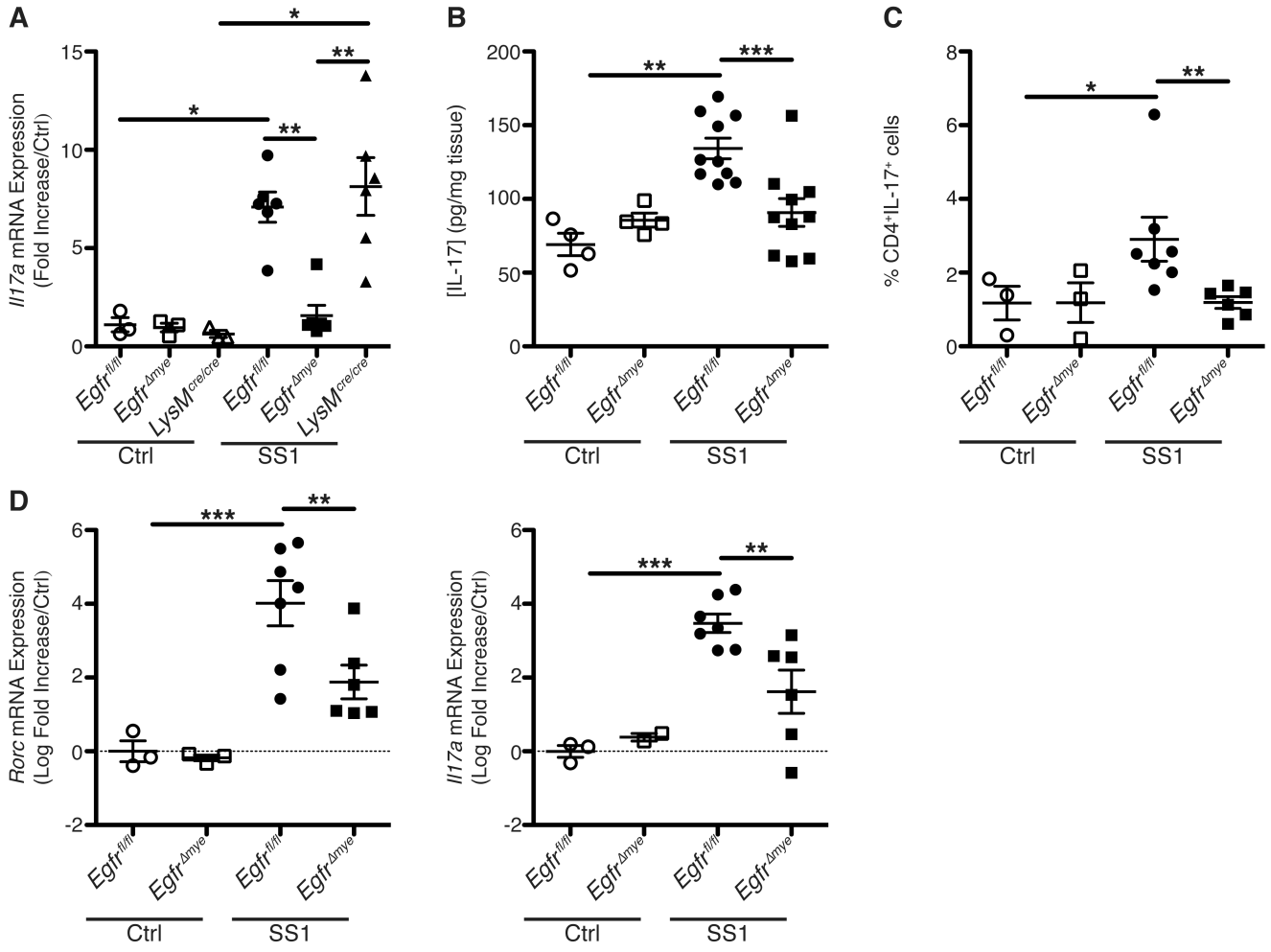

Figure 15. EGFR deficiency in macrophages leads to a diminished Th17 response to *H. pylori*. (A) mRNA levels of *Il17a* were assessed by RT-PCR in gastric tissues from *Egfr*$^{fl/fl}$, *Egfr*$^{\Delta mye}$, *and LysM*$^{cre/cre}$ mice 4 mo p.i. with *H. pylori* SS1. **P* < 0.05, ***P* < 0.01. *n* = 3 uninfected and 6 infected mice per genotype. (B) IL-17 protein levels were assessed by ELISA in gastric tissues from *Egfr*$^{fl/fl}$ and *Egfr*$^{\Delta mye}$ mice 4 mo p.i. with *H. pylori* SS1. ***P* < 0.01, ****P* < 0.001. *n* = 4 uninfected and 10 infected mice per genotype. (C) Assessment of CD4$^+$IL-17$^+$ T cells from perigastric lymph nodes (GLN) of *Egfr*$^{fl/fl}$ and *Egfr*$^{\Delta mye}$ mice 4 mo p.i. with *H. pylori* SS1 by flow cytometry. Isolated T cells were cultured in 96-well plates containing 5 μg/mL anti-CD3 and 1 μg/mL anti-CD28. Cells were then stimulated with 20 ng/mL PMA and 1 μg/mL ionomycin for 4 h. **P* < 0.05, ***P* < 0.01. *n* = 3 uninfected and 7 infected mice per genotype. (D) mRNA levels of Th17 markers, *Rorc* (*Rorγt*) and *Il17a,* were assessed by RT-PCR from magnetically selected CD4$^+$ T cells from the gastric lamina propria of *Egfr*$^{fl/fl}$ and *Egfr*$^{\Delta mye}$ mice 4 mo p.i. with *H. pylori* SS1. ***P* < 0.01, ****P* < 0.001. *n* = 3 uninfected and 6-7 infected mice per genotype. Statistical significance in all panels was calculated by one-way ANOVA with Newman-Keuls post-test.

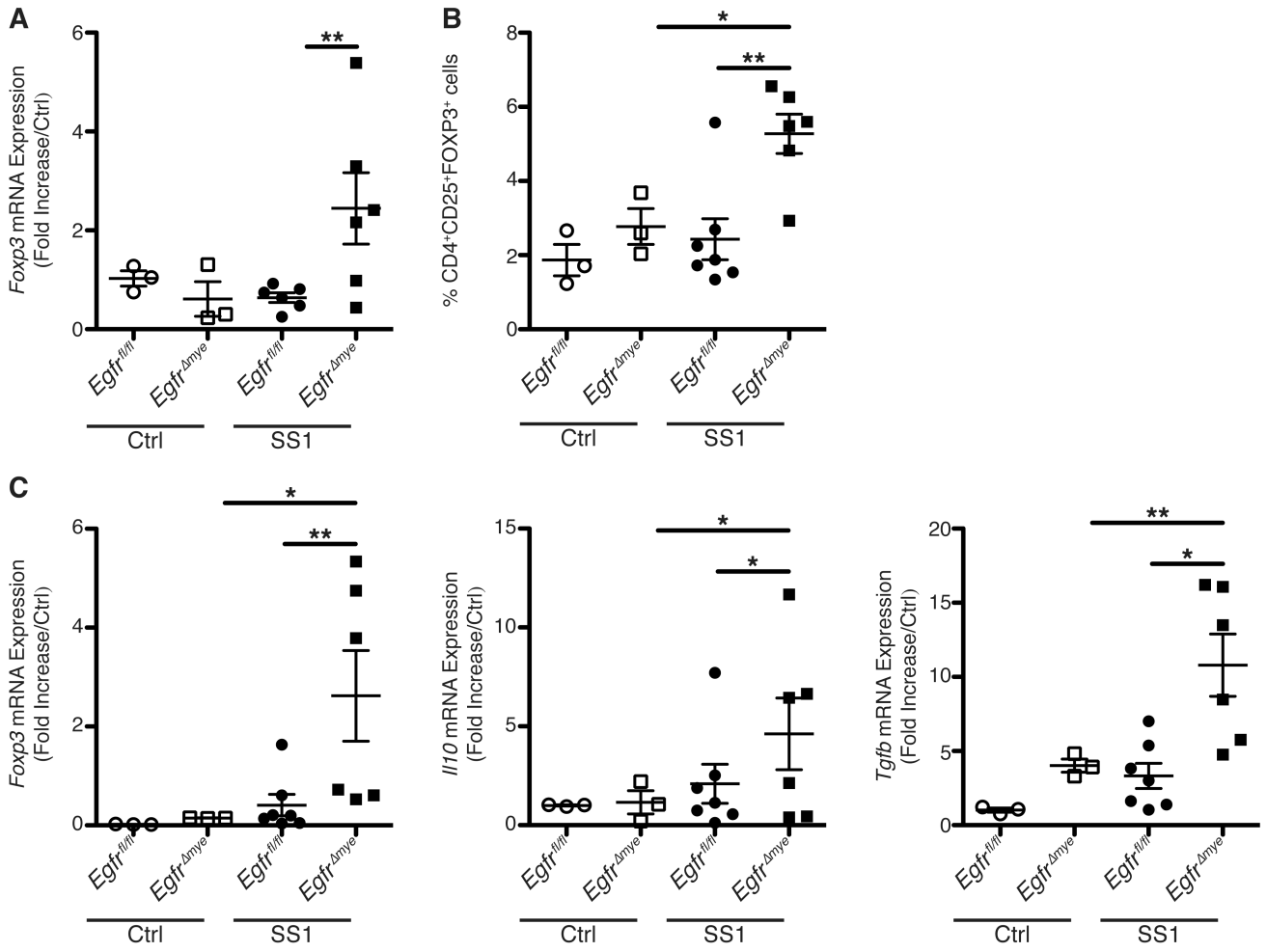

Figure 16. EGFR deficiency in macrophages leads to an enhanced Treg response during *H. pylori* infection. (A) mRNA levels of *Foxp3* were assessed by RT-PCR in gastric tissues from $Egfr^{fl/fl}$ and $Egfr^{\Delta mye}$ mice 4 mo p.i. with *H. pylori* SS1. $^{**}P < 0.01$. $n = 3$ uninfected and 6 infected mice per genotype. (B) Assessment of $CD4^+CD25^+FOXP3^+$ T cells from perigastric lymph nodes (GLN) of $Egfr^{fl/fl}$ and $Egfr^{\Delta mye}$ mice 4 mo p.i. with *H. pylori* SS1 by flow cytometry. Isolated T cells were not cultured or stimulated as in Figure 9C. $^{*}P < 0.05$, $^{**}P < 0.01$. $n = 3$ uninfected and 6-7 infected mice per genotype. (C) mRNA levels of Treg markers, *Foxp3, Il10,* and *Tgfb,* were assessed by RT-PCR from magnetically selected $CD4^+$ T cells from the gastric lamina propria of $Egfr^{fl/fl}$ and $Egfr^{\Delta mye}$ mice 4 mo p.i. with *H. pylori* SS1. $^{*}P < 0.05$, $^{**}P < 0.01$. $n = 3$ uninfected and 6-7 infected mice per genotype. Statistical significance in all panels was calculated by one-way ANOVA with Newman-Keuls post-test.

significantly larger than in *Egfr*$^{fl/fl}$ GLNs (Figure 16B). Significantly enhanced *Foxp3*, *Il10*, and *Tgfb* expression in CD4^{+} T cells from the lamina propria of *Egfr*$^{\Delta mye}$ mice further confirmed the enhancement of the Treg population during infection (Figure 16C). These data implicate a potential role for macrophage EGFR signaling in the Treg response during *H. pylori* infection.

We also assessed the role of macrophage EGFR in the initiation of the adaptive immune response to *H. pylori*. We examined the Th1, Th17, and Treg populations at 2 mo p.i. (Appendix A, Figure 22). In contrast to the 4 mo p.i. timepoint, there was no increase in Th1, Th17, or Treg populations with *H. pylori* infection in the *Egfr*$^{fl/fl}$ or *Egfr*$^{\Delta mye}$ GLNs when assessed by flow cytometry (Appendix A, Figure 22A, 22C, and 22E). There were, however, modest increases in the expression of the Th1- and Th17-related genes in the infected *Egfr*$^{fl/fl}$ mice that were decreased in the *Egfr*$^{\Delta mye}$ mice (Appendix A, Figure 22B and 22D). Together, these data suggest that the gastric T cell response is still developing at the 2 mo p.i. timepoint, and that the macrophage-T cell interaction is best assessed at 4 mo p.i. in the *H. pylori* model.

2.3 Discussion

EGFR regulates many epithelial cell functions, in addition to playing a pro-carcinogenic role in many cancers, including gastric cancer[59,69,74-76]. While EGFR signaling in macrophages has been demonstrated within the context of inflammation and cancer[82,83], our work reveals the central role that EGFR has in regulating macrophage activation and function in response to bacterial pathogens (Figure 17). Gastric carcinogenesis derives from deleterious, *H. pylori*-induced chronic inflammation that is substantially driven by macrophages[9,20,41,48,103,123]. We now show that EGFR signaling in macrophages has a causal role in gastric inflammation and is associated with *H. pylori*-induced gastric carcinogenesis. Specifically, human gastric macrophages have abundant levels of pEGFR, in the setting of both gastritis and intestinal metaplasia, and this continues in gastric carcinoma. As such, macrophage EGFR is a potential therapeutic target for this and other inflammation-mediated diseases and cancers.

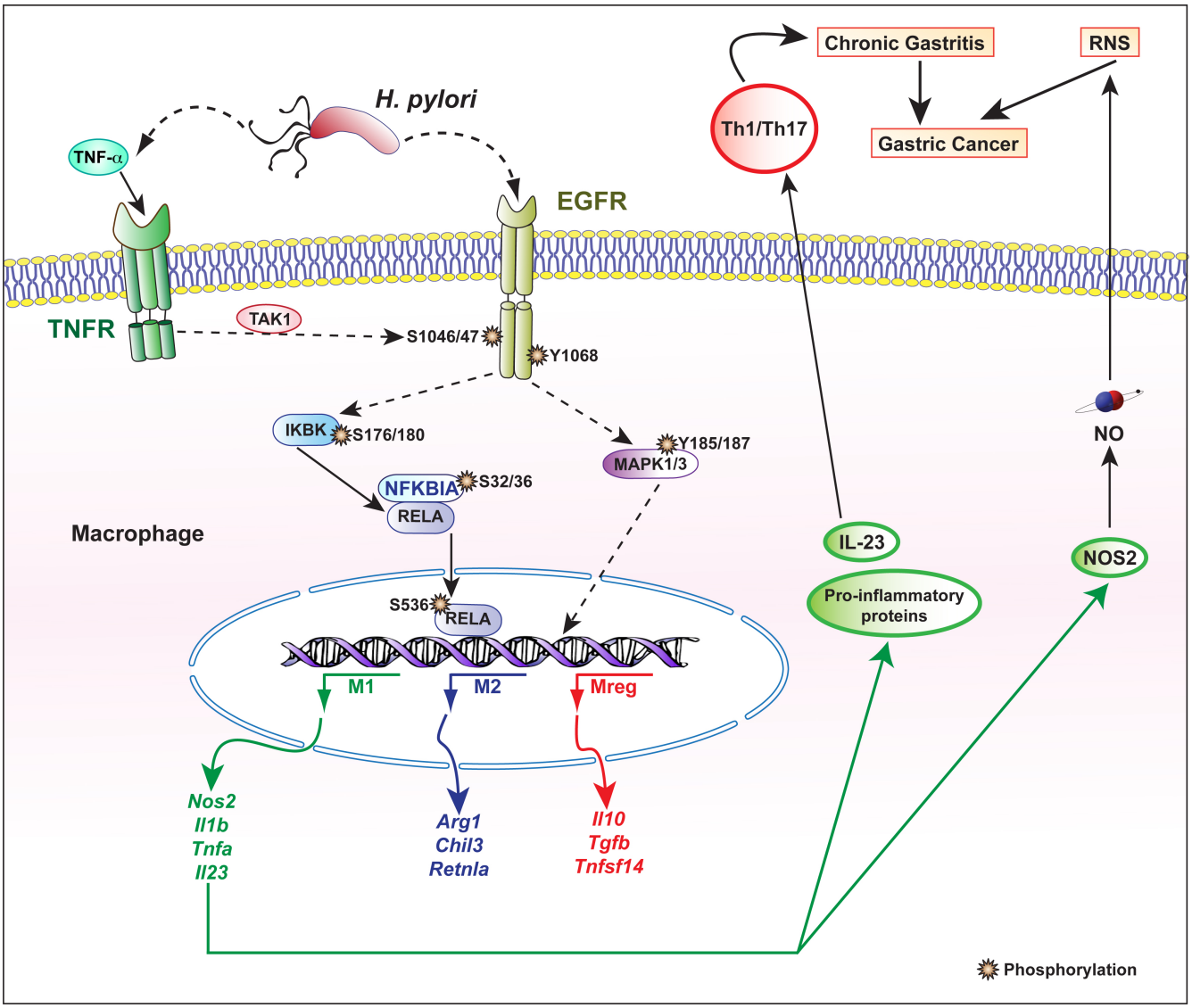

Figure 17. Summary of findings related to EGFR signaling in macrophages during *H. pylori* infection. EGFR signaling is activated by either an unknown ligand-dependent stimulus at tyrosine (Y) 1068 or by a ligand-independent mechanism at serine (S) 1046/47. TNF-α binds to TNF receptor (TNFR), leading to EGFR phosphorylation at S1046/47 via transforming growth factor beta-activated kinase 1 (TAK1). Once activated, EGFR signaling leads to NF-κB signaling by phosphorylation of IKBK (IKK), which phosphorylates NFKBKIA (IκBα) in order to release phosphorylated RELA (p65) for nuclear translocation. EGFR signaling also leads to phosphorylation of MAPK1/3 (ERK1/2). These signaling events lead to M1, M2, and Mreg gene expression. M1 activation, specifically, leads to the production of NOS2 and NO, causing reactive nitrogen species (RNS)-mediated DNA damage. Moreover, M1 activation leads to IL-23 production, along with other pro-inflammatory proteins, initiating a Th1/Th17 response. This leads to chronic gastritis, which when combined with RNS-mediated DNA damage, contributes to gastric carcinogenesis.

Myeloid-specific deletion of EGFR in mice significantly attenuated gastritis, with a commensurate increase in *H. pylori* burden. This decrease in gastric damage was marked by significantly decreased pro-inflammatory cytokine and chemokine levels. Similarly, the diminished clinical severity of infectious colitis in *Egfr*$^{\Delta mye}$ mice, despite increased *C. rodentium* burden, further implicates the importance of EGFR signaling in macrophages in the deleterious inflammatory response to bacterial infections. This concept was also supported by the decreased pro-inflammatory cytokine expression in colon tissues from infected *Egfr*$^{\Delta mye}$ mice.

Either inhibition of signaling or genetic knockout of EGFR led to decreased M1 and Mreg activation during bacterial infection *in vitro* and *in vivo*. Canonical stimuli for M1, M2, and Mreg activation also resulted in decreased gene expression of subset specific markers. Macrophage activation is critical for defining function, and our studies have established that EGFR assumes a central role in regulating this key step in macrophage biology. Importantly, we have utilized the term "activation," instead of "polarization", because this study is focused on gene expression patterns related specifically to macrophage activation. It should be noted, however, that we have assessed expression of *Arg2* and *Odc*, which encode for important enzymes involved in polyamine biosynthesis that we have previously shown to be upregulated in *H. pylori*-infected macrophages[95,103]. In BMmacs with either chemical inhibition or knockout of EGFR, there was no affect on *H. pylori*-induced expression of *Arg2* or *Odc* (data not shown), suggesting that EGFR signaling does not have global effects on all macrophage genes induced by *H. pylori*.

As M1 activation is responsible for pro-inflammatory, anti-microbial responses to bacterial pathogens, loss of M1 activation in *Egfr*$^{\Delta mye}$ mice is likely driving the decreased disease severity and increased bacterial load in the models utilized herein. Additionally, EGFR signaling in macrophages has marked effects on adaptive immunity, as it was required for Th17 responses, which have been implicated in clearance of *H. pylori*[124] and *C. rodentium*[125] infection.

The link between EGFR and NF-κB provides a mechanism for the decreased cytokine production by macrophages. Inhibition or deletion of EGFR led to significantly decreased NF-κB pathway signaling, including the upstream components MyD88, pIKBK, and pNFKBIA, as well as RELA

nuclear translocation and NF-κB activity. It should be noted that it has been reported that MyD88$^{-/-}$ mice exhibit attenuated gastritis and increased bacterial burden with *H. pylori* infection[126], consistent with our data herein with myeloid-specific deletion of *Egfr*. Thus MyD88 may provide a link between EGFR signaling and NF-κB in macrophages.

We have also implicated MAPK1/3 signaling as an additional target of EGFR signaling, which appears to be important in modulating macrophage activation in response to *H. pylori*. Since many potential pathways may be influenced by EGFR signaling, determining additional downstream targets of EGFR activation in macrophages is currently being investigated in our laboratory through proteomic approaches. These studies will enhance our understanding of mechanisms controlling macrophage responses.

Furthermore, phosphorylation of EGFR was detectable at S1046/47, as well as the canonical Y1068, indicating that initiation of EGFR signaling in macrophages can be ligand-independent[66,108]. We have implicated a potential role for TNF-α in such a ligand-independent mechanism. Future studies to determine the mechanism by which EGFR signaling is initiated in macrophages in response to bacterial infections are warranted. These studies could provide useful targets for therapeutic intervention in preventing EGFR activation in macrophages during chronic inflammation.

In sum, our work outlines a new role for EGFR signaling in regulating the macrophage-mediated host responses to bacterial infections. We have implicated EGFR as a central element in macrophage activation, with broad effects on immunopathogenesis (Figure 17). In the particular case of *H. pylori* infection, specific inhibition of pathways that activate macrophage EGFR signaling could prove a useful chemopreventive strategy in high risk subjects, since antibiotic treatment of *H. pylori* once precancerous lesions of atrophic gastritis and intestinal metaplasia have occurred does not reduce gastric cancer risk[39,127]. Further, this work provides an impetus for further studies regarding the role of EGFR in macrophages, especially as it relates to the treatment and prevention of other inflammatory diseases and associated carcinogenesis.

2.4 Materials and Methods

Reagents

All reagents used for cell culture are from Invitrogen (Carlsbad, CA, USA). Reagents for RNA extraction are from Qiagen (Valencia, CA, USA) Reagents for cDNA synthesis and quantitative real-time PCR were purchased from Bio-Rad (Hercules, CA, USA). Gefitinib (N-(3-Chloro-4-fluorophenyl)-7-methoxy-6-(3-morpholinopropoxy)quinazolin-4-amine) was obtained from Selleck Chemicals (Houston, TX, USA). AG1478 (N-(3-chlorophenyl)-6,7-dimethoxyquinazolin-4-amine) was obtained from Cayman Chemical (Ann Arbor, MI, USA). PD153035 (N-(3-bromophenyl)-6,7-dimethoxyquinazoline) was obtained from EMD Millipore (Billerica, MA, USA). The following compounds were obtained from EMD Millipore (Billerica, MA, USA): PD153035 (N-(3-bromophenyl)-6,7-dimethoxyquinazoline), and ERKi (3-(2-Aminoethyl)-5-((4-Ethoxyphenyl)Methylene)-2,4-Thiazolidinedione, HCl). Cytocholasin D, an inhibitor of actin polymerization was obtained from EMD Millipore (Billerica, MA, USA). ON-TARGET*plus* siRNA against *Egfr*, and scrambled targets were purchased from Dharmacon (Lafayette, CO, USA).

Antibodies

See Appendix A, Table 3 for information regarding all antibodies utilized for this study.

Bacteria, Cells, Culture Conditions and Infections

H. pylori PMSS1, SS1, and 7.13 were grown and used as previously described[47,96,103]. *C. rodentium* was cultured as previously described[106].

The murine macrophage cell line, RAW 264.7, was maintained in complete Dulbecco's modified Eagle's medium (DMEM), supplemented with 10% fetal bovine serum (FBS), 2 mM L-glutamine, 100 U/mL penicillin, 100 μg/mL streptomycin, 50 μg/mL gentamicin, 25 mM HEPES, and 10 mM sodium pyruvate. The human monocytic cell line, THP-1, was maintained in complete DMEM, supplemented with 10% FBS, 2 mM L-glutamine, 100 U/mL penicillin, 100 μg/mL streptomycin, and 50 μg/mL

gentamicin. THP-1 cells were differentiated into adherent macrophages with 10 ng/mL phorbol-12-myristate-13-acetate (PMA) for 24 hours. Cells were then washed and incubated in complete DMEM without PMA for 24 h prior to experimentation. RAW 264.7 cells and THP-1 cells were acquired from American Type Culture Collection (ATCC; Manassas, VA, USA). ATCC authenticates all cell lines before distribution. ATCC also tests for and confirms that all cell lines are free of Mycoplasma contamination. The murine, immortalized bone-marrow derived macrophage, NF-κB luciferase reporter cell line, NGL, were provided by Timothy Blackwell (Vanderbilt University Medical Center; Nashville, TN)[118,119], and were maintained in complete DMEM, supplemented with 10% FBS, 2 mM L-glutamine, 100 U/mL penicillin, 100 μg/mL streptomycin, and 50 μg/mL gentamicin. None of the cell lines utilized in this study are found in the database of commonly misidentified cell lines maintained by International Cell Line Authentication Committee.

BMmacs were isolated from all mouse genotypes utilized in this paper as previously described[128], with the following exceptions. Red blood cells were lysed with ammonium-chloride-potassium lysing buffer for 4 min prior to plating bone marrow cells. Recombinant macrophage colony stimulating factor (M-CSF) was used at a concentration of 20 ng/mL for seven days. Bone marrow-derived dendritic cells were isolated from all mouse genotypes as previously described[129]. Recombinant granulocyte-monocyte colony stimulating factor was used at a concentration of 40 ng/mL for nine days. M-CSF and granulocyte-macrophage colony stimulating factor (GM-CSF) were purchased from PeproTech (Rocky Hill, NJ, USA).

All cells were incubated in serum-free media for 14–16 h prior to infection for assays measuring pEGFR. All pharmacological inhibitors were added 1 h before infection. Cells were infected at a multiplicity of infection (MOI) of 100 for *H. pylori* experiments. Cells were infected at an MOI of 10 for all experiments with *C. rodentium*. Media without antibiotics were used for all experiments with live bacteria.

Animal Studies

Egfr$^{\Delta mye}$ and *Egfr*$^{fl/fl}$ x Villin$^{cre/+}$ were provided by Fang Yan (Vanderbilt University Medical Center; Nashville, TN). *Egfr*$^{fl/fl}$ mice were generated by backcrossing *Egfr*$^{fl/fl}$; Villin$^{cre/+}$ mice to WT mice to remove the *cre* allele. *LysM*$^{cre/cre}$ mice were purchased from Jackson Laboratories (Bar Harbor, ME). Excision of the *Egfr* alleles was confirmed by PCR (See Appendix A, Table 2 for primer information). Male mice between the ages of six to twelve weeks were exclusively utilized for these studies, regardless of genotype and mice were not removed from the cages into which they were weaned. Male mice were selected for this study because female mice have been shown to be protected from gastric damage in experimental *H. pylori* infection[130]. Sample sizes were based on previous studies from our laboratory[47,48,103] and mice were randomly selected for control and experimental groups, provided they met the sex and age requirements. Mice were infected orogastrically with 5 x 10^8 colony forming units (CFUs) with *H. pylori* SS1 or PMSS1. Inoculations occurred once for Gmac studies and three times, every other day, for all other *H. pylori* studies. Animals were sacrificed 48 h p.i. for Gmacs and 1 mo, 2 mo, or 4 mo p.i. for all other *H. pylori* studies. Colonization was assessed by serial dilution and culture. Histology was assessed in a completely blinded manner by a gastrointestinal pathologist, M. Blanca Piazuelo, using the updated Sydney System[48].

For the colitis studies, the same sex and age requirements utilized for *H. pylori* experiments were applied to the mice. Moreover, samples sizes were based on previous studies in our laboratory[106,113,131]. Mice were infected orogastrically with 5 x 10^8 CFUs once for all studies with *C. rodentium*. Animals were weighed daily and sacrificed 14 days post-infection. Colonization was assessed by serial dilution and culture. Histology was assessed in a completely blinded manner by M. Blanca Piazuelo, as previously described[113,131].

Human Tissues

Human gastric tissue samples were obtained as previously described[74,107]. Both a Vanderbilt University Medical Center TMA[74] and samples from Colombia[107] were utilized for this study.

Real-Time PCR

RNA was isolated from cells and tissues using RNeasy kits. cDNA was prepared from each sample using 1 mg of RNA and the iScript cDNA synthesis kit. PCR was performed as previously described[48]. Primers are listed in Appendix A, Table 2.

Western Blot Analysis

Cells were lysed in CellLytic MT Reagent (Sigma-Aldrich, St. Louis, MO, USA) or using the NE-PER Protein Extraction Kit (Pierce Biotechnology, Rockford, IL, USA). All lysis buffers were supplemented with the Protease Inhibitor Cocktail (Set III; Calbiochem, Darmstadt, Germany) and the Phosphatase Inhibitor Cocktail (Set I; Calbiochem, Darmstadt, Germany). Protein concentration was determined using the BCA protein assay (Pierce Biotechnology, Rockford, IL, USA). Primary and secondary antibodies are listed in Appendix A, Table 3. Densitometry was performed using ImageStudio (LI-COR, Version 4.0.21, Lincoln, NE, USA).

Transfections

RAW 264.7 cells in Opti-MEM I Reduced Serum Media were transfected using Lipofectamine 2000 (Invitrogen, Carlsbad, CA, USA) with 100 nM ON-TARGET*plus* siRNAs directed against *Egfr*, and scrambled targets. After 6 h, the cells were washed and then maintained for 36 h in serum-containing, antibiotic-free DMEM. Cells were then stimulated as described in the "Bacteria, Cells, Culture Conditions, and Infections" section of the Methods.

Measurement of Nitric Oxide

The concentration of the oxidized metabolite of NO, nitrite (NO_2^-) was assessed by the Griess reaction as previously described[47].

Measurement of NO-mediated Bacterial Killing

RAW 264.7 cells were plated in complete DMEM in 24 well plates and allowed to adhere. Cells were then washed and placed in complete DMEM, without antibiotics. Transwell filter supports were placed over the cells. *H. pylori* PMSS1 (MOI = 100) were then placed in the Transwell filter supports above the cells for 24 h. After 24 h, bacteria in the Transwells were quantified by serial dilution and culture. NO was measured by the Griess Reaction, described in the Methods, from the supernatants below the Transwell filter supports.

Measurement of Phagocytosis

Phagocytosis was measured by gentamicin protection assay as previously published[48].

NF-κB Reporter Assay

The NF-κB reporter assay was performed as previously published[118,119]. In brief, NGL cells were pre-treated with 10 μM gefitinib for 1 h and then infected with *H. pylori* PMSS1 and SS1 at MOI = 100 for 2, 3 and 4 h. Luciferase activity was assessed using the Luciferase Assay System kit (Promega, Madison, WI, USA).

Luminex Assay

A 32-plex assay (EMD Millipore, Cat. MCYTMAG-70K-PX32, Billerica, MA, USA) was performed on gastric tissues from uninfected and infected $Egfr^{fl/fl}$, $Egfr^{\Delta mye}$ and $LysM^{cre/cre}$ mice. Protein isolation, quantification and Luminex assay were performed as previously described[132].

Immunofluorescence Staining for CD68, pEGFR, tEGFR, and cleaved caspase 3

Immunofluorescence staining was performed on BMmacs after *H. pylori* infection, on murine gastric tissues from mice 4 months after infection with *H. pylori* SS1, and on human gastric tissues from Colombia and the Vanderbilt University TMA, as previously published[48,74]. Antigen retrieval was performed as previously described[74]. (See Appendix A, Table 3 for antibody information). Slides were

imaged using a SPOT RT slider camera system (Diagnostic Instruments, Inc., Sterling Heights, MI, USA) on a Nikon E800 microscope (Nikon, Inc. Melville, NY, USA). Images were all modestly adjusted in ImageJ with the brightness and contrast tool.

Quantification of Human TMA Immunofluorescence

The TMA was analyzed using CellProfiler (http://www.cellprofiler.org) software. Analysis was performed on images from the Ariol SL-50 platform (Leica Biosystems, Buffalo Grove, IL, USA). A CellProfiler pipeline was created that identified nuclei, $CD68^+$ cells and $pEGFR^+$ cells based on size and staining intensity. $CD68^+pEGFR^+$ cells were determined by the overlap of the CD68 and pEGFR staining, measured in pixels. All cells were required to have a nucleus to be counted in the analysis, thus eliminating red blood cells and non-specific staining. A serial section of the TMA was concurrently stained with hematoxylin and eosin (H&E) and histologic diagnosis was confirmed in order to ensure that only high quality cores were included in the analysis described in this section. Samples were excluded from this analysis if histologic diagnosis could not be made due to sample degradation.

Immunohistochemistry

Immunohistochemistry was performed on gastric biopsies from the Vanderbilt University TMA. Paraffin-embedded tissues were deparaffinized, antigen retrieval was performed, and tissues were stained for pEGFR as previously described[74]. See Appendix A, Table 3 for antibody information.

Apoptosis

Apoptosis was assayed using Annexin-V/7-AAD as previously published[103].

Purification of Gastric Macrophages

Gastric macrophages were purified as previously described[103].

T Cell Studies

Single-cell suspensions from GLNs of uninfected and *H. pylori* SS1 infected *Egfr*$^{fl/fl}$ and *Egfr*$^{\Delta mye}$ mice were cultured in Roswell Park Memorial Institute medium (RPMI) with 10% FBS, 10 mM HEPES, 100 U/mL penicillin, 100 μg/mL streptomycin, and 10 μg/mL gentamicin in 96-well plates coated with 5 μg/mL anti-CD3 and 1 μg/mL anti-CD28. Cells were stimulated with 20 ng/mL PMA and 1 μg/mL ionomycin for 4 h. Cells were then stained and assayed by flow cytometry, as described below. Cells from GLN utilized for assessing Treg populations were not cultured, and were stained directly upon isolation.

$CD4^+$ cells from the gastric lamina propria were purified utilizing the protocol for isolation and purification of Gmacs. Lamina propria cells were incubated in the presence of a 1:100 dilution of anti-CD4, biotin tagged antibody (BD Biosciences, San Diego, CA) for 1 h, followed by incubation with 100 mL streptavidin-conjugated iMag beads (BD Biosciences, San Diego, CA) for 1 h. $CD4^+$ cells were then magnetically selected and RNA isolated utilizing the 5 PRIME PerfectPure 96 CS Cell RNA kit (5 PRIME, Gaithersburg, MD) and cDNA synthesized as described above. Th1, Th17, and Treg genes were then assessed by RT-PCR. See Appendix A, Table 2 for primer information.

Flow Cytometry

Flow cytometry was performed a previously described[103]. Lamina propria cells were isolated from the stomach at 48 h p.i. with *H. pylori* SS1, as described[103]. Upon isolation, the cells were fixed and permeabilized with CytoFix/CytoPerm (BD Biosciences, Cat. No. 554714) for 20 min on ice. Following fixation and permeabilization, cells were washed 3 times with BD CytoFix/CytoPerm and then stained with a polyclonal rabbit anti-total EGFR antibody at 1:50, or a general rabbit IgG isotype control at 1:50, for 1 h on ice in BD CytoFix/CytoPerm. Cells were washed 3 times with BD CytoFix/CytoPerm and then stained for F4/80-PE, CD11b-PE-Cy7, and anti-rabbit-Alexa488 for 20 min on ice in flow cytometry staining buffer solution (eBiosciences, Cat. 04-4222-26). Upon completion of staining, cells were

washed 3 times in flow cytometry staining buffer solution and subsequently analyzed utilizing flow cytometry. See Appendix A, Table 3 for all antibody information.

Statistical Analysis

All the data shown represent the mean ± standard error of the mean (S.E.M.) At least three biological replicates were performed for all studies utilizing cell culture. Where data was normally distributed, two-tailed Student's *t* test was used to determine significance in experiments with only two groups, and one-way ANOVA with the Newman-Keuls test was used to determine significant differences between multiple test groups. In cases where data were not normally distributed, a one-way ANOVA with Kruskal-Wallis test, followed by a Mann-Whitney *U* test, was performed. All statistics were performed in GraphPad Prism 5.0 (GraphPad Software, San Diego, CA, USA). A P value of < 0.05 was considered to be significant.

Study Approval

Animals were used under protocol M/10/155, approved by the Institutional Animal Care and Use Committee (IACUC) at Vanderbilt University. WT C57BL/6 mice were also bred and maintained under IACUC protocol V/13/230. Human tissues were obtained from a Vanderbilt University Medical Center repository and non-human exemptions were granted by the Vanderbilt University Institutional Review Board, as all information was completely de-identified.

CHAPTER 3

EGFR SIGNALING IN MACROPHAGES DURING COLON CARCINOGENESIS

3.1 Introduction

Colorectal cancer is the third most common cancer globally[26] and accounts for approximately 10% of new cancer diagnoses annually[26]. The risk for colon carcinogenesis is linked to chronic inflammatory states, such as inflammatory bowel disease (IBD)[8,133,134]. Colitis-associated carcinogenesis (CAC) occurs in 20% of patients diagnosed with IBD, and mortality rates are over 50% in these patients[8,133,134]. While mechanisms by which chronic inflammation promotes colonic carcinogenesis are being investigated[8,133,134], unanswered questions remain.

The tumor microenvironment contains various immune cell types, including macrophages[8,133,134]. Macrophages represent a heterogeneous subset of innate immune cells with roles in tissue homeostasis, pro-inflammatory and anti-microbial responses, and wound repair[2,3,98], and are of particular interest given their highly plastic phenotypes that can both promote and inhibit tumorigenesis[135,136]. Macrophages can alter their function based on the activation program utilized – either M1 or M2 patterns[2,3,11,98]. M1 macrophages are pro-inflammatory, anti-microbial, and thought to be anti-tumorigenic, although this remains the subject of debate[2,3,98]. M2 macrophages are associated with wound healing and have pro-tumorigenic properties[11,98,135]. Macrophage activation is dependent upon the colon tumor microenvironment[5,136,137] and pathways that regulate this are incompletely understood[8,135]. Studies have implicated NF-κB signaling[138-140] and other pathways[141,142].

We demonstrated that EGFR signaling regulates macrophage activation across various stimuli in Chapter 2. EGFR phosphorylation occurs in macrophages and has major effects on expression of both M1 and M2 macrophage activation markers[143]. Importantly, we determined that EGFR signaling occurs in human gastric macrophages from gastritis to gastric adenocarcinoma (Chapter 2), leading us to speculate that EGFR signaling in macrophages may also have a role in CAC. EGFR signaling has been most commonly studied within the context of epithelial cell function and has been linked to

colorectal cancer initiation and progression[70-72]. The impact of EGFR protein levels and signaling capacity is an area of ongoing investigation[70-72].

Here, we demonstrate that EGFR signaling in macrophages has a profound effect on development of CAC. Early, inflammation-mediated stages of colon carcinogenesis in humans were marked by EGFR phosphorylation in macrophages. Myeloid-specific *Egfr* knockout mice exhibited decreased tumor multiplicity and tumor burden, while epithelial-specific *Egfr* knockout mice had no differences in phenotype. Loss of *Egfr* in myeloid cells resulted in decreased M2 and M1 macrophage activation, and decreased angiogenesis. Thus, EGFR signaling in macrophages may represent a potential target for therapeutic intervention in CAC.

3.2 Results

EGFR signaling occurs in human colonic macrophages during pre-cancerous stages of CAC

The majority of studies related to EGFR signaling during CRC have focused on epithelial cells[70-73,77]. Instead, we sought to determine if human colonic macrophages had detectable levels of pEGFR, a marker of active EGFR signaling, during IBD and associated CAC. We utilized an IBD-associated cancer TMA from Vanderbilt University Medical Center, which contained cases of inactive and active ulcerative colitis, dysplasia, and colitis-associated carcinoma[144]. pEGFR levels in $CD68^+$ macrophages were detected via immunofluorescence staining (Figure 18A) and quantified with CellProfiler image analysis software (http://www.cellprofiler.com). We observed a low percentage of $CD68^+pEGFR^+$ macrophages in inactive colitis that was significantly increased in active colitis and dysplasia (Figure 18B and 18C). The percentage of $CD68^+pEGFR^+$ macrophages was lower in CAC than in active colitis and dysplasia (Figure 18B and 18C). The histopathologic diagnosis of inactive colitis indicates an absence of neutrophils, but is typically characterized by expansion of the lamina propria immune cell compartment and relative dropout of the epithelium. As such, no differences in the overall percentage of macrophages were detected between disease groups (Appendix B, Figure 1). These data indicate that pEGFR is present in macrophages during pre-cancerous events associated with colonic inflammation, implying that EGFR signaling in macrophages has an important role in macrophage

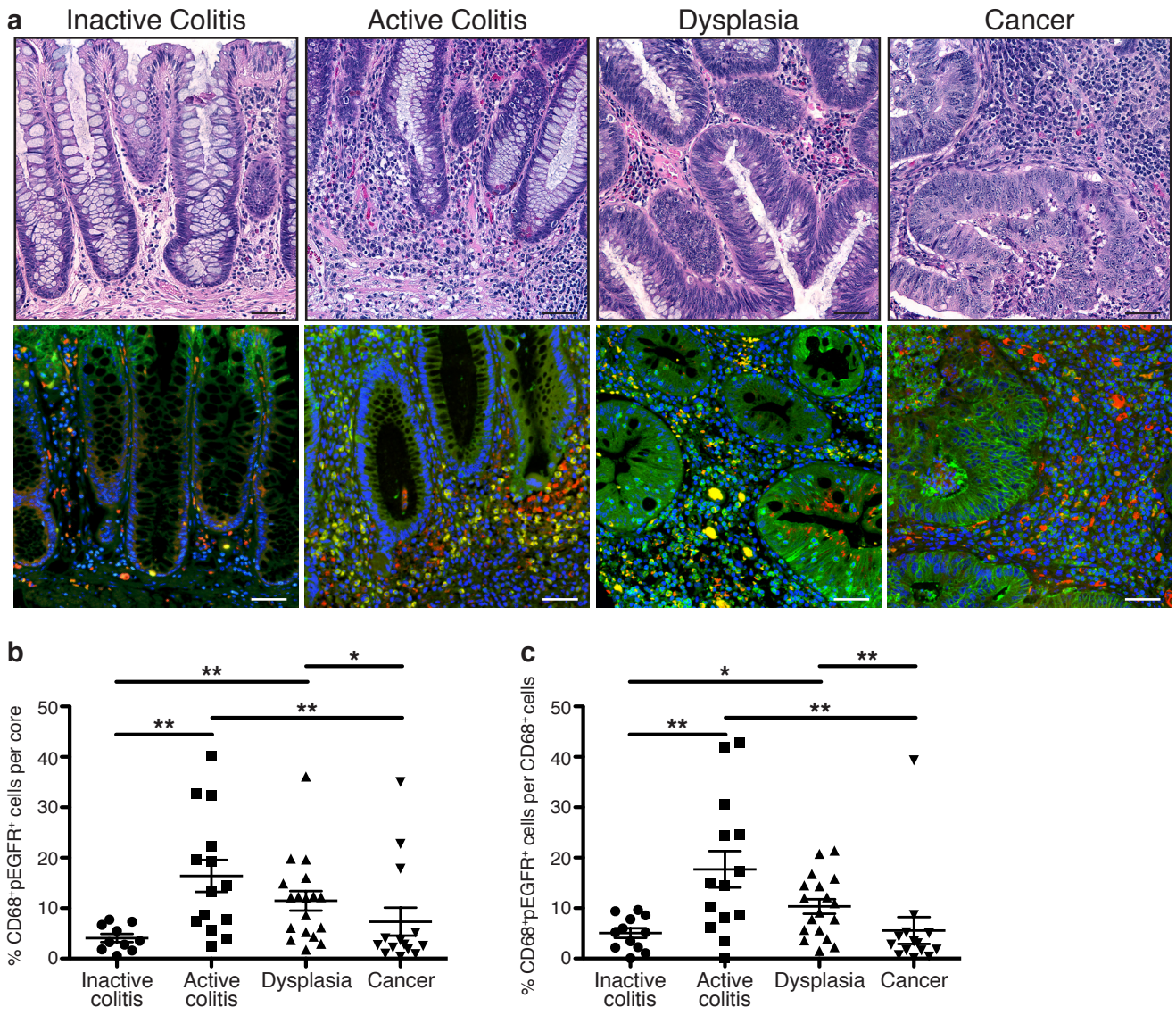

Figure 18. Macrophages have high levels of pEGFR Y1068 during inflammation driven, pre-cancerous stages of inflammatory bowel disease (IBD)-associated-colorectal cancer in human colonic tissues. (a) Representative hematoxylin and eosin (H&E)-stained images and representative immunofluorescence images of colonic tissues from the Vanderbilt University Medical Center IBD-associated colorectal cancer TMA. Red = CD68. Green = pEGFR Y1068. Yellow = Merge. Blue = DAPI. Scale bars = 50 μm. (b) Quantification of the percentage of $CD68^+pEGFR^+$ cells among the total number of cells in each individual core in the TMA, as determined by CellProfiler. (c) Quantification of the percentage of $CD68^+pEGFR^+$ cells among the total number of $CD68^+$ cells in each individual core in the TMA. For (a-c), *n* = 10 inactive colitis (normal or quiescent histology) samples, 14 active colitis (mild, moderate or severe histology) samples, 18 dysplasia samples, and 14 colorectal cancer samples. For (B-C), $*P < 0.05$, $**P < 0.01$ by one-way ANOVA with Kruskal-Wallis test, followed by Mann-Whitney *U* test.

function during initiation of carcinogenesis. It should be noted that, as expected, pEGFR staining was also abundant in colonic epithelial cells (CECs; Figure 18A).

EGFR signaling in macrophages contributes to AOM-DSS-induced colon tumorigenesis

We next sought to directly determine the role of EGFR signaling in macrophages during colon carcinogenesis. We utilized mice containing myeloid-specific, *Egfr* deletion (*Egfr*$^{\Delta mye}$) driven by LysM-Cre, which we have extensively characterized in models of gastric and colonic inflammation[143], and the appropriate control mice (*Egfr*$^{fl/fl}$). *Egfr*$^{fl/fl}$ and *Egfr*$^{\Delta mye}$ mice were subjected to the AOM-DSS model of CAC[145,146]. The AOM-DSS protocol utilized is outlined in Appendix B, Figure 2. No tumors were observed in the AOM-only or DSS-only groups, nor were differences in histologic colitis detectable between genotypes in the DSS-only group (data not shown). The lack of difference in the histologic colitis between genotypes in the DSS-only group is likely due to the prolonged recovery period, resulting in low colitis scores. Only data from the control and AOM-DSS groups are presented herein.

AOM-DSS-treated *Egfr*$^{\Delta mye}$ mice had significantly decreased tumor multiplicity and tumor burden, measured as the sum of the area of each tumor, versus AOM-DSS-treated *Egfr*$^{fl/fl}$ mice (Figure 19A and 19B). Further, *Egfr*$^{\Delta mye}$ mice were significantly protected from development of high-grade dysplasia, developing a maximum of low-grade dysplasia (Figure 19C). Representative H&E-stained images demonstrate the decrease in tumor size and protection from high-grade dysplasia in *Egfr*$^{\Delta mye}$ mice (Figure 19D). The myeloid-specific, *Egfr* knockout was maintained throughout the entire AOM-DSS protocol, as immunofluorescence images reveal the presence of many CD68^{+}tEGFR^{+} colonic macrophages in tissues from AOM-DSS-treated *Egfr*$^{fl/fl}$ mice, while only CD68^{+}tEGFR^{-} colonic macrophages are detectable in *Egfr*$^{\Delta mye}$ tissues (Figure 19E). Taken together, these data indicate that EGFR in myeloid cells is a potent promoter of tumorigenesis in mice.

Additionally, *Egfr*$^{\Delta mye}$ mice demonstrated significantly decreased histologic colitis with AOM-DSS versus *Egfr*$^{fl/fl}$ mice (Figure 19F). In conjunction with decreased histologic colitis, *Egfr*$^{\Delta mye}$ mice exhibited significant protection from weight loss associated with each cycle of DSS, as compared to *Egfr*$^{fl/fl}$ mice

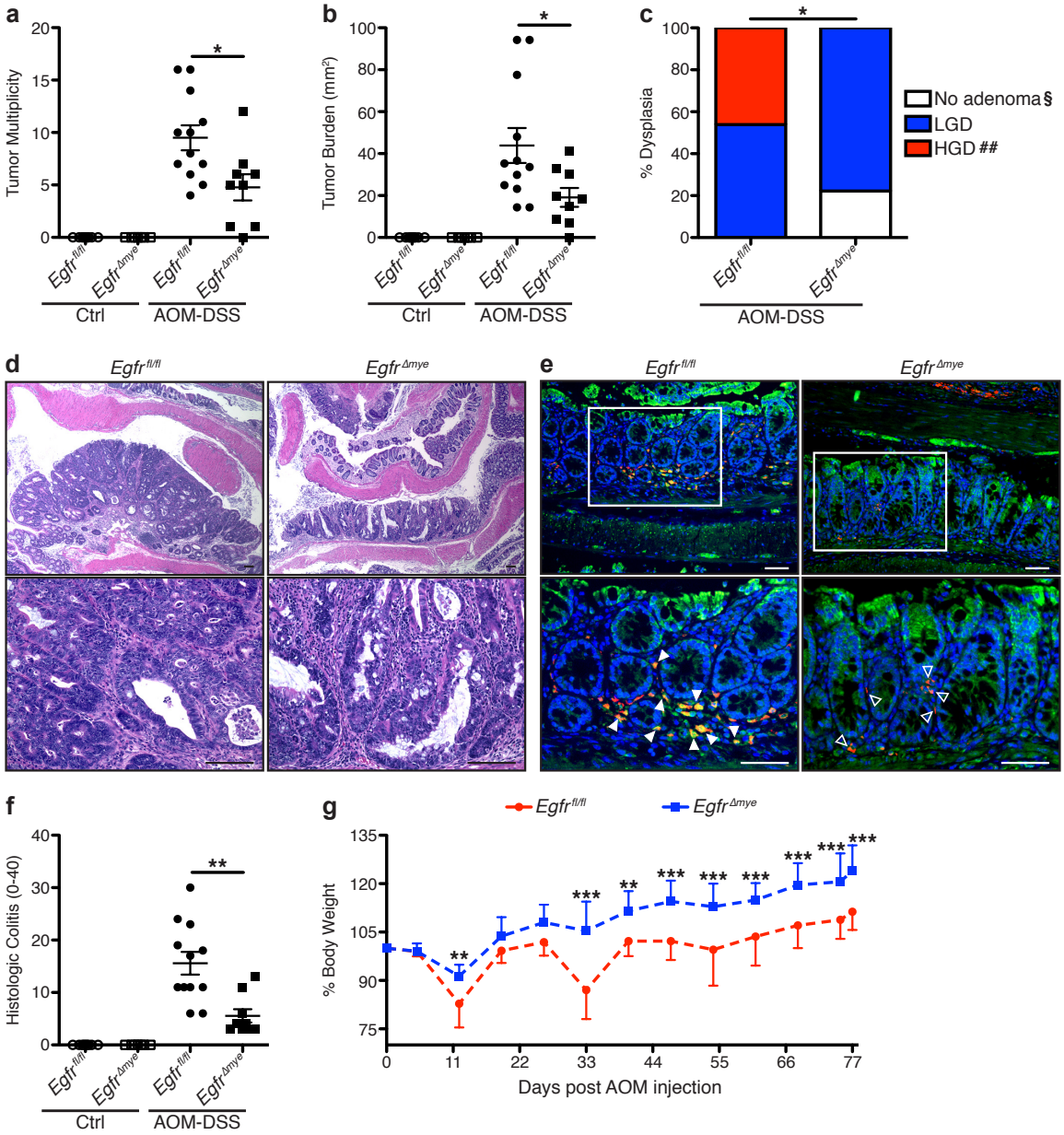

Figure 19. *Egfr*$^{\Delta mye}$ mice are significantly protected from tumorigenesis and dysplasia in the AOM-DSS model of colon tumorigenesis. (a) Tumor multiplicity was assessed by gross visual inspection, utilizing a dissecting microscope. (b) Tumor burden was determined by the addition of the calculated area of each identified tumor, as assessed with an electronic caliper for both length and width. (c) Percentage of cases with either no adenoma, low-grade dysplasia (LGD), and high-grade dysplasia (HGD) determined by a gastrointestinal pathologist (M. Kay Washington) in a blinded manner. By Chi Square test, **P* < 0.05. §*P* < 0.05 versus *Egfr*$^{fl/fl}$; ##*P* < 0.01 versus *Egfr*$^{fl/fl}$. *n* = 9-12 AOM-DSS-treated animals per genotype. (d) Representative H&E-stained images from AOM-DSS-treated mice. Scale bars = 100 μm. (e) Representative immunofluorescence images of tEGFR from AOM-DSS-treated mice. Red = CD68. Green = tEGFR. Yellow = Merge. Blue = DAPI. Scale bars = 50 μm. Solid arrows indicate CD68^{+}tEGFR^{+} macrophages. Open arrows indicate CD68^{+}tEGFR^{-} macrophages. White box indicates zoomed area. *n* = ≥ 3 mice per genotype assessed. (f) Histologic colitis was determined by M.K.W. (g) Percentage of initial body weight was assessed at the indicated time points. **P* < 0.05, ***P* < 0.01, ****P* < 0.001 versus *Egfr*$^{fl/fl}$ AOM-DSS by two-way ANOVA with Bonferroni post-test (ANOVA significance = *P* < 0.001). In (a), (b), and (f), *P < 0.05, **P < 0.01 by one-way ANOVA with Kruskal-Wallis test, followed by Mann-Whitney *U* test. In (a), (b), (f), and (g), *n* = 7-9 control and 9-12 AOM-DSS-treated mice per genotype.

(Figure 19G). These data indicate that *Egfr*$^{\Delta mye}$ mice are protected from the pro-inflammatory effects of the AOM-DSS model, which contributes to decreased CAC.

To assess the role of epithelial-specific EGFR in colon tumorigenesis, *Foxa3*$^{cre/+}$ mice were crossed with *Egfr*$^{fl/fl}$ mice. Forkhead box A3 (*Foxa3*) is expressed in all gastrointestinal epithelial cells from mouth to anus[147,148]. Isolated, naïve CECs from *Egfr*$^{fl/fl}$ mice crossed with *Foxa3*$^{cre/+}$ mice demonstrated absence of tEGFR (Appendix B, Figure 3A). Despite a report indicating that *Foxa3* is expressed in hematopoietic progenitor cells[149], we found no detectable deletion of EGFR in naïve splenocytes (Appendix B, Figure 3B), or BMmacs (Appendix B, Figure 3C). Thus, we termed these mice *Egfr*$^{\Delta GIepi}$, indicative of the epithelial-specific *Egfr* deletion in the gastrointestinal tract. It should be noted that direct comparisons of *Egfr*$^{\Delta mye}$ mice and *Egfr*$^{\Delta GIepi}$ mice are not possible because *Egfr*$^{\Delta GIepi}$ mice are on a mixed background, while *Egfr*$^{\Delta mye}$ mice are on a congenic C57BL/6 background.

When subjected to the AOM-DSS protocol, *Egfr*$^{fl/fl}$ (littermate controls of the *Egfr*$^{\Delta GIepi}$ mice, and not the same as *Egfr*$^{fl/fl}$ mice utilized in studies with *Egfr*$^{\Delta mye}$ mice) and *Egfr*$^{\Delta GIepi}$ mice exhibited no differences in tumor multiplicity and tumor burden (Appendix B, Figure 4A and 4B). Moreover, *Egfr*$^{fl/fl}$ and *Egfr*$^{\Delta GIepi}$ mice had similar susceptibility to low- and high-grade dysplasia (Appendix B, Figure 4C). Representative H&E-stained images reveal tumors of similar size and severity of dysplasia (Appendix B, Figure 4D).

Lack of differences between *Egfr*$^{fl/fl}$ and *Egfr*$^{\Delta GIepi}$ mice could be due to inefficient CRE-mediated excision of *Egfr*. However, loss of EGFR signaling was maintained in *Egfr*$^{\Delta GIepi}$ epithelial cells during AOM-DSS treatment (Appendix B, Figure 4E). pEGFR immunoperoxidase staining is robust in epithelial cells and immune cells in *Egfr*$^{fl/fl}$ mice, but is restricted to immune cells in *Egfr*$^{\Delta GIepi}$ mice (Appendix B, Figure 4E). In addition, no differences were observed in histologic colitis between *Egfr*$^{fl/fl}$ and *Egfr*$^{\Delta GIepi}$ mice (Appendix B, Figure 4F). *Egfr*$^{fl/fl}$ and *Egfr*$^{\Delta GIepi}$ mice also displayed similar weight loss during each cycle of DSS (Appendix B, Figure 4G). Taken together, EGFR signaling in immune cells, but not in epithelial cells, is critical for the promotion of tumorigenesis in mice.

EGFR signaling in macrophages enhances the innate immune response in colon tumors

The AOM-DSS model utilizes inflammation to drive tumorigenesis[145,146,150]. Based on decreased histologic colitis, combined with decreased tumor multiplicity and burden in *Egfr*$^{\Delta mye}$ mice, we sought to determine the nature of the innate immune response within the tumor microenvironment during AOM-DSS-induced CAC. We assessed 32 cytokines/chemokines via Luminex Multiplex Array. Analytes that were not different between genotypes or undetectable are in Appendix B, Table 1.

The C-C ligand chemokines, CCL3 (MIP-1α) and CCL4 (MIP-1β) protein levels were significantly decreased in *Egfr*$^{\Delta mye}$ tumors versus *Egfr*$^{fl/fl}$ tumors (Figure 20A). CCL3 and CCL4 are chemoattractants for innate immune cells, and are produced by macrophages[151]. Additionally, levels of the C-X-C ligand chemokines, CXCL9 (MIG) and CXCL10 (IP-10), were diminished in *Egfr*$^{\Delta mye}$ tumors (Figure 20A). CXCL9 and CXCL10 are also primarily produced by macrophages[152], but induce T cells infiltration[153]. CCL3, CCL4, CXCL9, and CXCL10 were induced to a similar degree in *Egfr*$^{fl/fl}$ and *Egfr*$^{\Delta GIepi}$ tumors, and no differences were detected between genotypes (Appendix B, Figure 5A). Taken together, the decreases in CCL3, CCL4, CXCL9, and CXCL10 are indicative of decreased macrophage responses that result in decreased innate and adaptive immune cell infiltration in tumor areas. These significant decreases in macrophage-driven immune responses indicate the essential role of myeloid EGFR in driving CAC.

In addition, *Egfr*$^{\Delta mye}$ tumors demonstrated significant differences in cytokine levels (Figure 20B and 20C). Leukemia inhibitory factor (LIF), a cytokine with pleiotropic effects on immune function, was decreased in *Egfr*$^{\Delta mye}$ tumors (Figure 20B). LIF protein levels were induced to a similar degree in *Egfr*$^{fl/fl}$ and *Egfr*$^{\Delta GIepi}$ tumors (Appendix B, Figure 5B). LIF overexpression is associated with poor prognosis in colorectal cancer[154,155], and decreased LIF levels in *Egfr*$^{\Delta mye}$ tumors are consistent with the decreased tumor multiplicity and burden. Moreover, colony stimulating factor 1 (CSF1; M-CSF) and IL-1α were significantly decreased in *Egfr*$^{\Delta mye}$ tumors (Figure 20C), but not altered between *Egfr*$^{fl/fl}$ and *Egfr*$^{\Delta GIepi}$ tumors (Appendix B, Figure 5C). CSF1 and IL-1α are produced by activated macrophages[140,156-158], and CSF1 represents a key factor in macrophage activation and downstream function. Taken together, the decreases in these three cytokines indicate an overall downregulation of immune/inflammatory

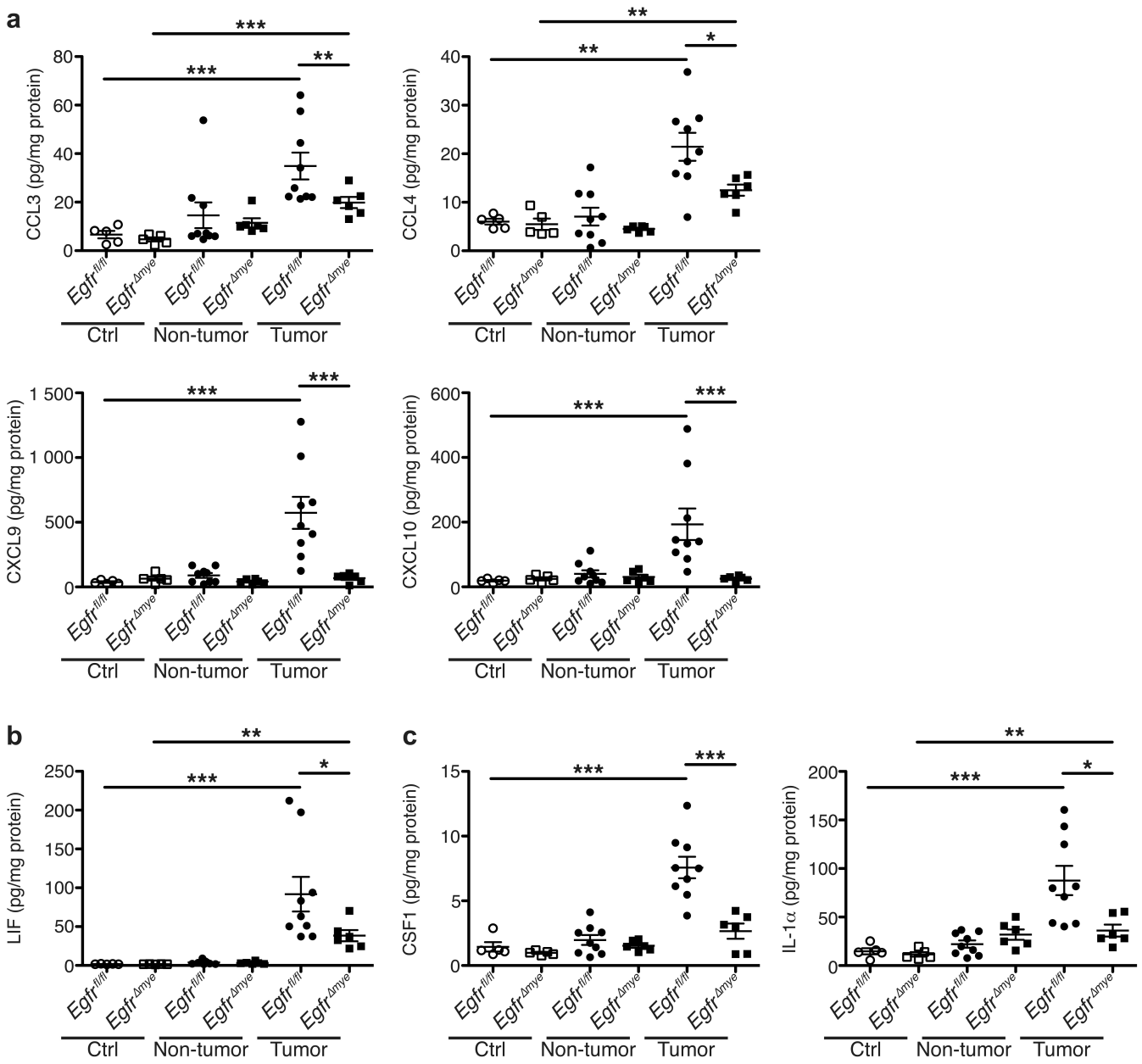

Figure 20. *Egfr*$^{\Delta mye}$ mice have significantly decreased cytokine and chemokine production within colon tumors. In a-c, protein levels were assessed by Luminex Multiplex Array from colonic tissues a 77 days post-AOM injection. (a) Levels of the C-C motif and C-X-C motif chemokines CCL3 (MIP-1α), CCL4 (MIP-1β), CXCL9 (MIG), and CXCL10 (IP-10). (b) Levels of the pleiotropic cytokine, LIF. (c) Levels of cytokines produced by activated macrophages, CSF1 (M-CSF) and IL-1α. In all panels, **P* < 0.05, ***P* < 0.01, ****P* < 0.001 by one-way ANOVA with Kruskal-Wallis test, followed by Mann-Whitney *U* test. In all panels, *n* = 5 control tissues and 6-9 tumors with paired non-tumor area per genotype.

responses within tumors lacking EGFR in myeloid cells, and imply that macrophage EGFR is a central driver of tumorigenesis in an inflammation-dependent model.

To further investigate the effects of reduced chemokine production, we assessed populations of immune cells by immunohistochemistry with the following markers: macrophages (CD68), neutrophils (myeloperoxidase, MPO), T cells (CD3), and B cells (CD45R). Abundance of these cells was scored in non-tumor and tumor tissue, and combined for an overall score. Consistent with decreased CCL3 and CCL4 levels (Figure 20A), there were significantly diminished macrophages and neutrophils in AOM-DSS-treated *Egfr*$^{\Delta mye}$ mice versus *Egfr*$^{fl/fl}$ mice (Figure 21A and 21B). T cell abundance was also significantly decreased in AOM-DSS-treated *Egfr*$^{\Delta mye}$ mice (Figure 21C), consistent with diminished CXCL9 and CXCL10 in these mice (Figure 20A). B cells were not different between genotypes (Figure 21D). Taken together, these data show diminished immune cell infiltration in the *Egfr*$^{\Delta mye}$ mice, which is dependent upon EGFR signaling in myeloid cells.

EGFR signaling in macrophages enhances M2 activation in colon tumors

Because macrophages were likely the major source of several of the chemokines and cytokines which were significantly reduced in *Egfr*$^{\Delta mye}$ tumors, we hypothesized that loss of EGFR led to altered macrophage activation in the tumor microenvironment. M2 macrophages are tumor-associated macrophages and have pro-tumorigenic properties[2,3,11,98]. Thus, the decrease in tumor multiplicity and burden could be due to a diminished M2 macrophage response in *Egfr*$^{\Delta mye}$ tumors.

Indeed, protein levels of IL-4, IL-10, and IL-13, drivers of M2 activation[2,3,11,98], were significantly upregulated in *Egfr*$^{fl/fl}$ tumors and decreased in *Egfr*$^{\Delta mye}$ tumors (Figure 22A). Moreover, mRNA levels of the M2 markers, *Arg1* and *Il10*, were also increased in *Egfr*$^{fl/fl}$ tumors and decreased in *Egfr*$^{\Delta mye}$ tumors (Figure 22B). Significant decreases in both the levels of cytokines that induce M2 activation and the expression of M2 macrophage markers indicate diminished M2 macrophage activation in *Egfr*$^{\Delta mye}$ mice, consistent with reduced colon tumorigenesis.

Egfr$^{fl/fl}$ and *Egfr*$^{\Delta Glepi}$ tumors did not demonstrate differences in IL-4 or IL-10 levels (Appendix B, Figure 6A), nor were differences detectable in *Arg1* and *Il10* mRNA levels (Appendix B, Figure 6B). IL-

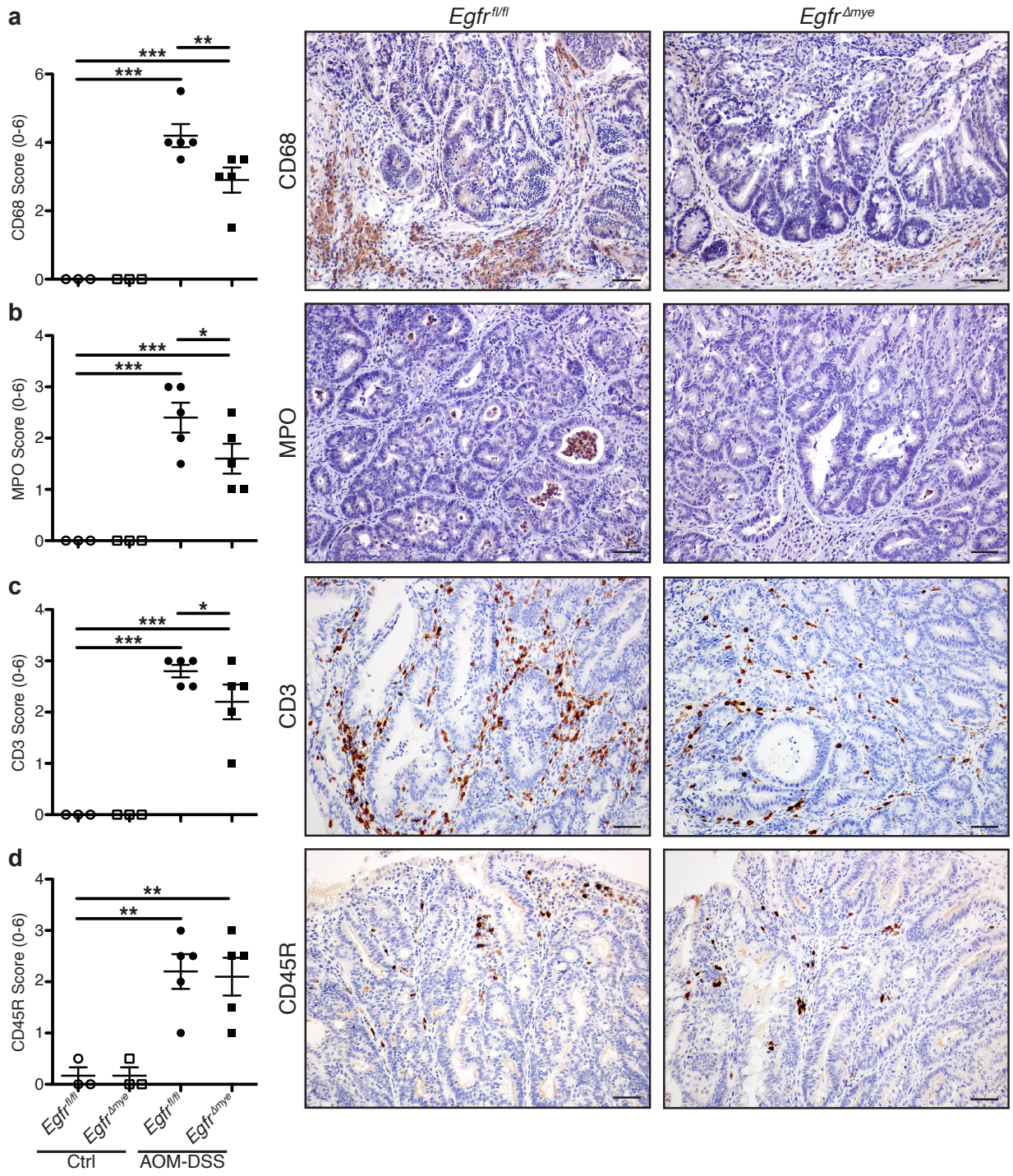

Figure 21. *Egfr*$^{\Delta mye}$ mice have significantly decreased macrophage, neutrophil and T cell infiltration during AOM-DSS treatment. (a) Quantification of CD68^{+} macrophage abundance with representative immunoperoxidase images of CD68 staining in AOM-DSS-treated mice. (b) Quantification of myeloperoxidase^{+} (MPO) neutrophil abundance with representative immunoperoxidase images of MPO staining in AOM-DSS-treated mice. (c) Quantification of CD3^{+} T cell abundance with representative immunoperoxidase images of CD3 staining in AOM-DSS-treated mice. (d) Quantification of CD45R^{+} B cell abundance with representative immunoperoxidase images of CD45R staining in AOM-DSS-treated mice. Scoring of immune cell abundance was performed by M.B.P. as described. In all panels, scale bars = 50 μm. In all panels, *n* = 3 control and 5 AOM-DSS-treated mice per genotype. In all panels, **P* < 0.05, ***P* < 0.01, ****P* < 0.001 by one-way ANOVA with Newman-Keuls post-test after the data were square-root transformed.

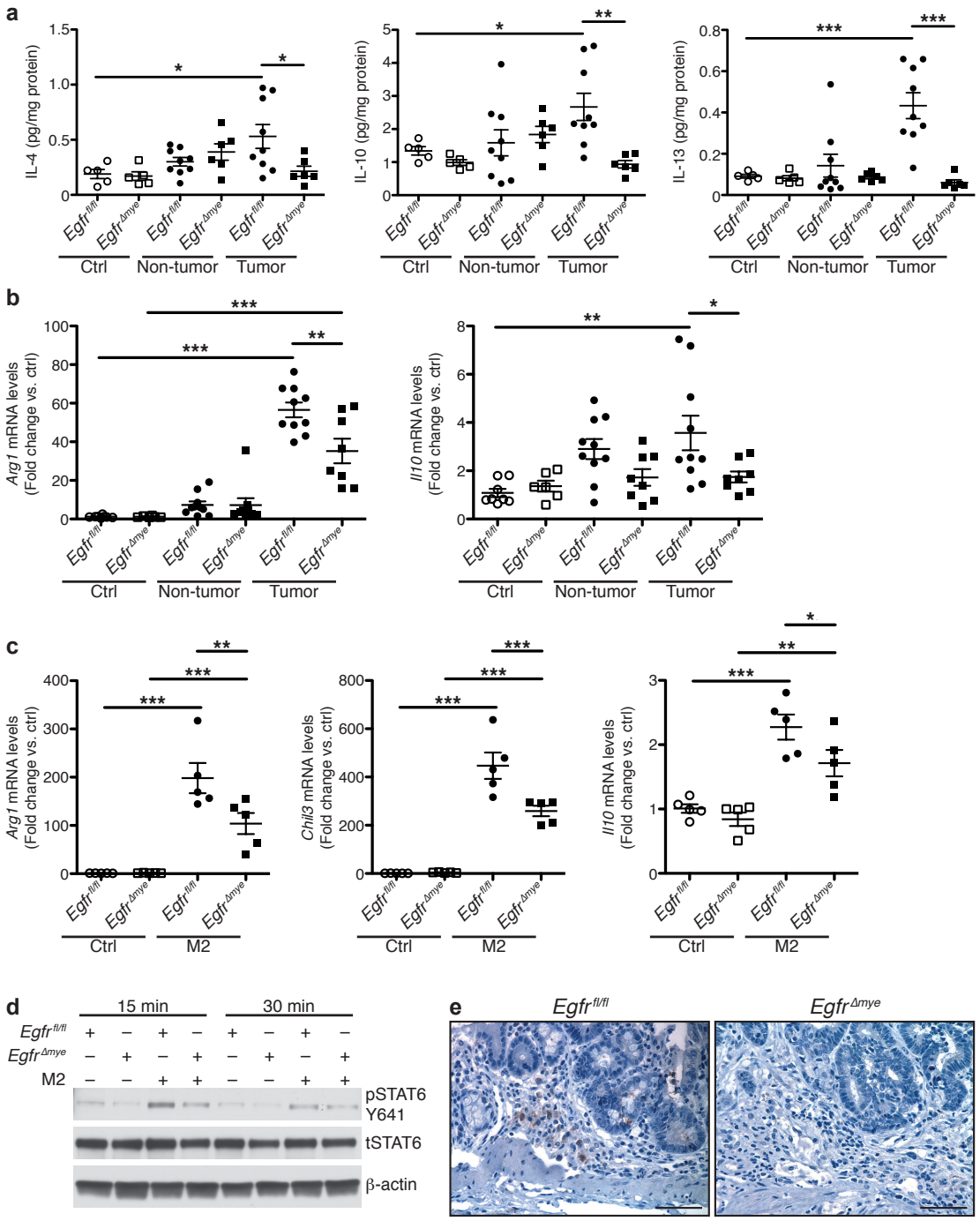

Figure 22. *Egfr*$^{\Delta mye}$ mice demonstrate decreased M2 macrophage activation during colon tumorigenesis. (a) Protein levels of the M2 stimuli, IL-4, IL-10, and IL-13, were assessed by Luminex Multiplex Array from colonic tissues 77 days post-AOM injection. *n* = 5 control tissues and 6-9 tumors with paired non-tumor area per genotype. (b) mRNA levels of M2 markers, *Arg1* and *Il10*, were assessed by qRT-PCR from colonic tissues 77 days post-AOM injection. *n* = 6-8 control tissues and 8-10 tumors with paired non-tumor area per genotype. In (a) and (b), **P* < 0.05, ***P* < 0.01, ****P* < 0.001 by one-way ANOVA with Kruskal-Wallis test, followed by Mann-Whitney *U* test. (c) mRNA levels of M2 markers, *Arg1*, *Chil3*, and *Il10*, were assessed by qRT-PCR in BMmacs 24 h post-treatment with classical M2 stimuli, IL-4 (10 ng/mL) and IL-10 (10 ng/mL). *n* = 5 biological replicates per genotype. In (c), **P* < 0.05, ***P* < 0.01, ****P* < 0.001 by one-way ANOVA with Newman-Keuls post-test. (d) Representative western blot of pSTAT6 levels in BMmacs stimulated with the M2 stimulus, IL-4 (10 ng/mL), for the indicated times. *n* = 3 biological replicates. (e) Representative images of pSTAT6 immunoperoxidase staining in AOM-DSS-treated tissues. Scale bar = 50 μm. *n* = 3 mice per genotype.

13 was detected at very low levels in *Egfr*$^{fl/fl}$ and *Egfr*$^{\Delta Glepi}$ tumors, but no significant differences were detected (Appendix B, Table 2). These data correlate with the finding that *Egfr*$^{fl/fl}$ and *Egfr*$^{\Delta Glepi}$ mice do not have significant differences in development of CAC.

To confirm that *Egfr* deletion in myeloid cells resulted in decreased M2 activation, we isolated BMmacs from *Egfr*$^{fl/fl}$ and *Egfr*$^{\Delta mye}$ mice and stimulated them *ex vivo* with IL-4 and IL-10. Markers of M2 macrophage activation were assessed by RT-PCR. IL-4/IL-10 stimulation led to a significant induction of *Arg1*, *Chil3*, and *Il10* in both *Egfr*$^{fl/fl}$ and *Egfr*$^{\Delta mye}$ BMmacs (Figure 22C). Importantly, *Arg1*, *Chil3*, and *Il10* mRNA levels were significantly decreased in *Egfr*$^{\Delta mye}$ BMmacs (Figure 22C), consistent with the findings in *Egfr*$^{\Delta mye}$ tumors. Together, these data further suggest that EGFR signaling regulates M2 macrophage activation.

To address the mechanism by which macrophage EGFR signaling alters M2 activation, we isolated BMmacs from *Egfr*$^{fl/fl}$ and *Egfr*$^{\Delta mye}$ mice, stimulated them *ex vivo* with IL-4, and assessed phospho-STAT6 (pSTAT6), a known mediator of M2 activation[17]. *Egfr*$^{\Delta mye}$ BMmacs exhibited decreased pSTAT6 levels when compared to *Egfr*$^{fl/fl}$ BMmacs (Figure 22D). Similarly, AOM-DSS-treated *Egfr*$^{\Delta mye}$ tissues demonstrated reduced pSTAT6 levels in immune cells (Figure 22E). These data reveal a potential link between EGFR and STAT6 in regulating M2 activation in macrophages.

Macrophage-specific EGFR signaling also augments M1 activation in colon tumors

Alterations in M2 macrophage activation in *Egfr*$^{\Delta mye}$ mice were not unexpected, given the close association between M2 macrophages and the tumor microenvironment[135,136]. However, we also observed significant alterations in both the levels of cytokines that induce M1 activation and in M1 markers in *Egfr*$^{\Delta mye}$ tumors.

IFN-γ and TNF-α potently induce M1 macrophage activation[7]. Protein levels of both IFN-γ and TNF-α were significantly upregulated in AOM-DSS-induced tumors in *Egfr*$^{fl/fl}$ mice and significantly reduced in *Egfr*$^{\Delta mye}$ tumors (Figure 23A), indicative of decreased capacity for M1 macrophage activation. mRNA levels of M1 markers *Nos2* and *Il1b* were upregulated in *Egfr*$^{fl/fl}$ tumors, and significantly decreased in *Egfr*$^{\Delta mye}$ tumors (Figure 23B). This decrease in M1 macrophage activation

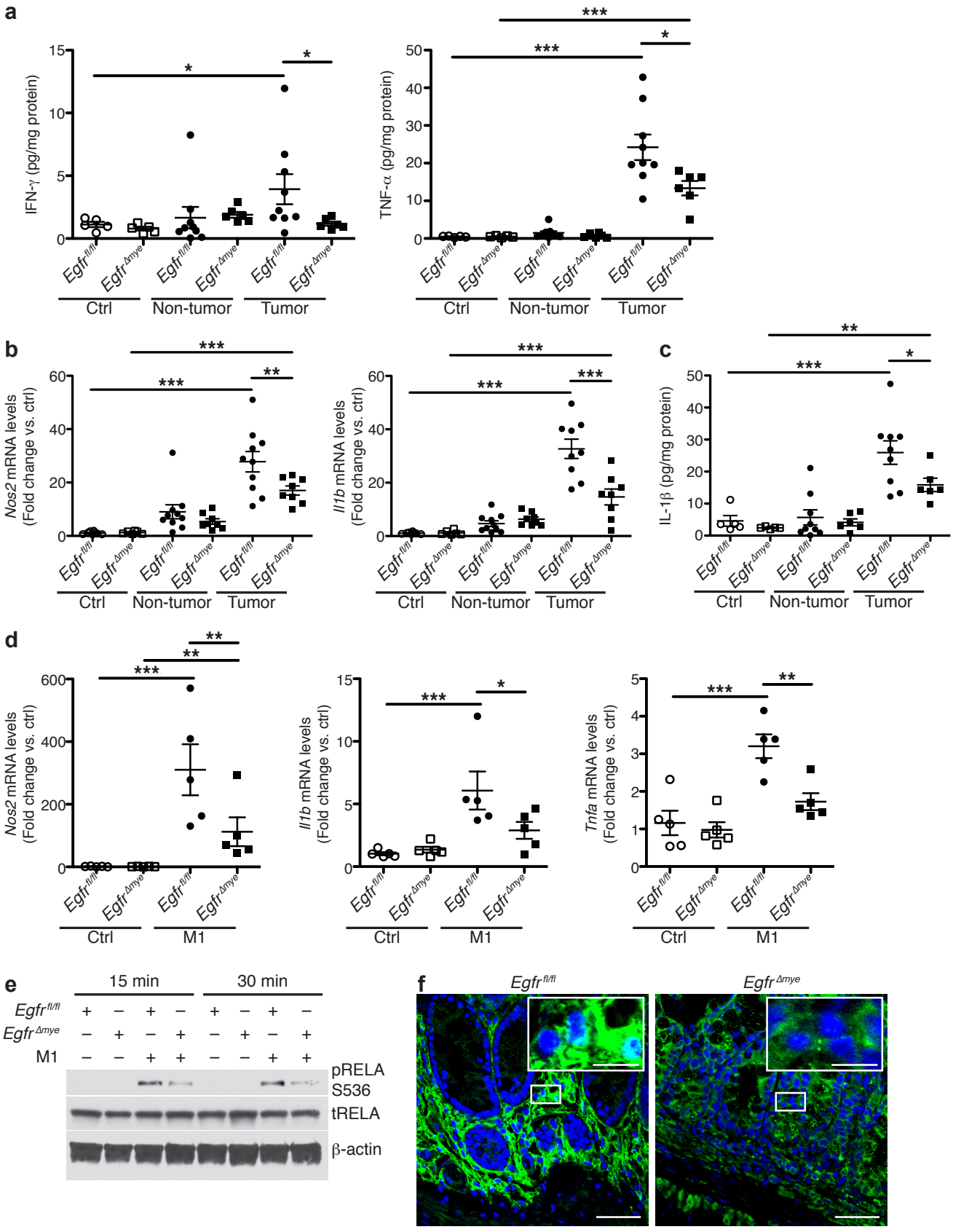
a
IFN-γ (pg/mg protein)
TNF-α (pg/mg protein)
Egfr fl/fl
Egfr Δmye
Ctrl
Non-tumor
Tumor
b
Nos2 mRNA levels (Fold change vs. ctrl)
Il1b mRNA levels (Fold change vs. ctrl)
c
IL-1β (pg/mg protein)
d
Nos2 mRNA levels (Fold change vs. ctrl)
Il1b mRNA levels (Fold change vs. ctrl)
Tnfa mRNA levels (Fold change vs. ctrl)
M1
e
15 min
30 min
M1
pRELA S536
tRELA
β-actin
f
Egfr fl/fl
Egfr Δmye

Figure 23. *Egfr*$^{\Delta mye}$ mice demonstrate decreased M1 macrophage activation during colon tumorigenesis. (a) Protein levels of M1 stimuli, IFN-γ and TNF-α, were assessed by Luminex Multiplex Array from colonic tissues 77 days post-AOM injection. *n* = 5 control tissues and 6-9 tumors with paired non-tumor area per genotype. (b) mRNA levels of M1 markers, *Nos2* and *Il1b*, were assessed by qRT-PCR from colonic tissues 77 days post-AOM injection. *n* = 6-8 control tissues and 8-10 tumors with paired non-tumor area per genotype. (c) Protein levels of the M1 marker, IL-1β, were assessed by Luminex Multiplex Array from colonic tissues 77 days post-AOM injection. *n* = 5 control tissues and 6-9 tumors with paired non-tumor area per genotype. In (a-c), **P* < 0.05, ***P* < 0.01, ****P* < 0.001 by one-way ANOVA with Kruskal-Wallis test, followed by Mann-Whitney *U* test. (d) mRNA levels of M1 markers, *Nos2*, *Il1b*, and *Tnfa*, were assessed by qRT-PCR in bone marrow derived macrophages (BMmacs) 24 h post-treatment with classical M1 stimuli, IFN-γ (200 U/mL) and TNF-α (10 ng/mL). *n* = 5 biological replicates per genotype. In (d), **P* < 0.05, ***P* < 0.01, ****P* < 0.001 by one-way ANOVA with Newman-Keuls post-test. (e) Representative western blot of pRELA (pp65) levels in BMmacs stimulated with the M1 stimuli, IFN-γ (200 U/mL) and lipopolysaccharide (10 ng/mL), for the indicated times. *n* = 3 biological replicates. (e) Representative confocal immunofluorescence images of cytoplasmic and nuclear RELA (p65) in AOM-DSS-treated tissues. Green = cytoplasmic RELA. White/Aqua = nuclear RELA. Blue = DAPI. Scale bar = 40 μm, Scale bar in inset = 10 μm. *n* = 3 mice per genotype.

was confirmed at the protein level, as IL-1β protein was also significantly decreased in *Egfr*$^{\Delta mye}$ tumors (Figure 23C). Protein levels of IFN-γ and TNF-α were detectable in *Egfr*$^{fl/fl}$ and *Egfr*$^{\Delta GIepi}$ tumors, but were not different between genotypes (Appendix B, Figure 7A). mRNA levels of *Nos2* and *Il1b* (Appendix B, Figure 7B), as well as IL-1β protein levels, were upregulated in *Egfr*$^{fl/fl}$ and *Egfr*$^{\Delta GIepi}$ tumors, but again were not different between genotypes.

To assess the role of EGFR signaling in M1 activation, we isolated BMmacs from *Egfr*$^{fl/fl}$ and *Egfr*$^{\Delta mye}$ mice and stimulated *ex vivo* with IFN-γ and TNF-α for 24 h. M1 stimulation resulted in robust expression of M1 markers *Nos2*, *Il1b*, and *Tnfa* (Figure 23D). Importantly, mRNA expression of *Nos2*, *Il1b*, and *Tnfa* was significantly reduced in *Egfr*$^{\Delta mye}$ BMmacs versus *Egfr*$^{fl/fl}$ BMmacs (Figure 19D), indicating that EGFR signaling is equally critical for M1 and M2 activation. Intriguingly, M1 activation may have critical role in colon tumorigenesis in this model that is regulated by EGFR signaling.

In Chapter 2, we have demonstrated that EGFR signaling is upstream of NF-κB in macrophages during *Helicobacter pylori* infection[143]. Moreover, we have reported that there is enhanced nuclear translocation of RELA (also known as p65) in two different models of colitis[159]. Thus, we hypothesized that EGFR and NF-κB signaling may regulate M1 activation. We isolated BMmacs from *Egfr*$^{fl/fl}$ and *Egfr*$^{\Delta mye}$ mice, stimulated with IFN-γ and lipopolysaccharide, and assessed phospho-RELA (pRELA) levels. *Egfr*$^{\Delta mye}$ BMmacs had diminished pRELA levels versus *Egfr*$^{fl/fl}$ BMmacs (Figure 23E). Moreover, AOM-DSS-treated *Egfr*$^{\Delta mye}$ tissues had markedly decreased RELA nuclear translocation in lamina propria cells (Figure 23F). Thus, EGFR signaling activates the NF-κB pathway to regulate M1 activation.

EGFR signaling in macrophages enhances angiogenesis in colon tumors

Angiogenesis is a hallmark of carcinogenesis[160], and is an essential means by which colon tumor growth is supported[161,162]. Several cytokines, including vascular endothelial growth factor (VEGF) A and CXCL1 (KC, GROα), the murine equivalent of CXCL8 (IL-8)[163], contribute to angiogenesis[164-167].

M1 macrophages are an important source of CXCL1[168] and both M1 and M2 macrophages are important sources of VEGFA[169].

Based on i) decreased tumor multiplicity/burden, and ii) decreased M2 and M1 macrophage activation in *Egfr*$^{\Delta mye}$ mice, we hypothesized that angiogenesis may be impaired, contributing to diminished tumorigenesis. *Egfr*$^{\Delta mye}$ tumors had decreased mRNA levels of *Cxcl1* and *Vegfa* (Figure 24A) and altered protein levels of CXCL1 and VEGF (Figure 24B) versus *Egfr*$^{fl/fl}$ tumors. *Egfr*$^{fl/fl}$ and *Egfr*$^{\Delta Glepi}$ tumors did not demonstrate any differences in mRNA or protein levels of these markers (Appendix B, Figure 8). Additionally, M1-activated *Egfr*$^{\Delta mye}$ BMmacs expressed significantly less *Cxcl1* and *Vegfa* (Appendix B, Figure 9A) and M2-activated *Egfr*$^{\Delta mye}$ BMmacs expressed less *Vegfa* (Appendix B, Figure 9B) versus *Egfr*$^{fl/fl}$ BMmacs. These data confirm that macrophages are a potential source of CXCL1 and VEGF, and that EGFR signaling is critical for expression of these pro-angiogenic mediators.

To confirm that decreased pro-angiogenic cytokines was accompanied by decreased angiogenesis, we performed immunoperoxidase staining for CD31, a marker of vascular endothelial cells[170]. Representative images demonstrate significantly enhanced angiogenesis in AOM-DSS-treated *Egfr*$^{fl/fl}$ versus *Egfr*$^{\Delta mye}$ mice (Figure 24C). Notably, angiogenesis in AOM-DSS-treated *Egfr*$^{\Delta mye}$ mice was not different than angiogenesis in control *Egfr*$^{fl/fl}$ and *Egfr*$^{\Delta mye}$ mice (Figure 24C). Both the number of CD31^{+} blood vessels per case (Figure 24D) and the total area of CD31^{+} blood vessels (Figure 24E) were significantly decreased in AOM-DSS-treated *Egfr*$^{\Delta mye}$ mice versus *Egfr*$^{fl/fl}$ mice. Thus, decreases in pro-angiogenic cytokine production were associated with decreased angiogenesis in *Egfr*$^{\Delta mye}$ mice. Decreased angiogenesis likely contributed to diminished tumorigenesis in this CAC model.

3.3 Discussion

EGFR signaling is a commonly studied pathway in carcinogenesis[59,69-71,74], although most studies related to EGFR signaling have been performed in epithelial cells[59,69-71,74]. This study outlines an important role for EGFR signaling in macrophages during inflammatory colon tumorigenesis (Figure 25). Herein, we demonstrate that EGFR signaling occurs in human macrophages during pre-cancerous

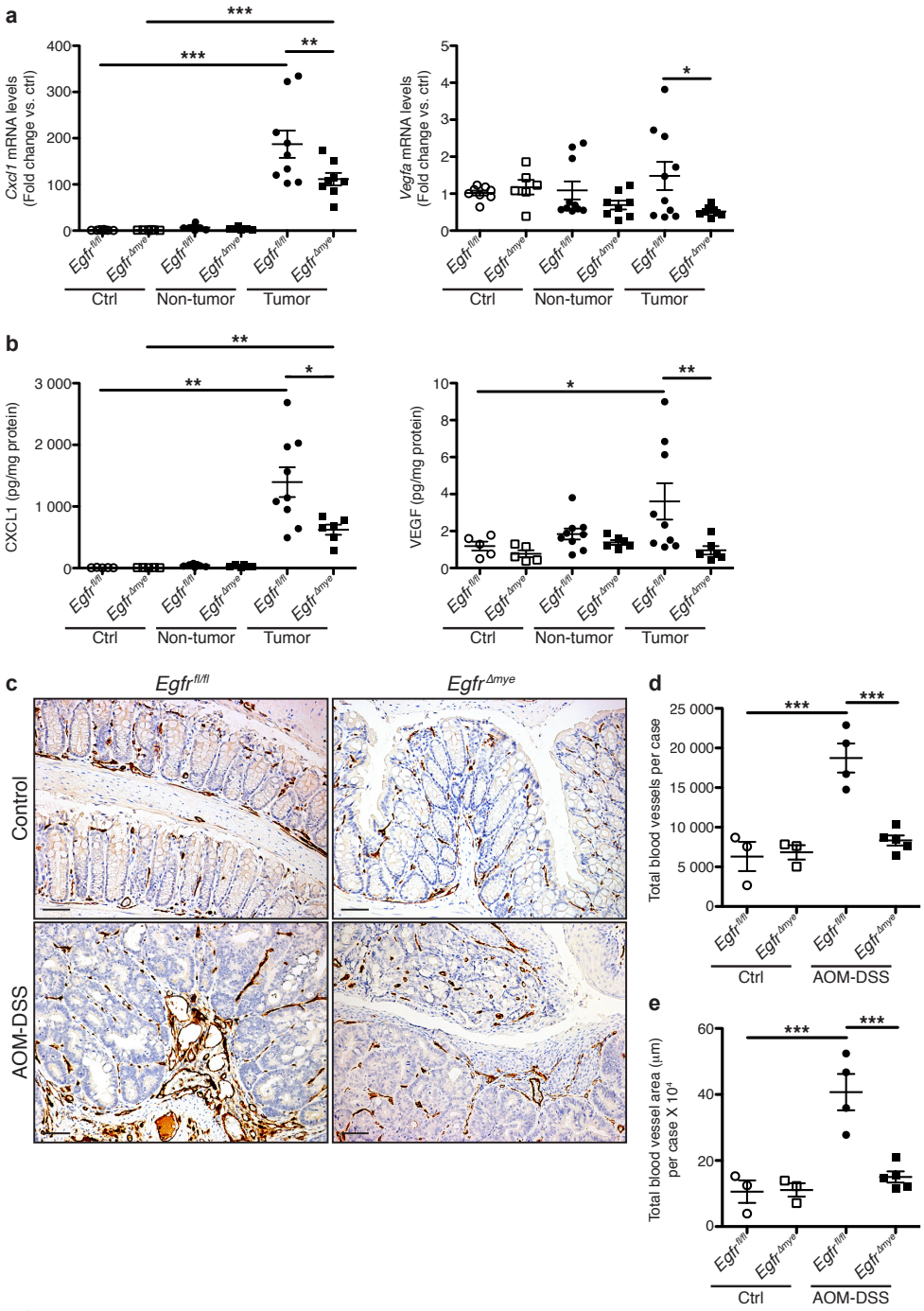

Figure 24. *Egfr*$^{\Delta mye}$ mice demonstrate decreased pro-angiogenic chemokine/cytokine production and angiogenesis during colon tumorigenesis. (a) mRNA levels of the pro-angiogenic chemokine, *Cxcl1*, and the pro-angiogenic cytokine, *Vegfa*, were assessed by qRT-PCR from colonic tissues 77 days post-AOM injection. *n* = 6-8 control tissues and 8-10 tumors with paired non-tumor area per genotype. (b) Protein levels of pro-angiogenic chemokine, CXCL1, and pro-angiogenic cytokine, VEGF, were assessed by Luminex Multiplex Array from colonic tissues 77 days post-AOM injection. *n* = 5 control tissues and 6-9 tumors with paired non-tumor area per genotype. In (a) and (b), **P* < 0.05, ***P* < 0.01, ****P* < 0.001 by one-way ANOVA with Kruskal-Wallis test, followed by Mann-Whitney *U* test. (c) Representative images of CD31$^+$ blood vessel immunohistochemistry in colonic tissues. Scale bars = 50 µm. (d) Quantification of the total number of CD31$^+$ blood vessels in (c). *n* = 3 control colonic tissues and 4-5 AOM-DSS-treated colonic tissues per genotype. (e) Quantification of the total CD31$^+$ blood vessel area within tissues in (c). *n* = 3 control colonic tissues and 4-5 AOM-DSS-treated colonic tissues per genotype. In (d) and (e), ****P* < 0.001 by one-way ANOVA with Newman-Keuls post-test.

stages of ulcerative colitis and dysplasia, both of which are marked by active inflammation[8,134]. Based on diminished $CD68^{+}pEGFR^{+}$ cells in CAC, we posit that EGFR signaling in human macrophages may be essential for initiation of inflammation-associated tumorigenesis. Myeloid-specific knockout of *Egfr* significantly protected mice from tumorigenesis in the AOM-DSS model of CAC. Intriguingly, gastrointestinal epithelial cell-specific knockout of *Egfr* did not have a phenotype that was significantly different from wild-type mice. Protection from tumorigenesis in $Egfr^{\Delta mye}$ mice was accompanied by restricted M2 and M1 macrophage activation, which likely contributed to decreased angiogenesis due to less production of pro-angiogenic cytokines and chemokines (Figure 25). These data point to a currently underappreciated role for EGFR signaling in myeloid cells, particularly macrophages, in promoting CAC.

A previous study utilizing *Wa5* mice, which carry a dominant-negative allele that impairs EGFR signaling, demonstrated that EGFR signaling inhibited CAC[171], the opposite of our current result. It should be noted that differences in colon tumorigenesis were only significant when *Wa5* mice were crossed with $Il10^{-/-}$ mice[171]. $Il10^{-/-}$ mice may have limitations as a model for CAC, because effects of the *Il10* deletion can be modulated by bacterial infections[172,173]. The AOM-DSS model is solely dependent upon inflammation as a driver of carcinogenesis[172,173]. The previous work that demonstrated a protective role for EGFR in colon tumorigenesis also utilized the AOM-DSS model of colon tumorigenesis, but noted no significant differences in tumor multiplicity[171]. Moreover, the *Wa5* allele affects all cell types, while our models used herein were myeloid- and gastrointestinal epithelial-cell-specific. Taken together, our study provides a strong body of evidence that EGFR signaling in macrophages is a critical component of CAC.

EGFR signaling appears to mediate M1 and M2 macrophage activation. Importantly, we demonstrated via multiple methods in a previously published study that EGFR signaling in macrophages had no effect on apoptosis[143]. Thus, the phenotypes observed are due to alterations in macrophage function, not cell viability. While the finding that decreased M2 activation, which is highly pro-tumorigenic[11,74,135], correlated with decreased tumor multiplicity and burden was not unexpected, the dramatic alteration of M1 activation was somewhat surprising. However, there are potential reasons

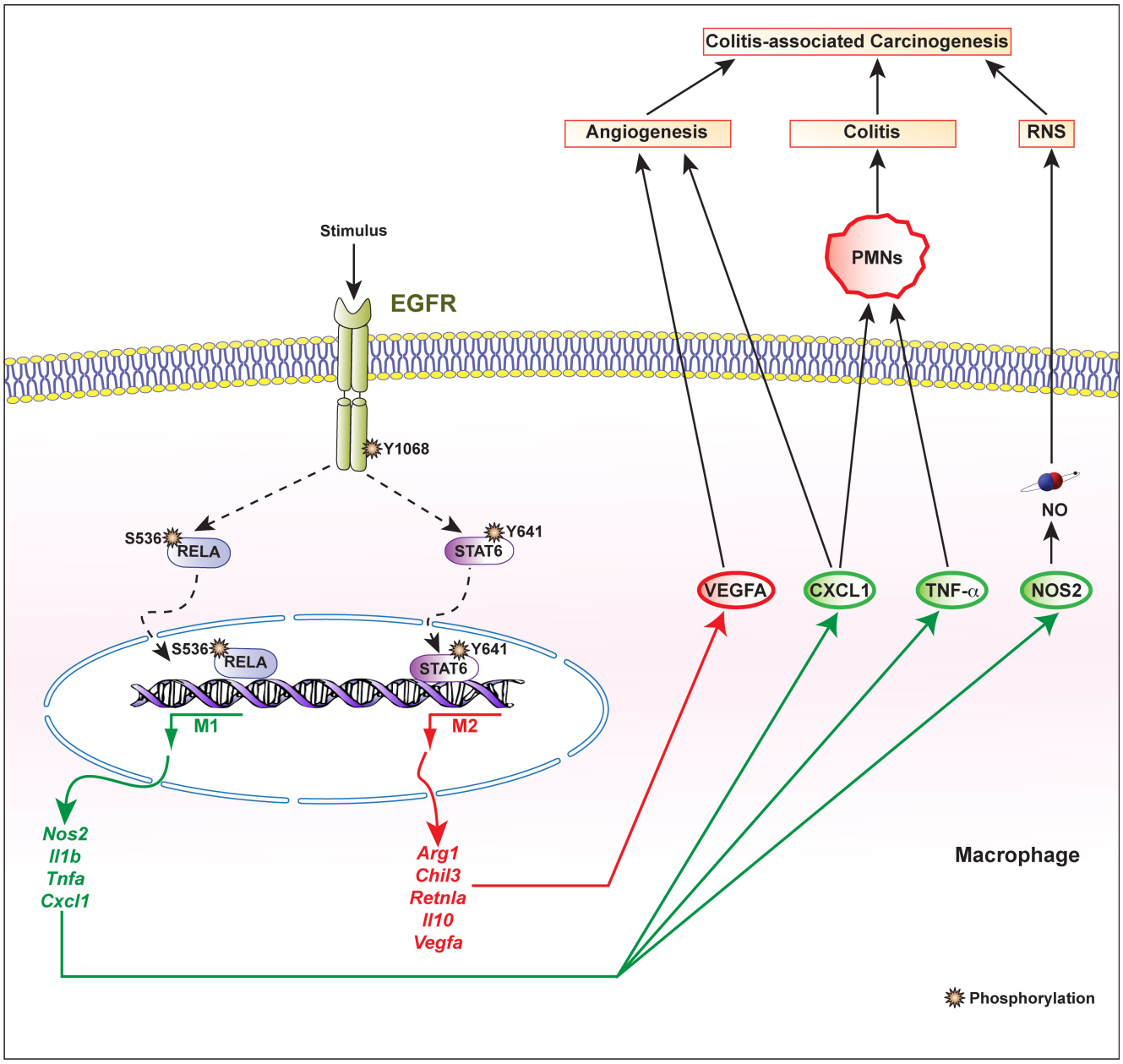

Figure 25. Summary of findings related to EGFR signaling in macrophages during colitis-associated carcinogenesis (CAC). EGFR activation occurs in macrophages during CAC, leading to NF-κB (RELA; p65) signaling and STAT6 signaling. NF-κB signaling leads to M1 gene expression, and STAT6 signaling leads to M2 gene expression. M1 activation leads to i) CXCL1 and TNF-α production, which recruit polymorphonuclear cells (PMNs) and increase colitis; ii) NOS2-mediated NO production, leading to reactive nitrogen species (RNS)-mediated DNA damage; and iii) CXCL1 production, which can promote angiogenesis. M2 activation leads to VEGFA production, which can also promote angiogenesis. Together, these effects contribute to increased risk for development of CAC.

why M1 activation may have an important role in tumorigenesis. Firstly, as we demonstrated, M1 macrophages are an important source of pro-angiogenic cytokines (VEGF) and chemokines (CXCL1). Secondly, M1 macrophages are a potent source of NOS2 (as shown herein) and NO[2,3,143]. It has been proposed that NO, a RNS, promotes colon tumorigenesis by causing DNA mutations and DNA instability[8,10]. Our work demonstrates that EGFR signaling has a role in promoting both M1 and M2 activation, potentially working synergistically to promote colon tumorigenesis.

In sum, our study outlines a novel role for EGFR signaling in macrophages during CAC. Robust EGFR signaling in human macrophages in stages leading to colitis-associated cancer indicates that macrophage pEGFR may serve as a potential biomarker for colorectal cancer risk in colitis patients. Moreover, our previous work showed that TNF-α induced EGFR signaling in macrophages[143]. Thus, one potential benefit of anti-TNF treatment, frequently used in IBD patients, may be suppression of macrophage EGFR signaling. Further studies are imperative to further assess the critical role that EGFR activation plays in immune cells in patients at risk for progression to colon cancer.

3.4 Materials and Methods

Reagents

Reagents used for cell culture were from Invitrogen (Carlsbad, CA, USA). Reagents for RNA extraction were from Qiagen (Valencia, CA, USA); those for cDNA synthesis and RT-PCR were from Bio-Rad (Hercules, CA, USA). Murine M-CSF, IFN-γ, IL-4, and IL-10 were from PeproTech (Rocky Hill, NJ, USA). Murine TNF-α was from Thermo Fisher Scientific (Waltham, MA, USA). Azoxymethane and LPS were from Sigma-Aldrich (St. Louis, MO, USA). DSS was from TdB Consultancy (Uppsala, Sweden).

Antibodies

See Appendix B, Table 4 for information regarding antibodies.

Cells and Culture Conditions

BMmacs were isolated and utilized as described in Chapter 2. Following differentiation, cells were placed in complete DMEM, supplemented with 10% FBS, 2 mM L-glutamine, 25 mM HEPES, and 10 mM sodium pyruvate for studies with IFN-γ, TNF-α, IL-4, IL-10, or LPS. Stimulation times and doses are indicated in figure legends.

Animal Studies

Egfr$^{fl/fl}$ and *Egfr*$^{\Delta mye}$ mice were utilized as described in Chapter 2. C57BL/6 *Egfr*$^{fl/fl}$ mice were crossed to CD-1/DBA *Foxa3*$^{cre/+}$ mice obtained from Timothy Wang (Columbia University Medical Center)[174], to generate *Egfr*$^{\Delta GIepi}$ mice. As *Egfr*$^{\Delta GIepi}$ mice contain one *Cre* allele, littermates were utilized for all experiments. Study approval is as described in Chapter 2.

Male mice, aged 6-12 weeks, were utilized for all studies. Samples sizes were based on previous AOM-DSS studies from our laboratory. Mice were not removed from the cages into which they were weaned. No other criteria were utilized for selection or randomization. Mice were subjected to the AOM-DSS colon tumorigenesis model[144,145]. Mice received one intraperitoneal AOM injection (12.5 mg/kg) on Day 0, and three doses of 4% DSS in their drinking water on Days 5, 26, and 47. The first two cycles of DSS lasted for 5 days, and the third for 4 days. Mice were weighed every 7 days from the start of the first DSS cycle and on Day 0 to determine the AOM dosage. Mice were sacrificed on Day 77.

Rarely, *Egfr*$^{\Delta mye}$ mice developed an enlarged spleen that was not attributable to AOM-DSS treatment. These mice were excluded from further analysis.

Tumor multiplicity was determined by visual inspection via dissecting microscope. Tumor burden was determined by the summation of tumor area, assessed by electronic caliper. Histologic colitis and dysplasia were determined by a gastrointestinal pathologist, M. Kay Washington in a blinded manner.

Human Tissues

The IBD-associated CAC human TMA was utilized as described[144].

Real-Time PCR

RNA isolated, cDNA synthesis, and RT-PCR was performed as described in Chapter 2. See Appendix B, Table 3 for primers utilized.

Western Blot Analysis

Western blot analysis was performed as described in Chapter 2.

Luminex Multiplex Array

Luminex Multiplex Array was performed as described in Chapter 2.

Immunofluorescence Staining for tEGFR and CD68, and RELA

Staining for tEGFR and CD68 in both the TMA and in murine tissues was performed as described[143], with the following exceptions in murine tissue. An initial blocking step was performed with Background Sniper (Biocare Medical), followed by incubation with anti-tEGFR. A second blocking step was performed with the Fab fragment of murine IgG for 15 min, followed 3% goat serum for 15 min, with subsequent incubation with anti-CD68. All other steps were as described. RELA staining and confocal microscopy was performed as described[159].

Immunoperoxidase Staining for pEGFR Y1068

Staining for pEGFR in human colonic biopsies was performed as described[74].

Immunoperoxidase Staining

CD68, MPO, and pSTAT6

After overnight heating at 37°C, sections were deparaffinized in xylene and rehydrated in graded alcohols. Sections were incubated with primary antibody overnight at room temperature. After washing, incubation with anti-rabbit HRP-polymer was performed for 30 min. Sections were rinsed and incubated with streptavidin-HRP (Biocare Medical, Concord, CA, USA) for 30 min.

CD3, CD45R, and CD31

Heat-induced antigen retrieval was performed on the Leica Bond Max using Epitope Retrieval 2 solution for 10 min (CD3, CD31) and 20 min (CD45R). Slides were incubated with primary antibody for 1 h and incubated with secondary antibody for 15 min. CD31 Images were captured using a high throughput Leica SCN400 Slide Scanner automated digital image system. Tissue samples were mapped using Ariol® Review software. The numbers and areas of $CD31^+$ blood vessels were determined in the Ariol® software.

Scoring of CD68, MPO, CD3, and CD45R Immunoperoxidase Staining

Slides were scored in a blinded manner by a gastrointestinal pathologist (M. Blanca Piazuelo) Samples were evaluated for staining in non-tumor and tumor areas using the following scale: 0=scarce positive cells, 1=low abundance of positive cells, 2=moderate abundance of positive cells, and 3=high abundance of positive cells. The two scores were combined for a highest possible score of 6.

Purification of colonic epithelial cells

Purification of colonic epithelial cells was performed as described[143].

Statistical Analysis

Data represent mean ± S.E.M. Where data were normally distributed, two-tailed Student's *t* test was used to determine significance in experiments with only two groups, and one-way ANOVA with the

Newman-Keuls test was used to determine significant differences between multiple test groups. In Figure 4, the data were square root transformed to ensure normal distribution prior to statistical analysis. In other cases where data were not normally distributed, a one-way ANOVA with Kruskal-Wallis test, followed by a Mann-Whitney *U* test, was performed. Please see Appendix B, Table 5 for all relevant *P* values as determined by Kruskal-Wallis test. Statistical analysis of all weight loss curves was performed by two-way ANOVA with Bonferroni post-test. All statistics were performed in Prism 5.0 (GraphPad Software, San Diego, CA, USA). A *P* value of < 0.05 was considered significant.

CHAPTER 4

TRIM28 IS A DOWNSTREAM TARGET OF EGFR IN MACROPHAGES

4.1 Introduction

EGFR signaling can encompass many different downstream pathways[59,60,71]. The studies outlined in Chapter 2 and Chapter 3 identified NF-κB signaling (Figure 13 and Figure 23), MAPK1/3 signaling (Figure 14) and STAT6 signaling (Figure 22) as being downstream of EGFR in macrophages. Next, we sought to determine other unique pathways that are downstream of EGFR in macrophages, especially considering that EGFR signaling in macrophages is a highly understudied area. Identification of pathways downstream of EGFR that are specific to macrophages may provide highly specific targets in the treatment of chronic inflammatory conditions.

4.2 Results

To address questions related to downstream signaling targets of EGFR in macrophages, we utilized the unbiased, phospho-proteomics based, SILAC approach. Three two-plex SILAC assays were performed in RAW 264.7 cells. Cells either treated with gefitinib (gefitinib only), infected with *H. pylori* PMSS1 (PMSS1 only), or treated with gefitinib and infected with *H. pylori* PMSS1 (PMSS1 + gefitinib) were labeled with “heavy” amino acids. Untreated, uninfected cells were labeled with “light” amino acids, and aliquots were utilized as the control sample in each two-plex SILAC experiment. Each SILAC experiment was performed in duplicate. The experimental design is outlined in Figure 26A.

Between two independent experiments, We identified 11,081 total phospho-peptides in the gefitinib only group, 12,088 total phospho-peptides in the PMSS1 only group and 12,997 total phospho-peptides in the PMSS1 + gefitinib group. There was significant overlap in the number of unique phospho-proteins identified between each replicate experiment, indicating a high degree of fidelity in these experiments (Figure 26B).

Upon completion of each set of SILAC experiments, the data from each replicate were normalized and phospho-peptides common to both replicates were compiled for further analysis. The

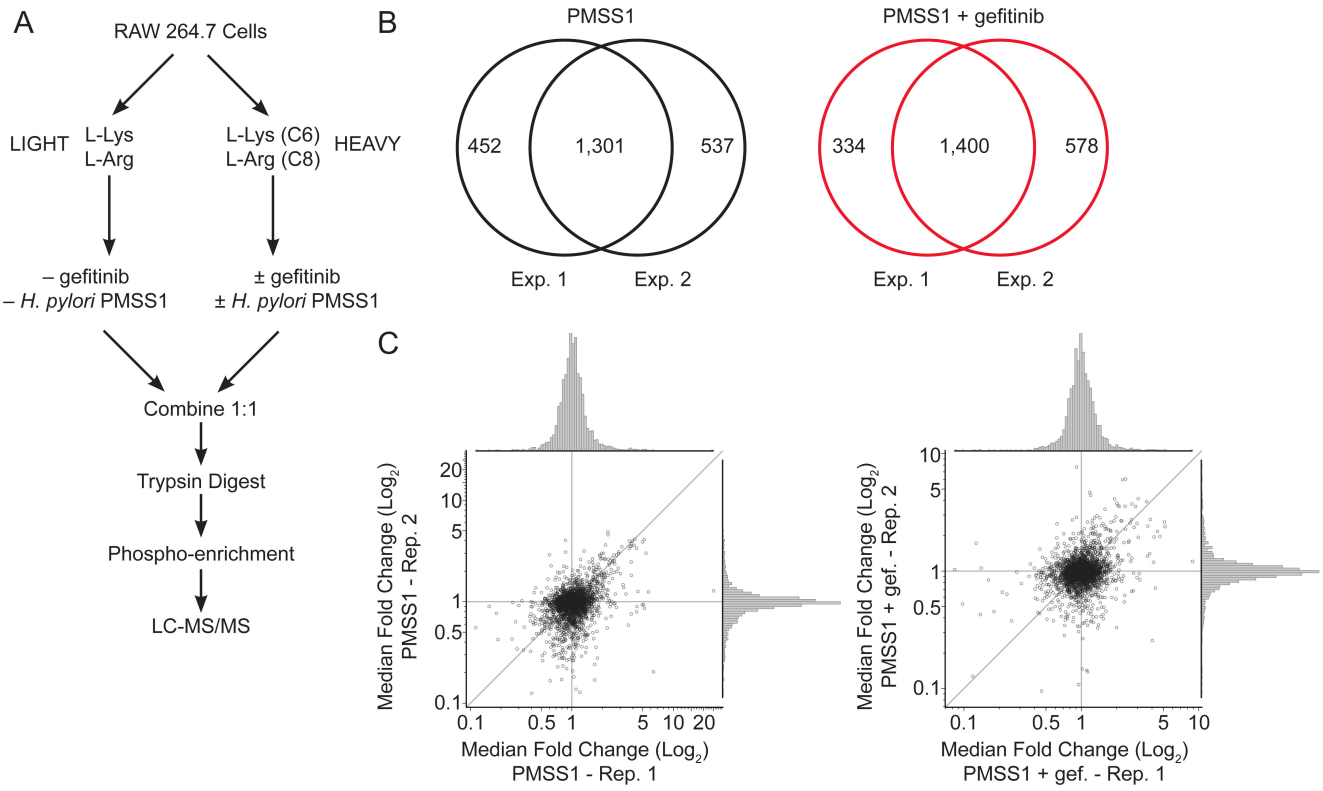

Figure 26. Schematic overview of SILAC experimental set-up and phosphopeptides identified in replicate experiments. (A) Diagram of experimental set-up for SILAC. (B) Venn diagrams depicting the number of phosphoproteins identified in each data set, both unique to one experimental replicate and overlapping between replicate experiments. (C) Scatterplots with normalized histograms demonstrating the degree of overlap in identified phosphopeptides in each experimental replicate.

normalized and combined datasets were then examined and we selected phospho-peptides for further analysis that met the following criteria. First, the gefitinib only data set was filtered such that phospho-peptides that had a positive or negative fold change of ≤ 1.2 were selected. Second, the PMSS1 only data set was filtered such that phospho-peptides that had a positive or negative fold change of ≥ 1.5 in the PMSS1-only cells were selected. The PMSS1 + gefitinib group was not filtered in any way so that phospho-peptides that were both affected or unaffected by gefitinib treatment and *H. pylori* infection could be identified. Finally, the phospho-peptides that were present in each replicate of the three data sets were selected and combined, provided they met the aforementioned criteria. The analysis pipeline is outlined in Figure 27A. We identified 104 unique phospho-peptides that were altered by *H. pylori* PMSS1 infection, but not altered by gefitinib treatment alone, according to the aforementioned criteria (Figure 27B). The data set was then manually curated to identify phospho-peptides that were altered by gefitinib treatment during *H. pylori* infection.

Once these parameters were applied, several phospho-peptides were selected for validation by western blotting. Phosphorylation of TRIM28 S473 was identified as being induced by *H. pylori* infection and significantly decreased in abundance by gefitinib treatment, during *H. pylori* infection (Figure 27B and Figure 28A). Western blotting confirmed the findings from the SILAC data sets. Indeed, TRIM28 pS473 is upregulated during *H. pylori* PMSS1 infection in RAW 264.7 cells, and gefitinib treatment reduces TRIM28 pS473 levels at multiple timepoints (Figure 28A-28D). Additionally, these data related to the phosphorylation of TRIM28 S473 was confirmed in both WT BMmacs treated with gefitinib and $Egfr^{fl/fl}$ and $Egfr^{\Delta mye}$ BMmacs (Figure 28E, 28F, and 28G). TRIM28 is a known transcriptional repressor in macrophages[175,176] and may represent a unique pathway by which EGFR signaling modulates macrophage activation. Further studies related to the role of TRIM28 pS473 in macrophages during *H. pylori* infection are planned.

Furthermore, two additional phospho-peptides – ribosomal protein S6 (RPS6) S235/236 and stathmin (STMN1) S25 – were confirmed via western blotting. RPS6 pS235/236 was induced by *H. pylori* infection and decreased with gefitinib treatment by both SILAC (Figure 29A) and western blotting (Figure 29B and 29C). STMN1 pS25 is induced by *H. pylori* infection, but is unaffected by gefitinib

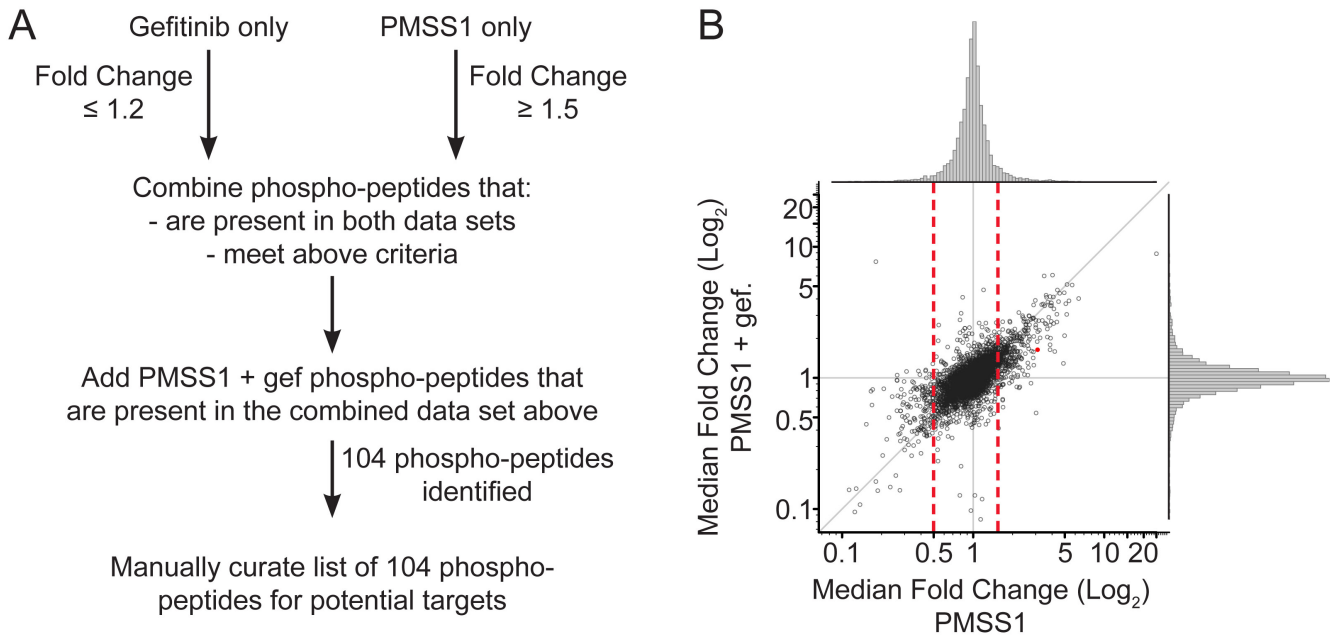

Figure 27. Pipeline of SILAC data analysis and identification of downstream targets of EGFR signaling during *H. pylori* infection of macrophages. (A) Pipeline of data analysis of phospho-peptides identified in SILAC analysis. The gefitinib only, PMSS1 only, and PMSS1 + gef. replicate experiments were combined prior to this analysis. (B) Scatterplot with normalized histogram demonstrating potential targets of interest that were up- or down-regulated by ≥1.5 fold versus control samples in the PMSS1 group. Red dot = TRIM28 pS473.

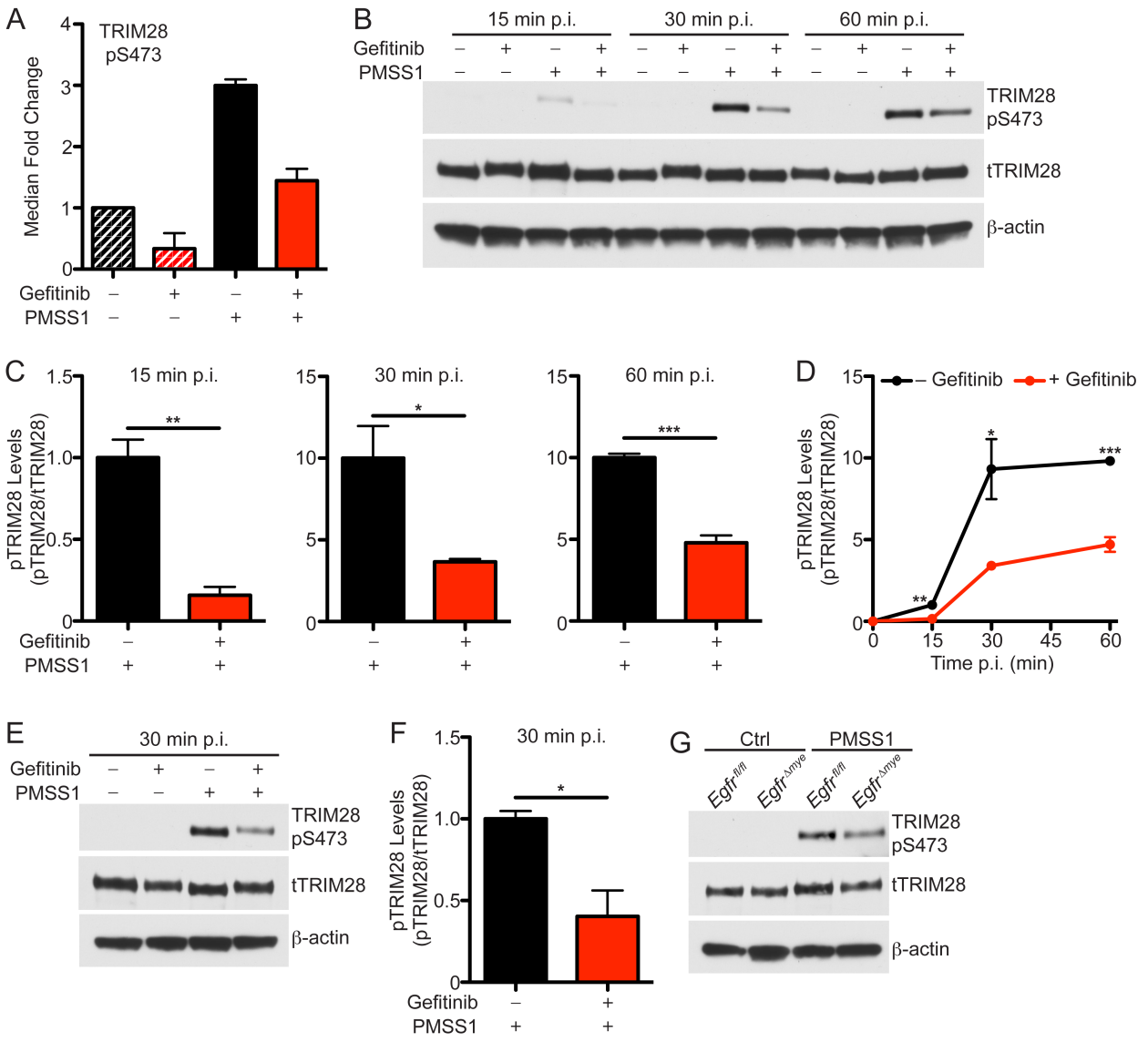

Figure 28. TRIM28 is a potential downstream target of EGFR signaling in macrophages. (A) Median fold change of TRIM28 pS473 in RAW 264.7 cells in replicate SILAC experiments in the gefitinib, PMSS1, and PMSS1 + gefitinib groups at 30 min p.i. (B) Representative western blot of TRIM28 pS473 levels in RAW 264.7 cells at indicated time points p.i. with *H. pylori* PMSS1 ± 10 μM gefitinib. *n* = 3 biological replicates. (C) Densitometric analysis of TRIM28 pS473 levels at 15, 30, and 60 min p.i. from (B). * $P < 0.05$, ** $P < 0.01$, *** $P < 0.001$ by two-tailed Student's *t* test. (D) Densitometric analysis of the kinetics of TRIM28 pS473 levels from (B). ** $P < 0.01$, *** $P < 0.001$ by one-way ANOVA with Newman-Keuls post-test. (E) Representative western blot of TRIM28 pS473 levels in WT BMmacs at indicated time point p.i. with *H. pylori* PMSS1 ± 10 μM gefitinib. *n* = 3 biological replicates. (F) Densitometric analysis of TRIM28 pS473 from (E). * $P < 0.05$ by two-tailed Student's *t* test. (G) Representative western blot of TRIM28 pS473 levels in $Egfr^{fl/fl}$ and $Egfr^{\Delta mye}$ BMmacs at indicated time point p.i. with *H. pylori* PMSS1. *n* = 2 biological replicates.

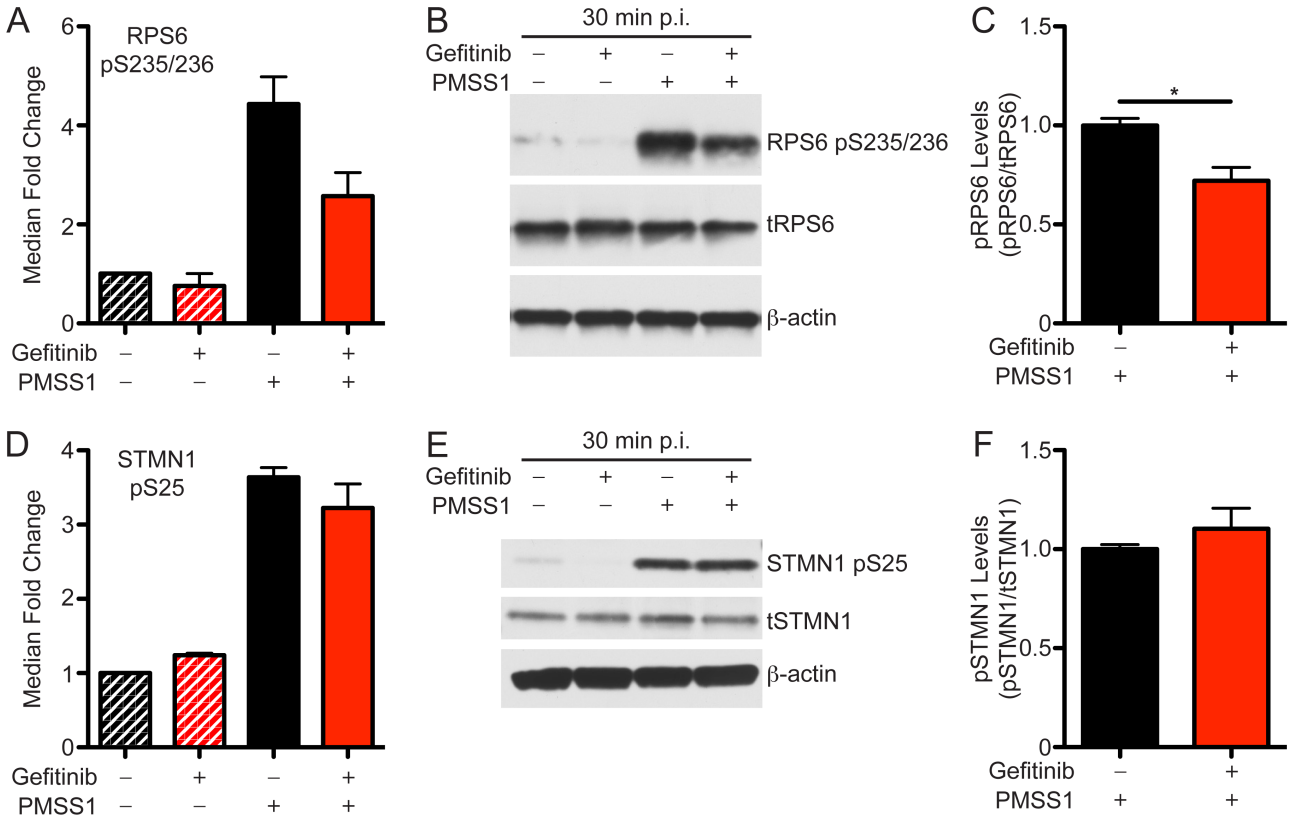

Figure 29. Validation of additional targets identified in SILAC experiments. (A) Median fold change of RPS6 pS235/236 in RAW 264.7 cells in replicate SILAC experiments in the gefitinib, PMSS1, and PMSS1 + gefitinib groups at 30 min p.i. (B) Representative western blot of RPS6 pS235/236 levels in RAW 264.7 cells at indicated time points p.i. with *H. pylori* PMSS1 ± 10 μM gefitinib. *n* = 3 biological replicates. (C) Densitometric analysis of RPS6 pS235/236 levels at 15, 30, and 60 min p.i. from (B). * $P < 0.05$ by two-tailed Student's *t* test. (D) Median fold change of STMN1 pS25 in RAW 264.7 cells in replicate SILAC experiments in the gefitinib, PMSS1, and PMSS1 + gefitinib groups at 30 min p.i. (E) Representative western blot of STMN1 pS25 levels in RAW 264.7 cells at indicated time points p.i. with *H. pylori* PMSS1 ± 10 μM gefitinib. *n* = 3 biological replicates. (F) Densitometric analysis of STMN1 pS25 levels at 15, 30, and 60 min p.i. from (E).

treatment by both SILAC (Figure 29D) and western blotting (Figure 29E and 29F). These data confirm the robustness of the SILAC experiments and demonstrate that further studies related to the phospho-peptides identified via SILAC are valid.

4.3 Discussion

The data discussed above are preliminary in nature. Two replicate SILAC analyses were performed, with limited follow-up studies. Further bioinformatic analyses are currently ongoing to create a more global understanding of the proteins involved in signaling downstream of EGFR in macrophages. Such studies will allow for mapping of pathways from the entire SILAC dataset and a better understanding of the relationships between identified phospho-peptides. Moreover, further analysis will provide insight into the kinases involved in the phosphorylation of identified peptides. Overall, the goal is to understand the role of EGFR signaling in macrophages on a global scale.

4.4 Materials and Methods

Reagents

All reagents for SILAC analysis were purchased from Fisher Scientific (Waltham, MA, USA).

Cell Culture

To label RAW 264.7 cells with the “light” and “heavy” amino acids, RAW cells were passaged in DMEM (Cat. no. PI-89985) with 10% dialyzed stem cell FBS (Cat. no. PI-88212), 2 mM L-glutamine, 25 mM HEPES, 10 mM sodium pyruvate, 0.23 mg/mL L-proline (Cat. no. PI-88211) and the following for either “light” or “heavy” cells. LIGHT: 0.1 mg/mL L-lysine-2HCl (Cat. no. PI-89987) and 0.1 mg/mL L-arginine-HCl (Cat. no. PI-89989). HEAVY: 0.1 mg/mL L-lysine-2HCl, ^{13}C6 and ^{15}N2 (Cat. no. PI-88209) and 0.1 mg/mL L-arginine-HCl, ^{13}C6 and ^{15}N4 (Cat. no. PI-89990). Following eight passages of cells in the “light” and “heavy” SILAC media, cells were tested for labeling by mass spectrometry. For SILAC, >

95% of proteins must be labeled with either “light” or “heavy” amino acids. Additional passages and labeling checks were performed as needed to achieve at least 95% labeling.

Once labeling was completed, “light” cells were utilized for untreated, uninfected control cells and “heavy” cells were utilized for gefitinib only cells, *H. pylori* PMSS1 only cells, and *H. pylori* PMSS1 + gefitinib cells. Cells were pre-treated for 1 h with 10 μM gefitinib and then infected for 30 min at an MOI of 100.

For confirmatory studies following SILAC analysis, culture of RAW 264.7 cells and BMmacs was performed as described in Chapter 2. Culture and usage of *H. pylori* PMSS1 was performed as described in Chapter 2.

Lysis of cells for SILAC

Following infection, cells were lysed in 50 mM Tris-HCl (pH 7.6), 150 nM NaCl, 1% NP-40, 2 mM EDTA in water. No protease or phosphatase inhibitors were added to lysis buffer. 1 mg protein was utilized for SILAC analysis.

Mass Spectrometry and SILAC analysis

The mass spectrometry and subsequent SILAC analysis was performed as previously described[74].

Western Blotting

Western blotting was performed as described in Chapter 2.

CHAPTER 5

ODC IN MACROPHAGES DURING BACTERIAL INFECTION

5.1 Introduction

Polyamine metabolism is a process critical for life occurring within all mammalian cell types[84,85]. Polyamines have ubiquitous roles in many cellular functions, including growth, proliferation, and differentiation[85]. Importantly, polyamines have also been implicated in the alteration of histone modifications and chromatin structure and thus might broadly affect DNA stability and transcription[90,92,93]. The production of the three major polyamines – putrescine, spermidine, and spermine – is tightly regulated and centers on the rate-limiting enzyme, ODC[84,97]. ODC utilizes the substrate, L-ornithine, to produce putrescine via a decarboxylation reaction[84,97]. Given its essential and central role in regulating polyamine metabolism within cells, ODC has been highly studied and implicated in several malignancies, including breast, colorectal, and gastric cancer[91,177-180]. However, most of the studies related to ODC have been focused on its role in epithelial cell function, leaving many questions surrounding the role of ODC in immune cells unanswered.

In particular, macrophages are a significant component of the innate immune cell compartment and play wide-ranging roles in immune surveillance, responses to pathogens, wound healing, embryonic development, and regulation of the tumor microenvironment[2,3]. An essential step in the responses to pathogens is macrophage activation. Macrophages have the capacity to alter cytokine/chemokine production and various other functions along the spectrum of M1 or M2 activation based on the stimulus detected[2,3,143]. M1 macrophages represent a highly pro-inflammatory and anti-microbial subset of macrophages[2,3,143]. M2 macrophages have various roles in wound repair, anti-parasitic responses, control of inflammation, and have been implicated in tumor development and growth[7,11,98]. The role of ODC has been well characterized in M2 macrophage responses to various parasitic and fungal infections[181-183], but the role of ODC in macrophages during M1 responses have been less well studied[184]. We have demonstrated that ODC expression is upregulated during bacterial infections[47,95,113,185], but the role in macrophage activation patterns requires further investigation.

To address this question, we utilized *Helicobacter pylori*, a globally pervasive human pathogen that represents the single greatest risk factor in the development of gastric cancer[21,23,27,102]. *H. pylori* establishes a chronic infection in humans, which can be recapitulated in mice[143], marked by continuous, low-grade inflammation and host tolerance of the pathogen[9,40,41,111]. We also utilized the *C. rodentium* infectious colitis model[113,131]. *C. rodentium* is an enteric bacterial pathogen that forms attaching and effacing lesions in the colon and is similar to enteropathogenic *Escherichia coli* infection in humans[104]. As macrophages are known to have a critical role in *H. pylori*-mediated gastritis[20,143] and *C. rodentium* colitis[143], we sought to interrogate the specific role of ODC in macrophages during these enteric infections, utilizing a myeloid/macrophage-specific *Odc* knockout mouse.

In this study, we have uncovered a novel mechanism by which ODC and its product, putrescine, regulates macrophage activation and function. We show that macrophage-derived ODC plays a critical role in the inhibition of M1 macrophage activation to promote persistence of infection. This defect in M1 macrophage activation is directly regulated by polyamine production that modulates chromatin structure, as determined by alterations in histone modification markers *in vitro* and *in vivo*, which prevents pro-inflammatory gene transcription.

5.2 Results

Myeloid-specific ODC deletion enhances gastritis and bacterial killing during *H. pylori* infection

As we have previously demonstrated that ODC plays a significant role in macrophage function during *H. pylori* infection *in vitro*[47,95,186], we hypothesized that macrophage-derived ODC would have significant effects on *H. pylori* pathogenesis, specifically in the regulation of gastric inflammation. As *H. pylori* is a human pathogen, we first assessed ODC levels in mononuclear cells in gastric biopsies from *H. pylori*-infected patients with chronic active gastritis from Colombia, where overall risk of gastric cancer is high[33,37]. We found that *H. pylori* infection leads to a significant increase in ODC levels in mononuclear cells, which includes abundant expression in cells with the appearance of macrophages (Figure 30A and 30B).

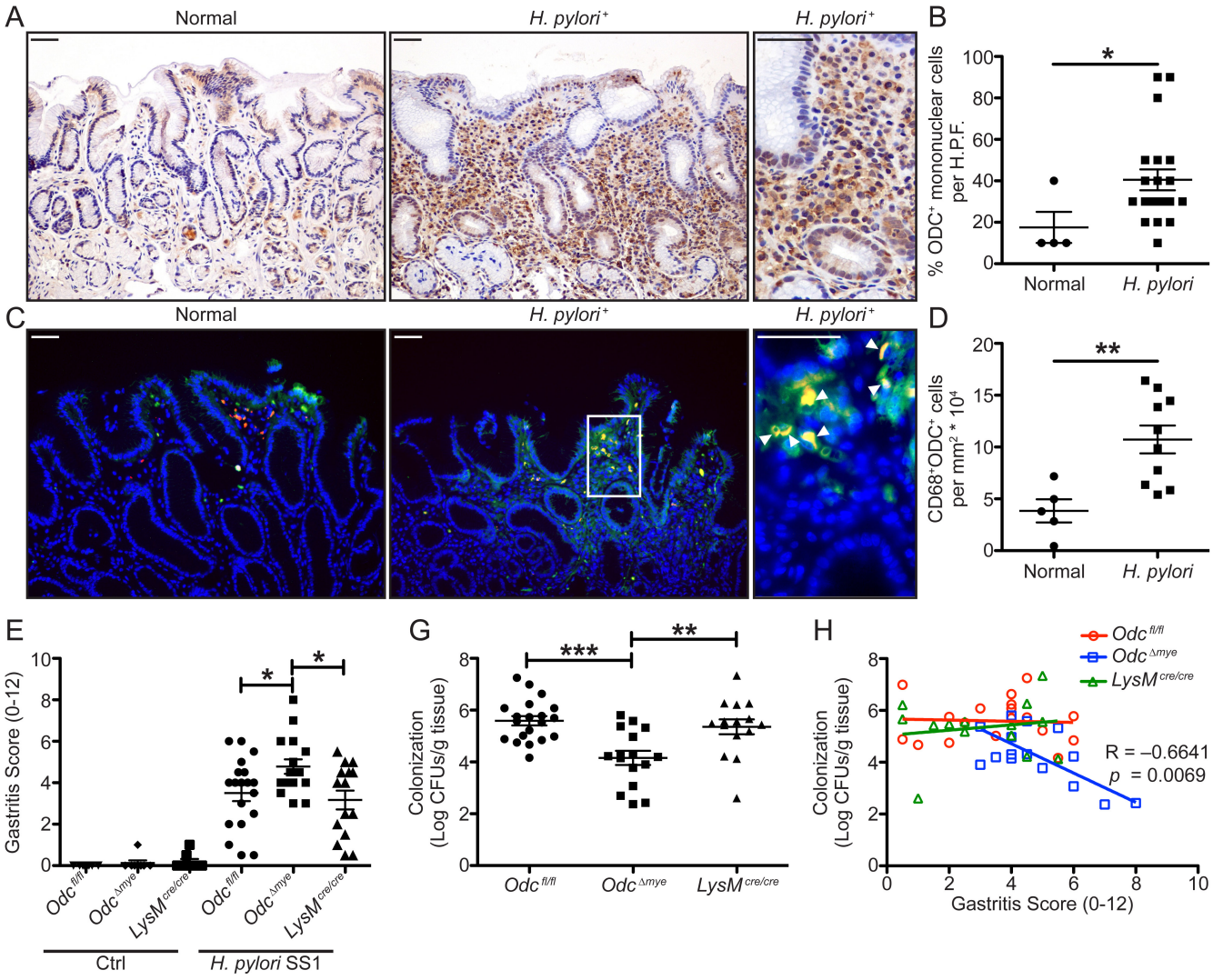
A
Normal
H. pylori+
H. pylori+
B
% ODC+ mononuclear cells per H.P.F.
100
80
60
40
20
0
*
Normal
H. pylori
C
Normal
H. pylori+
H. pylori+
D
CD68+ODC+ cells per mm2 * 10^4
20
15
10
5
0
**
Normal
H. pylori
E
Gastritis Score (0-12)
10
8
6
4
2
0
*
*
Odc fl/fl
Odc Δmye
LysM cre/cre
Odc fl/fl
Odc Δmye
LysM cre/cre
Ctrl
H. pylori SS1
G
Colonization (Log CFUs/g tissue)
8
6
4
2
0
***
**
Odc fl/fl
Odc Δmye
LysM cre/cre
H
Odc fl/fl
Odc Δmye
LysM cre/cre
Colonization (Log CFUs/g tissue)
R = –0.6641
p = 0.0069
0
2
4
6
8
10
Gastritis Score (0-12)
F
Odc fl/fl
Odc Δmye
LysM cre/cre
H. pylori SS1
I
Odc fl/fl
Odc Δmye
LysM cre/cre
H. pylori SS1

Figure 30. *Odc*$^{\Delta mye}$ mice have significantly increased histologic gastritis, but significantly decreased *H. pylori* burden after chronic infection. (a) Representative immunoperoxidase staining for ODC in human gastric biopsies from patients with normal mucosa and with *H. pylori*-positive gastritis. Scale bars = 50 μm. (b) Quantification of the percentage of ODC$^+$ mononuclear cells in gastric biopsies from (a). *n* = 4 normal biopsies and 20 *H. pylori*$^+$ gastric biopsies with chronic active gastritis. **P*<0.05 by Mann-Whitney *U* test. H.P.F. = high power field. (c) Representative immunofluorescence images of ODC from gastric biopsies in (a) and (b). Green = ODC, Red = CD68, Yellow = Merge, Blue = DAPI. Closed arrows indicate CD68$^+$ODC$^+$ macrophages. Boxed area indicates image shown in higher magnification. Scale bars = 50 μm. Note that different cases were utilized for representative images in (a) and (c). (d) Quantification of the number of CD68$^+$ODC$^+$ cells in the cases from (c). *n* = 5 normal biopsies and 10 *H. pylori*$^+$ gastric biopsies with chronic active gastritis. ***P*<0.05 by Student's *t* test. (e) Histologic gastritis scores were assessed 4 mo p.i. by a gastrointestinal pathologist in a blinded manner according to the updated Sydney System. (f) Representative H&E images from infected mice in (e). Scale bars = 100 μm. (g) Colonization of *H. pylori* SS1 was assessed by serial dilution and culture 4 mo p.i. In (e) and (g) **P*<0.05, ***P*<0.01, ****P*<0.001 by one-way ANOVA with Newman-Keuls post-test. *n* = 8-10 uninfected and 15-19 *H. pylori* SS1-infected mice per genotype. (h) Correlation between histologic gastritis in (e) and *H. pylori* SS1 colonization levels in (g). Correlation and significance determined by Pearson's product-moment correlation test. (i) Representative immunofluorescence images of ODC from infected mice in (e) and (g). Green = ODC, Red = CD68, Yellow = Merge, Blue = DAPI. Closed arrows indicate CD68$^+$ODC$^+$ macrophages. Open arrows indicate CD68$^+$ODC$^-$ macrophages. Scale bars = 50 μm. Data displayed as mean ± S.E.M.

To confirm that human macrophages express increased ODC during *H. pylori* infection, we performed immunofluorescence staining for ODC and CD68, a macrophage marker, on a subset of the cases from Colombia. Control staining in which no primary anti-ODC antibody was utilized was performed to confirm the specificity of the staining (Appendix C, Figure 1A). As expected, the number of $CD68^+$ macrophages was increased in the *H. pylori*$^+$ cases when compared to the normal cases (Appendix C, Figure 1B). While there was no difference in the number of $CD68^+ODC^-$ macrophages between normal and *H. pylori*$^+$ cases (Appendix C, Figure 1C), we found a significant increase in the number of $CD68^+ODC^+$ cells in the *H. pylori*-infected cases versus control cases (Figure 30C and 30D). Moreover, the percentage of $CD68^+ODC^+$ macrophages per the total number of $CD68^+$ macrophages was significantly higher in *H. pylori*$^+$ cases (Appendix C, Figure 1D) These data indicate that *H. pylori* infection is associated with upregulated ODC in human gastric macrophages, which led us to hypothesize that ODC has an important role in regulating macrophage function during infection.

To investigate the role of macrophage-derived ODC further, we generated mice with a myeloid-specific deletion of *Odc*, by crossing C57BL/6 *Odc*$^{fl/fl}$ mice with myeloid-specific *LysM*$^{cre/cre}$ driver mice, yielding the *Odc*$^{\Delta mye}$ mouse (Appendix C, Figure 2A). We assessed *Odc* mRNA levels in $CD11b^+$ myeloid cells and $CD11b^-$ non-myeloid cells from the gastric lamina propria of mice infected with *H. pylori* PMSS1 for 48 h, the peak of gastric macrophage infiltration[97,110], as well as in gastric epithelial cells (GECs). Importantly, only the $CD11b^+$ lamina propria cells demonstrated induction of *Odc* during *H. pylori* infection, which was ablated in *Odc*$^{\Delta mye}$ $CD11b^+$ cells (Appendix C, Figure 2B). Notably, *Odc* was not induced in $CD11b^-$ cells or GECs, and *Odc* mRNA levels were not altered in these cells derived from the *Odc*$^{fl/fl}$ and *Odc*$^{\Delta mye}$ mice (Appendix C, Figure 1C), consistent with the specificity of the knockout. We also demonstrated sufficient *Odc* knockdown in primary BMmacs by RT-PCR and western blotting during *H. pylori* infection (Appendix C, Figure 2C, 2D, 2E).

Additionally, expression levels of *Lyz2*, the gene on which the CRE recombinase was placed, and *Cre* were assessed in *H. pylori* SS1-infected gastric tissues and in *H. pylori* PMSS1-infected BMmacs from *Odc*$^{fl/fl}$, *Odc*$^{\Delta mye}$, and *LysM*$^{cre/cre}$ mice. At 4 mo p.i., gastric *Lyz2* mRNA was nearly undetectable, while *Cre* mRNA was abundant in both infected and uninfected *Odc*$^{\Delta mye}$ gastric tissue

(Appendix C, Figure 3A). Conversely, *Lyz2* was induced upon infection in $Odc^{fl/fl}$ gastric tissues and no *Cre* was detected (Appendix C, Figure 3A). These data were recapitulated in BMmacs from $Odc^{fl/fl}$, $Odc^{\Delta mye}$, and $LysM^{cre/cre}$ mice (Appendix C, Figure 3B). The maintenance of the *Lyz2* deletion and of high *Cre* expression during acute and chronic infection confirms the durability of the *Odc* deletion over time[143].

Upon confirmation of *Odc* knockdown in myeloid cells, $Odc^{fl/fl}$, $Odc^{\Delta mye}$, and $LysM^{cre/cre}$ mice were investigated for their response to infection with *H. pylori* SS1 for 4 mo, a model of chronic *H. pylori* infection[47,103,143,185]. $Odc^{\Delta mye}$ mice demonstrated significantly enhanced acute and chronic histologic gastritis, as compared to either $Odc^{fl/fl}$ or $LysM^{cre/cre}$ mice (Figure 30E and 30G). Consistent with previous studies[111,112,143,185] in which colonization and gastritis are typically inversely related, the enhanced gastritis was correlated with significantly decreased *H. pylori* burden in $Odc^{\Delta mye}$ mice (Figure 30G and 30H), indicating that ODC has an important role in regulating anti-microbial inflammation in the stomach. Importantly, there were no detectable phenotypic differences between the $Odc^{fl/fl}$ or $LysM^{cre/cre}$ mice, confirming all phenotypes are being driven by *Odc* deletion (Figure 30E-30H).

ODC knockout was confirmed by immunofluorescence in $CD68^+$ gastric macrophages from chronically-infected gastric tissues from $Odc^{fl/fl}$, $Odc^{\Delta mye}$, and $LysM^{cre/cre}$ mice. ODC co-localized with $CD68^+$ macrophages in both $Odc^{fl/fl}$ and $LysM^{cre/cre}$ gastric tissues, while ODC was not expressed in $CD68^+$ cells in $Odc^{\Delta mye}$ gastric tissues (Figure 30I). Control staining in which no primary anti-ODC antibody was utilized confirmed the specificity of the immunofluorescence (Appendix C, Figure 4). These data further confirmed successful deletion of *Odc* in macrophages, as well as maintenance of the knockout over time and during infection.

We next sought to determine if the role of ODC in macrophages was specific to *H. pylori* pathogenesis. *Odc* expression was also upregulated in BMmacs exposed to *C. rodentium* and was markedly attenuated in $Odc^{\Delta mye}$ BMmacs (Appendix C, Figure 5A). $Odc^{fl/fl}$ and $Odc^{\Delta mye}$ mice were inoculated with *C. rodentium* for 14 days. As in the chronic *H. pylori* model, $Odc^{\Delta mye}$ mice exhibited significantly increased levels of histologic inflammation and injury, represented by higher colitis scores, as compared to $Odc^{fl/fl}$ mice (Appendix C, Figure 5B and 5C). Moreover, tissues from $Odc^{\Delta mye}$ mice had

increased colon weight as a percentage of body weight on the day of sacrifice (Appendix C, Figure 5D), which is a marker of increased disease severity[131]. The significant increases in colitis and disease severity were concordant with the increased histologic gastritis observed in the *H. pylori* model, indicating that the role of ODC in regulating macrophage activation responses is conserved across various bacterial infections. However, differences in *C. rodentium* burden were not detected in colonic tissues between $Odc^{fl/fl}$ and $Odc^{\Delta mye}$ mice (Appendix C, Figure 5E); this finding is consistent with our prior reports that while diminished immune response can result in increased colonization[106,143], increased inflammation does not lead to decreased colonization in this model[187].

ODC deletion augments pro-inflammatory cytokine and chemokine production *in vivo*

Our *in vivo* findings demonstrated that macrophage-derived ODC has an anti-inflammatory role during bacterial pathogenesis. Thus, we hypothesized that the loss of ODC in macrophages leads to enhanced innate immune responses to *H. pylori*. We utilized a Luminex Multiplex Array to assess 25 distinct chemokines and cytokines in gastric tissues from chronically-infected $Odc^{fl/fl}$, $Odc^{\Delta mye}$, and $LysM^{cre/cre}$ mice. Nine analytes were significantly increased at the protein level in *H. pylori*-infected $Odc^{\Delta mye}$ gastric tissues, when compared to $Odc^{fl/fl}$ or $LysM^{cre/cre}$ gastric tissues. C-C motif ligand chemokines, CCL2 (MCP-1), CCL3 (MIP-1α), CCL4 (MIP-1β), and CCL5 (RANTES), and C-X-C motif ligand (CXCL) chemokines, CXCL1 (GROα, KC), CXCL2 (MIP2), and CXCL10 (IP-10), were all significantly increased in $Odc^{\Delta mye}$ gastric tissues (Figure 31). The enhanced chemokine production suggests that the deletion of macrophage ODC has a role in enhancing immune cell infiltration into the stomach, contributing to the significantly increased inflammation. Additionally, the cytokines IL-17 and TNF-α were detected at significantly higher levels in $Odc^{\Delta mye}$ gastric tissues at 4 mo p.i. (Figure 31). IL-17 is a hallmark of the Th17 response[188], especially in *H. pylori* infection[143], indicating an enhanced pro-inflammatory T cell response to *H. pylori* and a diminished ability to control infection[124] under conditions of macrophage *Odc* deletion. Many cell types can produce TNF-α, especially M1-activated macrophages[3]. Analytes that were either not induced by infection in any of the genotypes, were not significantly different between genotypes, or were not detected are listed in Appendix C, Table 1.

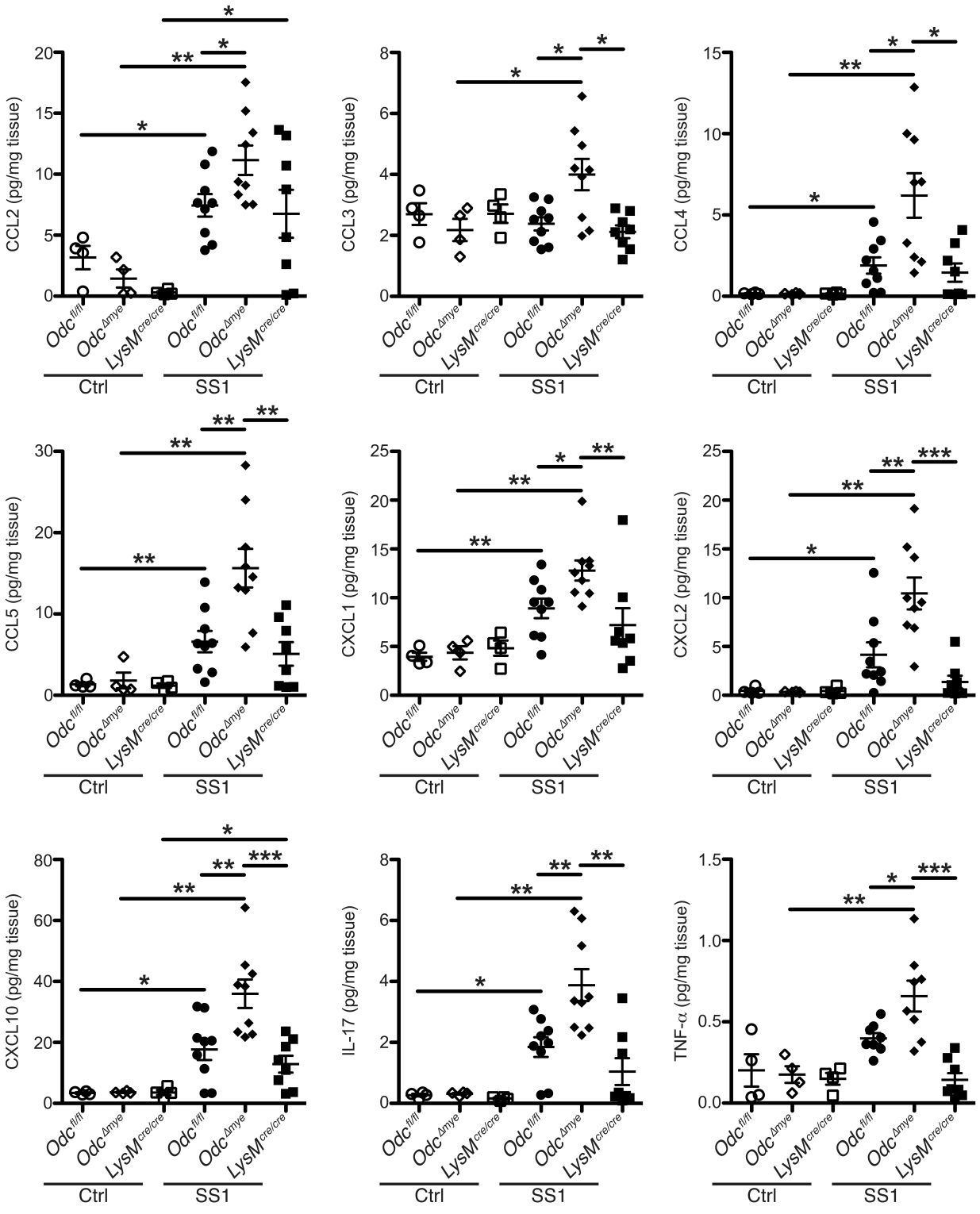

Figure 31. Cytokines and chemokines are significantly increased in *Odc*$^{\Delta mye}$ gastric tissues. Protein levels of the cytokines and chemokines CCL2 (MCP-1), CCL3 (MIP-1α), CCL4 (MIP-1β), CCL5 (RANTES), CXCL1 (KC/GRO-α), CXCL2 (MIP-2), CXCL10 (IP-10), IL-17, and TNF-α were assessed by Luminex Multiplex Array in gastric tissues 4 mo p.i. with *H. pylori* SS1. **P*<0.05, ***P*<0.01, ****P*<0.001 by one-way ANOVA with Kruskal-Wallis test, followed by Mann-Whitey *U* test. *n* = 4 uninfected and 8-9 *H. pylori* SS1-infected mice per genotype. Data displayed as mean ± S.E.M

ODC deletion leads to enhanced M1 macrophage activation during bacterial infections

The increased TNF-α levels in the context of myeloid-specific *Odc* deletion led us to hypothesize that ODC normally serves to suppress M1 macrophage activation. Thus, enhanced M1 responses in $Odc^{\Delta mye}$ mice would have the potential to orchestrate the highly pro-inflammatory immune response to both *H. pylori* and *C. rodentium*. To test our hypothesis, we expanded upon a previously utilized panel of genes marking M1 and M2 macrophage activation[143,185] and assessed expression levels of each marker in chronically-infected gastric tissues from $Odc^{fl/fl}$, $Odc^{\Delta mye}$, and $LysM^{cre/cre}$ mice. mRNA expression of M1 activation markers, *Il1b*, *Il6, Il12a* (*Il12p35*), *Il12b* (*Il12p40*), *Tnfa*, and *Nos2*, were induced during *H. pylori* infection in gastric tissues from each genotype (Figure 32A). Expression of each of these genes was markedly increased in $Odc^{\Delta mye}$ versus $Odc^{fl/fl}$ or $LysM^{cre/cre}$ gastric tissues (Figure 32A). Additionally, *C. rodentium*-infected colonic tissues demonstrated an induction of M1 marker expression that was further increased in $Odc^{\Delta mye}$ colonic tissues (Appendix C, Figure 6A). Taken together, these data demonstrate that the loss of ODC in myeloid cells significantly magnifies M1 macrophage activation in response to bacterial enteric pathogens.

Markers of M2 activation were also assessed in gastric and colonic tissues from *H. pylori*-infected mice. The following panel of M2 markers was utilized: *Arg1*, *Chil3* (*Ym1*), *Retnla* (*Relma*), *Il10*, *Tgfb*, and *Tnfsf14* (*Light*). *H. pylori* infection does not typically induce a robust M2 macrophage response[143,185]. Indeed, M2 genes *Arg1*, *Chil3*, *Retnla, Il10*, and *Tgfb* were not significantly induced in $Odc^{fl/fl}$ or $LysM^{cre/cre}$ gastric tissues (Appendix C, Figure 7A). *Tnfsf14* was significantly induced in $Odc^{fl/fl}$ and $LysM^{cre/cre}$ gastric tissues, but was significantly decreased in $Odc^{\Delta mye}$ gastric tissues (Appendix C, Figure 7A). Since *Tnfsf14* was the only M2 gene upregulated in infected gastric tissues, these data indicate that *H. pylori* infection does not induce a significant M2 response in mice during chronic infection.

Interestingly, $Odc^{\Delta mye}$ mice demonstrated enhanced *Arg1* expression in whole gastric tissue during *H. pylori* infection (Appendix C, Figure 7A); ARG1 is upstream of ODC and its upregulation may potentially represent a response to the loss of putrescine production by ODC in the myeloid-specific *Odc* knockout mice. However, based on previous studies, macrophages are not the likely source of

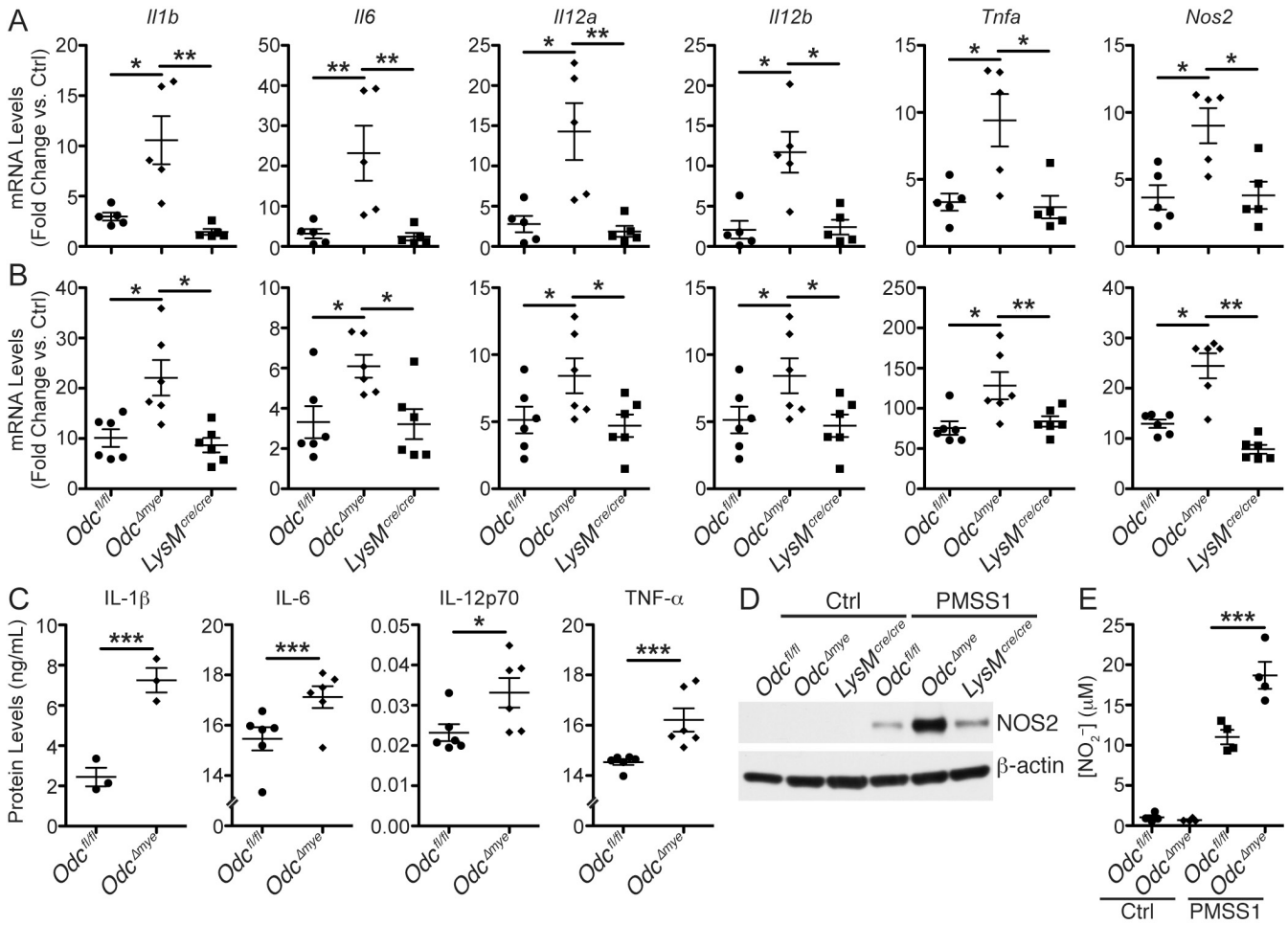

Figure 32. *Odc* deletion in macrophages enhances M1 macrophage activation during *H. pylori* infection. (a) mRNA levels of pro-inflammatory cytokines *Il1b*, *Il6*, *Il12a*, *Il12b*, *Tnfa*, and the gene *Nos2* were assessed by RT-PCR in gastric tissues 4 mo p.i. with *H. pylori* SS1. **P*<0.05, ***P*<0.01. *n* = 3 uninfected and 5 *H. pylori* SS1-infected mice per genotype. (b) mRNA levels of pro-inflammatory cytokines *Il1b*, *Il6*, *Il12a*, *Il12b*, *Tnfa*, and *Nos2* were assessed by RT-PCR in bone marrow-derived macrophages (BMmacs) 24 h p.i. with *H. pylori* PMSS1. **P*<0.05, ***P*<0.01. Statistical significance in (a) and (b) was calculated by one-way ANOVA with Kruskal-Wallis test, followed by Mann-Whitney *U* test. *n* = 6 mice per genotype. Note that the y-axis values for *Il1b*, *Il6,* and *Nos2* have been divided by a factor of 1000. All samples were analyzed as fold change against $Odc^{fl/fl}$ uninfected control samples. No differences were observed in the fold changes for uninfected samples from all genotypes. (c) Secreted levels of IL-1β, IL-6, IL-12p70, and TNF-α were measured by ELISA from supernatants of BMmacs 24 h p.i. with *H. pylori* PMSS1. **P*<0.05, ***P*<0.01 by one-way ANOVA with Newman-Keuls post-test. *n* = 3-6 mice per genotype. Note that none of the cytokines displayed were detected in supernatants from uninfected BMmacs. (d) Representative western blot of NOS2 levels in BMmacs 24 h p.i. with *H. pylori* PMSS1. *n* = 3 biological replicates. (e) Measurement of NO_2^- from BMmac supernatants 24 h p.i. with *H. pylori* PMSS1. ****P*<0.001 by one-way ANOVA with Newman-Keuls post-test. *n* = 4 mice per genotype. Data displayed as mean ± S.E.M.

Arg1 in these tissues[113,115]. Moreover, *Arg1* mRNA levels were significantly higher in $Odc^{\Delta mye}$ GECs than in $Odc^{fl/fl}$ GECs following *H. pylori* infection (Appendix C, Figure 7B), indicating that epithelial cells may be the source of increased *Arg1*. Taken together, these data indicate that ODC does not have a major role in regulating M2 activation, but that *Odc* deletion in macrophages allows for enhanced M1 activation.

To confirm the specificity of these findings to macrophages, we assessed macrophage activation in BMmacs from each of the genotypes infected *ex vivo* with either *H. pylori* or *C. rodentium*. As in the gastric tissues, *Il1b*, *Il6*, *Il12a*, *Il12b*, *Tnfa*, and *Nos2* mRNA levels were significantly increased in $Odc^{\Delta mye}$ BMmacs infected with *H. pylori* (Figure 32B). Representative M1 genes, *Il1b*, *Tnfa*, and *Nos2* were also increased in *C. rodentium*-infected $Odc^{\Delta mye}$ BMmacs (Appendix C, Figure 8) versus $Odc^{fl/fl}$ or $LysM^{cre/cre}$ BMmacs. Moreover, $Odc^{\Delta mye}$ BMmacs had significantly increased secreted levels of IL-1β, IL-6, IL-12p70, and TNF-α (Figure 32C), as well as increased NOS2 protein levels (Figure 32D) and NO production (Figure 32E) in response to *H. pylori* infection. Densitometry further confirmed the significant increase in NOS2 protein levels in $Odc^{\Delta mye}$ BMmacs (Appendix C, Figure 9). These data clearly demonstrate enhanced M1 macrophage activation at the functional level in *Odc*-deficient macrophages.

M2 marker gene expression revealed a more complicated picture in *H. pylori*-infected BMmacs. *Arg1*, *Chil3*, *Retnla*, and *Tnfsf14* were not induced by *H. pylori* infection, regardless of genotype (Appendix C, Figure 10A). However, *H. pylori* infection induced *Il10* and *Tgfb* mRNA expression, which was significantly increased in $Odc^{\Delta mye}$ BMmacs versus the control genotypes (Appendix C, Figure 10A). Protein levels of IL-10 confirmed the mRNA data, while TGF-β secretion was not altered between genotypes (Appendix C, Figure 10B). As M1 activation was consistently increased in <u>both</u> gastric tissues and BMmacs from $Odc^{\Delta mye}$ mice, and M2 activation was not, these data indicate that ODC is a key regulator of M1 macrophage activation during bacterial infections. In contrast, the potential role of ODC in M2 activation during bacterial infections is much less apparent.

To determine if the role of ODC was conserved in human macrophages, we utilized THP1 cells, a human monocytic cell line that can be differentiated into macrophages with PMA. We determined that *H. pylori* infection induced ODC expression at the mRNA and protein levels (Appendix C, Figure 11A,

B). We then treated THP1 cells with DFMO, an irreversible and specific ODC inhibitor[186], for 3 or 5 days and then infected with *H. pylori* PMSS1 for 6 h. We assessed M1 and M2 activation by RT-PCR. DFMO-treated, *H. pylori*-infected THP1 cells had a significant increase in induction of *IL1B*, *IL12A*, *IL12B*, and *TNFA* when compared to untreated, *H. pylori*-infected cells (Appendix C, Figure 11C). *IL10* expression was induced by infection, but DFMO treatment did not further alter expression (Appendix C, Figure 11D). Importantly, the data related to M1 marker expression demonstrate that ODC also has a role in regulating M1 activation in human macrophages.

Macrophage activation can occur in many settings beyond the context of bacterial infection[2,3,7,98]. We next sought to determine the global role of ODC in macrophage activation in BMmacs by utilizing prototypical stimuli of M1 and M2 activation that are not dependent upon bacterial infection. An M1 response was induced by stimulation with IFN-γ and LPS[3] and an M2 response was elicited via stimulation with IL-4[3]. M(IFN-γ/LPS) macrophages from $Odc^{\Delta mye}$ mice, as with *H. pylori*- or *C. rodentium*-infected macrophages, demonstrated significantly increased *Il1b*, *Tnfa*, and *Nos2* expression as compared to $Odc^{fl/fl}$ or $LysM^{cre/cre}$ BMmacs (Appendix C, Figure 12A). Interestingly, M(IL-4) macrophages from $Odc^{\Delta mye}$ mice had further upregulation of *Arg1* and *Chil3* (Appendix C, Figure 12B). Thus, ODC has the capacity to regulate subsets of macrophage activation in a stimulus-dependent manner. These data demonstrate the central role of ODC in regulating macrophage activation in general.

The role of ODC in macrophages is dependent upon the polyamine, putrescine.

As the rate-limiting enzyme in polyamine synthesis, ODC converts L-ornithine to the polyamine, putrescine[47,84,186], which can then be converted into spermidine and spermine. We determined putrescine, spermidine, and spermine levels by liquid chromatography-mass spectrometry (LC-MS) using deuterated d_8-polyamines as internal standards. Deletion of *Odc* resulted in significantly diminished putrescine and spermidine levels in macrophages at 6 h and 24 h p.i. (Figure 33A). *Odc* deletion resulted in modest spermine accumulation (Figure 33A), which has been demonstrated previously during ODC inhibition with DFMO[91]. Moreover, *H. pylori* infection resulted in increased

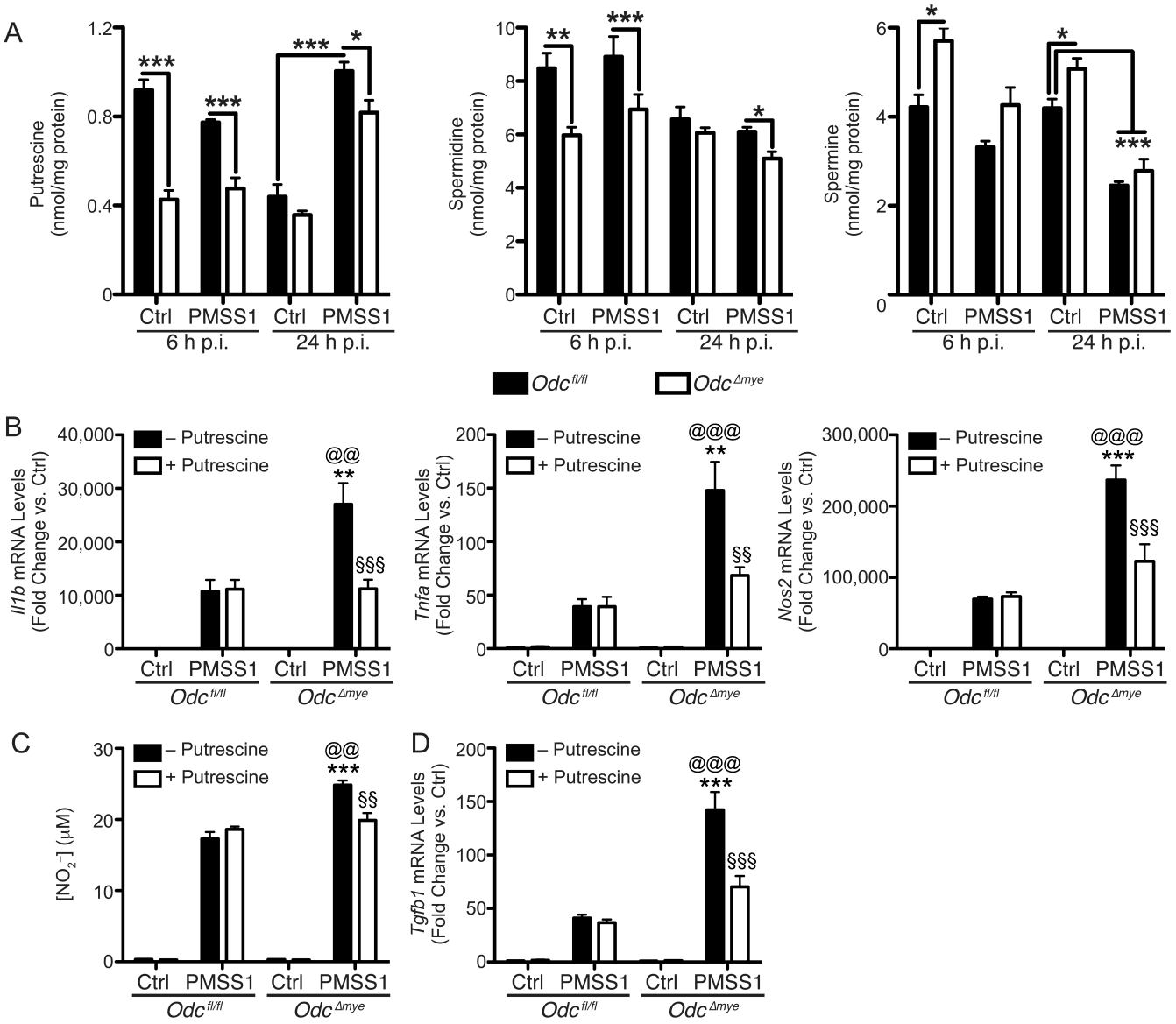

Figure 33. The effects of *Odc* deletion in macrophages are due to putrescine depletion. (a) Measurement of polyamine levels in BMmacs 6 h and 24 h p.i. with *H. pylori* PMSS1 by mass spectrometry. ***P<0.001 by one-way ANOVA with Newman-Keuls post-test. n = 3-4 mice per genotype. (b) mRNA levels of M1 cytokines *Il1b*, *Tnfa*, and *Nos2* were assessed by RT-PCR in BMmacs 24 h p.i. with *H. pylori* PMSS1 ± 25 mM putrescine added 60 min prior to infection. (c) Measurement of NO_2^- from BMmac supernatants 24 h p.i. with *H. pylori* PMSS1 ± 25 μM putrescine added 60 min prior to infection. (d) mRNA levels of the M2 cytokine, *Tgfb1*, were assessed by RT-PCR in BMmacs 24 h p.i. with *H. pylori* PMSS1 ± 25 μM putrescine added 60 min prior to infection. In (b-d), **P<0.01, ***P<0.001 vs. $Odc^{fl/fl}$ + PMSS1; @@P<0.01, @@@P<0.001 vs. $Odc^{fl/fl}$ + PMSS1 + putrescine; §§P<0.01, §§§P<0.001 vs. $Odc^{\Delta mye}$ + PMSS1 by one-way ANOVA with Newman-Keuls post-test. n = 4 biological replicates. Data displayed as mean ± S.E.M.

putrescine levels and decreased spermine levels in *Odc*$^{fl/fl}$ BMmacs at 24 h p.i. (Figure 33A), indicating that infection can modulate polyamine metabolism.

We hypothesized that addition of excess putrescine to the *Odc*$^{\Delta mye}$ BMmacs would serve to complement the deletion of *Odc* and reverse the enhanced M1 activation during *H. pylori* infection. Indeed, *H. pylori*-stimulated expression of *Nos2*, *Il1b*, and *Tnfa* in *Odc*$^{\Delta mye}$ BMmacs was no longer statistically increased compared to *Odc*$^{fl/fl}$ BMmacs when putrescine was added to the cells (Figure 33B). Moreover, the addition of putrescine significantly reduced NO production from infected *Odc*$^{\Delta mye}$ BMmacs, such that it was no longer significantly higher than NO production from *Odc*$^{fl/fl}$ BMmacs (Figure 33C). Putrescine had no effect on gene expression in *Odc*$^{fl/fl}$ BMmacs (Figure 33B, 33C, 33D). Intriguingly, the addition of putrescine had no effect on M2 macrophage activation (Appendix C, Figure 13), beyond its effect on *Tgfb* (Figure 33D).

ODC deletion in macrophages also enhances NLRP3-inflammasome activation.

IL-1β is the secreted effector protein of the NLR family, pyrin domain containing (NLRP) 3-driven inflammasome[189]. As we observed enhanced *Il1b* gene expression, we hypothesized that ODC may also affect NLRP3-inflammasome activation. We first assessed mRNA levels of NLRP3-inflammasome markers – *Nlrp3* and caspase 1 (*Casp1*), in both gastric tissues and BMmacs from *Odc*$^{fl/fl}$, *Odc*$^{\Delta mye}$, and *LysM*$^{cre/cre}$ mice. As expected, *Nlrp3* and *Casp1* expression was significantly higher in *Odc*$^{\Delta mye}$ mice during *H. pylori* infection than in the control genotypes in both chronically-infected gastric tissue and acutely-infected BMmacs (Appendix C, Figure 14A and 14C). Additionally, the levels of total IL-1β in *H. pylori*-infected gastric tissues were significantly increased in *Odc*$^{\Delta mye}$ mice (Appendix C, Figure 14B). Both pro- IL-1β (Appendix C, Figure 14D) and secreted IL-1β (Figure 32C) levels were substantially higher in *Odc*$^{\Delta mye}$ BMmacs. The role of ODC in regulating NLRP3-inflammasome activation is also dependent upon putrescine production, as the addition of excess putrescine substantially decreased *Nlrp3* and *Casp1* expression in *Odc*$^{\Delta mye}$ BMmacs, such that expression was no longer statistically different than *Nlrp3* and *Casp1* levels in *Odc*$^{fl/fl}$ BMmacs (Appendix C, Figure 14E). These data indicate that the combination of increased expression of *Il1b* and NLRP3 inflammasome

constituents are contributing to increased IL-1β levels. Moreover, IL-1β is a potent pro-inflammatory cytokine[189] and thus may be substantially contributing to the enhanced histologic gastritis observed in $Odc^{\Delta mye}$ mice following chronic *H. pylori* infection.

ODC deletion promotes histone modifications leading to euchromatin formation and transcription.

To this point, our studies have implicated ODC in macrophages as a major regulator of gastric inflammation, cytokine and chemokine production, and M1 macrophage activation. Overall, our data indicate that mice with *Odc*-deficient macrophages exhibit a substantial increase in pro-inflammatory gene transcription. Previous studies have demonstrated that both ODC and the polyamines generated have the ability to influence histone modifications and, therefore, regulate gene transcription[190,191]. To gain an understanding of the role of ODC in altering macrophage gene transcription in response to bacterial infection, we assessed histone modifications at histone 3, lysine 4 (H3K4), known to be found at enhancer regions[192], as well as, H3K9, which is a specific residue known to mark global alterations in chromatin structure and gene transcription levels[193]. Specifically, H3K4 mono-methylation (H3K4me1) is associated with primed, active enhancers and upregulated transcriptional levels[192]. H3K9 acetylation (H3K9ac) is associated with euchromatin formation and increased gene expression, while H3K9 di-/tri-methylation (H3K9me2/3) is associated with heterochromatin formation and decreased gene expression[193]. Under conditions of *H. pylori* infection, $Odc^{\Delta mye}$ BMmacs demonstrated significantly increased H3K4me1 and H3K9ac levels and decreased H3K9me2/3 levels versus $Odc^{fl/fl}$ BMmacs (Figure 34A and 34B), indicative of enhanced gene transcription and correlating with the observed alterations in macrophage activation patterns in the present study. Importantly, a marked increase in H3K9 acetylation was noted in $CD68^{+}$ gastric macrophages from *H. pylori*-infected $Odc^{\Delta mye}$ mice versus *H. pylori*-infected $Odc^{fl/fl}$ mice (Figure 34C). Similar alterations in H3K9 acetylation and methylation were observed in *C. rodentium*-infected BMmacs (Appendix C, Figure 15). Intriguingly, these changes in H3K4me1, H3K9ac, and H3K9me2/3 levels only significantly occurred upon *H. pylori* or *C. rodentium*

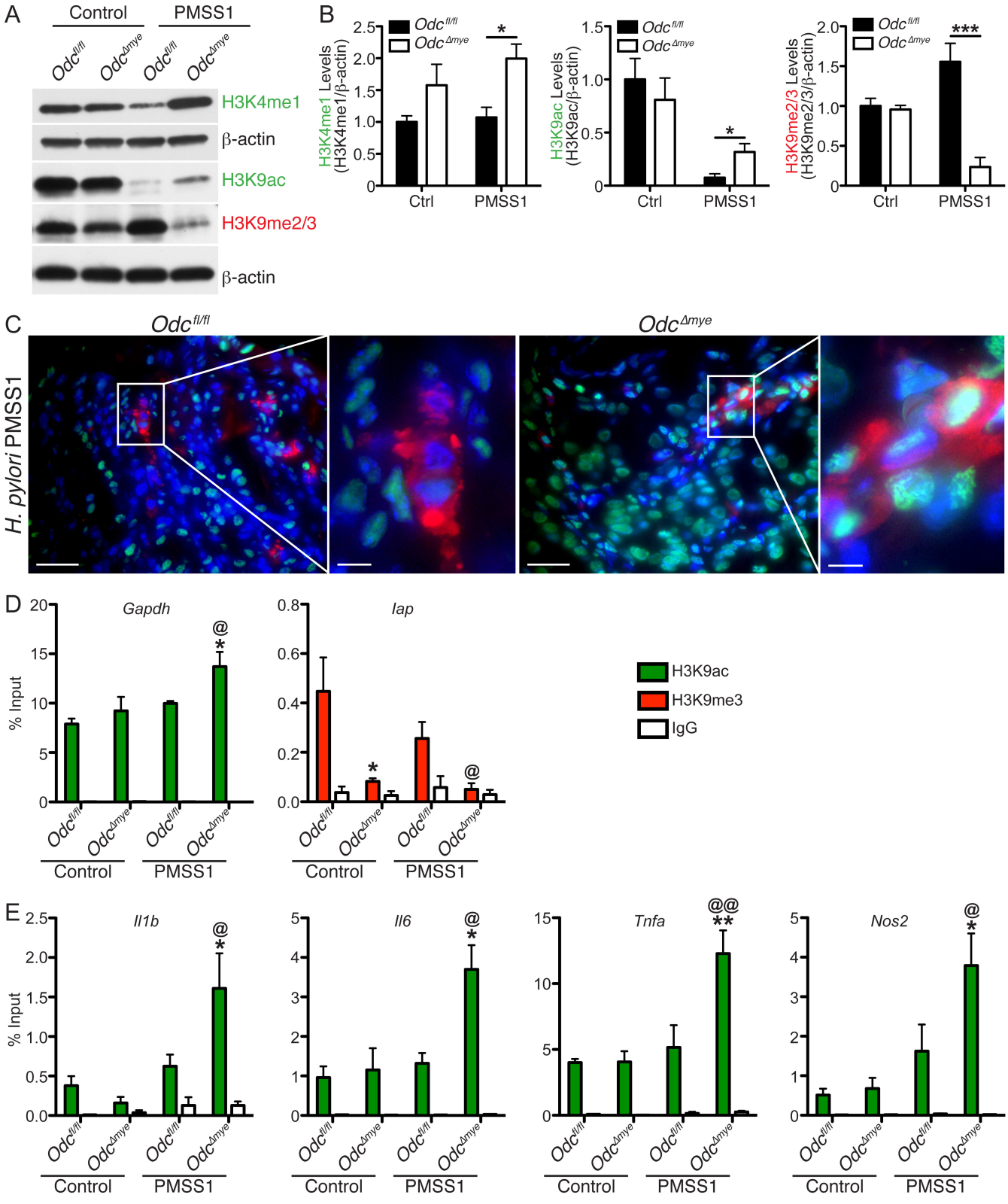
A
Control
PMSS1
Odc fl/fl
Odc Δmye
H3K4me1
β-actin
H3K9ac
H3K9me2/3
β-actin
B
H3K4me1 Levels (H3K4me1/β-actin)
H3K9ac Levels (H3K9ac/β-actin)
H3K9me2/3 Levels (H3K9me2/3/β-actin)
Ctrl
PMSS1
C
Odc fl/fl
Odc Δmye
H. pylori PMSS1
D
Gapdh
Iap
% Input
H3K9ac
H3K9me3
IgG
Control
PMSS1
E
Il1b
Il6
Tnfa
Nos2
% Input

Figure 34. *Odc* deletion in macrophages alters H3K4 and H3K9 modifications during *H. pylori* infection. (a) Representative western blot of H3K4me1, H3K9ac, and H3K9me2/3 levels in BMmacs 24 h p.i. with *H. pylori* PMSS1. *n* = 3 biological replicates. (b) Densitometric analysis of H3K4me1, H3K9ac, and H3K9me2/3 levels in (a). **P*<0.05, ****P*<0.001 by one-way ANOVA with Newman-Keuls post-test. *n* = 3 biological replicates. (c) Representative immunofluorescence images of H3K9ac in *H. pylori*-infected gastric tissues 4 mo. p.i. Green = H3K9ac, Red = CD68, Blue = DAPI. Scale bars = 50 μm. Boxed area indicates image shown at higher magnification. Scale bar = 10 μm. *n* = 3 biological replicates per genotype. Note that a cell is considered double positive if the cell surface is red and the nucleus is green. (d) Expression of *Gapdh* and *Iap* was assessed by RT-PCR in BMmacs from $Odc^{fl/fl}$ and $Odc^{\Delta mye}$ mice 24 h p.i. with *H. pylori* PMSS1 with subsequent ChIP with the denoted antibodies. **P*<0.05. *n* = 3 biological replicates. (e) Expression of *Il1b*, *Il6*, *Tnfa*, and *Nos2* promoter sequences was assessed by RT-PCR in BMmacs from $Odc^{fl/fl}$ and $Odc^{\Delta mye}$ mice 24 h p.i. with *H. pylori* PMSS1 with subsequent ChIP with the denoted antibodies. **P*<0.05. *n* = 3 biological replicates. In (d) and (e), statistical significance was calculated by one-way ANOVA with Newman-Keuls post-test on square-root transformed data. Data displayed as mean ± S.E.M.

infection, implying that the alterations in histone modifications are specific to the macrophage response to stimulation and not occurring during basal conditions.

As with the expression of markers of M1 macrophage and NLRP3-inflammasome activation, the addition of putrescine reversed the histone modifications in *Odc*$^{\Delta mye}$ BMmacs, such that they then resembled the H3K9ac and H3K9me2/3 levels in *Odc*$^{fl/fl}$ BMmacs during *H. pylori* infection (Appendix C, Figure 16). The addition of excess spermidine or spermine, the other two principal polyamines, did not change H3K9ac or H3K9me2/3 levels in either *Odc*$^{fl/fl}$ or *Odc*$^{\Delta mye}$ BMmacs (Appendix C, Figure 16), indicating that putrescine plays a more critical role in regulating histone modifications during *H. pylori* infection in macrophages.

To verify that the loss of ODC in macrophages was directly affecting transcription of the pro-inflammatory M1 markers through H3K9 alterations- namely enhanced acetylation and diminished methylation, we performed chromatin immunoprecipitation (ChIP), followed by RT-PCR in *Odc*$^{fl/fl}$ and *Odc*$^{\Delta mye}$ BMmacs. ChIP was performed with both anti-H3K9ac and anti-H3K9me3 antibodies in order to assess gene expression during both chromatin modifications. Immunoprecipitation with an anti-H3K9ac antibody resulted in significantly increased glyceraldehyde 3-phosphate dehydrogenase (*Gapdh*) expression in *H. pylori*-infected *Odc*$^{\Delta mye}$ BMmacs (Figure 34D). *Gapdh* expression is a marker of transcriptionally active euchromatin[194]. *Gapdh* was not substantially immunoprecipitated with an anti-H3K9me3 antibody (Appendix C, Figure 17A), consistent with this gene representing a maker of euchromatin rather than heterochromatin. Inversely, immunoprecipitation with an anti-H3K9me3 antibody demonstrated significantly decreased expression of inhibitor of apoptosis (*Iap*), a marker indicative of heterochromatin[195], in *H. pylori*-infected *Odc*$^{\Delta mye}$ BMmacs versus *H. pylori*-infected *Odc*$^{fl/fl}$ BMmacs (Figure 34D). Moreover, *Iap* was not markedly immunoprecipitated with an anti-H3K9ac antibody (Appendix C, Figure 16A). Myogenic differentiation 1 (*Myod1*) is indicative of transcriptionally inactive euchromatin[194] and was unchanged between genotypes with immunoprecipitation with either antibody (Appendix C, Figure 17B). Taken together, these data demonstrate that the loss of ODC leads to an enhancement in transcriptionally active euchromatin levels during infection and a decrease in heterochromatin levels, which would result in enhanced gene transcription.

To test if alterations in chromatin modifications were specifically altering pro-inflammatory gene expression, we also assessed *Il1b*, *Il6*, *Tnfa*, and *Nos2* promoter levels by ChIP-PCR. *Il1b*, *Il6*, *Tnfa*, and *Nos2* promoter levels were significantly increased in $Odc^{\Delta mye}$ BMmacs versus $Odc^{fl/fl}$ BMmacs during H3K9ac immunoprecipitation (Figure 34E), and were not significantly immunoprecipitated with an anti-H3K9me3 antibody (Appendix C, Figure 18). Taken together, these data verify that chromatin alterations during *Odc* deletion in macrophages drive enhanced pro-inflammatory gene expression, which then contributes to increased immune cell activation, exhibited as enhanced histologic gastritis that leads to diminished *H. pylori* bacterial burden.

ODC driven histone modifications are essential for alterations in M1 macrophage activation.

Finally, to determine if histone modifications, specifically methylation and acetylation events, are the mechanism by which the loss of ODC alters M1 macrophage activation, we utilized pharmacological inhibitors of histone methylation and acetylation in $Odc^{fl/fl}$ and $Odc^{\Delta mye}$ BMmacs and assessed expression of M1 macrophage activation markers.

BIX 01924 is a selective inhibitor of euchromatic histone lysine methyltransferase 2 (EHMT2; also known as G9a histone methyltransferase), which is known to interact specifically with H3K9[196]. We hypothesized that inhibition of EHMT2 would remove the inhibitory methylation present in $Odc^{fl/fl}$ BMmacs, leading to increased expression of M1 macrophage activation markers. Indeed, BIX 01924 treatment resulted in significantly increased *Il1b*, *Tnfa*, and *Nos2* expression in $Odc^{fl/fl}$ BMmacs during *H. pylori* infection (Figure 35A). As expected, treatment with BIX 01924 did not significantly alter M1 marker expression in $Odc^{\Delta mye}$ BMmacs (Figure 35A). Moreover, BIX 01924 treatment did not alter M2 macrophage activation marker expression in either genotype (Appendix C, Figure 19A). These data further support the concept that that the loss of ODC in the $Odc^{\Delta mye}$ BMmacs allowed for potentiation of M1 marker expression by relieving the methylation of H3K9, therefore leading to increased immune response and gastric inflammation.

Anacardic acid is a selective inhibitor of lysine acetyltransferase 2A (KAT2A; also known as GCN5), which has been previously shown to interact with H3K9[197]. Inhibition of KAT2A significantly

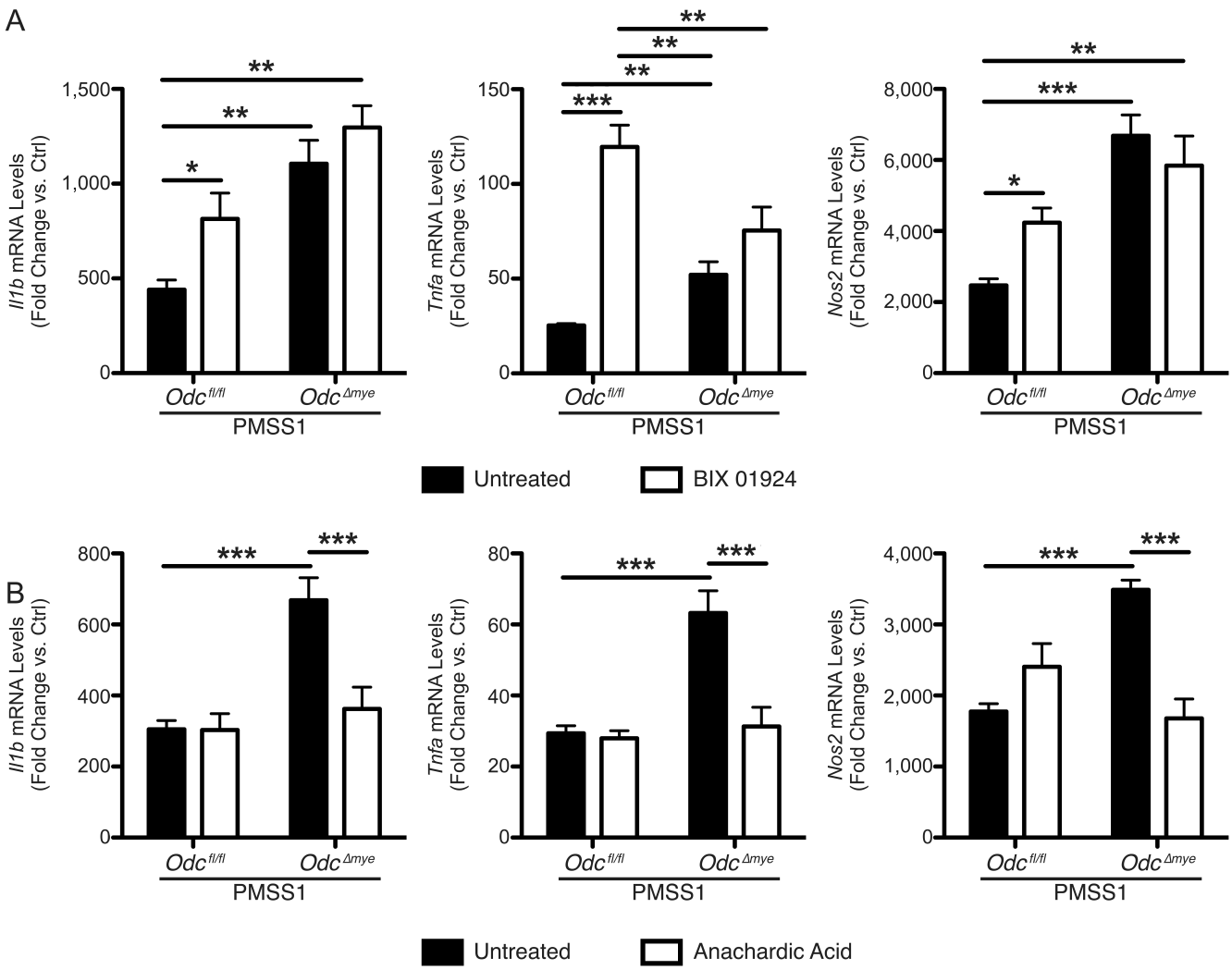

Figure 35. Alterations in histone modifications and chromatin structure in ODC-deficient macrophages alters M1 macrophage activation during *H. pylori* infection. (a) mRNA levels of pro-inflammatory cytokines *Il1b*, *Tnfa*, and *Nos2* were assessed by RT-PCR in BMmacs 24 h p.i. with *H. pylori* PMSS1 ± 5 μM BIX 01924 added 60 min prior to infection. **P*<0.05, ***P*<0.01, ****P*<0.001 by one-way ANOVA with Kruskal-Wallis test, followed by Mann-Whitney *U* test. *n* = 5 mice per genotype. (b) mRNA levels of pro-inflammatory cytokines *Il1b*, *Tnfa*, and *Nos2* were assessed by RT-PCR in BMmacs 24 h p.i. with *H. pylori* PMSS1 ± 10 μM anacardic acid added 60 min prior to infection. ****P*<0.001 by one-way ANOVA with Kruskal-Wallis test, followed by Mann-Whitney *U* test. *n* = 5 mice per genotype. Data displayed as mean ± S.E.M.

reduced M1 marker expression in *Odc*$^{\Delta mye}$ BMmacs, such that expression was similar to M1 marker expression in *Odc*$^{fl/fl}$ BMmacs during *H. pylori* infection (Figure 35B). Anacardic acid treatment did not alter M1 marker gene expression in *H. pylori*-infected *Odc*$^{fl/fl}$ BMmacs (Figure 35B). Additionally, anacardic acid did not alter the expression of M2 macrophage markers, again indicating that the role of ODC in regulating histone modifications is specific to the M1 response (Appendix C, Figure 19B).

Taken together, these studies demonstrate that loss of ODC in macrophages leads to an M1 response that is driven by ODC/putrescine-mediated histone modifications that alter chromatin structure and the capacity for active gene transcription. This increased M1 response is a key orchestrator of the increased gastric inflammatory response.

5.3 Discussion

ODC and polyamines have been well studied in epithelial cells within the context of cancer and in macrophages within the context of parasitic and fungal infections. The present study now reveals a novel mechanism by which ODC and its product, putrescine, regulate M1 macrophage activation via alterations of histone modifications to directly alter pro-inflammatory gene expression during bacterial infection (Figure 36). We demonstrate that loss of ODC in macrophages has profound effects on M1 macrophage activation and thus, on the pathogenesis of both *H. pylori* and *C. rodentium* in mice. We further demonstrate that deletion of ODC leads to alterations in *H. pylori* survival during gastric infection, implicating ODC in macrophages as a mediator of bacterial persistence within a host. This is a critical advancement of our understanding of the immune privilege that is associated with this particular infection, as long-term persistence is the hallmark of *H. pylori* infection and is directly linked to damaging inflammation and increased cancer risk[9,40,111].

ODC is detectable in abundance in human gastric myeloid cells during *H. pylori* infection, indicating the potential importance of the enzyme in regulating the host response to the pathogen[47]. Previous studies demonstrated that pharmacologic inhibition of ODC with DFMO diminished both inflammation and *H. pylori* colonization in mice[47,186], although it should be noted that we have shown that DFMO can have direct inhibitory effects on *H. pylori*[186]. Based on the robust induction of ODC in

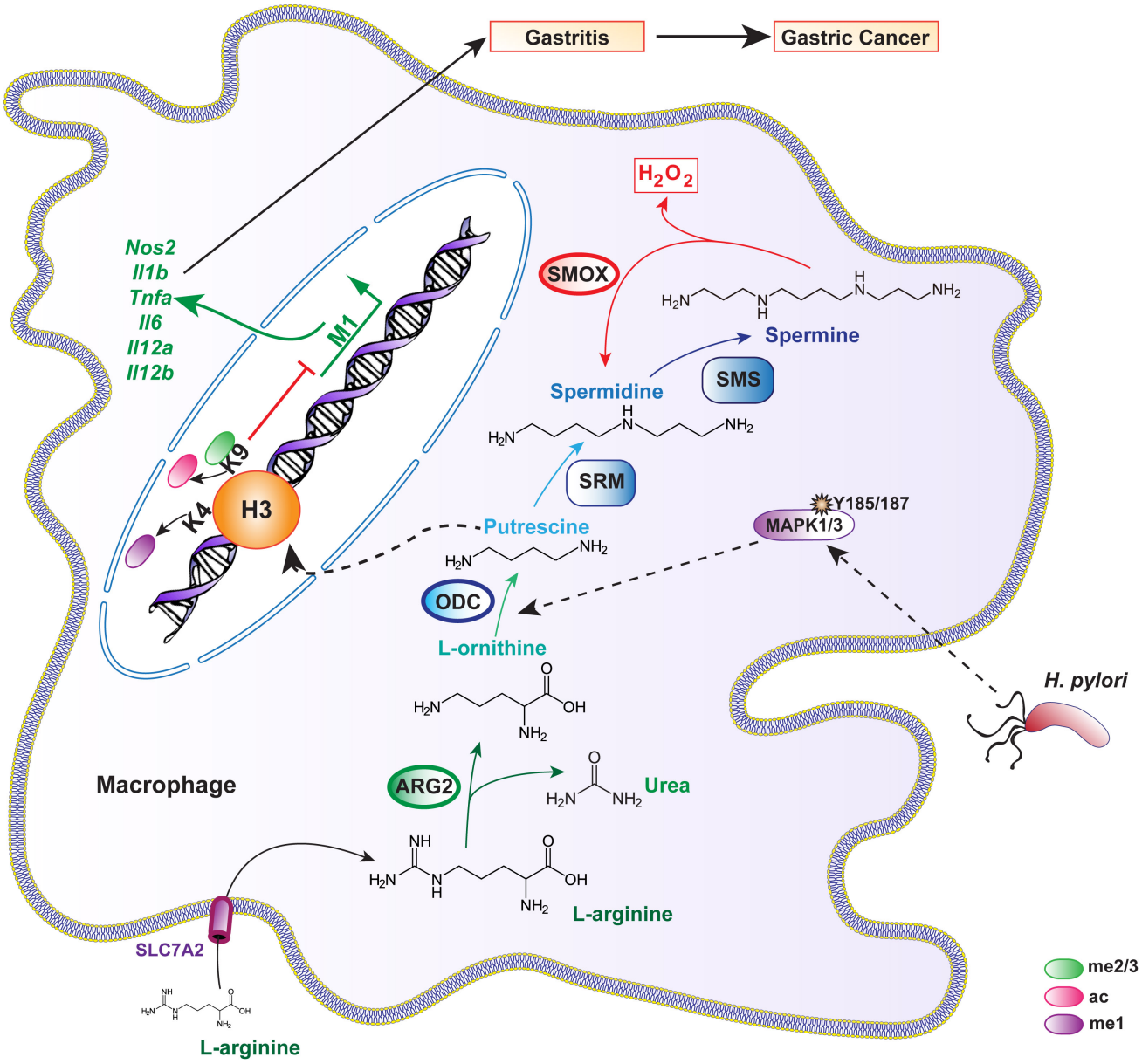

Figure 36. Summary of findings related to ODC in macrophages during *H. pylori* infection. The production of the polyamines – putrescine, spermidine, and spermine – is tightly regulated. Solute carrier family 7, member 2 (SLC7A2) imports L-arginine into cells. L-arginine is converted to L-ornithine by arginase 2 (ARG2). Ornithine decarboxylase (ODC) converts L-ornithine to putrescine. Putrescine is converted to spermidine and spermine by spermidine synthase (SRM) and spermine synthase (SMS), respectively. *H. pylori* infection leads to the induction of ODC via mitogen activated kinase (MAPK) 1/3 (ERK1/2) signaling. ODC-mediated putrescine production alters the modifications on lysine (K) 4 and K9 of histone 3 (H3). Putrescine leads to the replacement of H3K4 mono-methylation (me1) and H3K9 acetylation (ac), which activate transcription, with H3K9 di-/tri-methylation (me2/3), which represses transcription. The increase in H3K9me2/3, and decrease in H3K4me1 and H3K9ac leads to diminished M1 gene expression. Decreased M1 gene expression leads to decreased gastritis, allowing for *H. pylori* survival. Persistent *H. pylori* infection and chronic active gastritis creates a vicious cycle, leading to gastric cancer.

macrophages during *H. pylori* infection[95], we anticipated that myeloid-specific deletion of ODC might result in decreased inflammation and decreased colonization. However, we observed significantly increased inflammation, accompanied by a reduction in *H. pylori* colonization. We attribute this finding to dramatically enhanced M1 macrophage activation, upregulated cytokine and chemokine expression, and significantly increased production of NO, which is a potent anti-microbial mediator. Clearly, ODC expression in macrophages actually impairs the host response. The ability of *H. pylori* to upregulate ODC, via MAPK1/3 and MYC signaling[95,97], is advantageous for the creation of a less inflammatory environment in which the pathogen can establish a persistent infection. However, even in the tolerant environment, persistent infection is still accompanied by chronic inflammation, leading to increased risk for gastric cancer[40,41,111]. Thus, inhibition of ODC may prove to be a potential target to enhance the clearance of long-term infection.

C. rodentium-infected *Odc*$^{\Delta mye}$ mice also had substantially increased disease severity, again attributable to increased M1 macrophage activation. Several previous studies have demonstrated that the severity of colitis is positively correlated with *C. rodentium* colonization[113,187,198,199]. The fact that colonization was not different in our model, despite increased colitis, potentially indicates that colonization was actually impaired, as we would have expected increased colonization accompanying increased colitis. The concordance in macrophage activation patterns and histologic inflammation between the *H. pylori* and *C. rodentium* models in our study, combined with the studies with classical M1 and M2 stimuli, indicate that the role of ODC in macrophages is broadly applicable across various models of mucosal inflammation and is an important mediator of general macrophage activation and biology in mice and humans.

ODC serves as such a potent mediator of macrophage function via its role in the alteration of chromatin structure and gene transcription. ODC and polyamines are known to modulate chromatin modifications, DNA stability, and gene expression[90,92,93]. However, we have now demonstrated for the first time that ODC and polyamines have the ability to directly regulate the expression of pro-inflammatory genes within the context of bacterial infections. This is a critical expansion of our understanding of macrophage activation and function. Putrescine is the product of the enzymatic

conversion of L-ornithine by ODC. In our study, putrescine, but not spermidine or spermine, was capable of reversing the activation patterns observed in *Odc*$^{\Delta mye}$ BMmacs infected with either *H. pylori* or *C. rodentium*. These studies indicate that putrescine is a potent regulatory molecule in macrophage activation. Further studies are required to determine the mechanism by which putrescine modulates histone modifications.

In summary, our work outlines a new role for ODC in regulating macrophage activation during bacterial infections. ODC is a well-known mediator of cancer risk across various types of cancer, including gastric and colorectal cancers[91,177-180]. Importantly, chronic inflammation contributes to the process of carcinogenesis and we now implicate ODC as having a role in the establishment of chronic inflammation by tempering the M1 macrophage response to bacterial pathogens. A novel finding in the current study is that these phenotypes are due to the alteration of chromatin structures by modifications of putrescine levels within macrophages. These studies provide further impetus for studies related to the role of ODC in macrophages as a potential pathway to better understanding the etiology, prevention, and treatment of inflammatory diseases and associated cancer risk.

5.4 Materials and Methods

Reagents

All reagents used for cell culture were from Invitrogen (Carlsbad, CA, USA). Reagents for RNA extraction are from Qiagen (Valencia, CA, USA). Reagents for cDNA synthesis and RT-PCR were purchased from Bio-Rad (Hercules, CA, USA). The following reagents were obtained from PeproTech (Rocky Hill, NJ, USA): murine recombinant M-CSF; murine recombinant IFN-γ; murine recombinant IL-4. The following reagents were obtained from Sigma-Aldrich (St. Louis, MO, USA): LPS from Escherichia coli O111:E4; anacardic acid (2-hydroxy-6-pentadecylbenzoic acid, 6-pentadecylsalicylic acid); putrescine; spermine; spermidine; putrescine-d_4 (1,4-diaminobutane-2,2,3,3-d_4 dihydrochloride); spermidine-d_8 (spermidine-(butane-d_8) trihydrochloride); and spermine-d_8 (spermine-(butane-d_8) tetrahydrochloride). Dansyl chloride was obtained from Acros Organics (Geel, Belgium). BIX01924 (2-

(hexahydro-4-methyl-1*H*-1,4-diazepin-1-yl)-6,7-dimethoxy-*N*-[1-(phenylmethyl)-4-piperidinyl]-4-quinazolinamine trihydrochloride) was obtained from Fisher Scientific (Waltham, MA, USA).

Antibodies

See Appendix C, Table 2 for information regarding antibodies utilized for this study.

Bacteria, Cells, Culture Conditions, and Infections

Helicobacter pylori PMSS1 and SS1 were cultured as previously described in Chapter 2. *C. rodentium* was cultured as previously described in Chapter 2.

BMmacs were isolated and differentiated as previously described in Chapter 2. THP1 cells were utilized as described in Chapter 2.

All pharmacological inhibitors (except DFMO) or polyamines were added 1 h before infection. Cells were infected at a MOI of 100 for *H. pylori* studies and at a MOI of 10 for *C. rodentium* studies. All infection studies were performed with live bacteria.

Animal Studies

$Odc^{fl/fl}$ mice were generated and provided by John L Cleveland (Moffitt Cancer Center) $Odc^{\Delta mye}$ mice were generated by crossing $Odc^{fl/fl}$ mice with $LysM^{cre/cre}$ mice from our stock of breeding colonies. Animals were used under protocol M/10/155, approved by the IACUC at Vanderbilt University.

All *in vivo H. pylori* studies were performed as described in Chapter 2.

On rare occasions, $Odc^{\Delta mye}$ and $LysM^{cre/cre}$ mice would develop a substantially enlarged spleen that was not attributable to *H. pylori* or *C. rodentium* infection, as control mice would also manifest this condition.

If marked splenomegaly was observed at time of sacrifice, that mouse was excluded from further analysis.

Real-Time PCR

RNA isolation, cDNA synthesis, and RT-PCR were performed as described in Chapter 2. See Appendix C, Table 3 for primers utilized in this study.

Western Blot Analysis

Western blot analysis was performed as previously described in Chapter 2. See Appendix C, Table 2 for all antibodies used in this study with accompanying information regarding dilutions utilized.

Luminex Multiplex Array

Luminex Multiplex Array was performed as previously described in Chapter 2.

ELISAs

The following R&D DuoSet ELISA kits were utilized for cytokine measurements: IL-1β (DY401), TNF-α (DY410), IL-6 (DY406), IL-12p70 (DY419), IL-10 (DY417), and TGF-β (DY1679). All ELISAs were performed according to kit instructions.

Measurement of Nitric Oxide

The concentration of the oxidized metabolite of NO, nitrite (NO_2^-) was assessed by the Griess reaction as previously described in Chapter 2.

DFMO Studies in THP1 Cells

THP1 cells were treated with 5 mM DFMO in T-75 flasks for 3 or 5 days. Cells were then counted, plated, and treated with 10 ng/mL PMA for 18 h to differentiate the cells into macrophages. 5 mM DFMO was maintained in the media during PMA treatment. Following differentiation, cells were place in

antibiotic-, PMA-, and DFMO-free media and infected with *H. pylori* PMSS1 (MOI = 100) for 6 h. All RNA and protein assays were performed as described above.

Immunofluorescence Staining for ODC, CD68, and H3K9ac in Murine Tissues

Immunofluorescence staining for ODC, CD68, and H3K9ac in murine tissues was performed utilizing a staining protocol that was previously described[143], with the following alterations. As the source for each of the three antibodies is rabbit, tissues were blocked with 5% goat serum and rabbit Fab fragment for 30 minutes at room temperature following incubation in primary and secondary antibodies for either ODC or H3K9ac prior to incubation with anti-CD68. A secondary anti-rabbit antibody with an Alexa488 tag was utilized. Slides were imaged using a SPOT RT slider camera system (Diagnostic Instruments, Inc., Sterling Heights, MI, USA) on a Nikon E800 microscope (Nikon, Inc. Melville, NY, USA). Images were all modestly adjusted in ImageJ with the brightness and contrast tool.

Immunoperoxidase Staining for ODC

Staining for ODC in human gastric biopsies was performed as previously described[47].

Immunofluorescence Staining for ODC and CD68 Human Tissues

Immunofluorescence staining for ODC and CD68 in human tissues was performed utilizing a staining protocol that was previously described[143]. Quantification of $CD68^{+}ODC^{+}$ and $CD68^{+}ODC^{-}$ cells was performed by four blinded observers and the scoring was averaged.

Human Tissues

De-identified human gastric samples from Colombia were obtained and utilized as previously described[143]. All patients participating in studies in Colombia were enrolled with informed consent, and the de-identified coded tissues were provided under nonhuman exemptions approved by the Vanderbilt University Institutional Review Board.

Purification of gastric epithelial cells and gastric macrophages

Purification of gastric epithelial cells and gastric macrophages was performed as previously described[143].

Measurement of Polyamines

All studies related to polyamine measurements were conducted in serum-free media. Putrescine, spermidine, and spermine were quantified by LC-MS using a Thermo TSQ Vantage Triple Quadrupole instrument operated in positive ion mode. Cell pellets were extracted using acetonitrile/20 mM NH_4OAc pH 8 (70:30). Extracts were derivatized by reaction with 20 mM dansyl chloride in 100 mM $NaHCO_3$ pH 10 for 20 min. Polyamines were quantified using deuterated internal standards d_4-putrescine, d_8-spermidine, and d_8-spermine.

ChIP-PCR

Chromatin immunoprecipitation (ChIP) was performed utilizing the EpiTect Chip ChIP-Grade Antibody Kit – H3K9ac (Qiagen, cat. no. GAM-1209) and the EpiTect Chip ChIP-Grade Antibody Kit – H3K9me3 (Qiagen, cat. no. GAM-6204). All reagents were provided in the EpiTect Chip One-day Kit (Qiagen, cat. no. 334471). All kit instructions were followed as stated, including PCR master mix set-up and recommended PCR protocol. Primers for *Gapdh* and *Myod1* were provided with the ChIP antibody kits listed above. Primers for *Il1b*, *Il6*, *Tnfa*, and *Nos2* promoter sites are listed in Appendix C, Table 3.

Statistical Analysis

All the data shown represent the mean ± S.E.M. At least three biological replicates were performed for all studies utilizing cell culture. Where data was normally distributed, two-tailed Student's *t* test was used to determine significance in experiments with only two groups, and one-way ANOVA with the Newman-Keuls test was used to determine significant differences between multiple test groups. In cases where data were not normally distributed, a one-way ANOVA with Kruskal-Wallis test, followed by a Mann-Whitney *U* test, was performed, unless otherwise noted. All statistics were performed in

GraphPad Prism 5.0 (GraphPad Software, San Diego, CA, USA). A *P* value of < 0.05 was considered to be significant.

CHAPTER 6

SUMMARY, FUTURE DIRECTIONS, AND FINAL CONCLUSIONS

Macrophages represent an extremely diverse subset of innate immune cells, with functions spanning the gamut from development to immune surveillance and clearance of pathogens to maintenance of tissue homeostasis. Macrophages fill a highly necessary niche within mammalian life, but when left uncontrolled can contribute to malignancies. As this dissertation has demonstrated, the mechanisms by which macrophage activation is controlled are of significant importance in furthering our understanding of disease pathology, both within the context of bacterial infections and carcinogenesis. Clearly, both EGFR and ODC have profound, but opposite, roles in regulating macrophage activation across various stimuli. The overall findings of this dissertation are outlined in Figure 37 and described in more detail in the subsequent sections.

6.1 Summary and Future Directions

Chapter 2 outlined the role of EGFR signaling in the regulation of macrophage activation and function during bacterial infections. *H. pylori* is one of the most prevalent and successful human pathogens and the single greatest risk factor for gastric cancer, and macrophages are an essential component of *H. pylori* pathogenesis. As such, the study of macrophage activation within this context is especially important. EGFR signaling proved to be critical for M1 and Mreg activation during *H. pylori* infection, and for M2 activation during stimulation with IL-4. Importantly, EGFR signaling was also important in macrophage activation during *C. rodentium* infection and treatment with known macrophage stimuli (IFN-γ, LPS, IL-4, and IL-10).

The studies presented in Chapter 2 have revealed a profound role of EGFR signaling in macrophages during both bacterial infection and carcinogenesis. Yet, many questions remain unanswered and further studies are required to better understand the role of EGFR signaling in macrophages.

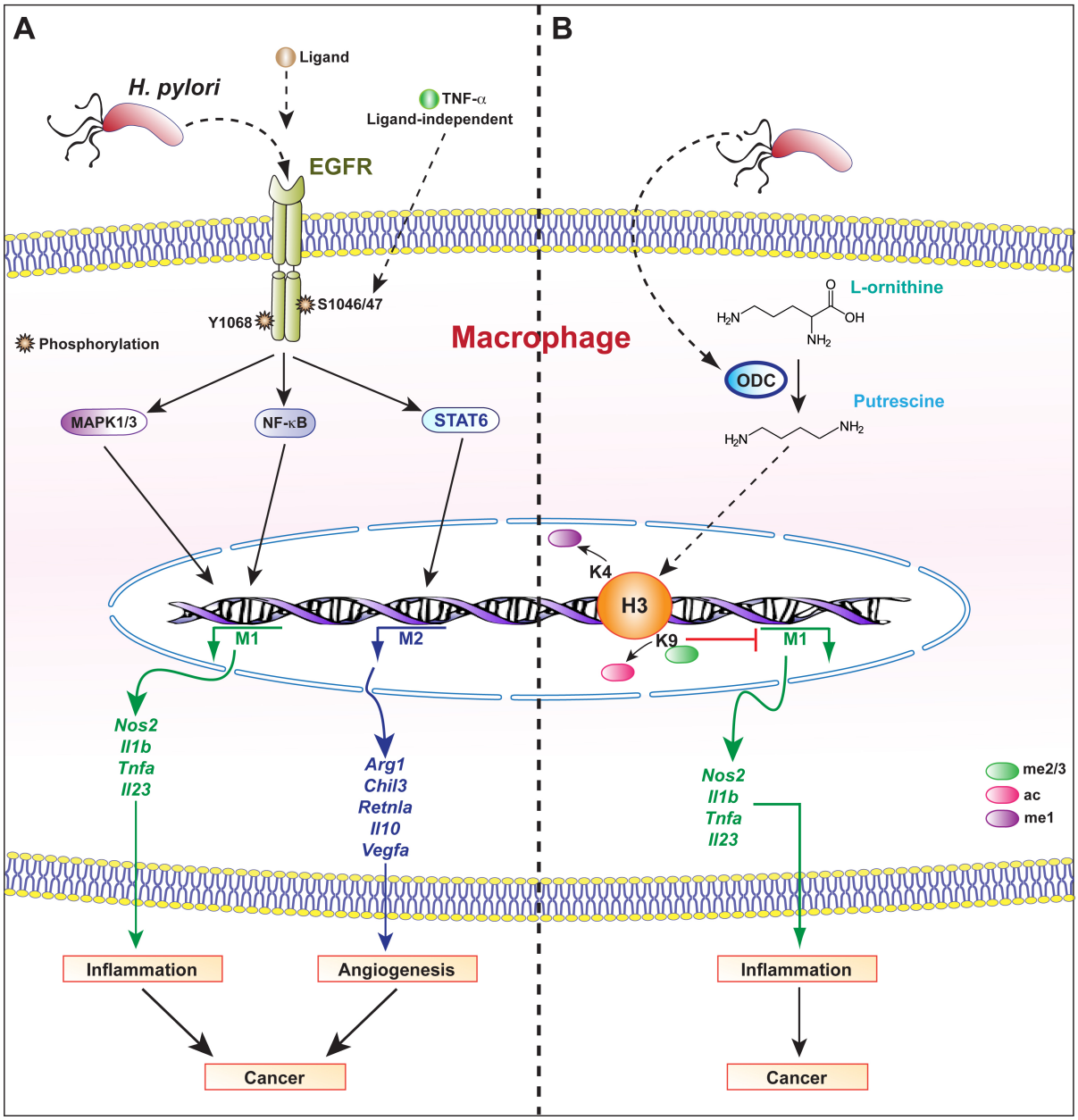

Figure 37. Summary of the main findings of this dissertation. A. Epidermal growth factor receptor (EGFR) signaling is initiated during both *H. pylori* infection and colon carcinogenesis. Phosphorylation occurs at tyrosine (Y) 1068 via a ligand-dependent mechanism and at serine (S) 1046/47 via a ligand-independent mechanism. EGFR signaling then induces mitogen-activated protein kinase (MAPK) 1/3 signaling, nuclear factor kappa-light-chain-enhancer of activated B cells (NF-κB) signaling, and Signal transducer and activator of transcription (STAT) 6 signaling, depending upon the cytokine milieu/stimulus detected. MAPK1/3 signaling and NF-κB signaling lead to M1 activation and STAT6 signaling leads to M2 activation. M1 activation contributes to the establishment of a persistant inflammatory state, while M2 activation enhances angiogenesis. The combination of M1 and M2 activation contribute to carcinogenesis. B. H. pylori infection leads to the induction of ornithine decarboxylase (ODC). ODC converts L-ornithine into putrescine, one of the three main polyamines. Putrescine alters histone 3 (H3) modifications by an unknown mechanism. In putrescine replete conditions, H3 has abundant di-/tri-methylation (me2/3) on lysine 9 (K9), while H3K4 mono-methylation (me1) and H3K9 acetylation (ac) are not present. This combination of histone modifications leads to decreased M1 activation because of decreased transcription of pro-inflammatory genes. A diminished M1 response leads to bacterial persistence and reduced, but not absent, gastritis *in vivo*.

While the role of EGFR in regulating macrophage activation is clear, the activation of EGFR signaling in macrophages remains largely unknown. Our studies have implicated both ligand-independent activation of EGFR signaling through TNF-α signaling (Figure 8G) and ligand-dependent signaling via an unknown mechanism. Further studies are required to better understand the mechanism by which EGFR transactivation occurs. Canonical EGFR signaling is mediated by one of seven known ligands[62]. Our studies have demonstrated that EGF and HB-EGF do not lead to significant phosphorylation at Y1068, the marker of canonical activation. However, further studies with the five remaining ligands need to be performed. To determine if bacterial or host factors are necessary to activate EGFR signaling, supernatants from cultures of *H. pylori*, macrophages, and epithelial cells can be applied to macrophages to determine if soluble constituents from either bacterial or host cells are necessary for activation. Phospho-peptide mapping by mass spectrometry can be performed to gather unbiased data regarding EGFR phosphorylation at various tyrosines, serines, and threonines to better inform further studies related to EGFR transactivation.

Furthermore, future studies related to the role of EGFR signaling in gastric cancer are necessary. The AOM-DSS model of colon carcinogenesis is a highly tractable model used routinely in many laboratories. However, few models exist in which to interrogate gastric cancer in mice. The Mongolian gerbil model of gastric cancer is not feasible to study the role of EGFR signaling in macrophages, as cell-specific tools and reagents do not exist. Thus, our laboratory is working to create an FVB/N insulin-gastrin (INS-GAS) mouse strain that carries the myeloid-specific *Egfr* deletion (INS-GAS:*Egfr*$^{\Delta mye}$). INS-GAS mice are a model of hypergastrinemia that results in hyperplasia, dysplasia, and occasionally gastric carcinoma[200]. Currently, the *Egfr*$^{\Delta mye}$ mice are being crossed with WT FVB/N mice to ensure the mice are on the correct background. Once the background alteration is accomplished, FVB/N *Egfr*$^{\Delta mye}$ will be crossed with FVB/N INS-GAS mice, and appropriate controls will be derived from the INS-GAS:*Egfr*$^{\Delta mye}$ mice. Once all necessary genotypes are created, chronic *H. pylori* infections will be initiated and endpoint parameters of histologic gastritis, hyperplasia, dysplasia, and carcinoma will be assessed. These studies will definitively address questions related to the role of

EGFR signaling in macrophage in gastric carcinogenesis. However, these studies are several years away due to the complicated nature of the mouse strains being created.

Beyond bacterial infection, Chapter 3 demonstrated that EGFR signaling in macrophages had a significant role in colon carcinogenesis, even more so than EGFR signaling in epithelial cells, the canonical cell type in which EGFR signaling is studied. Taken together, these data indicate that EGFR is a master regulator of macrophage biology. This has broad implications in our understanding of the etiology of inflammation-mediated diseases. However, our understanding of the role of EGFR in regulation of macrophage activation in human macrophages *in vivo* remains extremely limited.

Thus, further studies linking EGFR signaling, macrophage activation, and carcinogenesis in humans are necessary. We plan to perform serial sectioning of gastric and CAC TMAs available at Vanderbilt University Medical Center. Sections will be stained for CD68 and pEGFR or NOS2 (M1 marker) or ARG1 (M2 marker) for immunofluorescence imaging on the Ariol platform. Following imaging, CellProfiler will be utilized to quantify $CD68^{+}pEGFR^{+}$ macrophages, M1 macrophages, and M2 macrophages in each section. Correlations can then be made between the level of EGFR signaling in macrophages and the activation state of macrophages in both gastric and colon cancers. Moreover, primary human blood monocyte-derived macrophages can be studied *in vitro* to further elucidate the role of EGFR signaling in human macrophages. These studies would serve to begin to address the role of EGFR signaling in macrophage activation in humans during carcinogenesis and may provide biomarkers for stratification of cancer risk or therapeutic targets for intervention during cancer.

Chapter 4 represents the newest direction of research related to the role of EGFR signaling in macrophages. SILAC analysis allowed for an unbiased and global view of signaling pathways that are affected by EGFR in macrophages. While these studies are still in an early stage, they may prove highly informative and may produce novel therapeutic targets for intervention in inflammatory diseases. Once more bioinformatic analyses are complete, future studies will be focused on elucidating the mechanism by which EGFR signaling modulates candidate pathways and how those pathways contribute to the regulation of macrophage activation and function.

The overarching theme of this dissertation was to elucidate mechanisms by which macrophage activation is regulated. EGFR signaling is now known to be a pro-inflammatory pathway, enhancing M1 macrophage activation. However, Chapter 5 demonstrated that the role of ODC and polyamines is to downregulate M1 macrophage activation during *H. pylori* and *C. rodentium* infection and promote an anti-inflammatory response *in vivo*. For the first time, ODC, and its product, putrescine, were demonstrated to directly regulate the transcription of pro-inflammatory genes by modulating histone structure. ODC has been widely studied within the context of carcinogenesis, but not within bacterial infection. These findings demonstrate the profound effect that polyamines have on macrophage function, which should be extended to other inflammation-mediated diseases, including cancer. ODC is already a known therapeutic target in the treatment of cancer, but these studies suggest that ODC inhibition could be useful in the treatment of diseases, like persistent bacterial infections, which require a more potent pro-inflammatory and anti-microbial response. While the studies presented within Chapter 5 have elucidated a novel role for ODC and polyamines in the regulation of macrophage activation, several unanswered questions remain.

Firstly, ODC is the rate-limiting enzyme for synthesis of putrescine from L-ornithine. Putrescine can then be converted into spermidine and spermine. It was surprising that only the addition of excess putrescine, and not spermidine or spermine, was able to complement phenotypes related to gene expression and histone modifications in $Odc^{\Delta mye}$ BMmacs. The *in vivo* relevance of this finding remains unclear. Thus, chronic *H. pylori* SS1 infections in $Odc^{fl/fl}$ and $Odc^{\Delta mye}$ mice should be performed with and without putrescine supplementation. There is one previous study that utilized a 1% putrescine solution in the drinking water to provide mice with excess putrescine[201]. Such a study could be performed in our model of *H. pylori* infection to confirm the critical role for putrescine specifically in regulating macrophage activation. It would also be interesting to conduct studies in which the polyamine content of the diet is highly controlled. Our laboratory is currently using defined diets with varying levels of L-arginine which is upstream of polyamine synthesis and observing substantial effects on *C. rodentium*-induced colitis. A diet with defined polyamines could potentially be synthesized for these studies.

Moreover, the exact mechanism by which putrescine leads to alterations in histone modifications is unknown. It is important to know what proteins putrescine interacts with, and where those proteins are within the cell. I propose treating macrophages with radiolabeled putrescine, infecting with *H. pylori* across a time course, and then extracting protein lysates from control and infected cells. Following extraction of the protein lysate, mass spectrometry could be utilized to identify proteins that are interacting with the radiolabeled putrescine. Follow-up studies can be performed on relevant identified proteins to better understand the mechanism by which putrescine is influencing histone modifications and gene expression.

Thirdly, the study presented in Chapter 5 was limited to macrophages and no questions were addressed related to the interaction between ODC-deficient macrophages and adaptive immune cells. GLNs and isolated gastric $CD4^+$ T cells from chronically infected mice can be utilized to interrogate the role of ODC and polyamine production in macrophages in the initiation and establishment of T helper responses in the stomach. These studies will provide critical information regarding the relationship between macrophages and T cells in the context of polyamine metabolism.

Finally, the role of ODC in macrophages in carcinogenesis remains unknown. *C. rodentium* infection in $Odc^{\Delta mye}$ mice resulted in exacerbated colitis (Appendix C, Figure 5), providing a rationale for utilization of the AOM-DSS model of colitis-associated carcinogenesis in these mice. I hypothesize that the enhanced M1 macrophage activation noted in the *C. rodentium* model will translate to enhanced tumorigenesis, as the loss of M1 activation proved to be protective in the $Egfr^{\Delta mye}$ AOM-DSS studies. Alternatively, the enhanced M1 response in ODC deficient macrophages may prove to be anti-tumorigenic. Clearly, these are questions that need to be addressed further.

6.2 Final Conclusions

While pro-inflammatory EGFR and anti-inflammatory ODC represent opposite sides of the spectrum in controlling macrophage activation, these studies leave the clear impression that there is much knowledge to be gained about macrophage biology. EGFR and ODC are both highly studied proteins in epithelial cells, but the studies presented herein have only begun to scratch the surface of

their roles in macrophage biology. Further investigation is needed to better delineate the roles of each of these proteins in the regulation of macrophage function within every niche in which macrophages operate. Ultimately, these studies could lead to novel therapeutic targets to better treat and potentially prevent inflammation-mediated diseases and their long-term sequelae, especially carcinoma, in humans.

As the studies in this Chapters 2-4 have made clear, EGFR signaling robustly occurs within macrophages under various conditions, and this signaling has profound effects on macrophage activation and function. Given the ubiquitous nature of EGFR signaling in other cell types and the central role of this signaling pathway in many disease states, EGFR signaling in macrophages should be a topic of intense study. Moreover, the data presented in these chapters demonstrate that EGFR signaling in macrophages is as critical for disease progression – especially in CAC – as signaling within epithelial cells.

ODC is equally as central to life and cellular function as EGFR and polyamine metabolism has been widely studied for decades, and polyamines are known to have ubiquitous effects on cellular function[84,85]. The studies presented in Chapter 5 provide novel insight into the role of ODC and its product, putrescine, in the regulation of macrophage activation at the transcriptional level. Polyamines have been known to influence transcription for some time[90,92,93], but this is the first instance where such regulation has relevance in bacterial infection models and across various known macrophage stimuli. These data provide evidence that polyamine metabolism is a key regulator of macrophage function, which could be relevant in many disease models that involve persistent inflammation.

As our understanding of carcinogenesis has improved, the role of inflammation has come to the forefront[7-9,82,133,134,136,160,202]. Macrophages contribute significantly to inflammation because they serve as both initiators of innate immune responses and recruit adaptive immune cells in order to establish chronic inflammation[7]. Advances in our understanding of the regulation of macrophage activation and function may identify potential points of chemotherapeutic intervention in persons with chronic inflammatory states. Controlling inflammation may be the key to prevent both gastric and colorectal cancers, especially as the risks both are significantly augmented by chronic inflammatory

states[8,9,133,135,202]. EGFR and ODC represent two halves of the same question in that EGFR promotes M1 macrophage activation, while ODC tempers M1 macrophage activation. The data presented herein provide a compelling rationale for further studies related to proteins that are not traditionally thought to be mediators of macrophage activation and function. Perhaps by expanding our perception of what is thought to be relevant within immune cells, as opposed to other cell types, we may gain a better understanding of the etiology, prevention, and treatment of inflammatory diseases and associated cancer risk.

REFERENCES

1 Benoit M, Desnues B, Mege JL (2008). Macrophage polarization in bacterial infections. *J Immunol* **181:** 3733-3739.

2 Mosser DM (2003). The many faces of macrophage activation. *J Leukoc Biol* **73:** 209-212.

3 Mosser DM, Edwards JP (2008). Exploring the full spectrum of macrophage activation. *Nat Rev Immunol* **8:** 958-969.

4 Murray PJ, Wynn TA (2011). Protective and pathogenic functions of macrophage subsets. *Nat Rev Immunol* **11:** 723-737.

5 Norton SE, Dunn ET, McCall JL, Munro F, Kemp RA (2016). Gut macrophage phenotype is dependent on the tumor microenvironment in colorectal cancer. *Clin Trans Immunol* **5:** e76.

6 Biswas SK, Mantovani A (2010). Macrophage plasticity and interaction with lymphocyte subsets: cancer as a paradigm. *Nat Immunol* **11:** 889-896.

7 Ostuni R, Kratochvill F, Murray PJ, Natoli G (2015). Macrophages and cancer: From mechanisms to therapeutic implications. *Trends Immunol* **36:** 229-239.

8 Feagins LA, Souza RF, Spechler SJ (2009). Carcinogenesis in IBD: Potential targets for the prevention of colorectal cancer. *Nat Rev Gastroenterol Hepatol* **6:** 297-305.

9 Hardbower DM, de Sablet T, Chaturvedi R, Wilson KT (2013). Chronic inflammation and oxidative stress: The smoking gun for *Helicobacter pylori*-induced gastric cancer? *Gut Microbes* **4:** 475-481.

10 Payne CM, Bernstein C, Bernstein H, Gerner EW, Garewal H (1999). Reactive nitrogen species in colon carcinogenesis. *Antiox Redox Sig* **1:** 449-467.

11 Anderson CF, Mosser DM (2002). A novel phenotype for an activated macrophage: The type 2 activated macrophage. *J Leuko Biol* **72:** 101-106.

12 Biswas SK, Gangi L, Paul S, Schioppa T, Saccani A, Sironi M *et al* (2005). A distinct and unique transcriptional program expressed by tumor-associated macrophages (defective NF-κB and enhanced IRF-3/STAT1 activation). *Blood* **107:** 2112-2122.

13 Pander J, Heusinkveld M, van der Straaten T, Jordanova ES, Baak-Pablo R, Gelderblom H *et al* (2011). Activation of tumor-promoting type 2 macrophages by EGFR-targeting antibody Cetuximab. *Clin Cancer Res* **17:** 5668-5673.

14 Fleming BD, Mosser DM (2011). Regulatory macrophages: Setting the threshold for therapy. *Eur J Immunol* **41:** 2498-2502.

15 Ghisletti S, Barozzi I, Mietton F, Polletti S, De Santa F, Venturini E *et al* (2010). Identification and characterization of enhancers controlling the inflammatory gene expression program in macrophages. *Immunity* **32:** 317-328.

16 Lawrence T, Natoli G (2011). Transcriptional regulation of macrophage polarization: Enabling diversity with identity. *Nat Rev Immunol* **11:** 750-761.

17 Wang N, Liang H, Zen K (2014). Molecular mechanisms that influence the macrophage M1-M2 polarization balance. *Front Immunol* **5:** 614.

18 Foster SL, Hargreaves DC, Medzhitov R (2007). Gene-specific control of inflammation by TLR-induced chromatin modifications. *Nature* **447:** 972-978.

19 Ruffell D, Mourkioti F, Gambardella A, Kirstetter P, Lopez RG, Rosenthal N *et al* (2009). A CREB-C/EBPβ cascade induces M2 macrophage-specific gene expression and promotes muscle injury repair. *Proc Natl Acad Sci USA* **106:** 17475-17480.

20 Kaparakis M, Walduck AK, Price JD, Pedersen JS, van Rooijen N, Pearse MJ *et al* (2008). Macrophages are mediators of gastritis in acute *Helicobacter pylori* infection in C57BL/6 mice. *Infect Immun* **76:** 2235-2239.

21 Cover TL, Blaser MJ (2009). *Helicobacter pylori* in health and disease. *Gastroenterology* **136:** 1863-1873.

22 Peek RM, Blaser MJ (2002). *Helicobacter pylori* and gastrointestinal tract adenocarcinomas. *Nat Rev Cancer* **2:** 28-37.

23 Mera R, Fontham ETH, Bravo LE, Bravo JC, Piazuelo MB, Camargo MC *et al* (2005). Long term follow up of patients treated for *Helicobacter pylori* infection. *Gut* **54:** 1536-1540.

24 Parsonnet J, Friedman GD, Vandersteen DP, Chang Y, Vogelman JH, Orentreich N *et al* (1991). *Helicobacter pylori* infection and the risk of gastric carcinoma. *N Engl J Med* **325:** 1127-1131.

25 (1994). Schistosomes, liver flukes and *Helicobacter pylori*. IARC working group on the evaluation of carcinogenic risks to humans. *IARC Monogr Eval Carcinog Risks Hum* **61:** 1-241.

26 Global Burden of Disease Cancer C, Fitzmaurice C, Dicker D, Pain A, Hamavid H, Moradi-Lakeh M *et al* (2015). The global burden of cancer 2013. *JAMA Oncol* **1:** 505-527.

27 Blaser MJ, Perez-Perez GI, Kleanthous H, Cover TL, Peek RM, Chyou PH *et al* (1995). Infection with *Helicobacter pylori* strains possessing CagA is associated with an increased risk of developing adenocarcinoma of the stomach. *Cancer Res* **55:** 2111-2115.

28 Lin WC, Tsai HF, Kuo SH, Wu MS, Lin CW, Hsu PI *et al* (2010). Translocation of *Helicobacter pylori* CagA into human B lymphocytes, the origin of mucosa-associated lymphoid tissue lymphoma. *Cancer Res* **70:** 5740-5748.

29 Murata-Kamiya N (2011). Pathophysiological functions of the CagA oncoprotein during infection by *Helicobacter pylori*. *Microbes Infect* **13:** 799-807.

30 Raju D, Hussey S, Ang M, Terebiznik MR, Sibony M, Galindo-Mata E *et al* (2012). Vacuolating cytotoxin and variants in Atg16L1 that disrupt autophagy promote *Helicobacter pylori* infection in humans. *Gastroenterology* **142:** 1160-1171.

31 Kim JM, Kim JS, Lee JY, Kim Y-J, Youn H-J, Kim IY *et al* (2007). Vacuolating cytotoxin in *Helicobacter pylori* water-soluble proteins upregulates chemokine expression in human eosinophils via Ca^{2+} influx, mitochondrial reactive oxygen intermediates, and NF-κB activation. *Infect Immun* **75:** 3373-3381.

32 Tsugawa H, Suzuki H, Saya H, Hatakeyama M, Hirayama T, Hirata K *et al* (2012). Reactive oxygen species-induced autophagic degradation of *Helicobacter pylori* CagA is specifically suppressed in cancer stem-like cells. *Cell Host Microbe* **12:** 764-777.

33 de Sablet T, Piazuelo MB, Shaffer CL, Schneider BG, Asim M, Chaturvedi R *et al* (2011). Phylogeographic origin of *Helicobacter pylori* is a determinant of gastric cancer risk. *Gut* **60:** 1189-1195.

34 Zambon CF, Basso D, Navaglia F, Belluco C, Falda A, Fogar P *et al* (2005). Pro- and anti-inflammatory cytokines gene polymorphisms and *Helicobacter pylori* infection: interactions influence outcome. *Cytokine* **29:** 141-152.

35 Hardbower DM, Peek RM, Jr., Wilson KT (2014). At the bench: *Helicobacter pylori*, dysregulated host responses, DNA damage, and gastric cancer. *J Leukoc Biol* **96:** 201-212.

36 Ferlay J, Soerjomataram I, Dikshit R, Eser S, Mathers C, Rebelo M *et al* (2015). Cancer incidence and mortality worldwide: sources, methods and major patterns in GLOBOCAN 2012. *Int J Cancer* **136:** E359-386.

37 Chaturvedi R, de Sablet T, Asim M, Piazuelo MB, Barry DP, Verriere TG *et al* (2015). Increased *Helicobacter pylori*-associated gastric cancer risk in the Andean region of Colombia is mediated by spermine oxidase. *Oncogene* **34:** 3429-3440.

38 Chaturvedi R, de Sablet T, Coburn LA, Gobert AP, Wilson KT (2012). Arginine and polyamines in *Helicobacter pylori*-induced immune dysregulation and gastric carcinogenesis. *Amino Acids* **42:** 627-640.

39 Ford AC, Forman D, Hunt RH, Yuan Y, Moayyedi P (2014). *Helicobacter pylori* eradication therapy to prevent gastric cancer in healthy asymptomatic infected individuals: Systematic review and meta-analysis of randomised controlled trials. *BMJ* **348:** g3174.

40 Peek RM, Fiske C, Wilson KT (2010). Role of innate immunity in *Helicobacter pylori*-induced gastric malignancy. *Physiol Rev* **90:** 831-858.

41 Robinson K, Argent RH, Atherton JC (2007). The inflammatory and immune response to *Helicobacter pylori* infection. *Best Pract Res Clin Gastroenterol* **21:** 237-259.

42 Wilson KT, Crabtree JE (2007). Immunology of *Helicobacter pylori*: Insights Into the failure of the immune response and perspectives on vaccine studies. *Gastroenterology* **133:** 288-308.

43 Augusto AC, Miguel F, Mendonça S, Pedrazzoli Jr J, Gurgueira SA (2007). Oxidative stress expression status associated to *Helicobacter pylori* virulence in gastric diseases. *Clin Biochemn* **40:** 615-622.

44 Ramarao N, Gray-Owen SD, Meyer TF (2000). *Helicobacter pylori* induces but survives the extracellular release of oxygen radicals from professional phagocytes using its catalase activity. *Molec Microbiol* **38:** 103-113.

45 Wang G, Hong Y, Olczak A, Maier SE, Maier RJ (2006). Dual roles of *Helicobacter pylori* NapA in inducing and combating oxidative stress. *Infect Immun* **74:** 6839-6846.

46 Terebiznik MR, Vazquez CL, Torbicki K, Banks D, Wang T, Hong W *et al* (2006). *Helicobacter pylori* VacA toxin promotes bacterial intracellular survival in gastric epithelial cells. *Infect Immun* **74:** 6599-6614.

47 Chaturvedi R, Asim M, Hoge S, Lewis ND, Singh K, Barry DP *et al* (2010). Polyamines impair immunity to *Helicobacter pylori* by inhibiting L-arginine uptake required for nitric oxide production. *Gastroenterology* **139:** 1686-1698.

48 Gobert AP, Verriere T, Asim M, Barry DP, Piazuelo MB, de Sablet T *et al* (2014). Heme oxygenase-1 dysregulates macrophage polarization and the immune response to *Helicobacter pylori*. *J Immunol* **193:** 3013-3022.

49 Wroblewski LE, Peek RM, Jr., Wilson KT (2010). *Helicobacter pylori* and gastric cancer: Factors that modulate disease risk. *Clin Microbiol Rev* **23:** 713-739.

50 Kao JY, Zhang M, Miller MJ, Mills JC, Wang B, Liu M *et al* (2010). *Helicobacter pylori* immune escape is mediated by dendritic cell-induced Treg skewing and Th17 suppression in mice. *Gastroenterology* **138:** 1046-1054.

51 Gray BM, Fontaine CA, Poe SA, Eaton KA (2013). Complex T cell interactions contribute to *Helicobacter pylori* gastritis in mice. *Infect Immun* **81:** 740-752.

52 Eaton KA, Mefford M, Thevenot T (2001). The role of T cell subsets and cytokines in the pathogenesis of *Helicobacter pylori* gastritis in mice. *J Immunol* **166:** 7456-7461.

53 Shi Y, Liu XF, Zhuang Y, Zhang JY, Liu T, Yin Z *et al* (2010). *Helicobacter pylori*-induced Th17 responses modulate Th1 cell responses, benefit bacterial growth, and contribute to pathology in mice. *J Immunol* **184:** 5121-5129.

54 Peterson RA, 2nd, Hoepf T, Eaton KA (2003). Adoptive transfer of splenocytes in SCID mice implicates $CD4^+$ T cells in apoptosis and epithelial proliferation associated with *Helicobacter pylori*-induced gastritis. *Comp Med* **53:** 498-509.

55 Lundgren A, Stromberg E, Sjoling A, Lindholm C, Enarsson K, Edebo A *et al* (2005). Mucosal FOXP3-expressing $CD4^+CD25^{high}$ regulatory T cells in *Helicobacter pylori*-infected patients. *Infect Immun* **73:** 523-531.

56 Muller A, Solnick JV (2011). Inflammation, immunity, and vaccine development for *Helicobacter pylori*. *Helicobacter* **16 Suppl 1:** 26-32.

57 Robinson K, Kenefeck R, Pidgeon EL, Shakib S, Patel S, Polson RJ *et al* (2008). *Helicobacter pylori*-induced peptic ulcer disease is associated with inadequate regulatory T cell responses. *Gut* **57:** 1375-1385.

58 Wang YH, Gorvel JP, Chu YT, Wu JJ, Lei HY (2010). *Helicobacter pylori* impairs murine dendritic cell responses to infection. *PLoS One* **5:** e10844.

59 Scaltriti M, Baselga J (2006). The epidermal growth factor receptor pathway: A model for targeted therapy. *Clin Cancer Res* **12:** 5268-5272.

60 Jorissen RN, Walker F, Pouliot N, Garrett TPJ, Ward CW, Burgess AW (2003). Epidermal growth factor receptor: Mechanisms of activation and signalling. *Exp Cell Res* **284:** 31-53.

61 Chen J, Zeng F, Forrester SJ, Eguchi S, Zhang M-Z, Harris RC (2016). Expression and function of the epidermal growth factor receptor in physiology and disease. *Physiol Rev* **96:** 1025-1069.

62 Schneider MR, Wolf E (2009). The epidermal growth factor receptor ligands at a glance. *J Cell Physiol* **218:** 460-466.

63 Marikovsky M, Breuing K, Liu PY, Eriksson E, Higashiyama S, Farber P *et al* (1993). Appearance of heparin-binding EGF-like growth factor in wound fluid as a response to injury. *Proc Natl Acad Sci USA* **90:** 3889-3893.

64 Schlessinger J (2002). Ligand-induced, receptor-mediated dimerization and activation of EGF receptor. *Cell* **110:** 669-672.

65 Medts, T, de Diesbach, P, Cominelli, A, N'Kuli, F, Tyteca, D, Courtoy PJ (2010). Acute ligand-independent Src activation mimics low EGF-induced EGFR surface signalling and redistribution into recycling endosomes. *Exp Cell Res* **316:** 3239-3253.

66 Nishimura M, Shin M, Singhirunnusorn P, Suzuki S, Kawanishi M, Koizumi K *et al* (2009). Tak1-mediated serine/threonine phosphorylation of epidermal growth factor receptor via p38/extracellular signal-regulated kinase: NF-κB-independent survival pathways in tumor necrosis factor alpha signaling. *Mol Cell Biol* **29:** 5529-5539.

67 Hobbs SS, Goettel JA, Liang D, Yan F, Edelblum KL, Frey MR *et al* (2011). TNF transactivation of EGFR stimulates cytoprotective COX-2 expression in gastrointestinal epithelial cells. *Am J Physiol Gastrointest Liver Physiol* **301**: 220-229.

68 Oda K, Matsuoka Y, Funahashi A, Kitano H (2005). A comprehensive pathway map of epidermal growth factor receptor signaling. *Mol Sys Biol* **1:** 2005 0010.

69 Nicholson RI, Gee JMW, Harper ME (2001). EGFR and cancer prognosis. *Eur J Cancer* **37:** 9-15.

70 Markman B, Javier Ramos F, Capdevila J, Tabernero J (2010). EGFR and KRAS in colorectal cancer. *Adv Clin Chem* **51:** 71-119.

71 Krasinskas AM (2011). EGFR Signaling in colorectal carcinoma. *Pathol Res Int* **2011:** 932932.

72 Spano JP, Lagorce C, Atlan D, Milano G, Domont J, Benamouzig R *et al* (2005). Impact of EGFR expression on colorectal cancer patient prognosis and survival. *Ann Oncol* **16:** 102-108.

73 Sasaki T, Hiroki K, Yamashita Y (2013). The role of epidermal growth factor receptor in cancer metastasis and microenvironment. *BioMed Res Int* **2013:** 546318.

74 Chaturvedi R, Asim M, Piazuelo MB, Yan F, Barry DP, Sierra JC *et al* (2014). Activation of EGFR and ErbB2 by *Helicobacter pylori* results in survival of gastric epithelial cells with DNA damage. *Gastroenterology* **146:** 1739-1751.

75 Tokunaga, A, Onda, M, Okuda, T, Teramoto, T, Fujita, I, Mizutani, T, *et al* (1995). Clinical significance of epidermal growth factor (EGF), EGF receptor, and c-*erbB*-2 in human gastric cancer. *Cancer* **15:** 1418-1425.

76 Yan F, Cao H, Chaturvedi R, Krishna U, Hobbs SS, Dempsey PJ *et al* (2009). Epidermal growth factor receptor activation protects gastric epithelial cells from *Helicobacter pylori*-induced apoptosis. *Gastroenterology* **136:** 1297-1307.

77 Yang JL, Qu XJ, Russell PJ, Goldstein D (2004). Regulation of epidermal growth factor receptor in human colon cancer cell lines by interferon alpha. *Gut* **53:** 123-129.

78 Tietzel I, Mosser DM (2002). The modulation of macrophage activation by tyrosine phosphorylation. *Front Biosci* **7:** 494-502.

79 Scholes AG, Hagan S, Hiscott P, Damato BE, Grierson I (2001). Overexpression of epidermal growth factor receptor restricted to macrophages in uveal melanoma. *Arch Ophthalmol* **119:** 373-377.

80 Chan G, Nogalski MT, Yurochko AD (2009). Activation of EGFR on monocytes is required for human cytomegalovirus entry and mediates cellular motility. *Proc Natl Acad Sci USA* **106:** 22369-22374.

81 Gao P, Wang X-m, Qian D-h, Qin Z-X, Jin J, Xu Q *et al* (2013). Induction of oxidative stress by oxidized LDL via meprinα-activated epidermal growth factor receptor in macrophages. *Cardiovasc Res* **97**: 533-543.

82 Lanaya H, Natarajan A, Komposch K, Li L, Amberg N, Chen L *et al* (2014). EGFR has a tumour-promoting role in liver macrophages during hepatocellular carcinoma formation. *Nat Cell Biol* **16:** 972-981.

83 Lu N, Wang L, Cao H, Liu L, Van Kaer L, Washington MK *et al* (2014). Activation of the epidermal growth factor receptor in macrophages regulates cytokine production and experimental colitis. *J Immunol* **192:** 1013-1023.

84 Pegg AE (2006). Regulation of ornithine decarboxylase. *J Biol Chem* **281:** 14529-14532.

85 Pegg AE (2009). Mammalian polyamine metabolism and function. *IUBMB Life* **61:** 880-894.

86 Gobert AP, Wilson KT (2017). Human and *Helicobacter pylori* interactions determine the outcome of gastric diseases. *Curr Topics Microbiol Immunol* **400:** 27-52.

87 Murray-Stewart TR, Woster PM, Casero RA, Jr. (2016). Targeting polyamine metabolism for cancer therapy and prevention. *Biochem J* **473:** 2937-2953.

88 Singh K, Al-Greene NT, Verriere TG, Coburn LA, Asim M, Barry DP *et al* (2016). The L-Arginine transporter Solute Carrier Family 7, Member 2 mediates the immunopathogenesis of attaching and effacing bacteria. *PLoS Pathog* **12:** e1005984.

89 Pekarova M, Lojek A (2015). The crucial role of L-arginine in macrophage activation: What you need to know about it. *Life Sci* **137:** 44-48.

90 Brooks WH (2013). Increased polyamines alter chromatin and stabilize autoantigens in autoimmune diseases. *Front Immunol* **4:** 91.

91 Casero RA, Jr., Marton LJ (2007). Targeting polyamine metabolism and function in cancer and other hyperproliferative diseases. *Nat Rev Drug Disc* **6:** 373-390.

92 Hobbs CA, Gilmour SK (2000). High levels of intracellular polyamines promote histone acetyltransferase activity resulting in chromatin hyperacetylation. *J Cell Biochem* **77:** 345-360.

93 Huang Y, Marton LJ, Woster PM, Casero RA (2009). Polyamine analogues targeting epigenetic gene regulation. *Essays Biochem* **46:** 95-110.

94 Chaturvedi R, Asim M, Romero-Gallo J, Barry DP, Hoge S, de Sablet T *et al* (2011). Spermine oxidase mediates the gastric cancer risk associated with *Helicobacter pylori* CagA. *Gastroenterology* **141:** 1696-1708 e1691-1692.

95 Cheng Y, Chaturvedi R, Asim M, Bussiere FI, Scholz A, Xu H *et al* (2005). *Helicobacter pylori*-induced macrophage apoptosis requires activation of ornithine decarboxylase by c-Myc. *J Biol Chem* **280:** 22492-22496.

96 Gobert AP, Cheng Y, Wang J, Boucher JL, Iyer RK, Cederbaum SD *et al* (2002). *Helicobacter pylori* induces macrophage apoptosis by activation of arginase II. *J Immunol* **168:** 4692-4700.

97 Asim M, Chaturvedi R, Hoge S, Lewis ND, Singh K, Barry DP *et al* (2010). *Helicobacter pylori* induces ERK-dependent formation of a phospho-c-Fos c-Jun activator protein-1 complex that causes apoptosis in macrophages. *J Biol Chem* **285:** 20343-20357.

98 Martinez FO, Gordon S (2014). The M1 and M2 paradigm of macrophage activation: Time for reassessment. *F1000Prime Rep* **6:** 13.

99 Krausgruber T, Blazek K, Smallie T, Alzabin S, Lockstone H, Sahgal N *et al* (2011). IRF5 promotes inflammatory macrophage polarization and TH1-TH17 responses. *Nat Immunol* **12:** 231-238.

100 Liu B, Neufeld AH (2003). Activation of epidermal growth factor receptor signals induction of nitric oxide synthase-2 in human optic nerve head astrocytes in glaucomatous optic neuropathy. *Neurobiol Dis* **13:** 109-123.

101 Sibony M, Jones NL (2012). Recent advances in *Helicobacter pylori* pathogenesis. *Curr Opin Gastroenterol* **28:** 30-35.

102 Nomura A, Stemmermann GN, Chyou PH, Kato I, Perez-Perez GI, Blaser MJ (1991). *Helicobacter pylori* infection and gastric carcinoma among Japanese Americans in Hawaii. *N Engl J Med* **325:** 1132-1136.

103 Lewis ND, Asim M, Barry DP, de Sablet T, Singh K, Piazuelo MB *et al* (2011). Immune evasion by *Helicobacter pylori* is mediated by induction of macrophage arginase II. *J Immunol* **186:** 3632-3641.

104 Kelly M, Hart E, Mundy R, Marchès O, Wiles S, Badea L *et al* (2006). Essential role of the type III secretion system effector NleB in colonization of mice by *Citrobacter rodentium*. *Infect Immun* **74:** 2328-2337.

105 Schreiber HA, Loschko J, Karssemeijer RA, Escolano A, Meredith MM, Mucida D *et al* (2013). Intestinal monocytes and macrophages are required for T cell polarization in response to *Citrobacter rodentium*. *J Exp Med* **210:** 2025-2039.

106 Van Kaer L, Algood HM, Singh K, Parekh VV, Greer MJ, Piazuelo MB *et al* (2014). CD8alphaalpha(+) innate-type lymphocytes in the intestinal epithelium mediate mucosal immunity. *Immunity* **41:** 451-464.

107 Gobert AP, Asim M, Piazuelo MB, Verriere T, Scull BP, de Sablet T *et al* (2011). Disruption of nitric oxide signaling by *Helicobacter pylori* results in enhanced inflammation by inhibition of heme oxygenase-1. *J Immunol* **187:** 5370-5379.

108 Singhirunnusorn P, Ueno Y, Matsuo M, Suzuki S, Saiki I, Sakurai H (2007). Transient suppression of ligand-mediated activation of epidermal growth factor receptor by tumor necrosis factor-α through the Tak1-p38 signaling pathway. *J Biol Chem* **282:** 12698-12706.

109 Lee T, Threadgill DW (2009). Generation and validation of mice carrying a conditional allele of the epidermal growth factor receptor. *Genesis* **47:** 85-92.

110 Algood HM, Gallo-Romero J, Wilson KT, Peek RM, Jr., Cover TL (2007). Host response to *Helicobacter pylori* infection before initiation of the adaptive immune response. *FEMS Immunol Med Microbiol* **51:** 577-586.

111 Israel DA, Peek RM, Jr. (2006). The role of persistence in *Helicobacter pylori* pathogenesis. *Curr Opin Gastroenterol* **22:** 3-7.

112 Noto JM, Gaddy JA, Lee JY, Piazuelo MB, Friedman DB, Colvin DC *et al* (2013). Iron deficiency accelerates *Helicobacter pylori*-induced carcinogenesis in rodents and humans. *J Clin Invest* **123:** 479-492.

113 Gobert AP, Cheng Y, Akhtar M, Mersey BD, Blumberg DR, Cross RK *et al* (2004). Protective role of arginase in a mouse model of colitis. *J Immunol* **173:** 2109-2117.

114 Chaturvedi R, Asim M, Lewis ND, Algood HM, Cover TL, Kim PY *et al* (2007). L-arginine availability regulates inducible nitric oxide synthase-dependent host defense against *Helicobacter pylori*. *Infect Immun* **75:** 4305-4315.

115 Lewis ND, Asim M, Barry DP, Singh K, de Sablet T, Boucher JL *et al* (2010). Arginase II restricts host defense to *Helicobacter pylori* by attenuating inducible nitric oxide synthase translation in macrophages. *J Immunol* **184:** 2572-2582.

116 Backert S, Naumann M (2010). What a disorder: Proinflammatory signaling pathways induced by *Helicobacter pylori*. *Trends Microbiol* **18:** 479-486.

117 Brandt S, Kwok T, Hartig R, Konig W, Backert S (2005). NF-κB activation and potentiation of proinflammatory responses by the *Helicobacter pylori* CagA protein. *Proc Natl Acad Sci USA* **102:** 9300-9305.

118 Everhart MB, Han W, Sherrill TP, Arutiunov M, Polosukhin VV, Burke JR *et al* (2006). Duration and intensity of NF-κB activity determine the severity of endotoxin-induced acute lung injury. *J Immunol* **176:** 4995-5005.

119 Han W, Li H, Cai J, Gleaves LA, Polosukhin VV, Segal BH *et al* (2013). NADPH oxidase limits lipopolysaccharide-induced lung inflammation and injury in mice through reduction-oxidation regulation of NF-κB activity. *J Immunol* **190:** 4786-4794.

120 Orton RJ, Sturm OE, Vyshemirsky V, Calder M, Gilbert DR, Kolch W (2005). Computational modelling of the receptor-tyrosine-kinase-activated MAPK pathway. *Biochem J* **392:** 249-261.

121 Schulze WX, Deng L, Mann M (2005). Phosphotyrosine interactome of the ErbB-receptor kinase family. *Molec Sys Biol* **1:** 2005 0008.

122 Dienz O, Rincon M (2009). The effects of IL-6 on CD4 T cell responses. *Clin Immunol* **130:** 27-33.

123 Gobert AP, Mersey BD, Cheng Y, Blumberg DR, Newton JC, Wilson KT (2002). Cutting edge: Urease release by *Helicobacter pylori* stimulates macrophage inducible nitric oxide synthase. *J Immunol* **168:** 6002-6006.

124 DeLyria ES, Redline RW, Blanchard TG (2009). Vaccination of mice against *Helicobacter pylori* induces a strong Th-17 response and immunity that is neutrophil dependent. *Gastroenterology* **136:** 247-256.

125 Mangan PR, Harrington LE, O'Quinn DB, Helms WS, Bullard DC, Elson CO *et al* (2006). Transforming growth factor-beta induces development of the T(H)17 lineage. *Nature* **441:** 231-234.

126 Rad R, Brenner L, Krug A, Voland P, Mages J, Lang R *et al* (2007). Toll-like receptor-dependent activation of antigen-presenting cells affects adaptive immunity to *Helicobacter pylori*. *Gastroenterology* **133:** 150-163 e153.

127 Dalal RS, Moss SF (2014). At the bedside: *Helicobacter pylori*, dysregulated host responses, DNA damage, and gastric cancer. *J Leukoc Biol* **96:** 213-224.

128 Weischenfeldt J, Porse B (2008). Bone marrow-derived macrophages (BMM): Isolation and applications. *Cold Spring Harbor Prot* **2008:** 1-6.

129 Matheu MP, Sen D, Cahalan MD, Parker I (2008). Generation of bone marrow derived murine dendritic cells for use in 2-photon imaging. *J Visual Exp* **17**: 773.

130 Sheh A, Ge Z, Parry NM, Muthupalani S, Rager JE, Raczynski AR *et al* (2011). 17beta-estradiol and tamoxifen prevent gastric cancer by modulating leukocyte recruitment and oncogenic pathways in *Helicobacter pylori*-infected INS-GAS male mice. *Cancer Prev Res* **4:** 1426-1435.

131 Singh K, Chaturvedi R, Barry DP, Coburn LA, Asim M, Lewis ND *et al* (2011). The apolipoprotein E-mimetic peptide COG112 inhibits NF-κB signaling, proinflammatory cytokine expression, and disease activity in murine models of colitis. *J Biol Chem* **286:** 3839-3850.

132 Coburn LA, Horst SN, Chaturvedi R, Brown CT, Allaman MM, Scull BP *et al* (2013). High-throughput multi-analyte Luminex profiling implicates eotaxin-1 in ulcerative colitis. *PLoS One* **8:** e82300.

133 Brower V (2005). Feeding the flame: new research adds to role of inflammation in cancer development. *J Natl Can Inst* **97:** 251-253.

134 Terzic J, Grivennikov S, Karin E, Karin M (2010). Inflammation and colon cancer. *Gastroenterology* **138:** 2101-2114 e2105.

135 Erreni M, Mantovani A, Allavena P (2011). Tumor-associated macrophages (TAM) and inflammation in colorectal cancer. *Cancer Microenviron* **4:** 141-154.

136 Isidro RA, Appleyard CB (2016). Colonic macrophage polarization in homeostasis, inflammation, and cancer. *Am J Physiol Gastrointest Liver Physiol* **311:** G59-73.

137 Georgoudaki AM, Prokopec KE, Boura VF, Hellqvist E, Sohn S, Ostling J *et al* (2016). Reprogramming tumor-associated macrophages by antibody targeting inhibits cancer progression and metastasis. *Cell Rep* **15:** 2000-2011.

138 Greten FR, Eckmann L, Greten TF, Park JM, Li ZW, Egan LJ *et al* (2004). IKKβ links inflammation and tumorigenesis in a mouse model of colitis-associated cancer. *Cell* **118:** 285-296.

139 Sakamoto K, Maeda S, Hikiba Y, Nakagawa H, Hayakawa Y, Shibata W *et al* (2009). Constitutive NF-κB activation in colorectal carcinoma plays a key role in angiogenesis, promoting tumor growth. *Clin Cancer Res* **15:** 2248-2258.

140 Xie W, Li M, Xu N, Lv Q, Huang N, He J *et al* (2013). MiR-181a regulates inflammation responses in monocytes and macrophages. *PLoS One* **8:** e58639.

141 De Simone V, Franze E, Ronchetti G, Colantoni A, Fantini MC, Di Fusco D *et al* (2015). Th17-type cytokines, IL-6 and TNF-α synergistically activate STAT3 and NF-κB to promote colorectal cancer cell growth. *Oncogene* **34:** 3493-3503.

142 Yu H, Pardoll D, Jove R (2009). STATs in cancer inflammation and immunity: A leading role for STAT3. *Nat Rev Cancer* **9:** 798-809.

143 Hardbower DM, Singh K, Asim M, Verriere TG, Olivares-Villagomez D, Barry DP *et al* (2016). EGFR regulates macrophage activation and function in bacterial infection. *J Clin Invest* **126:** 3296-3312.

144 Parang B, Kaz AM, Barrett CW, Short SP, Ning W, Keating CE *et al* (2016). BVES regulates c-Myc stability via PP2A and suppresses colitis-induced tumourigenesis. *Gut* **0**: 1-11.

145 De Robertis M, Massi E, Poeta ML, Carotti S, Morini S, Cecchetelli L *et al* (2011). The AOM/DSS murine model for the study of colon carcinogenesis: From pathways to diagnosis and therapy studies. *Journal Carcinog* **10:** 9.

146 West NR, McCuaig S, Franchini F, Powrie F (2015). Emerging cytokine networks in colorectal cancer. *Nat Rev Immunol* **15:** 615-629.

147 Hiemisch H, Schutz G, Kaestner KH (1997). Transcriptional regulation in endoderm development: Characterization of an enhancer controlling Hnf3g expression by transgenesis and targeted mutagenesis. *EMBO J* **16:** 3995-4006.

148 Katz JP, Perreault N, Goldstein BG, Actman L, McNally SR, Silberg DG *et al* (2005). Loss of Klf4 in mice causes altered proliferation and differentiation and precancerous changes in the adult stomach. *Gastroenterology* **128:** 935-945.

149 Holmfeldt P, Ganuza M, Marathe H, He B, Hall T, Kang G *et al* (2016). Functional screen identifies regulators of murine hematopoietic stem cell repopulation. *J Exp Med* **213:** 433-449.

150 Barrett CW, Fingleton B, Williams A, Ning W, Fischer MA, Washington MK *et al* (2011). MTGR1 is required for tumorigenesis in the murine AOM/DSS colitis-associated carcinoma model. *Cancer Res* **71:** 1302-1312.

151 Chandrasekar B, Deobagkar-Lele M, Victor ES, Nandi D (2013). Regulation of chemokines, CCL3 and CCL4, by interferon gamma and nitric oxide synthase 2 in mouse macrophages and during Salmonella enterica serovar typhimurium infection. *J Infect Dis* **207:** 1556-1568.

152 Porta C, Rimoldi M, Raes G, Brys L, Ghezzi P, Di Liberto D *et al* (2009). Tolerance and M2 (alternative) macrophage polarization are related processes orchestrated by p50 nuclear factor kappaB. *Proc Natl Acad Sci USA* **106:** 14978-14983.

153 Valbuena G, Bradford W, Walker DH (2003). Expression analysis of the T-cell-targeting chemokines CXCL9 and CXCL10 in mice and humans with endothelial infections caused by rickettsiae of the spotted fever group. *Am J Pathol* **163:** 1357-1369.

154 Yu H, Yue X, Zhao Y, Li X, Wu L, Zhang C *et al* (2014). LIF negatively regulates tumour-suppressor p53 through Stat3/ID1/MDM2 in colorectal cancers. *Nature Commun* **5:** 5218.

155 Yue X, Wu L, Hu W (2015). The regulation of leukemia inhibitory factor. *Cancer Cell Microenviron* **2**: e877.

156 Huaux F, Lo Re S, Giordano G, Uwambayinema F, Devosse R, Yakoub Y *et al* (2015). IL-1alpha induces CD11b(low) alveolar macrophage proliferation and maturation during granuloma formation. *J Pathol* **235:** 698-709.

157 Sweet MJ, Hume DA (2003). CSF-1 as a regulator of macrophage activation and immune responses. *Arch Immunol Ther Exp (Warsz)* **51:** 169-177.

158 Van Overmeire E, Stijlemans B, Heymann F, Keirsse J, Morias Y, Elkrim Y *et al* (2016). M-CSF and GM-CSF receptor signaling differentially regulate monocyte maturation and macrophage polarization in the tumor microenvironment. *Cancer Res* **76:** 35-42.

159 Singh K, Chaturvedi R, Asim M, Barry DP, Lewis ND, Vitek MP *et al* (2008). The apolipoprotein E-mimetic peptide COG112 inhibits the inflammatory response to *Citrobacter rodentium* in colonic epithelial cells by preventing NF-κB activation. *J Biol Chem* **283:** 16752-16761.

160 Hanahan D, Weinberg RA (2000). The hallmarks of cancer. *Cell* **100:** 57-70.

161 Mousa L, Salem ME, Mikhail S (2015). Biomarkers of angiogenesis in colorectal cancer. *Biomark Cancer* **7:** 13-19.

162 Rmali KA, Puntis MC, Jiang WG (2007). Tumour-associated angiogenesis in human colorectal cancer. *Colorec Dis* **9:** 3-14.

163 Hol J, Wilhelmsen L, Haraldsen G (2010). The murine IL-8 homologues KC, MIP-2, and LIX are found in endothelial cytoplasmic granules but not in Weibel-Palade bodies. *J Leukoc Biol* **87:** 501-508.

164 Angelo LS, Kurzrock R (2007). Vascular endothelial growth factor and its relationship to inflammatory mediators. *Clin Cancer Res* **13:** 2825-2830.

165 Heidemann J, Ogawa H, Dwinell MB, Rafiee P, Maaser C, Gockel HR *et al* (2003). Angiogenic effects of interleukin 8 (CXCL8) in human intestinal microvascular endothelial cells are mediated by CXCR2. *J Biol Chem* **278:** 8508-8515.

166 Li A, Dubey S, Varney ML, Dave BJ, Singh RK (2003). IL-8 directly enhanced endothelial cell survival, proliferation, and matrix metalloproteinases production and regulated angiogenesis. *J Immunol* **170:** 3369-3376.

167 Ning Y, Manegold PC, Hong YK, Zhang W, Pohl A, Lurje G *et al* (2011). Interleukin-8 is associated with proliferation, migration, angiogenesis and chemosensitivity *in vitro* and *in vivo* in colon cancer cell line models. *Int J Cancer* **128:** 2038-2049.

168 Engstrom A, Erlandsson A, Delbro D, Wijkander J (2014). Conditioned media from macrophages of M1, but not M2 phenotype, inhibit the proliferation of the colon cancer cell lines HT-29 and CACO-2. *Int J Oncol* **44:** 385-392.

169 Wu WK, Llewellyn OP, Bates DO, Nicholson LB, Dick AD (2010). IL-10 regulation of macrophage VEGF production is dependent on macrophage polarisation and hypoxia. *Immunobiol* **215:** 796-803.

170 Pusztaszeri MP, Seelentag W, Bosman FT (2006). Immunohistochemical expression of endothelial markers CD31, CD34, von Willebrand factor, and Fli-1 in normal human tissues. *J Histochem Cytochem* **54:** 385-395.

171 Dube PE, Yan F, Punit S, Girish N, McElroy SJ, Washington MK *et al* (2012). Epidermal growth factor receptor inhibits colitis-associated cancer in mice. *J Clin Invest* **122:** 2780-2792.

172 Kanneganti M, Mino-Kenudson M, Mizoguchi E (2011). Animal models of colitis-associated carcinogenesis. *J Biomed Biotechnol* **2011:** 342637.

173 Uronis JM, Muhlbauer M, Herfarth HH, Rubinas TC, Jones GS, Jobin C (2009). Modulation of the intestinal microbiota alters colitis-associated colorectal cancer susceptibility. *PLoS One* **4:** e6026.

174 Shibata W, Takaishi S, Muthupalani S, Pritchard DM, Whary MT, Rogers AB *et al* (2010). Conditional deletion of IkappaB-kinase-beta accelerates *Helicobacter*-dependent gastric apoptosis, proliferation, and preneoplasia. *Gastroenterology* **138:** 1022-1034 e1021-1010.

175 Chang CW, Chou HY, Lin YS, Huang KH, Chang CJ, Hsu TC *et al* (2008). Phosphorylation at Ser473 regulates heterochromatin protein 1 binding and corepressor function of TIF1β/KAP1. *BMC Mol Biol* **9:** 61.

176 Eames HL, Saliba DG, Krausgruber T, Lanfrancotti A, Ryzhakov G, Udalova IA (2012). KAP1/TRIM28: An inhibitor of IRF5 function in inflammatory macrophages. *Immunobiol* **217:** 1315-1324.

177 Gerner EW, Meyskens FL, Jr. (2004). Polyamines and cancer: Old molecules, new understanding. *Nat Rev Cancer* **4:** 781-792.

178 Linsalata M, Orlando A, Russo F (2014). Pharmacological and dietary agents for colorectal cancer chemoprevention: Effects on polyamine metabolism. *Int J Oncol* **45:** 1802-1812.

179 Soda K (2011). The mechanisms by which polyamines accelerate tumor spread. *J Exp Clin Cancer Res* **30:** 95.

180 Wallace HM, Fraser AV (2004). Inhibitors of polyamine metabolism: review article. *Amino Acids* **26:** 353-365.

181 Heby O, Persson L, Rentala M (2007). Targeting the polyamine biosynthetic enzymes: A promising approach to therapy of African sleeping sickness, Chagas' disease, and leishmaniasis. *Amino Acids* **33:** 359-366.

182 Liao CP, Lasbury ME, Wang SH, Zhang C, Durant PJ, Murakami Y *et al* (2009). Pneumocystis mediates overexpression of antizyme inhibitor resulting in increased polyamine levels and apoptosis in alveolar macrophages. *J Biol Chem* **284:** 8174-8184.

183 Seabra SH, DaMatta RA, de Mello FG, de Souza W (2004). Endogenous polyamine levels in macrophages is sufficient to support growth of *Toxoplasma gondii*. *J Parisitol* **90:** 455-460.

184 Van den Bossche J, Lamers WH, Koehler ES, Geuns JM, Alhonen L, Uimari A *et al* (2012). Pivotal Advance: Arginase-1-independent polyamine production stimulates the expression of IL-4-induced alternatively activated macrophage markers while inhibiting LPS-induced expression of inflammatory genes. *J Leukoc Biol* **91:** 685-699.

185 Hardbower DM, Asim M, Murray-Stewart T, Casero RA, Jr., Verriere T, Lewis ND *et al* (2016). Arginase 2 deletion leads to enhanced M1 macrophage activation and upregulated polyamine metabolism in response to *Helicobacter pylori* infection. *Amino Acids* **48**: 2375-2388.

186 Barry DP, Asim M, Leiman DA, de Sablet T, Singh K, Casero RA, Jr. *et al* (2011). Difluoromethylornithine is a novel inhibitor of *Helicobacter pylori* growth, CagA translocation, and interleukin-8 induction. *PLoS One* **6:** e17510.

187 Williams CS, Bradley AM, Chaturvedi R, Singh K, Piazuelo MB, Chen X *et al* (2013). MTG16 contributes to colonic epithelial integrity in experimental colitis. *Gut* **62:** 1446-1455.

188 Korn T, Bettelli E, Oukka M, Kuchroo VK (2009). IL-17 and Th17 Cells. *Ann Rev Immunol* **27:** 485-517.

189 Tschopp J, Schroder K (2010). NLRP3 inflammasome activation: The convergence of multiple signalling pathways on ROS production? *Nat Rev Immunol* **10:** 210-215.

190 Venkatesh S, Workman JL (2015). Histone exchange, chromatin structure and the regulation of transcription. *Nat Rev Mol Cell Biol* **16:** 178-189.

191 Voss TC, Hager GL (2014). Dynamic regulation of transcriptional states by chromatin and transcription factors. *Nat Rev Genet* **15:** 69-81.

192 Shlyueva D, Stampfel G, Stark A (2014). Transcriptional enhancers: From properties to genome-wide predictions. *Nat Rev Genet* **15:** 272-286.

193 Georgopoulos K (2002). Haematopoietic cell-fate decisions, chromatin regulation and ikaros. *Nat Rev Immunol* **2:** 162-174.

194 Mal A, Harter ML (2003). MyoD is functionally linked to the silencing of a muscle-specific regulatory gene prior to skeletal myogenesis. *Proc Natl Acad Sci USA* **100:** 1735-1739.

195 Rangasamy D (2013). Distinctive patterns of epigenetic marks are associated with promoter regions of mouse LINE-1 and LTR retrotransposons. *Mobile DNA* **4:** 27.

196 Tao H, Li H, Su Y, Feng D, Wang X, Zhang C *et al* (2014). Histone methyltransferase G9a and H3K9 dimethylation inhibit the self-renewal of glioma cancer stem cells. *Mol Cell Biochem* **394:** 23-30.

197 Srivastava S, Bhowmick K, Chatterjee S, Basha J, Kundu TK, Dhar SK (2014). Histone H3K9 acetylation level modulates gene expression and may affect parasite growth in human malaria parasite Plasmodium falciparum. *FEBS J* **281:** 5265-5278.

198 Bailey MT, Dowd SE, Parry NM, Galley JD, Schauer DB, Lyte M (2010). Stressor exposure disrupts commensal microbial populations in the intestines and leads to increased colonization by *Citrobacter rodentium*. *Infect Immun* **78:** 1509-1519.

199 Basu R, O'Quinn DB, Silberger DJ, Schoeb TR, Fouser L, Ouyang W *et al* (2012). Th22 cells are an important source of IL-22 for host protection against enteropathogenic bacteria. *Immunity* **37:** 1061-1075.

200 Wang TC, Dangler CA, Chen D, Goldenring JR, Koh T, Raychowdhury R *et al* (2000). Synergistic interaction between hypergastrinemia and *Helicobacter* infection in a mouse model of gastric cancer. *Gastroenterology* **118:** 36-47.

201 Tao Y, Liu D, Mo G, Wang H, Liu XJ (2015). Peri-ovulatory putrescine supplementation reduces embryo resorption in older mice. *Human Reprod* **30:** 1867-1875.

202 Crusz SM, Balkwill FR (2015). Inflammation and cancer: Advances and new agents. *Nat Rev Clin Oncol* **12:** 584-596.

Appendix A

Supplementary Figures for Chapter 2

EGFR Regulates Macrophage Activation and Function in Bacterial Infection

Dana M. Hardbower[1,2], Kshipra Singh[2], Mohammad Asim[2], Thomas G. Verriere[2], Danyvid Olivares-Villagómez[1], Daniel P. Barry[2], Margaret M. Allaman[2], M. Kay Washington[1], Richard M. Peek, Jr.[2,3], M. Blanca Piazuelo[2], and Keith T. Wilson[1,2,3,4,5]

[1]Department of Pathology, Microbiology, and Immunology; Vanderbilt University Medical Center; Nashville, TN, USA

[2]Division of Gastroenterology, Hepatology, and Nutrition, Department of Medicine; Vanderbilt University Medical Center; Nashville, TN, USA

[3]Department of Cancer Biology; Vanderbilt University Medical Center; Nashville, TN, USA

[4]Center for Mucosal Inflammation and Cancer, Vanderbilt University Medical Center; Nashville, TN, USA

[5]Veterans Affairs Tennessee Valley Healthcare System; Nashville, TN, USA

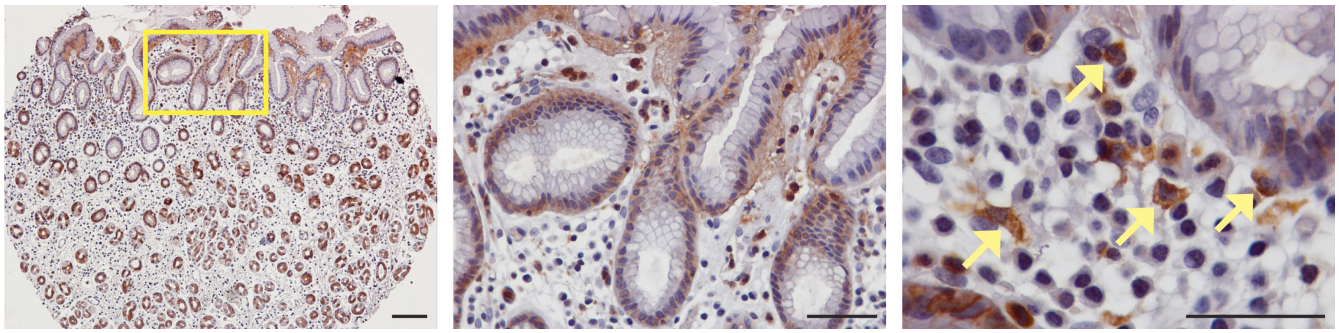

Appendix A, Figure 1. Mononuclear cells in human gastritis tissues have high levels of pEGFR. Representative image of a gastric tissue core from the Vanderbilt University Medical Center human tissue microarray (TMA) assessed for pEGFR expression by immunoperoxidase staining. Middle and right images are magnifications of the area in the yellow box in the left image. Yellow arrows indicate $pEGFR^{+}$ mononuclear cells. Scale bars = 100 μM. *n* = 41 gastritis samples.

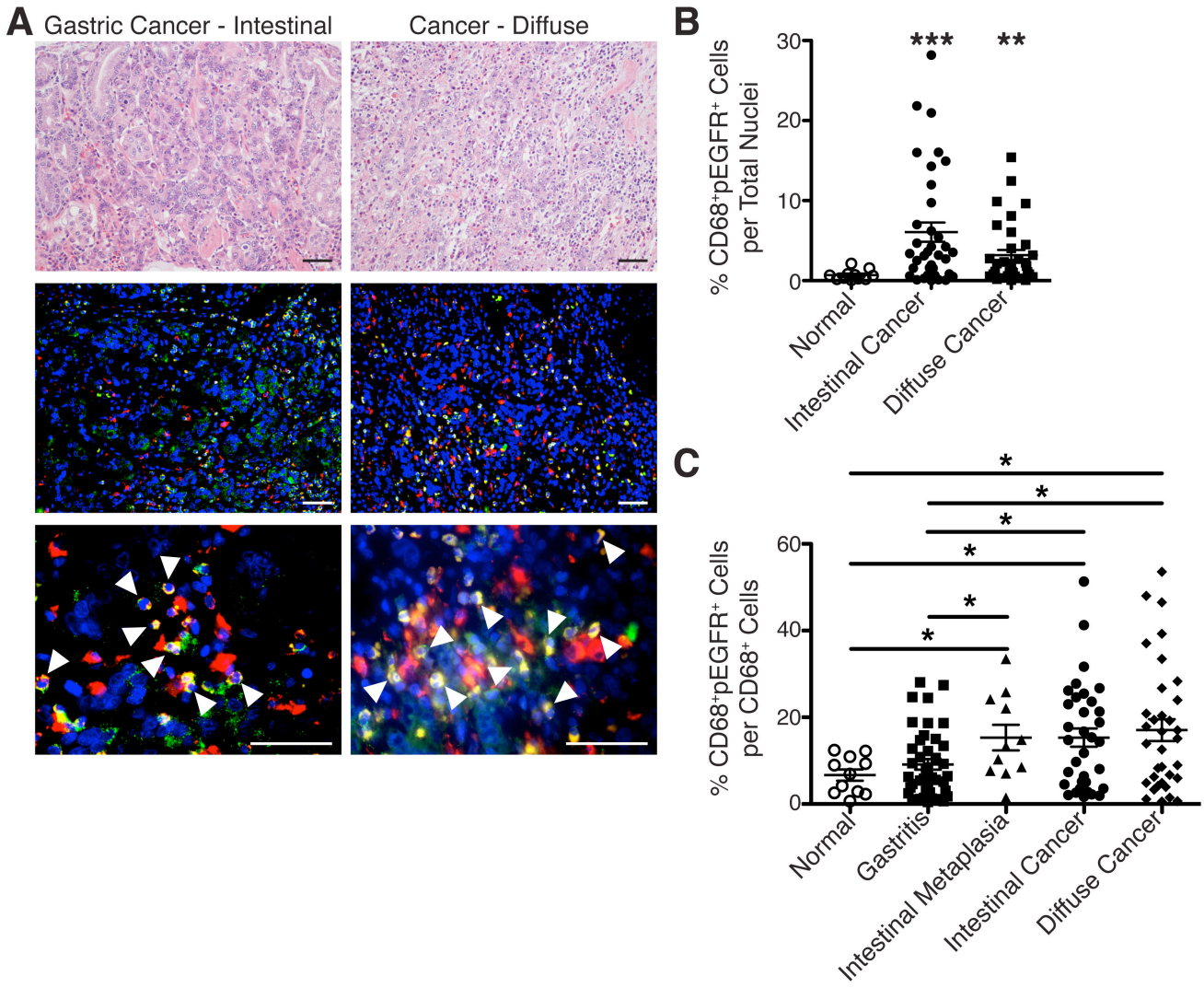

Appendix A, Figure 2. CD68$^+$pEGFR$^+$ macrophages are present in human cases of gastric cancer. (A) Representative hematoxylin and eosin (H&E) and immunofluorescence images for cases of intestinal type and diffuse type gastric adenocarcinoma from the Vanderbilt University Medical Center human TMA. Red = CD68, Green = EGFR pY1068, Yellow = merge and Blue = DAPI. Scale bars = 50 μM. White arrows indicate CD68$^+$pEGFR$^+$ macrophages. *n* = 12 normal samples, 35 intestinal-type cancer, and 35 diffuse-type cancer. (B) Quantification of the percentage of CD68$^+$pEGFR$^+$ macrophages per the total number of cells in each individual core. $^{**}P < 0.01$, $^{***}P < 0.001$ vs. Normal. *n* = 12 normal samples, 35 intestinal-type cancer, and 35 diffuse-type cancer. (C) Quantification of the percentage of CD68$^+$pEGFR$^+$ macrophages per the total number of CD68$^+$ cells in each individual core. $^{*}P < 0.05$. *n* = 12 normal samples, 41 gastritis samples, 11 intestinal metaplasia samples, 35 intestinal-type cancer, and 35 diffuse-type cancer. In (B) and (C), statistical significance was calculated by one-way ANOVA with Kruskal-Wallis test, followed by Mann-Whitney *U* test. Note: The "Normal" data displayed in Panels B and C is the same "Normal" data as in Figure 1D, since there was only one set of normal biopsies on the TMA.

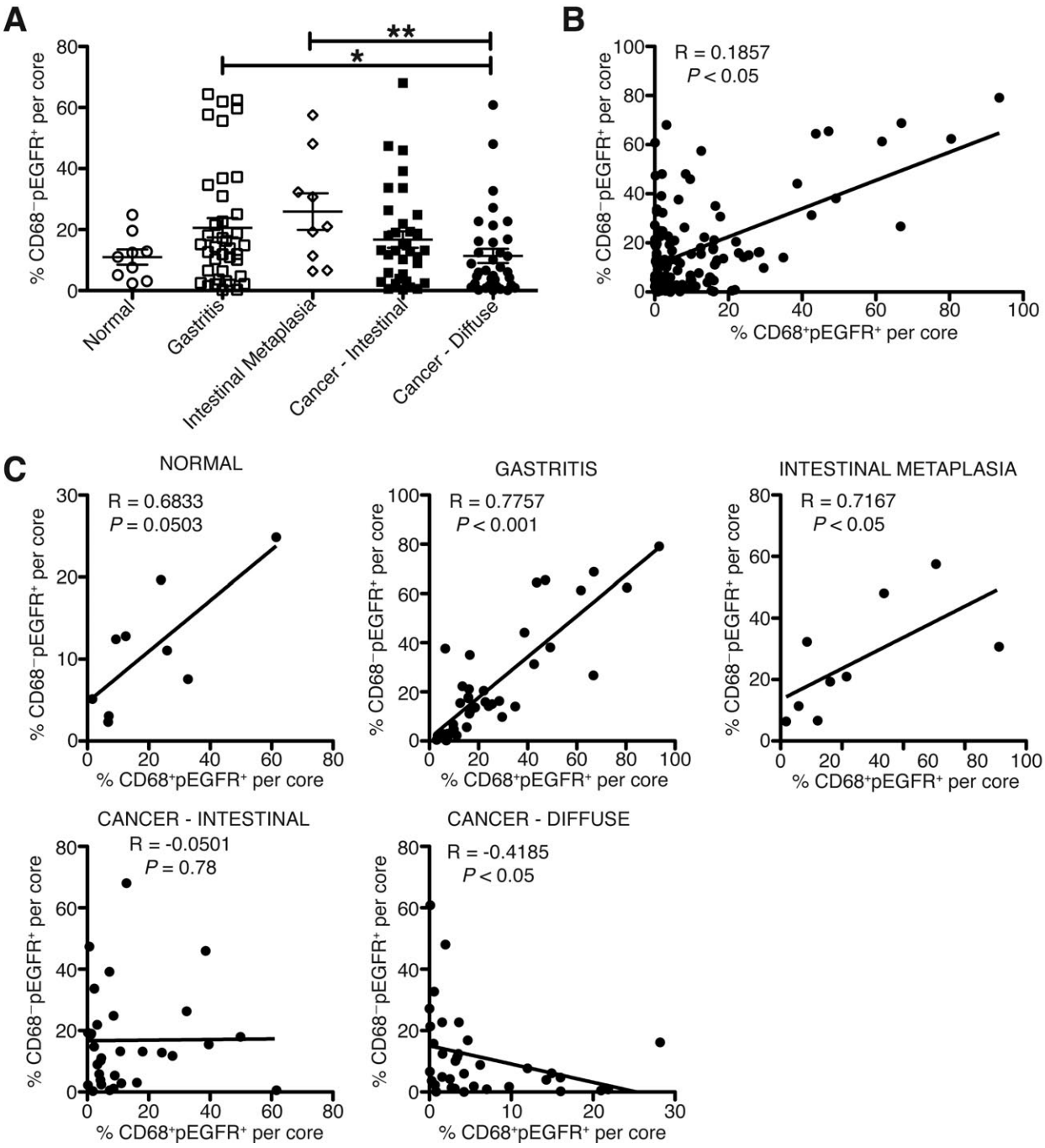

Appendix A, Figure 3. pEGFR levels in CD68$^+$ macrophages and CD68$^-$ cells are correlated in pre-cancerous stages, but not during cancer. (A) Quantification of the percentage of CD68$^-$pEGFR$^+$ cells per the total number of cells in each individual core from the TMA utilized in Figure 1 and in Appendix A, Figures 1 and 2. **P* < 0.05, ***P* < 0.01. Statistical significance was calculated by one-way ANOVA with Kruskal-Wallis test, followed by Mann-Whitney *U* test. (B) Overall correlation between CD68$^+$pEGFR$^+$ macrophages and CD68$^-$pEGFR$^+$ cells; data are from all cores in the TMA. (C) Correlation between CD68$^+$pEGFR$^+$ macrophages and CD68$^-$pEGFR$^+$ cells in each core in cases within the same histologic stage of disease. Correlation in (B) and (C) was calculated using the Spearman's rank correlation coefficient. In all panels, *n* = 12 normal samples, 41 gastritis samples, 9 intestinal metaplasia samples, 35 intestinal-type cancer, and 35 diffuse-type cancer.

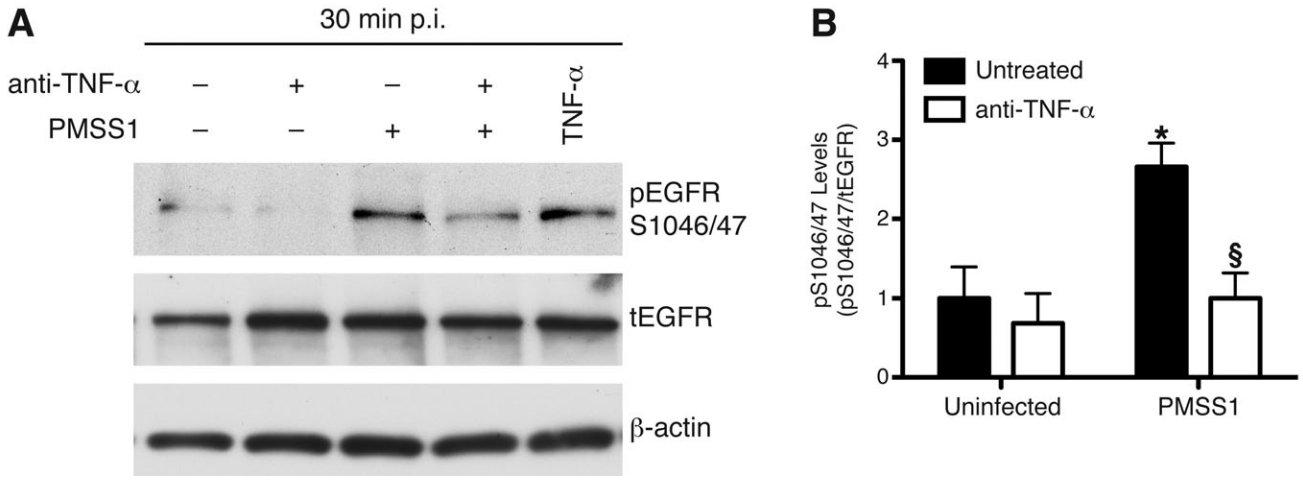

Appendix A, Figure 4. EGFR phosphorylation in macrophages is ligand-independent and TNF-α dependent at the pS1046/47 residue. (A) Representative western blot of EGFR pS1046/47 in RAW 264.7 cells at 30 min p.i. ± anti-TNF-α neutralizing antibody (10 ng/mL) with *H. pylori* PMSS1 infection. Recombinant murine TNF-α (20 ng/mL) also stimulates pS1046/47 at 30 min post-stimulation. *n* = 3 biological replicates. (B) Densitometric analysis of the levels of pS1046/47 in (A). **P* < 0.05 vs. uninfected, untreated control. §*P* < 0.05 vs. untreated, PMSS1-infected cells. *n* = 3 biological replicates. Statistical significance was calculated by one-way ANOVA with Newman-Keuls post-test.

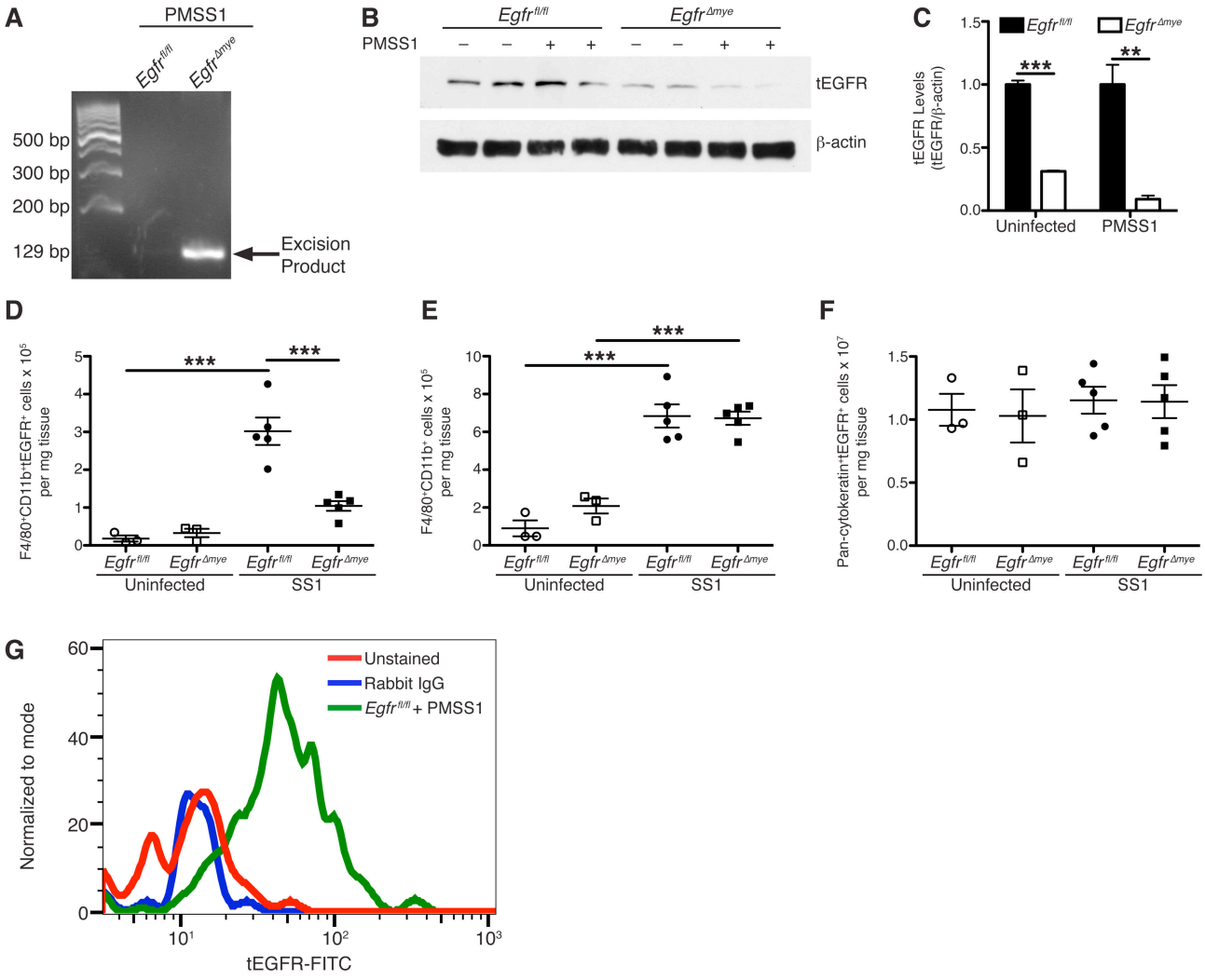

Appendix A, Figure 5. Confirmation of EGFR deletion in *Egfr*$^{\Delta mye}$ bone marrow-derived macrophages and gastric macrophages before and after infection with *H. pylori*. (A) Representative DNA gel of PCR confirmation of *Egfr* excision in *Egfr*$^{\Delta mye}$ bone marrow-derived macrophages (BMmacs) 24 h post-infection (p.i.) with *H. pylori* PMSS1. *n* = 3 biological replicates. (B) Representative western blot confirming tEGFR knockdown in *Egfr*$^{\Delta mye}$ BMmacs 24 h p.i. with *H. pylori* PMSS1. (C) Densitometric analysis of tEGFR levels from (B). $^{**}P < 0.01$, $^{***}P < 0.001$. Statistical significance was calculated by Student's *t* test between uninfected *Egfr*$^{fl/fl}$ and *Egfr*$^{\Delta mye}$ BMmacs and between infected *Egfr*$^{fl/fl}$ and *Egfr*$^{\Delta mye}$ BMmacs. (D) Confirmation of tEGFR knockdown in F4/80$^+$CD11b$^+$ gastric macrophages (Gmacs) from *Egfr*$^{\Delta mye}$ mice 48 h p.i. with *H. pylori* SS1 by flow cytometry. $^{***}P < 0.001$. *n* = 3 uninfected and 5 *H. pylori* SS1 infected mice per genotype. (E) Assessment of the total number of F4/80$^+$CD11b$^+$ Gmacs in the stomachs of *Egfr*$^{fl/fl}$ and *Egfr*$^{\Delta mye}$ mice from (D) by flow cytometry. $^{***}P < 0.001$. *n* = 3 uninfected and 5 *H. pylori* SS1 infected mice per genotype. Statistical significance in (D) and (E) was calculated by one-way ANOVA with Newman-Keuls post-test. (F) Assessment of tEGFR levels in pan-cytokeratin$^+$ gastric epithelial cells from the same *Egfr*$^{fl/fl}$ and *Egfr*$^{\Delta mye}$ mice in (D) and (E). *n* = 3 uninfected and 5 *H. pylori* SS1 infected mice per genotype. (G) Representative flow cytometry tracings of tEGFR staining, including a rabbit IgG isotype control from (D). The population of interest was first selected by gating on the F4/80$^+$CD11b$^+$ cells and then assessing tEGFR-FITC staining.

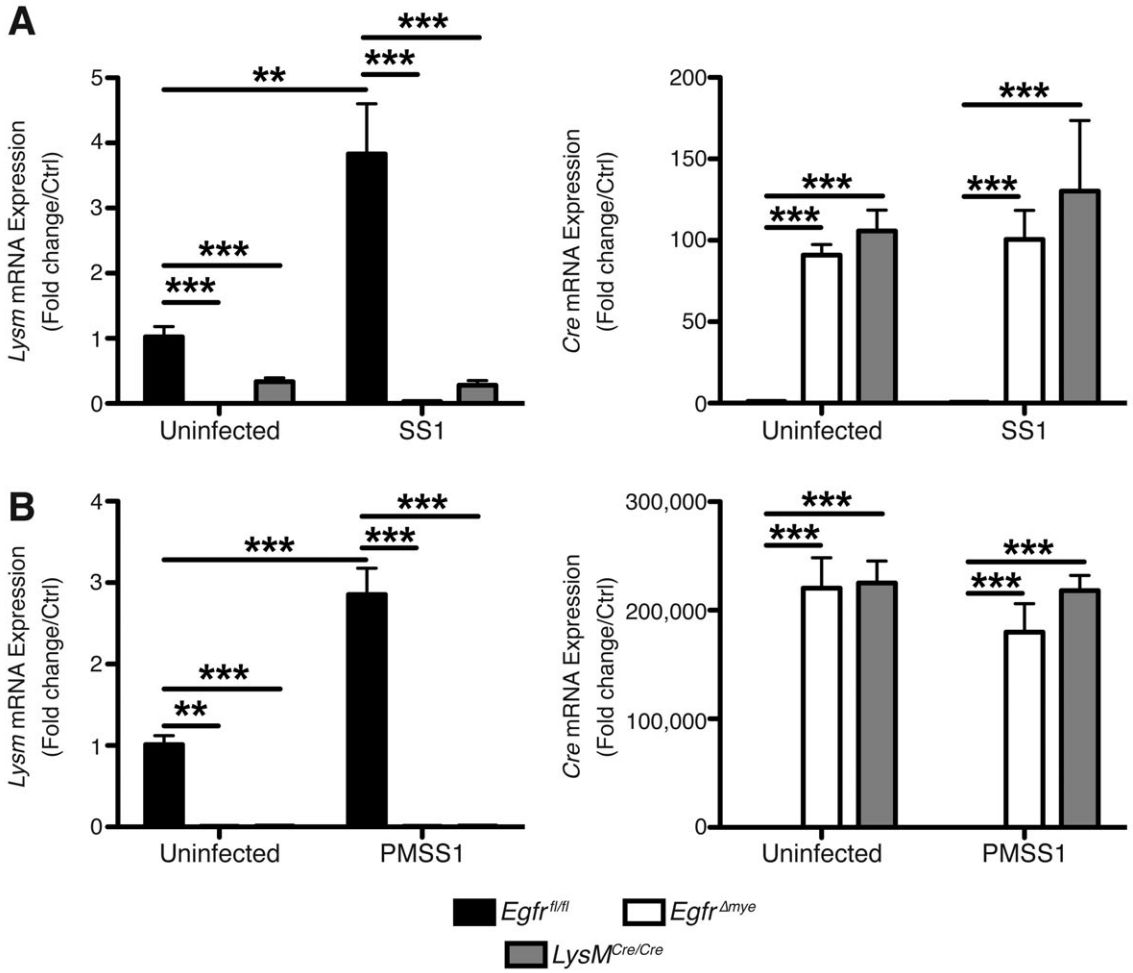

Appendix A, Figure 6. *Egfr*$^{\Delta mye}$ gastric tissues and BMmacs have no *Lysm* expression and substantial *Cre* expression. (A) *Lysm* and *Cre* mRNA levels were assessed by RT-PCR in *Egfr*$^{fl/fl}$, *Egfr*$^{\Delta mye}$, and *LysM*$^{Cre/Cre}$ gastric tissues 4 mo p.i. with *H. pylori* SS1. ***P* < 0.01, ****P* < 0.001. *n* = 3 uninfected and 8 infected mice per genotype. (B) *Lysm* and *Cre* mRNA levels were assessed by RT-PCR in *Egfr*$^{fl/fl}$, *Egfr*$^{\Delta mye}$, and *LysM*$^{Cre/Cre}$ BMmacs 24 h p.i. with *H. pylori* PMSS1. ***P* < 0.01, ****P* < 0.001. *n* = 3 biological replicates per genotype. Statistical significance in all panels was calculated by one-way ANOVA with Newman-Keuls post-test.

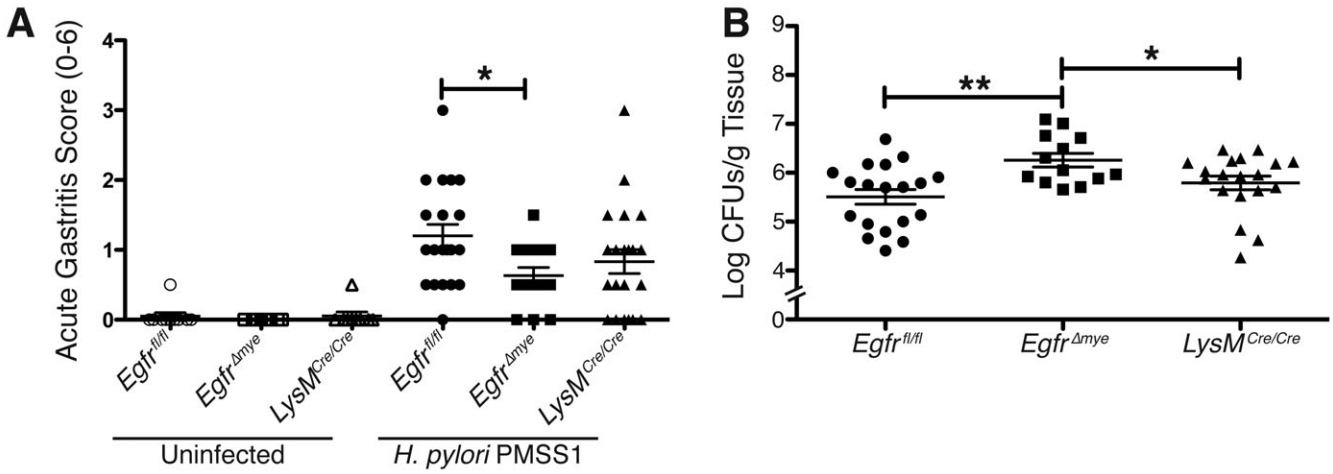

Appendix A, Figure 7. *Egfr*$^{\Delta mye}$ mice have increased bacterial burden and decreased disease pathology during acute *H. pylori* infection. (A) Acute gastritis, specifically scoring neutrophilic infiltrate, was assessed 1 mo p.i by a gastrointestinal pathologist, according to the updated Sydney System, in a blinded manner. *P < 0.05. n = 8-10 uninfected and 15-21 *H. pylori* PMSS1 infected mice per genotype. (B) Colonization levels of *H. pylori* PMSS1 were assessed 1 mo p.i. by serial dilution and culture. *P < 0.05, **P < 0.01. n = 15-21 *H. pylori* PMSS1 infected mice per genotype. Significance in all panels was calculated by one-way ANOVA with Newman-Keuls post-test.

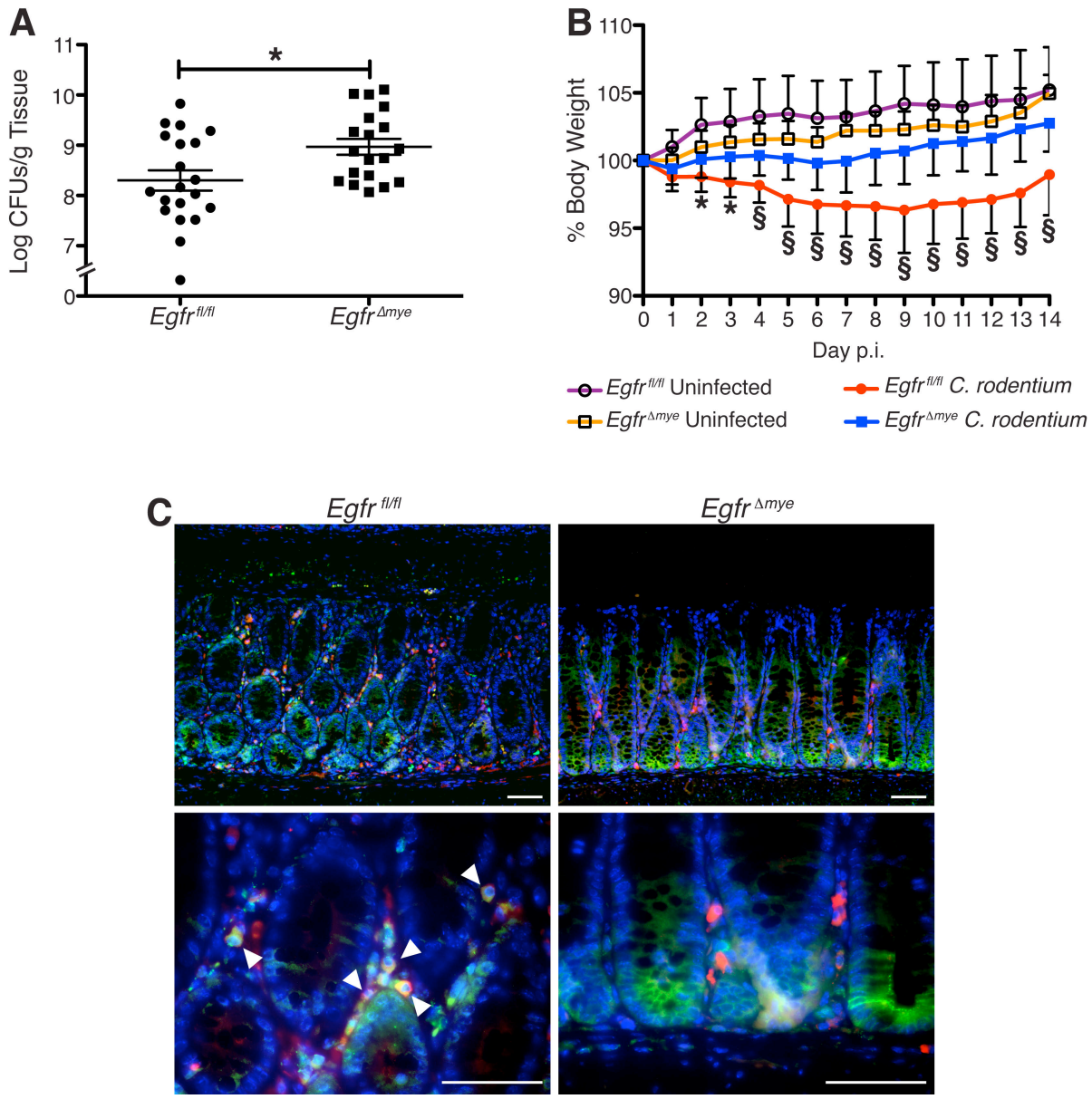

Appendix A, Figure 8. *Egfr*$^{\Delta mye}$ mice have increased bacterial burden and decreased clinical disease severity during *C. rodentium* infection. (A) Colonization levels of *C. rodentium* in colonic tissues were assessed 14 d p.i. by serial dilution and culture. **P* < 0.05. *n* = 8-10 uninfected and 19-20 *C. rodentium* infected mice per genotype. Statistical significance was calculated by Student's *t* test (B) Percentage of initial body weight was assessed on each day of the 14-day infection model. **P* < 0.01, §*P* < 0.001 vs. *Egfr*$^{fl/fl}$ *C. rodentium*. *n* = 8-10 uninfected and 19-20 *C. rodentium* infected mice per genotype. Statistical significance was calculated by one-way ANOVA with the Kruskal-Wallis test, followed by Mann-Whitney *U* test. (C) Representative immunofluorescence images of pEGFR from infected mice in (A) and (B). Green = EGFR pY1068, Red = CD68, Yellow = merge, Blue = DAPI. Arrows indicate CD68$^+$pEGFR$^+$ macrophages. Scale bars = 50 μM. *n* ≥ 3 mice per genotype.

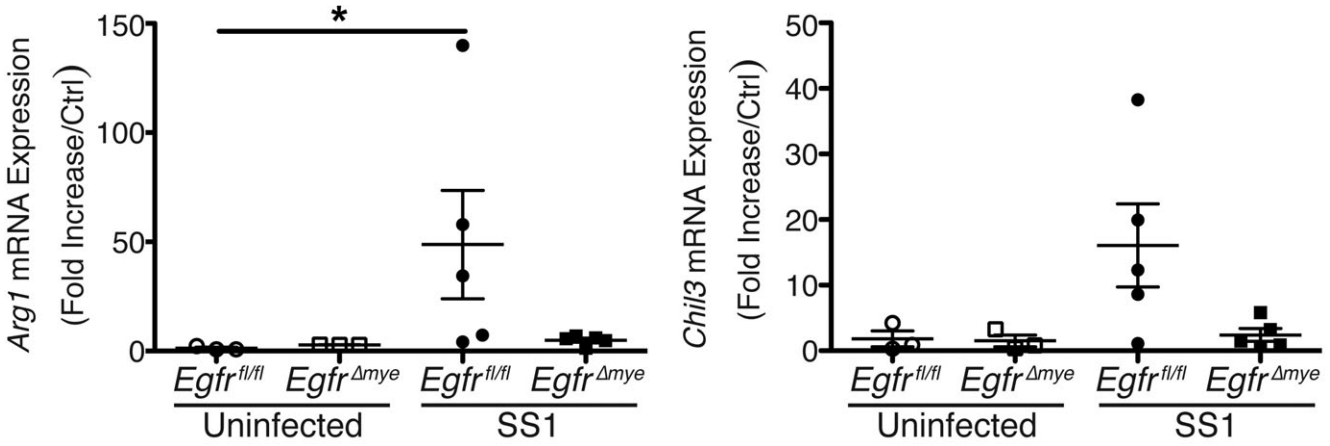

Appendix A, Figure 9. Markers of M2 activation are not significantly altered in *Egfr*$^{\Delta mye}$ gastric tissue during infection with *H. pylori*. *Arg1* and *Chil3* mRNA expression was assessed by RT-PCR in gastric tissues 4 mo p.i. with *H. pylori* SS1. **P* < 0.05. *n* = 3 uninfected and 5 *H. pylori* SS1 infected mice per genotype. Significance was calculated by one-way ANOVA with Newman-Keuls post-test.

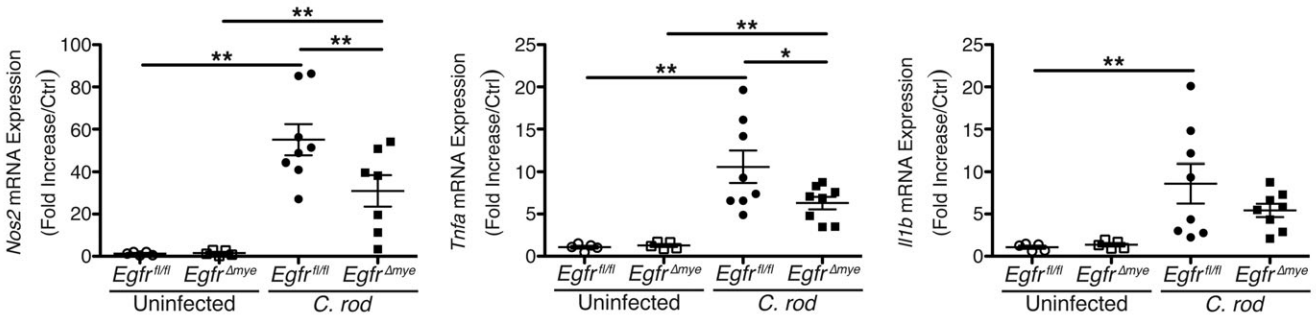

Appendix A, Figure 10. Markers of M1 activation are significantly decreased in *Egfr*$^{\Delta mye}$ colonic tissue during *C. rodentium* infection. *Nos2*, *Tnfa*, and *Il1b* mRNA expression were assessed by RT-PCR in colonic tissue 14 d p.i. **P* < 0.05, ***P* < 0.01. *n* = 5 uninfected and 7-8 *C. rodentium* infected mice per genotype. Statistical significance was calculated by one-way ANOVA with Kruskal-Wallis test, followed by Mann-Whitney *U* test.

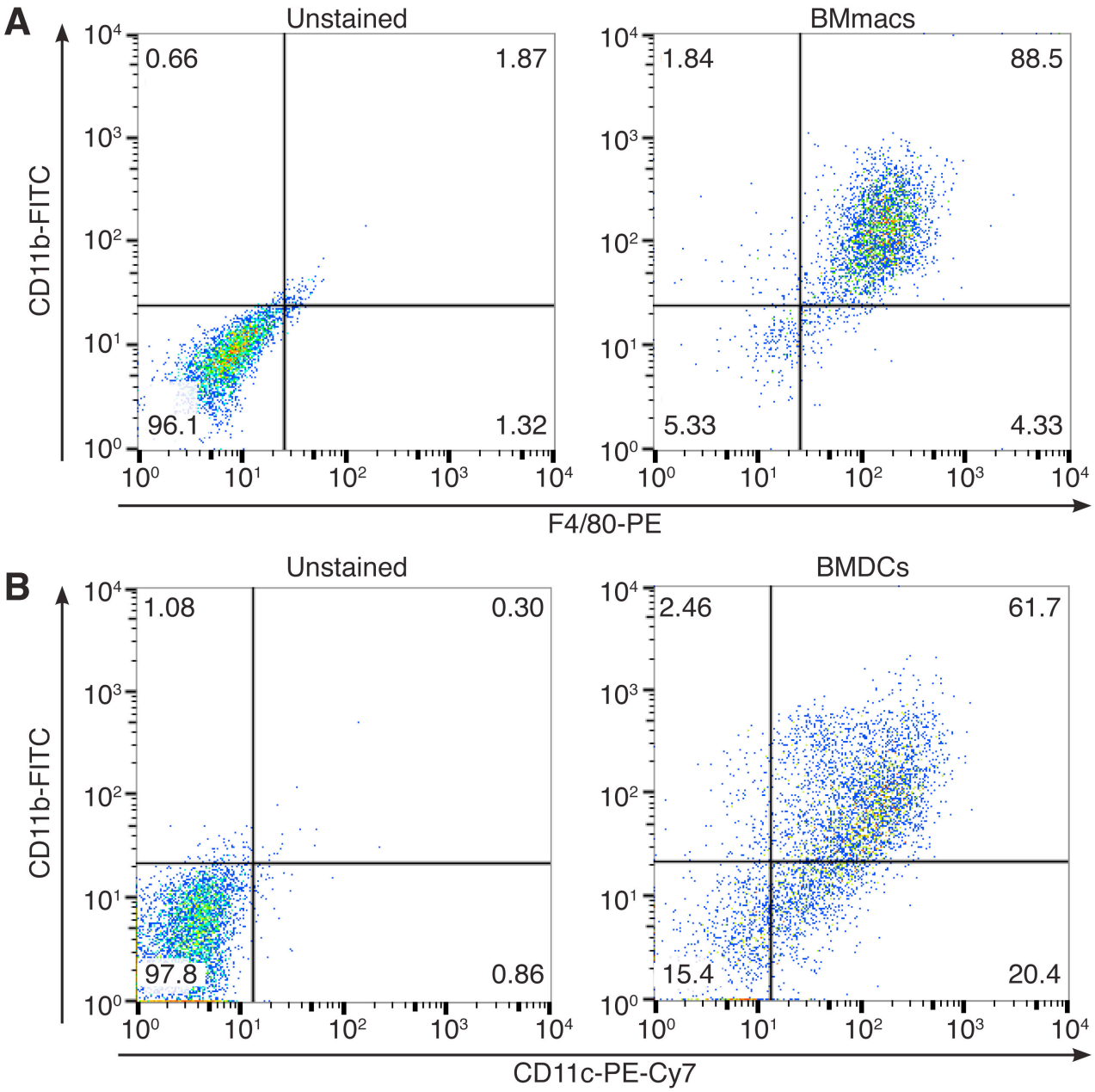

Appendix A, Figure 11. Isolation and differentiation of macrophages and dendritic cells from murine bone marrow. (A) Representative flow cytometry scatter plots demonstrating populations of $CD11b^{+}F4/80^{+}$ BMmacs. (B) Representative flow cytometry scatter plots demonstrating populations of $CD11b^{+}CD11c^{+}$ bone marrow derived dendritic cells (BMDCs). In both panels, *n* = 4 biological replicates.

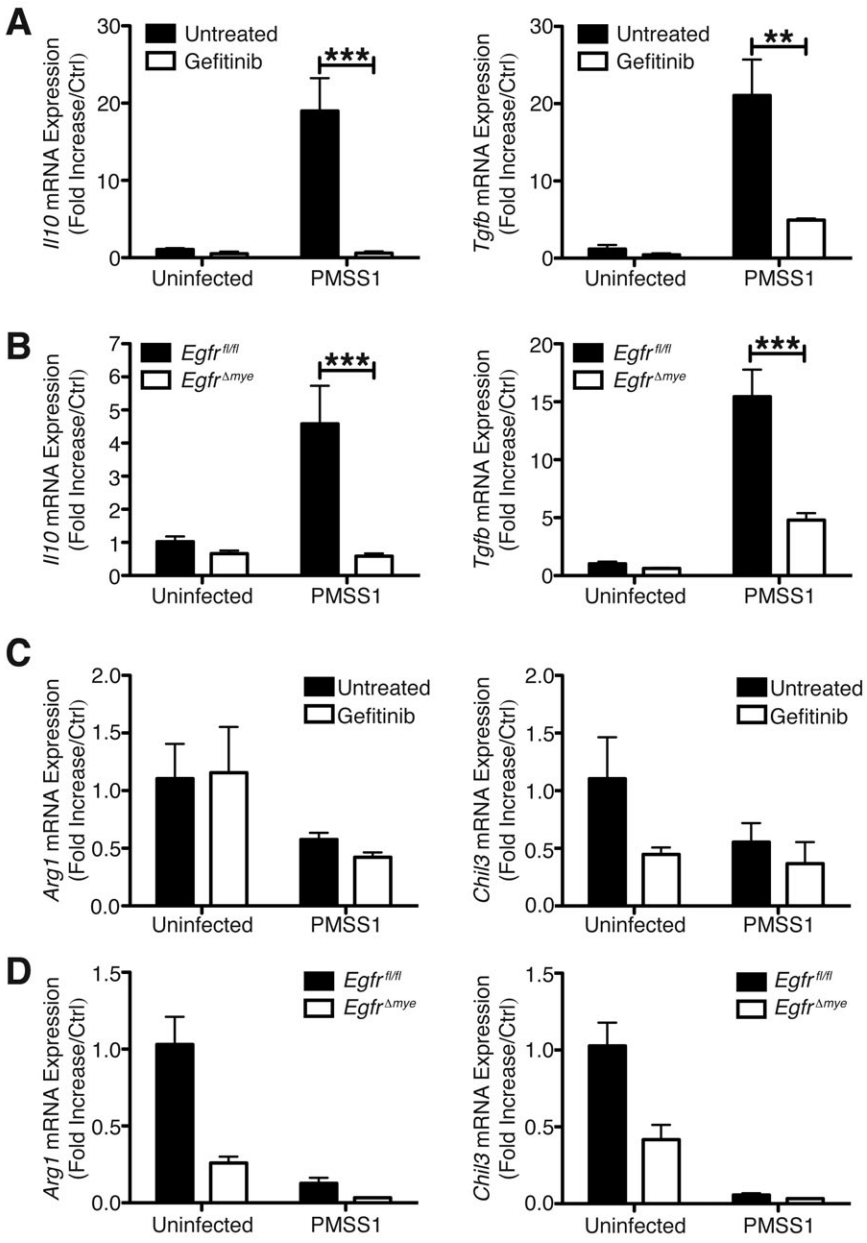

Appendix A, Figure 12. Markers of Mreg activation are significantly decreased during *H. pylori* infection, but markers of M2 activation are not significantly altered in EGFR signaling-deficient BMmacs. (A) *Il10* and *Tgfb* mRNA levels were assessed by RT-PCR in wildtype (WT) BMmacs ± 10 μM gefitinib 24 h p.i. with *H. pylori* PMSS1. ***P* < 0.01, ****P* < 0.001. *n* = 4 biological replicates. (B) *Il10* and *Tgfb* mRNA levels were assessed by RT-PCR in $Egfr^{fl/fl}$ and $Egfr^{\Delta mye}$ BMmacs 24 h p.i. with *H. pylori* PMSS1. ****P* < 0.001. *n* = 4 mice per genotype. Statistical significance in (A) and (B) was calculated by one-way ANOVA with Newman-Keuls post-test. (C) *Arg1* and *Chil3* mRNA levels were assessed by RT-PCR in WT BMmacs ± 10 μM gefitinib 24 h p.i. with *H. pylori* PMSS1. *n* = 4 biological replicates. (D) *Arg1* and *Chil3* mRNA levels were assessed by RT-PCR in $Egfr^{fl/fl}$ and $Egfr^{\Delta mye}$ BMmacs 24 h p.i. with *H. pylori* PMSS1. *n* = 4 mice per genotype.

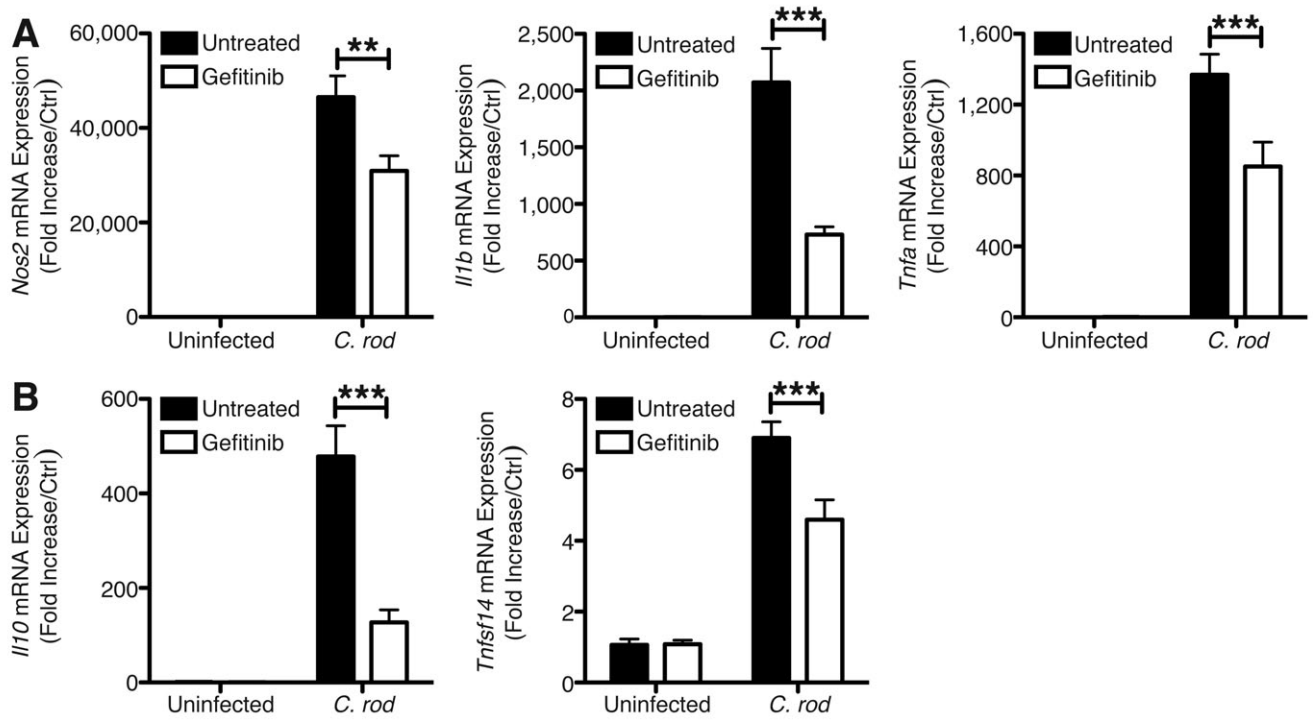

Appendix A, Figure 13. M1 and Mreg activation markers are significantly decreased in EGFR signaling-deficient BMmacs infected with *C. rodentium*. (A) mRNA levels M1 activation markers, *Nos2*, *Il1b*, and *Tnfa*, were assessed by in WT BMmacs ± 10 μM gefitinib 6 h p.i. by RT-PCR. ***P* < 0.01, ****P* < 0.001. *n* = 5 biological replicates. (B) mRNA levels Mreg activation markers, *Il10*, and *Tgfb*, were assessed in WT BMmacs ± 10 μM gefitinib 6 h p.i. by RT-PCR. ****P* < 0.001. *n* = 5 biological replicates. Statistical significance in all panels was calculated by one-way ANOVA with Newman-Keuls post-test.

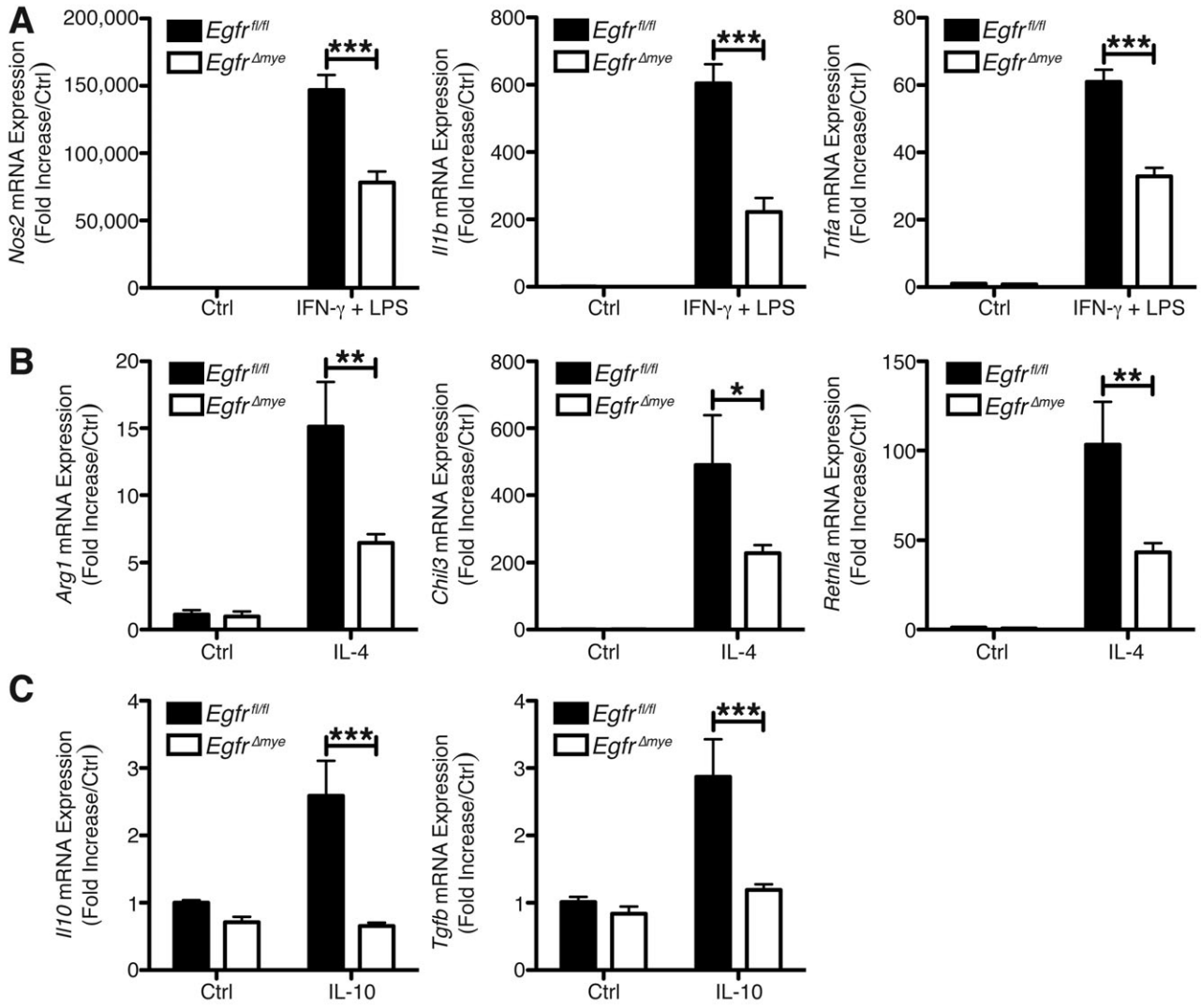

Appendix A, Figure 14. EGFR signaling regulates macrophage activation during stimulation with classical M1, M2, and Mreg activation stimuli. (A) *Nos2*, *Il1b*, and *Tnfa* mRNA levels were assessed by RT-PCR in *Egfr*$^{fl/fl}$ and *Egfr*$^{\Delta mye}$ BMmacs 24 h post stimulation with IFN-γ (200 U/mL) and LPS (10 ng/mL). ***$P < 0.001$. $n = 3$ mice per genotype. (B) *Arg1, Chil3*, and *Retnla* mRNA levels were assessed by RT-PCR in *Egfr*$^{fl/fl}$ and *Egfr*$^{\Delta mye}$ BMmacs 24 h post stimulation with IL-4 (10 ng/mL). *$P < 0.05$, **$P < 0.01$. $n = 3$ mice per genotype. (C) *Il10* and *Tgfb* mRNA levels were assessed by RT-PCR in *Egfr*$^{fl/fl}$ and *Egfr*$^{\Delta mye}$ BMmacs 24 h post stimulation with IL-10 (10 ng/mL). ***$P < 0.001$. $n = 3$ mice per genotype. Statistical significance in all panels was calculated by one-way ANOVA with Newman-Keuls post-test.

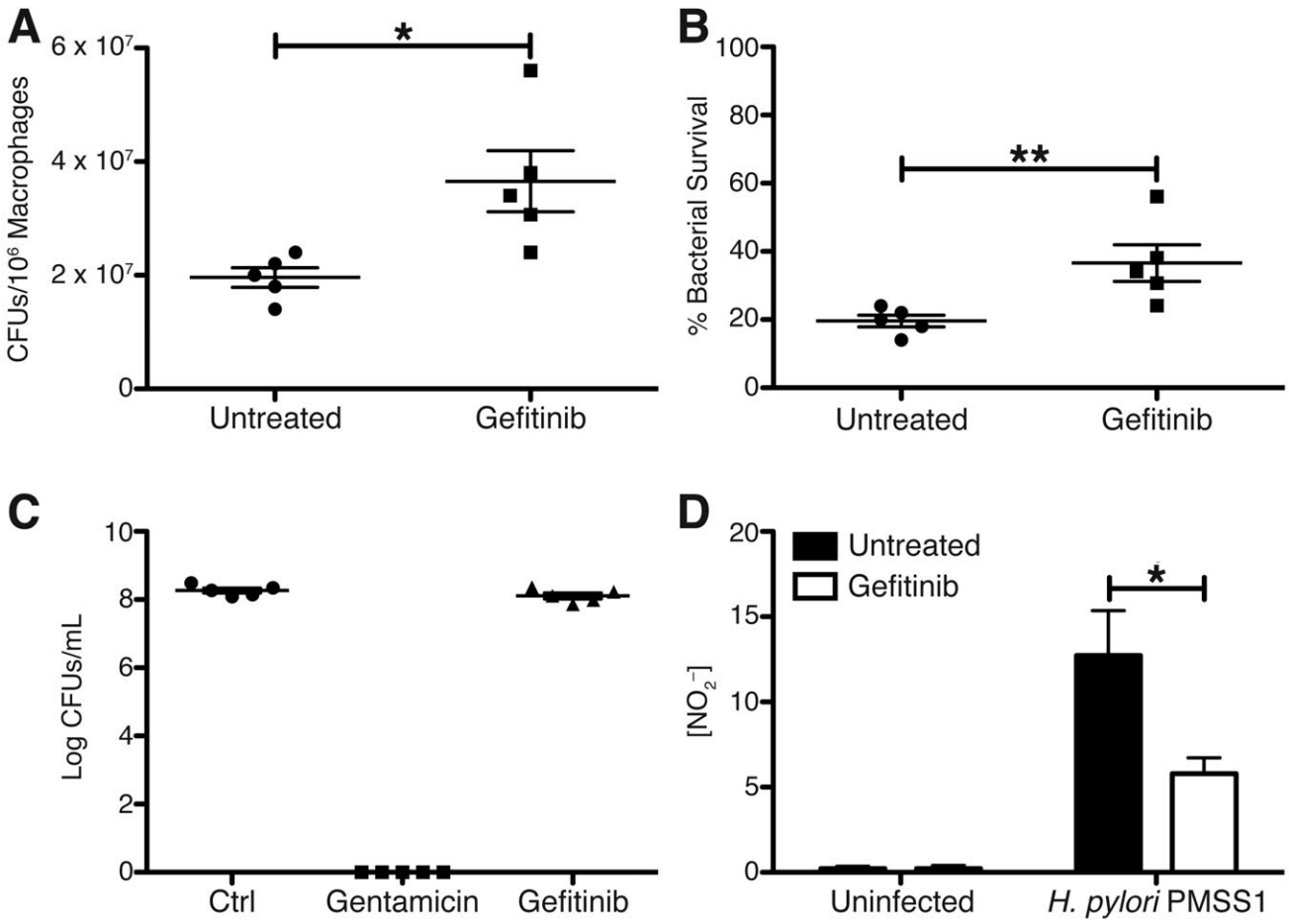

Appendix A, Figure 15. EGFR inhibition enhances bacterial survival by inhibiting NO production and NO-mediated killing. RAW 264.7 cells and *H. pylori* PMSS1 were co-cultured across Transwell Filter supports for 24 h. (A) *H. pylori* survival was assessed by serial dilution and culture from Transwell filter supports above RAW 264.7 cells ± 10 μM gefitinib. **P* < 0.05. *n* = 5 biological replicates. (B) Percent of bacteria that survived NO-mediated killing based on the initial MOI of 100 and the bacteria cultured in (A). ***P* < 0.01. *n* = 5 biological replicates. Statistical significance in (A) and (B) was calculated by Student's *t* test. (C) A set of control conditions for these assays. Culture of *H. pylori* PMSS1 in DMEM + 10% FBS does not result in bacterial death. Gentamicin treatment served as a positive control, leading to 100% bacterial death. Treatment of *H. pylori* PMSS1 with 10 μM gefitinib did not result in bacterial death. *n* = 5 biological replicates. (D) Measurement of NO_2^- from RAW 264.7 cell supernatants ± 10 μM gefitinib 24 h p.i. with *H. pylori* PMSS1. **P* < 0.05. *n* = 5 biological replicates. Statistical significance was calculated by one-way ANOVA with Newman-Keuls post-test.

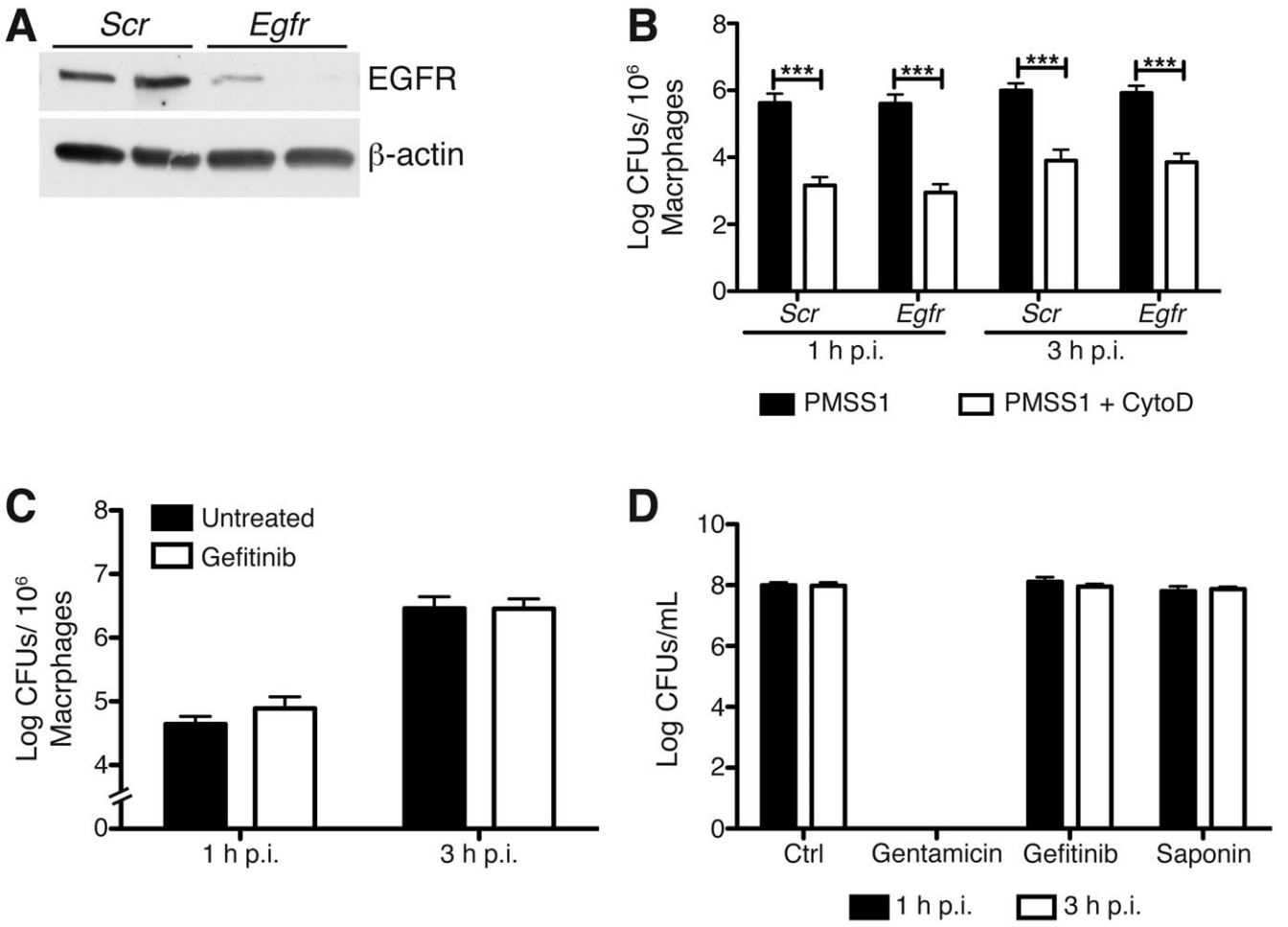

Appendix A, Figure 16. EGFR inhibition cells does not affect phagocytosis of *H. pylori* PMSS1. (A) Confirmation of *Egfr* knockdown by siRNA in RAW 264.7 cells by western blot. *n* = 2 biological replicates. (B) The amount of *H. pylori* PMSS1 that was phagocytosed by RAW 264.7 cells ± 10 μM cytochalasin D (CytoD) at 1 h and 3 h p.i. was assessed by serial dilution and culture. ***$P < 0.001$. Statistical significance was calculated by one-way ANOVA with Newman-Keuls post-test. *n* = 3 biological replicates. *Scr* = scrambled siRNA. *Egfr* = *Egfr* siRNA. (C) The amount of *H. pylori* that was phagocytosed by RAW 264.7 cells ± 10 μM gefitinib at 1 h and 3 h p.i. was assessed by serial dilution and culture. *n* = 3 biological replicates. (D) Confirmation that gentamicin treatment (200 μg/mL) for 30 min kills >99% of *H. pylori* PMSS1 and that 10 μM gefitinib treatment for 1 h and 0.1% saponin treatment for 30 min kills <1% of *H. pylori* PMSS1. *n* = 3 biological replicates.

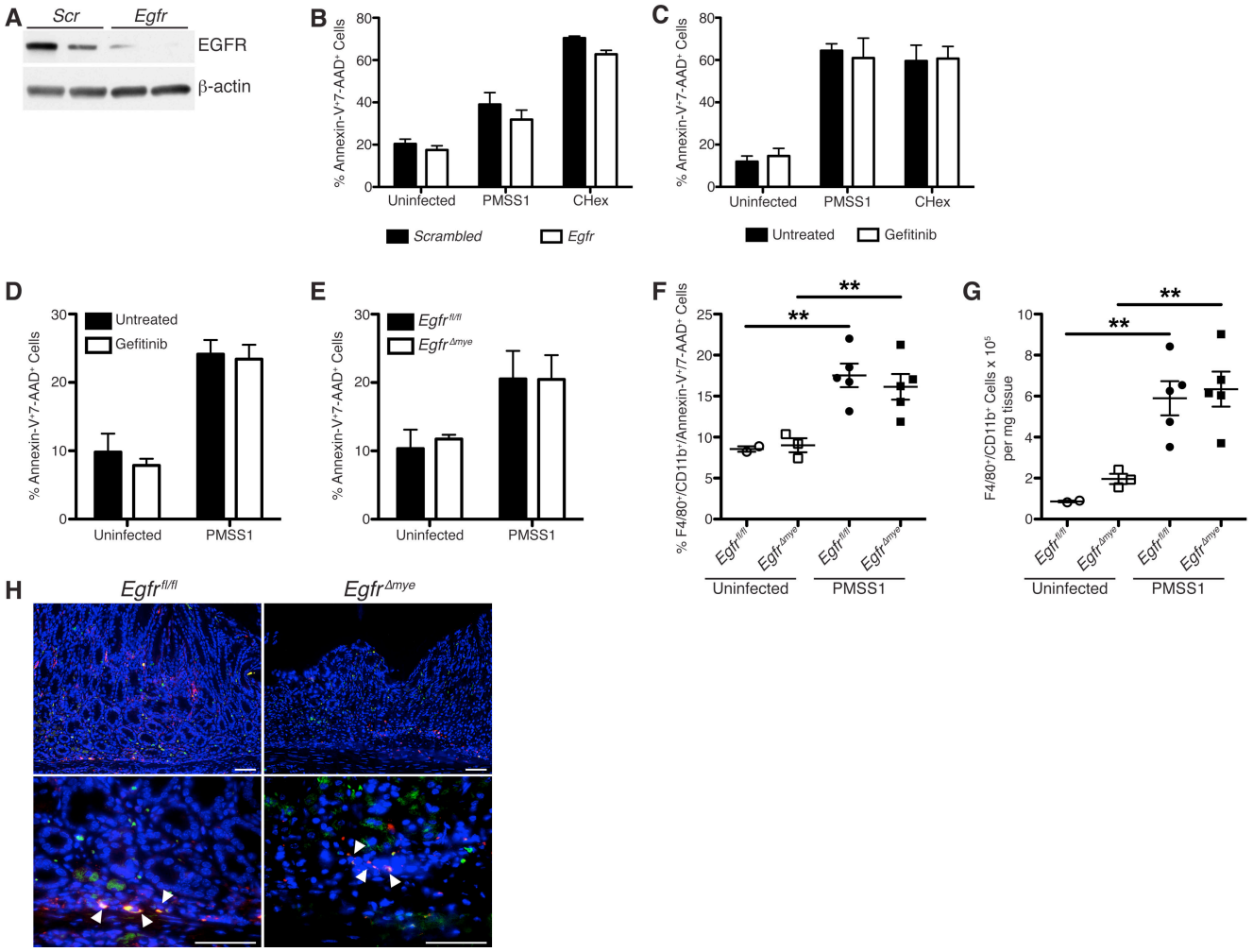

Appendix A, Figure 17. EGFR knockdown or inhibition does not affect apoptosis of macrophages during *H. pylori* PMSS1 infection. (A) Confirmation of *Egfr* knockdown by siRNA in RAW 264.7 cells by western blot. *n* = 2 biological replicates. (B) Percentage of Annexin-V$^+$7-AAD$^+$ RAW 264.7 cells ± *Egfr* siRNA knockdown 24 h p.i. with *H. pylori* PMSS1. *n* = 3 biological replicates. CHex = cyclohexamide (5 μg/mL). (C) Percentage of Annexin-V$^+$7-AAD$^+$ RAW 264.7 cells ± 10 μM gefitinib 24 h p.i. with *H. pylori* PMSS1. *n* = 3 biological replicates. CHex = cyclohexamide (5 μg/mL). (D) Percentage of Annexin-V$^+$7-AAD$^+$ WT BMmacs ± 10 μM gefitinib 24 h p.i. with *H. pylori* PMSS1. *n* = 3 biological replicates. (E) Percentage of Annexin-V$^+$7-AAD$^+$ *Egfr*$^{fl/fl}$ and *Egfr*$^{\Delta mye}$ BMmacs 24 h p.i. with *H. pylori* PMSS1. *n* = 3 biological replicates. (F) Percentage of F4/80$^+$CD11b$^+$Annexin-V$^+$7-AAD$^+$ Gmacs from *Egfr*$^{fl/fl}$ and *Egfr*$^{\Delta mye}$ mice 48 h p.i. with *H. pylori* SS1. **P < 0.01. *n* = 3 uninfected and 5 *H. pylori* PMSS1 infected mice per genotype. (G) Number of F4/80$^+$CD11b$^+$ Gmacs from *Egfr*$^{fl/fl}$ and *Egfr*$^{\Delta mye}$ mice 48 h p.i. with *H. pylori* SS1. **P < 0.01. *n* = 3 uninfected and 5 *H. pylori* PMSS1 infected mice per genotype. Statistical significance in (F)-(G) was calculated by one-way ANOVA with Newman-Keuls post-test. (H) Representative immunofluorescence images of cleaved caspase 3 staining in *Egfr*$^{fl/fl}$ and *Egfr*$^{\Delta mye}$ gastric tissues 4 mo p.i. with *H. pylori* SS1. Green = cleaved caspase 3, Red = CD68, Yellow = merge, Blue = DAPI. Arrows indicate CD68$^+$cleaved caspase 3$^+$ macrophages. Scale bars = 50 μM. *n* ≥ 3 mice per genotype.

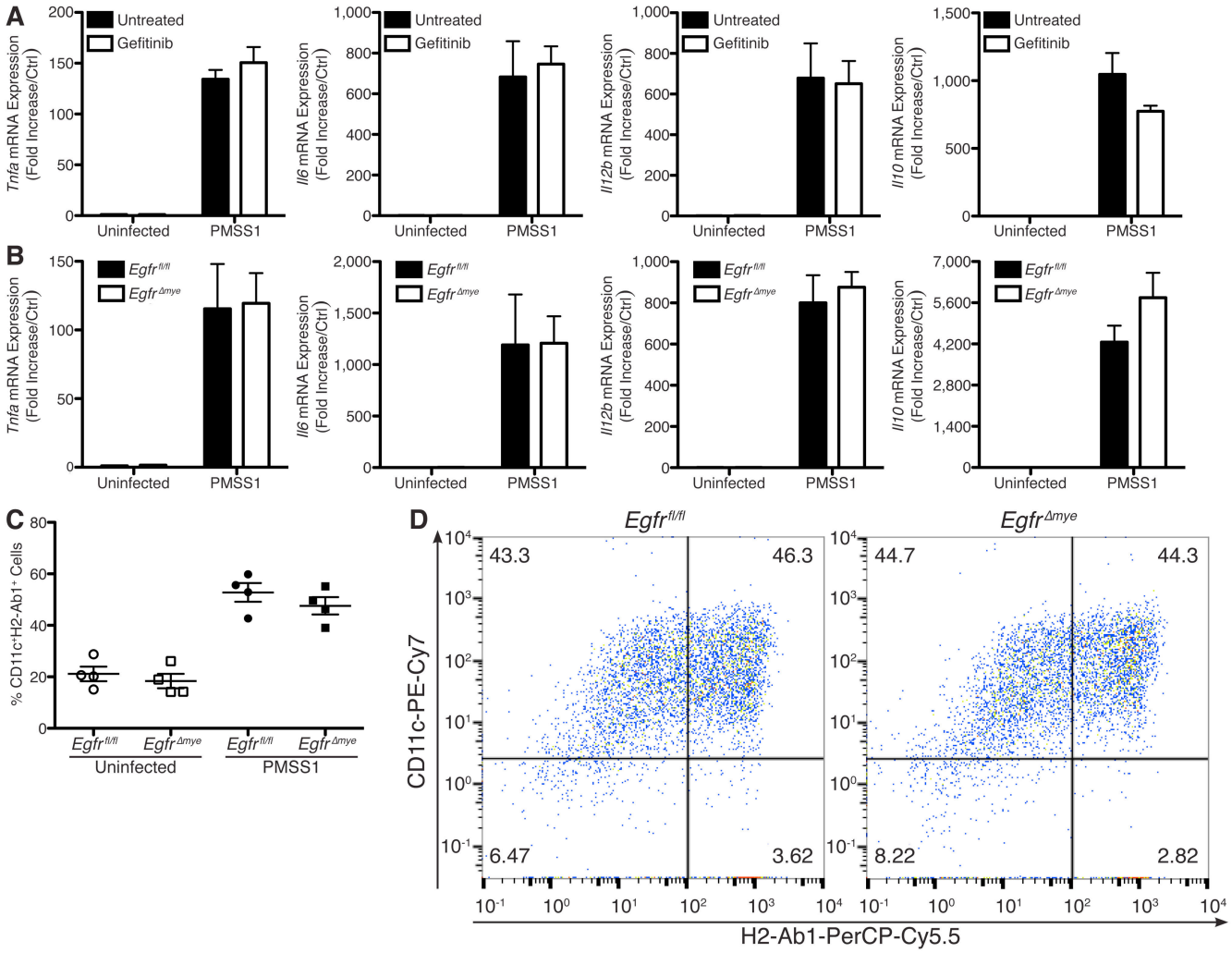

Appendix A, Figure 18. EGFR inhibition or knockout does not affect cytokine production or antigen presentation by bone marrow-derived dendritic cells. (A) mRNA levels of prototypical dendritic cell cytokines, *Tnfa*, *Il6*, *Il12b* (*Il12p40*), and *Il10*, were assessed by RT-PCR 24 h p.i. with *H. pylori* PMSS1 in WT BMDCs ± 10 μM gefitinib. *n* = 4 biological replicates. (B) mRNA levels of prototypical dendritic cell cytokines, *Tnfa*, *Il6*, *Il12b*, and *Il10*, were assessed by RT-PCR 24 h p.i. with *H. pylori* PMSS1 in $Egfr^{fl/fl}$ and $Egfr^{\Delta mye}$ BMDCs. *n* = 4 mice per genotype. (C) Antigen presentation ability was assessed by determining levels of surface H2-Ab1 (MHCII) on $Egfr^{fl/fl}$ and $Egfr^{\Delta mye}$ $CD11c^{+}$ BMDCs 24 h p.i. with *H. pylori* PMSS1. *n* = 4 biological replicates. (D) Representative flow cytometry scatter plots for *H. pylori*-infected $Egfr^{fl/fl}$ and $Egfr^{\Delta mye}$ BMDCs from (C). *n* = 4 biological replicates.

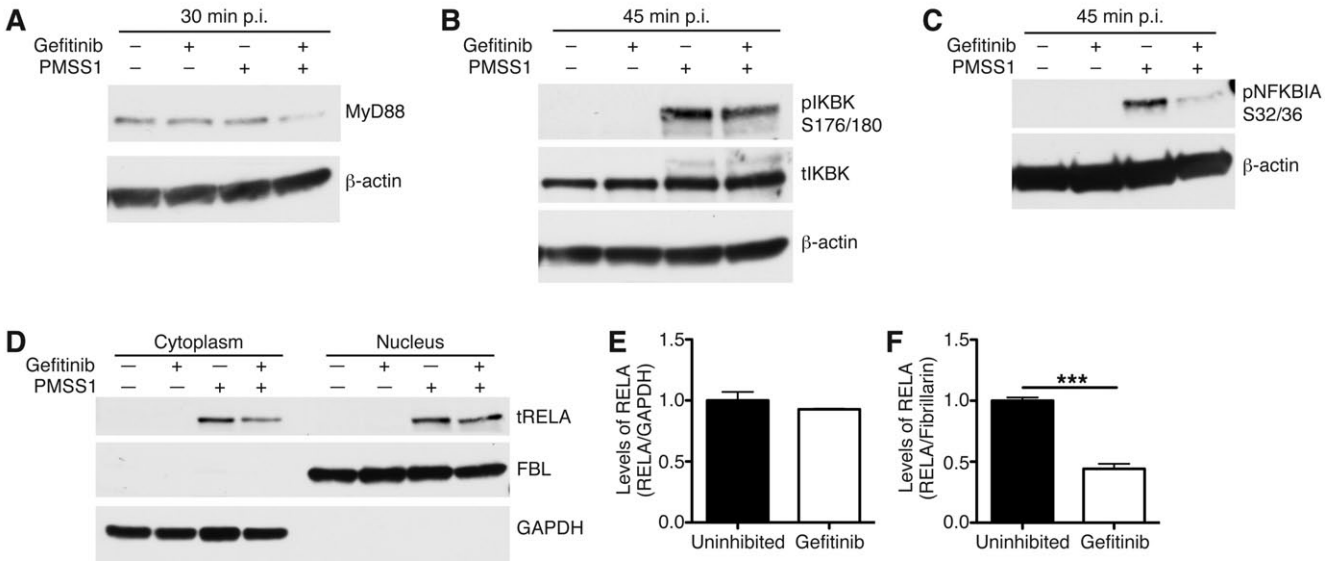

Appendix A, Figure 19. EGFR inhibition leads to markedly decreased NF-κB signaling. (A) Representative western blot of MyD88 protein levels in WT BMmacs ± 10 μM gefitinib. *n* = 3 biological replicates. (B) Representative western blot of pIKBK (pIKK) and tIKBK (tIKK) protein levels in WT BMmacs ± 10 μM gefitinib. *n* = 3 biological replicates. (C) Representative western blot of pNFKBIA (pIκB) protein levels in WT BMmacs ± 10 μM gefitinib. *n* = 3 biological replicates. (D) Representative western blot of tRELA (p65) protein levels in the cytoplasm and nucleus of WT BMmacs ± 10 μM gefitinib. *n* = 3 biological replicates. (E) Densitometric analysis of tRELA protein levels the cytoplasm in (D) *n* = 3 biological replicates. (F) Densitometric analysis of tRELA levels in the nucleus in (D). ***$P < 0.001$. *n* = 3 biological replicates. Statistical significance was calculated by Student's *t* test.

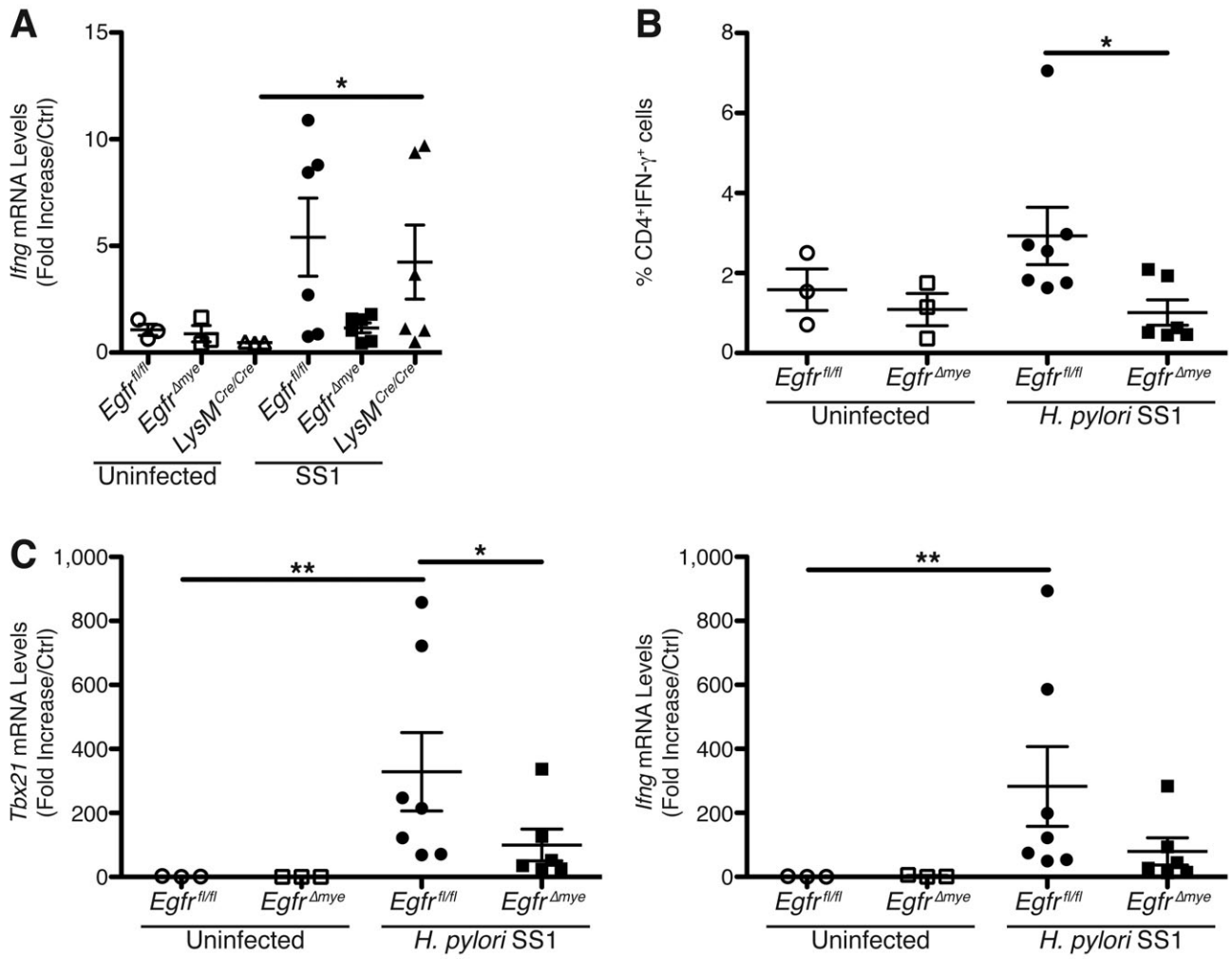

Appendix A, Figure 20. Macrophage EGFR signaling has a modest effect on the Th1 response to *H. pylori* 4 mo p.i. (A) *Ifng* mRNA expression was assessed by RT-PCR in $Egfr^{fl/fl}$, $Egfr^{\Delta mye}$, and $LysM^{Cre/Cre}$ gastric tissues 4 mo p.i. with *H. pylori* SS1. $^*P < 0.05$. $n = 3$ uninfected and 6 *H. pylori* SS1 infected mice per genotype. (B) Assessment of $CD4^+IFN\text{-}\gamma^+$ T cells from gastric lymph nodes (GLN) of $Egfr^{fl/fl}$ and $Egfr^{\Delta mye}$ mice 4 mo p.i. by flow cytometry. Isolated T cells were cultured in 96-well plates containing 5 μg/mL anti-CD3 and 1 μg/mL anti-CD28. Cells were then stimulated with 20 ng/mL PMA and 1 μg/mL ionomycin for 4 h. $^*P < 0.05$. $n = 3$ uninfected and 6-7 *H. pylori* SS1 infected mice per genotype. (C) *Tbx21* (*Tbet*) and *Ifng* mRNA expression was assessed by RT-PCR from magnetically selected $CD4^+$ T cells from the gastric lamina propria of $Egfr^{fl/fl}$ and $Egfr^{\Delta mye}$ mice 4 mo p.i. $^*P < 0.05$, $^{**}P < 0.01$. $n = 3$ uninfected and 6-7 *H. pylori* SS1 infected mice per genotype. Statistical significance in all panels was calculated by one-way ANOVA with Kruskal-Wallis test, followed by Mann-Whitney *U* test.

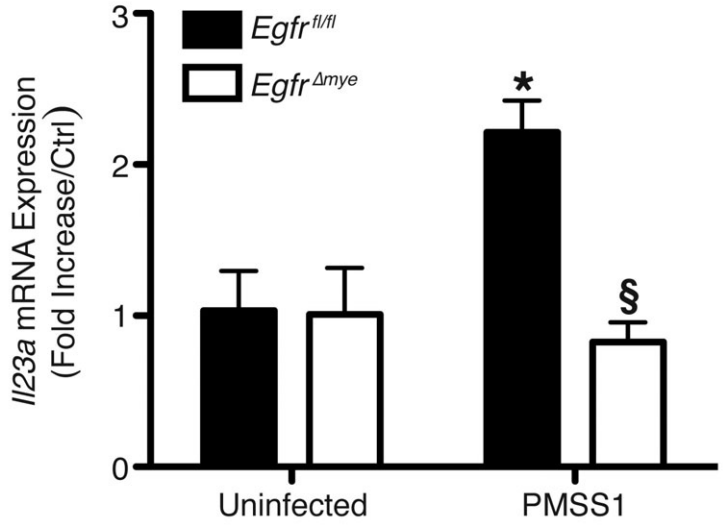

Appendix A, Figure 21. Macrophage EGFR signaling results in *IL23a* expression in gastric tissues and primary macrophages in response to *H. pylori.* *Il23a* (*Il23p19*) mRNA expression was assessed by RT-PCR in $Egfr^{fl/fl}$ and $Egfr^{\Delta mye}$ BMmacs 24 h p.i. with *H. pylori* PMSS1. **P* < 0.05 vs. $Egfr^{fl/fl}$ control BMmacs. §*P* < 0.05 vs. PMSS1-infected $Egfr^{fl/fl}$ BMmacs. *n* = 4 mice per genotype. Statistical significance in all panels was calculated by one-way ANOVA with Newman-Keuls post-test.

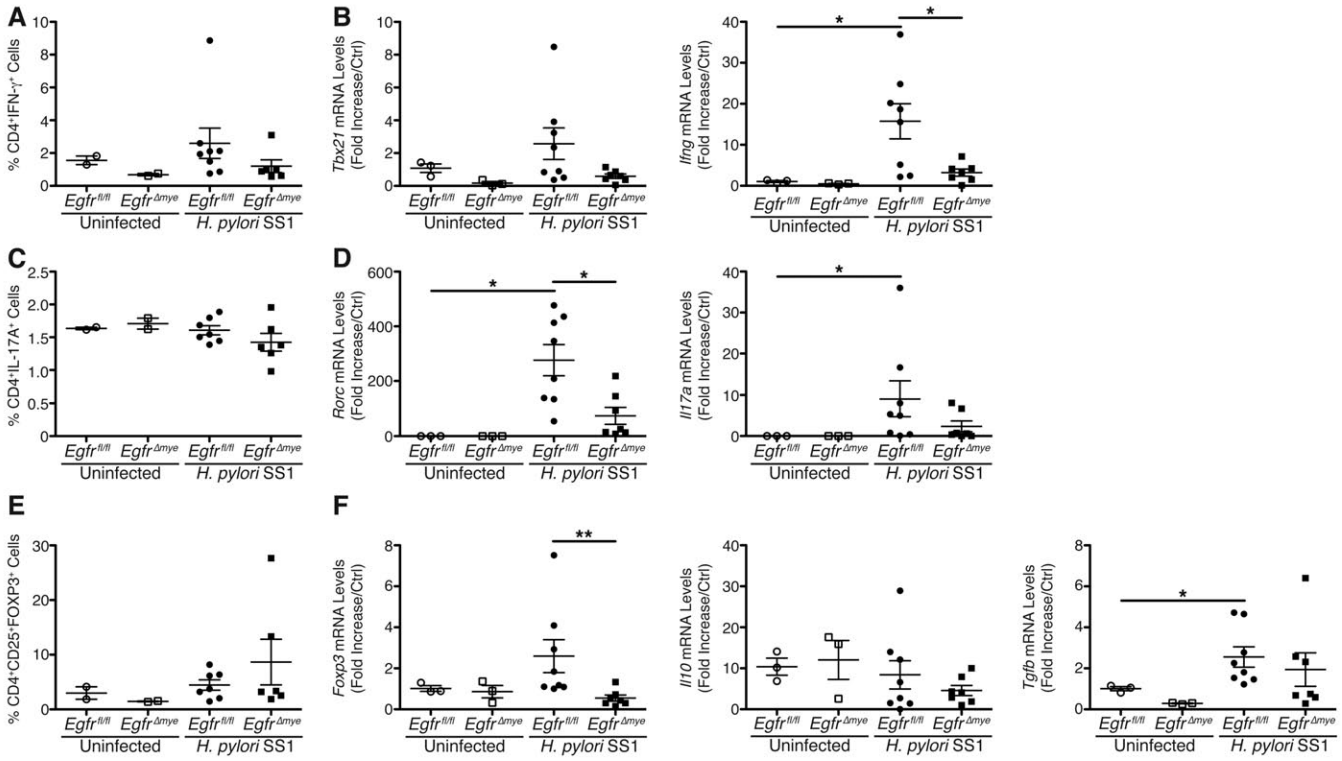

Appendix A, Figure 22. Macrophage EGFR signaling has a modest effect on Th1, Th17, and Treg responses to *H. pylori* 2 mo p.i. (A) Assessment of $CD4^+IFN\text{-}\gamma^+$ T cells from GLNs of $Egfr^{fl/fl}$ and $Egfr^{\Delta mye}$ mice 4 mo p.i. by flow cytometry. Isolated T cells were cultured in 96-well plates containing 5 μg/mL anti-CD3 and 1 μg/mL anti-CD28. Cells were then stimulated with *H. pylori* French-pressed lysate for 4 h. $^*P < 0.05$. (B). *Tbx21* (*Tbet*) and *Ifng* mRNA expression was assessed by RT-PCR from magnetically selected $CD4^+$ T cells from the gastric lamina propria of $Egfr^{fl/fl}$ and $Egfr^{\Delta mye}$ mice 4 mo p.i. $^*P < 0.05$, $^{**}P < 0.01$. (C) Assessment of $CD4^+IL\text{-}17^+$ T cells from GLNs of $Egfr^{fl/fl}$ and $Egfr^{\Delta mye}$ mice 4 mo p.i. by flow cytometry. Cells isolated and stimulated as in (A). (D) *Rorc* (*Rorgt*) and *Il17a* mRNA expression was assessed by RT-PCR from magnetically-selected $CD4^+$ T cells from the gastric lamina propria of $Egfr^{fl/fl}$ and $Egfr^{\Delta mye}$ mice 4 mo p.i. $^*P < 0.05$. (E) Assessment of $CD4^+CD25^+FOXP3^+$ T cells from GLNs of $Egfr^{fl/fl}$ and $Egfr^{\Delta mye}$ mice 4 mo p.i. by flow cytometry. Cells isolated and stimulated as in (A). (F) *Foxp3, Il10,* and *Tgfb* mRNA expression was assessed by RT-PCR from magnetically selected $CD4^+$ T cells from the gastric lamina propria of $Egfr^{fl/fl}$ and $Egfr^{\Delta mye}$ mice 4 mo p.i. $^*P < 0.05$, $^{**}P < 0.01$. In all panels, n = 2-3 uninfected and 6-8 *H. pylori* SS1 infected mice per genotype. Statistical significance in all panels was calculated by one-way ANOVA with Kruskal-Wallis test, followed by Mann-Whitney *U* test.

Analyte	Concentration of Analyte (pg/mg protein); Mean ± S.E.M.					
	***Egfr*$^{fl/fl}$**		***Egfr*$^{\Delta mye}$**		***LysM*$^{Cre/Cre}$**	
	Uninfected	***H. pylori* SS1**	**Uninfected**	***H. pylori* SS1**	**Uninfected**	***H. pylori* SS1**
CCL2	4.10 ± 1.70	24.20 ± 6.78 *	14.26 ± 3.98	16.14 ± 4.21	15.59 ± 1.01	26.08 ± 4.75
CCL11	50.62 ± 9.20	47.73 ± 6.00	54.40 ± 2.95	47.32 ± 4.33	41.25 ± 4.79	59.80 ± 7.42
CSF1	2.83 ± 0.49	4.69 ± 0.31	2.85 ± 0.37	4.08 ± 0.44	4.50 ± 1.81	3.62 ± 0.37
CSF2	1.21 ± 0.54	0.74 ± 0.16	1.73 ± 0.88	1.18 ± 0.59	1.42 ± 1.15	2.55 ± 0.93
CSF3	4.29 ± 0.60	8.54 ± 1.56	4.54 ± 0.89	5.68 ± 0.62	4.42 ± 1.19	8.19 ± 0.70
IFNG	2.63 ± 0.45	4.57 ± 1.21	2.90 ± 0.31	2.68 ± 0.30	2.61 ± 0.04	3.38 ± 0.38
IL-1α	48.07 ± 6.10	38.85 ± 5.73	44.49 ± 5.58	43.36 ± 5.05	35.06 ± 3.76	42.53 ± 5.07
IL-1β	4.21 ± 1.23	9.75 ± 1.72 *	4.96 ± 1.36	7.20 ± 1.30	9.01 ± 2.27	10.37 ± 1.19
IL-2	2.63 ± 0.42	2.78 ± 0.27	2.53 ± 0.27	2.22 ± 0.32	2.57 ± 0.14	2.62 ± 0.19
IL-6	0.70 ± 0.38	1.33 ± 0.36	0.91 ± 0.19	1.13 ± 0.24	0.70 ± 0.35	1.58 ± 0.26
IL-7	0.97 ± 0.19	1.85 ± 0.35	1.73 ± 0.39	1.20 ± 0.30	1.74 ± 0.36	2.28 ± 0.21
IL-9	0.36 ± 0.25	15.24 ± 2.82 ***	0.51 ± 0.25	4.75 ± 1.89 §	0.34 ± 0.13	26.17 ± 10.92
IL-10	3.25 ± 0.52	3.23 ± 0.50	4.84 ± 0.80	3.42 ± 0.79	4.31 ± 1.40	5.05 ± 1.47
IL-12p40	0.16 ± 0.06	0.34 ± 0.11	0.29 ± 0.05	0.13 ± 0.02[A]	0.27 ± 0.07	0.38 ± 0.05 aa
IL-12p70	11.33 ± 2.94	12.95 ± 3.59	8.12 ± 3.31	9.20 ± 1.09	11.72 ± 0.24	11.40 ± 1.08
IL-15	5.29 ± 2.09	7.09 ± 1.53	5.22 ± 2.13	3.93 ± 0.90	6.51 ± 1.53	7.75 ± 0.58
IL-17	0.98 ± 0.18	4.94 ± 0.49 **	1.33 ± 0.25	3.03 ± 0.78	0.89 ± 0.14	5.51 ± 1.16
TNF-a	1.22 ± 0.23	3.10 ± 1.13	1.49 ± 0.20	1.44 ± 0.18	1.65 ± 0.05	2.70 ± 0.45
VEGFA	3.23 ± 0.31	4.47 ± 0.60	4.11 ± 0.82	3.71 ± 0.22	2.98 ± 0.19	4.24 ± 0.33
Analytes Not Detected: CXCL2, IL-3, IL-4, IL-5, IL-13, LIF, LIX						

Appendix A, Table 1. Luminex analytes that did not demonstrate significant differences in gastric tissue between *Egfr*$^{fl/fl}$, *Egfr*$^{\Delta mye}$ and *LysM*$^{Cre/Cre}$ mice. 32 distinct analytes were assessed in gastric tissue from uninfected and infected mice from each of the three genotypes. Listed are the analytes that showed no significant differences as a result of infection, no significant differences between genotypes or were not detected. *Egfr*$^{fl/fl}$: n = 5 uninfected, 11 infected. *Egfr*$^{\Delta mye}$: n = 3 uninfected, 8 infected. *LysM*$^{Cre/Cre}$: n = 2 uninfected, 9 infected. * P < 0.05, ** P < 0.01 *** P < 0.001 vs. *Egfr*$^{fl/fl}$ Uninfected. § P < 0.05 vs. *Egfr*$^{fl/fl}$ *H. pylori* SS1. aa P < 0.01 for. *LysM*$^{Cre/Cre}$ *H. pylori* SS1 vs *Egfr*$^{\Delta mye}$ *H. pylori* SS1. Statistical significance was calculated by one-way ANOVA with Kruskal-Wallis test, followed by Mann-Whitney U test. [A]P = 0.07 between *Egfr*$^{fl/fl}$ *H. pylori* SS1 and *Egfr*$^{\Delta mye}$ *H. pylori* SS1.

Species	Target	Sequence
Mouse	*β-actin*	F: CCAGAGCAAGAGAGGTATCC
		R: CTGTGGTGGTGAAGCTGTAG
Mouse	*Nos2*	F: CACCTTGGAGTTCACCCAGT
		R: ACCACTCGTACTTGGGATGC
Mouse	*Tnfa*	F: CTGTGAAGGGAATGGGTGTT
		R: GGTCACTGTCCCAGCATCTT
Mouse	*Il1b*	F: ACCTGCTGGTGTGTGACGTTCC
		R: GGGTCCGACAGCACGAGGCT
Mouse	*Arg1*	F: AAGAAAAGGCCGATTCACCT
		R: CACCTCCTCTGCTGTCTTCC
Mouse	*Chia1*	F: ACTTTGATGGCCTCAACCTG
		R: AATGATTCCTGCTCCTGTGG
Mouse	*Retnla*	F: GGGATGACTGCTACTGGGTG
		R: TCAACGAGTAAGCACAGGCA
Mouse	*Il10*	F: CCAAGCCTTATCGGAAATGA
		R: TCACTCTTCACCTGCTCCAC
Mouse	*Tgfb*	F: TCCTTGCCTGCGGAAGTG
		R: GGAGAGCATTGAGCAGTTCGA
Mouse	*Tnfsf14*	F: CTGCATCAACGTCTTGGAGA
		R: GATACGTCAAGCCCCTCAAG
Mouse	*Egfr*[A]	F: CCTCGTCTGTGGAAGAACTA
		R: CTCAGCCAGATGATGTTGAC
Mouse	*Tbx21*	F: GCCAGGGAACCGCTTATATG
		R: GACGATCATCTGGGTCACATTGT
Mouse	*Ifng*	F: GGCCATCAGCAACAACATAAGCGT
		R: TGGGTTGTTGACCTCAAACTTGGC
Mouse	*Rorc*	F: CCGCTGAGAGGGCTTCAC
		R: TGCAGGAGTAGGCCACATTACA
Mouse	*Il17a*	F: ATCCCTCAAAGCTCAGCGTGTC
		R: GGGTCTTCATTGCGGTGGAGAG
Mouse	*Foxp3*	F: GAGAGCAGGCAGTTCAGGAC
		R: CGGGAGCATATACCAGGCAC
Mouse	*Il23a*	F: CCAGCAGCTCTCTCGGAATC
		R: TCATAGTCCCGCTGGTGC
Mouse	*Lysm*	F: TGGGATCAATTGCAGTGCT
		R: CACCACCCTCTTTGCACATT
Mouse	*Cre*	F: GATTTCGACCAGGTTCGTTC
		R: GCTAACCAGCGTTTTCGTTC

Appendix A, Table 2. List of primers used for PCR and RT-PCR. [A]Indicates primers were used to confirm excision of the *Egfr* alleles in *Egfr*$^{\Delta mye}$ mice.

Antibody	Dilution	Application	Source (Location)
Rabbit polyclonal anti-pEGFR Y1068	1:1,000	WB	Cell Signaling (Danvers, MA) Cat. No. 2234
Rabbit polyclonal anti-pEGFR S1046/47	1:1,000	WB	Cell Signaling (Danvers, MA) Cat. No. 2238
Rabbit polyclonal anti-tEGFR	1:5,000 1:100 1:50	WB IF FC	Cell Signaling (Danvers, MA) Cat. No. 2232
Mouse monoclonal anti-b-actin	1:10,000	WB	Sigma-Aldrich (St. Louis, MO) Cat. No. A1978
Rabbit polyclonal anti-MyD88	1:1000	WB	Cell Signaling (Danvers, MA) Cat. No. 3699
Rabbit polyclonal anti-pIKBK S176/180	1:2000	WB	Cell Signaling (Danvers, MA) Cat. No. 2697
Rabbit polyclonal anti-tIKBK	1:2000	WB	Cell Signaling (Danvers, MA) Cat. No. 2682
Mouse monoclonal anti-pNFKBIA S32/36	1:1000	WB	Life Technologies (Carlsbad, CA) Cat. No. MA515224
Rabbit polyclonal anti-tRELA	1:5,000	WB	EMD Millipore (Billerica, MA) Cat. No. PC138
Rabbit polyclonal anti-FBL	1:5,000	WB	Santa Cruz (Dallas, TX) Cat. No. SC-25397
Mouse monoclonal anti-GAPDH	1:10,000	WB	EMD Millipore (Billerica, MA) Cat. No. MAB374
Goat anti-mouse IgG, HRP labeled	1: 30,000	WB	Jackson ImmunoResearch (St. Louis, MO) Cat. No. 115-035-003
Goat anti-rabbit IgG, HRP labeled	1:3,000-1:6,000	WB	Jackson ImmunoResearch (St. Louis, MO) Cat. No. 111-035-003
Rabbit polyclonal anti-NOS2	1:5,000 1:100	WB FC	Pierce (Waltham, MA)**
Rabbit polyclonal anti-Clvd CASP3 D175	1:400	IF	Cell Signaling (Danvers, MA) Cat. No. 9661
Anti-mouse F4/80-Alexa488	1:100	FC	Invitrogen (Carlsbad, CA) Cat. No.
Anti-mouse F4/80-PE	1:100	FC	Invitrogen (Carlsbad, CA) Cat. No. MF48004
Anti-mouse CD4-PerCP-Cy5.5	1:200	FC	Biolegend (San Diego, CA) Cat. No. 100540
Hamster anti-mouse IFNG-FITC	1:100	FC	BD Biosciences (San Jose, CA) Cat. No. 562019
Rat anti-mouse IL-17A-PE	1:100	FC	BD Biosciences (San Jose, CA) Cat. No. 561020
Anti-mouse CD25-PE	1:100	FC	eBioscience (San Diego, CA) Cat. No. 12-0281-83
Rat anti-mouse FOXP3-Alexa488	1:00	FC	BD Biosciences (San Jose, CA) Cat. No. 560407
Mouse monoclonal Pan-cytokeratin PE	1:100	FC	Abcam (Cambridge, UK) Cat. No. AB52460

Rat anti-mouse CD11b-FITC	1:100	FC	Biolegend (San Diego, CA) Cat. No. 101219
Rant anti-mouse CD11b-PE-Cy7	1:100	FC	BD Biosciences (San Jose, CA) Cat. No. 552850
Hamster anti-mouse CD11c-PE-Cy7	1:100	FC	BD Biosciences (San Jose, CA) Cat. No. 558079
Anti-mouse H2-AB1-PerCP-Cy5.5	1:100	FC	Biolegend (San Diego, CA) Cat. No. 562363
Goat Anti-rabbit IgG-Alexa488	1:200	FC	Jackson ImmunoResearch (St. Louis, MO) Cat. No. 111-095-003
Rabbit IgG (isotype control)	1:50	FC	Jackson ImmunoResearch (St. Louis, MO) Cat. No. 011-000-003
Rabbit polyclonal anti-pEGFR	Pre-diluted	IF/IHC	Biocare Medical (Concord, CA) Cat. No. API 300
Rabbit HRP Polymer	Pre-diluted	IF/IHC	Biocare Medical (Concord, CA) Cat. No. RHRP520
Goat anti-HRP, Alexa488	1:400	IF	Jackson ImmunoResearch (St. Louis, MO) Cat. No. 123-545-021
Mouse monoclonal anti-CD68	Pre-diluted	IF	Santa Cruz Biotechnology (West Grove, PA) Cat. No. SC-7084
Goat anti-mouse IgG, Alexa555	1:500	IF	Life Technologies (Carlsbad, CA) Cat. No. A31570
Rat polyclonal anti-F4/80	1:50	IF	Invitrogen (Carlsbad, CA) Cat. No. MF48000
Rabbit anti-rat IgG, TRITC	1:100	IF	Sigma-Aldrich (St. Louis, MO) Cat. No. T4280
Mouse Anti-TNF-a	10 ng/mL	NEUT	Cell Signaling (Danvers, MA) Cat. No. 11969
Mouse Anti-HB-EGF	25 ng/mL	NEUT	Sigma-Aldrich (St. Louis, MO) Cat. No. AF259NA

Appendix A, Table 3. A list of all antibodies used for this study, including the dilution, application and company from which the antibodies were purchased. WB = western blotting, FC = flow cytometry, IF = immunofluorescence, IHC = immunohistochemistry. NEUT = neutralization. **No longer available.

Appendix B

Supplementary Figures for Chapter 3

EGFR-mediated Macrophage Activation Promotes Colitis-associated Tumorigenesis

Dana M. Hardbower[1, 2], Lori A. Coburn[2, 4, 6], Mohammad Asim[2], Kshipra Singh[2], Johanna C. Sierra[2],

Daniel P. Barry[2], Alain P. Gobert[2, 4], M. Blanca Piazuelo[2, 4], M. Kay Washington[1],

and Keith T. Wilson[1, 2, 3, 4, 5, 6 *]

[1]Department of Pathology, Microbiology and Immunology; Vanderbilt University Medical Center; Nashville, TN, USA

[2]Division of Gastroenterology, Hepatology and Nutrition, Department of Medicine; Vanderbilt University Medical Center; Nashville, TN, USA

[3]Department of Cancer Biology; Vanderbilt University Medical Center; Nashville, TN, USA

[4]Center for Mucosal Inflammation and Cancer, Vanderbilt University Medical Center; Nashville, TN, USA

[5]Vanderbilt Ingram Cancer Center; Vanderbilt University Medical Center; Nashville, TN, USA

[6]Veterans Affairs Tennessee Valley Healthcare System; Nashville, TN, USA

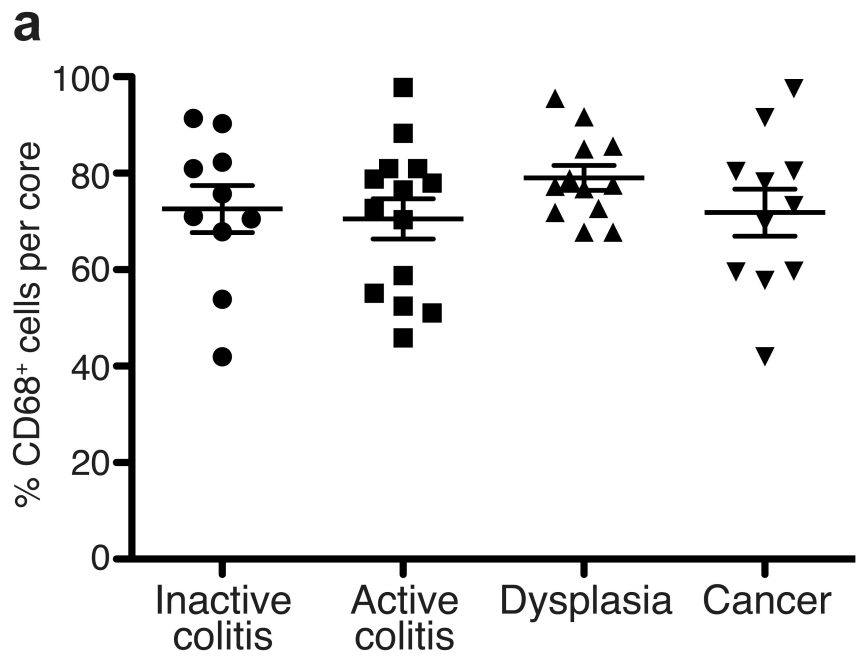

Appendix B, Figure 1. Percentages of macrophages in human CAC TMA. (a) Quantification of the percentage of $CD68^+$ cells among the total number of nuclei in each individual core in the TMA. For (a-c), *n* = 10 inactive colitis (normal or quiescent histology) samples, 14 active colitis (mild, moderate or severe histology) samples, 12 dysplasia samples, and 11 colorectal cancer samples.

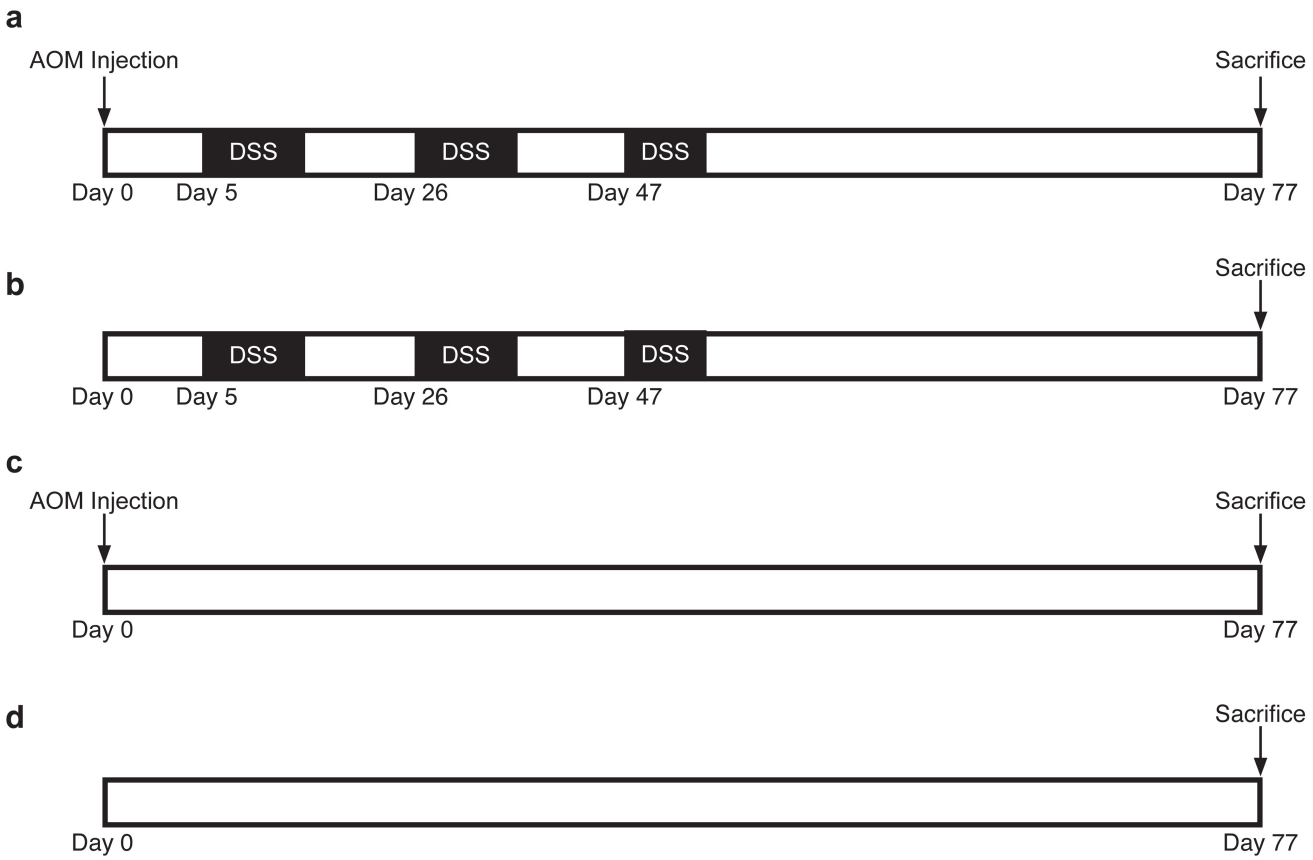

Appendix B, Figure 2. Schematic of the AOM-DSS protocol utilized in these studies. (a) AOM-DSS group: Mice were injected with 12.5 mg/kg AOM on Day 0. Animals then received 3 cycles of 4% DSS beginning on Day 5 (for 5 days), Day 26 (for 5 days), and Day 47 (for 4 days). Mice were sacrificed on Day 77 post-AOM injection. (b) DSS only group: Mice did not receive an AOM injection, but received 3 cycles of 4% DSS as in the AOM-DSS group. Mice were sacrificed on Day 77. (c) AOM only group: Mice were injected with 12.5 mg/kg AOM on Day 0 and were then maintained on normal drinking water throughout the protocol. Mice were sacrificed on Day 77 post-AOM injection. (d) Control group: Mice did not receive an AOM injection nor did mice receive DSS in their drinking water. Mice were sacrificed on Day 77.

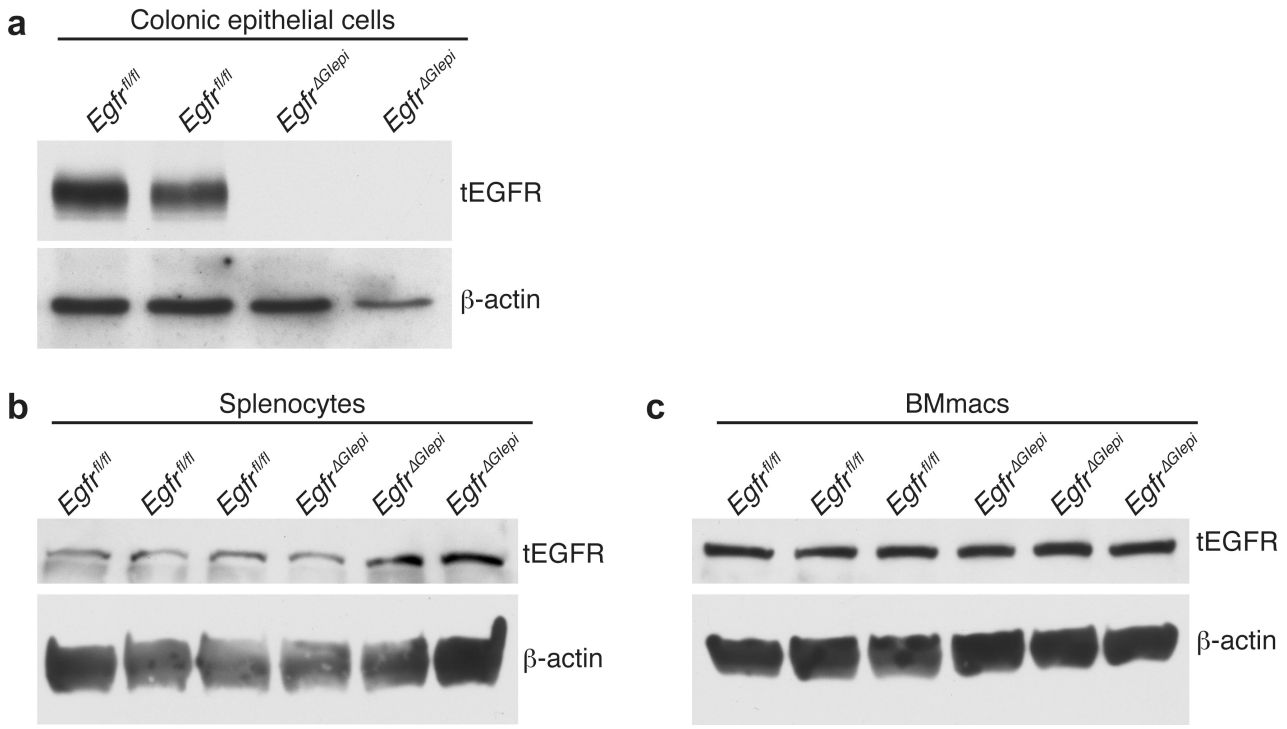

Appendix B, Figure 3. *Egfr*$^{\Delta GIepi}$ colonic epithelial cells demonstrated tEGFR knockout, but splenocytes and bone marrow-derived macrophages did not. (a) Representative Western blot of tEGFR levels in colonic epithelial cells from naïve *Egfr*$^{fl/fl}$ *and Egfr*$^{\Delta GIepi}$ mice. (b) Representative Western blot of tEGFR levels in splenocytes from naïve *Egfr*$^{fl/fl}$ *and Egfr*$^{\Delta GIepi}$ mice. (c) Representative Western blot of tEGFR levels in bone marrow-derived macrophages (BMmacs) from naïve *Egfr*$^{fl/fl}$ *and Egfr*$^{\Delta GIepi}$ mice.

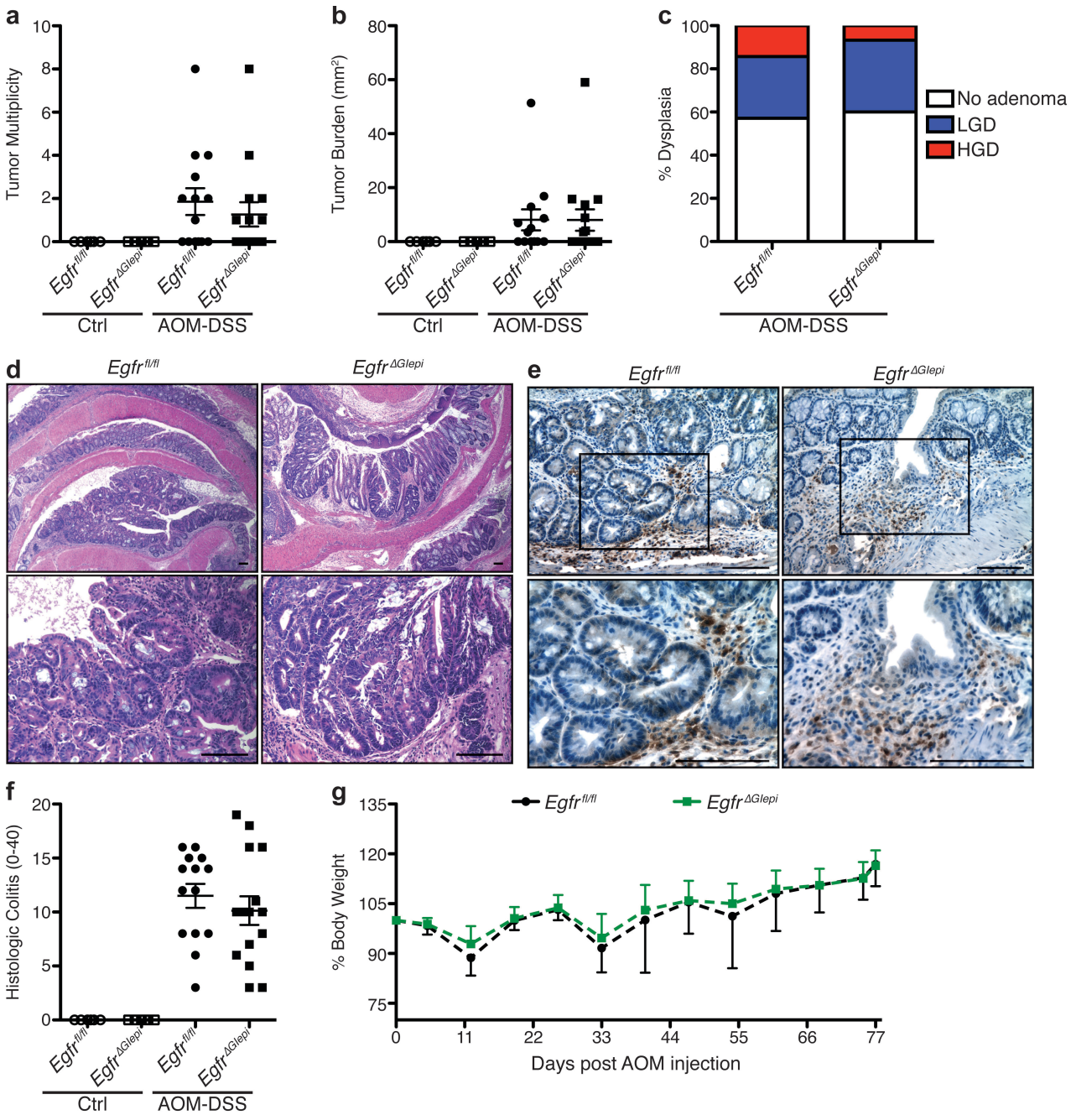

Appendix B, Figure 4. *Egfr*$^{\Delta Glepi}$ mice did not demonstrate altered tumorigenesis compared to *Egfr*$^{fl/fl}$ mice. (a) Tumor multiplicity was assessed by gross visual inspection, utilizing a dissecting microscope. (b) Tumor burden was determined by the addition of the calculated area of each identified tumor, as assessed with an electronic caliper for both length and width. (c) Percentage of cases with either no adenoma, low-grade dysplasia (LGD), and high-grade dysplasia (HGD) was determined by a gastrointestinal pathologist (M.K.W.) in a blinded manner. (d) Representative H&E-stained images from AOM-DSS-treated mice. Scale bars = 100 μm. (e) Representative immunoperoxidase images of pEGFR Y1068 from mice in (a-f). Scale bars = 50 μm. *n* = 6 mice per genotype assessed. (f) Histologic colitis was determined by M.K.W. in a blinded manner. (g) Percentage of initial body weight was assessed at indicated time points. In (a-c) and (f-g), *n* = 6 control and 14-15 AOM-DSS treated mice per genotype.

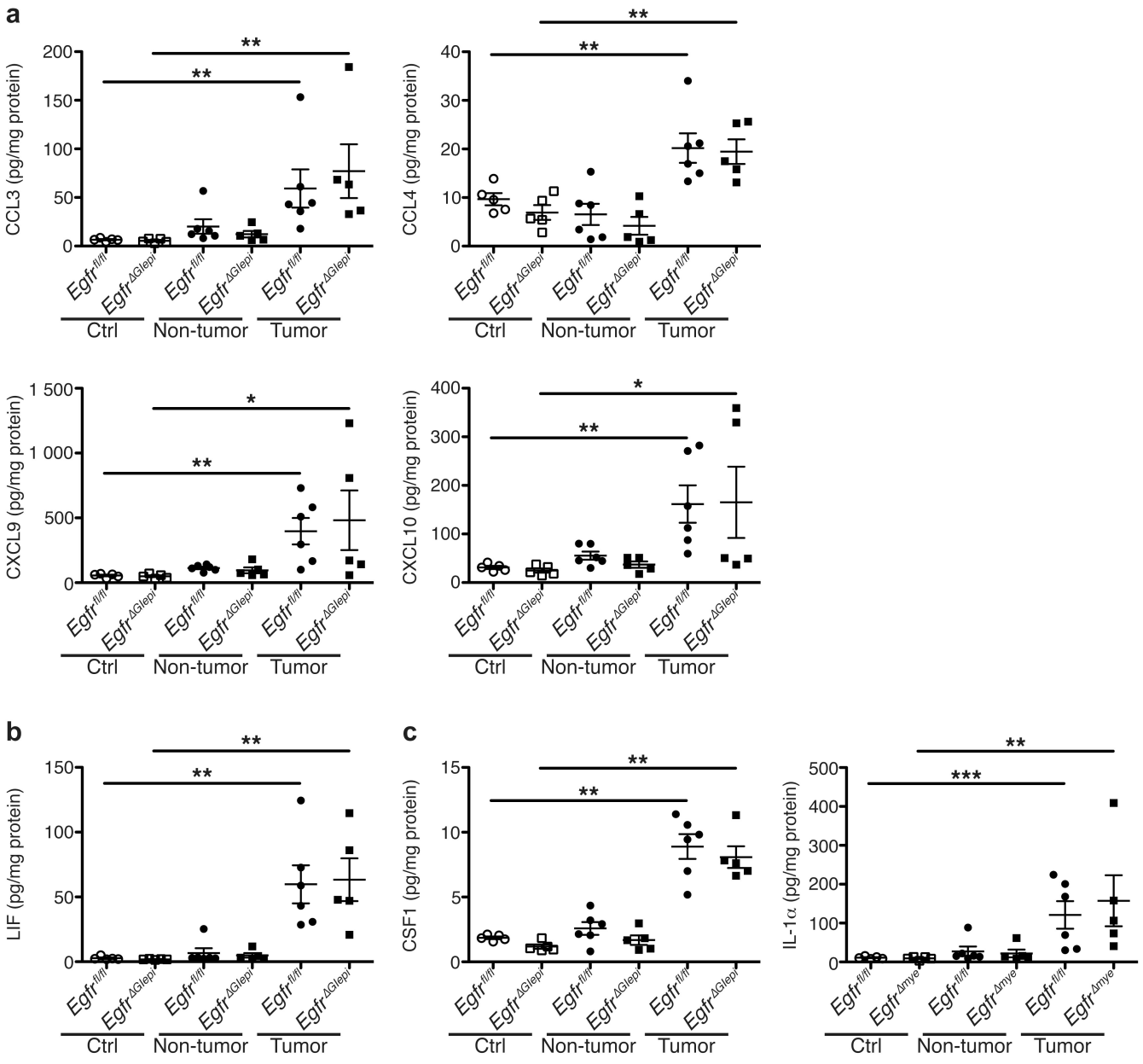

Appendix B, Figure 5. *Egfr*$^{\Delta Glepi}$ mice demonstrate no alterations in cytokine and chemokine production within tumors. (a) Protein levels of the general C-C motif and C-X-C motif chemokines CCL3 (MIP-1α), CCL4 (MIP-1β), CXCL9 (MIG), and CXCL10 (IP-10) were assessed by Luminex Multiplex Array from colonic tissues 77 days post-AOM injection. (b) Protein levels of the pleiotropic cytokine, LIF, were assessed by Luminex Multiplex Array from colonic tissues 77 days post-AOM injection. (c) Protein levels of cytokines produced by activated macrophages, CSF1 (M-CSF) and IL-1α were assessed by Luminex Multiplex Array from colonic tissues 77 days post-AOM injection. In all panels, n = 5 control tissues and 5-6 tumors with paired non-tumor area per genotype. In all panels, *P < 0.05, **P < 0.01, ***P < 0.001 by one-way ANOVA with Kruskal-Wallis test, followed by Mann-Whitney U test.

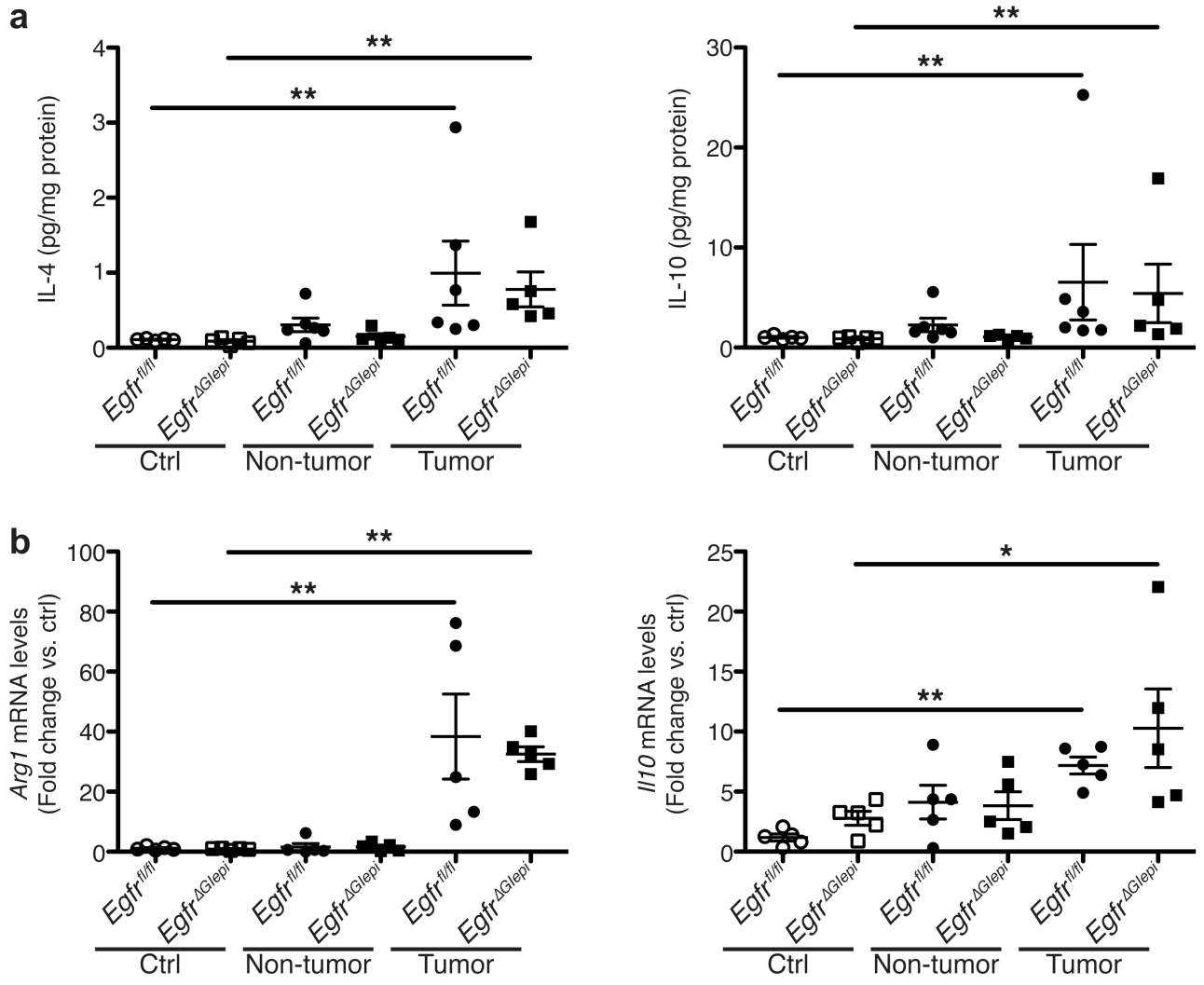

Appendix B, Figure 6 *Egfr*$^{\Delta GIepi}$ mice demonstrate no alterations in M2 macrophage activation during colon tumorigenesis. (a) Protein levels of M2 stimuli, IL-4 and IL10, were assessed by Luminex Multiplex Array from colonic tissues 77 days post-AOM injection. *n* = 5 control tissues and 5-6 tumors with paired non-tumor area per genotype. (b) mRNA levels of M2 markers, *Arg1* and *Il10*, were assessed by qRT-PCR from colonic tissues 77 days post-AOM injection. *n* = 5 control tissues and 5 tumors with paired non-tumor area per genotype. In all panels, **P* < 0.05, ***P* < 0.01 by one-way ANOVA with Kruskal-Wallis test, followed by Mann-Whitney *U* test.

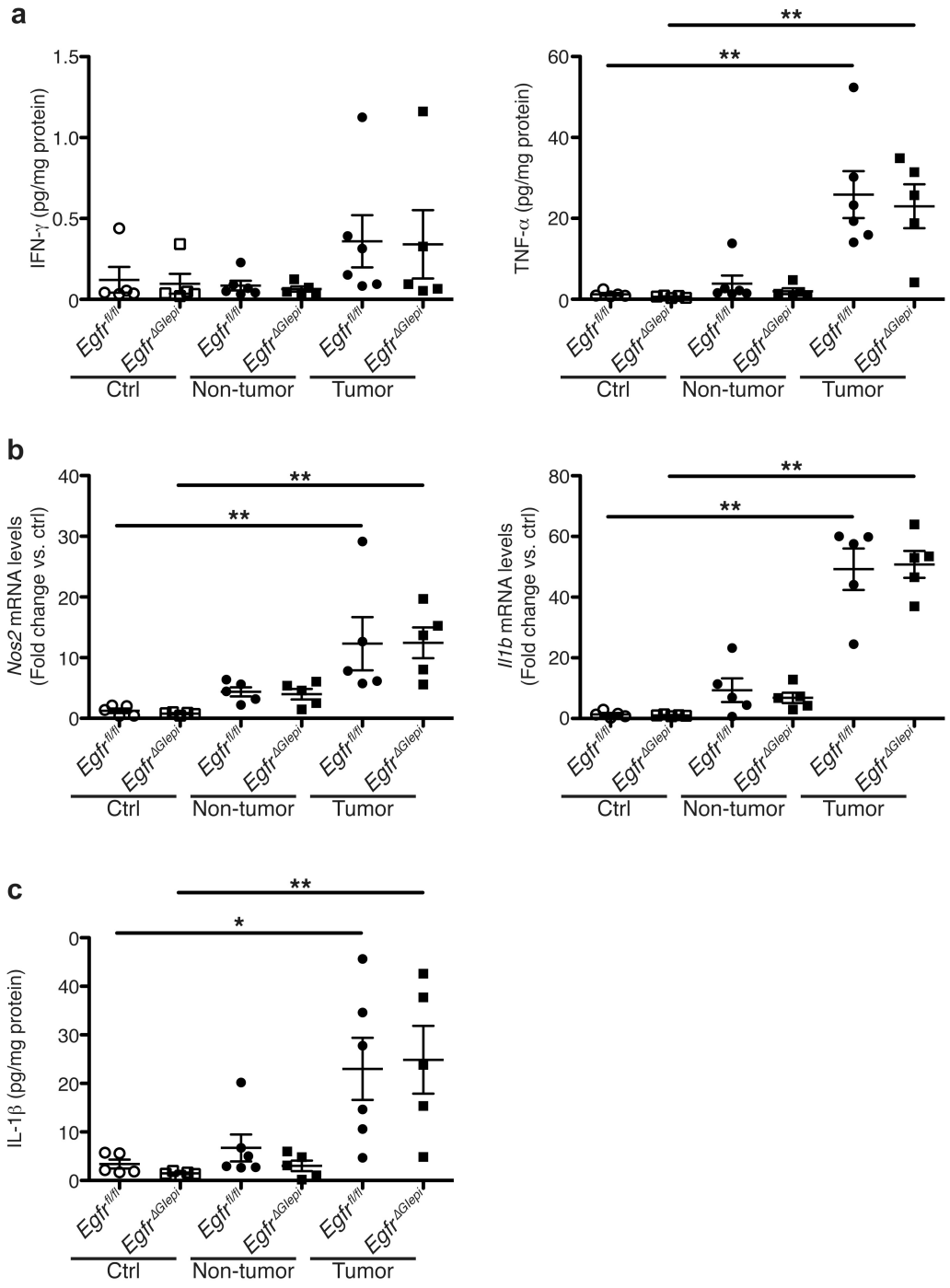

Appendix B, Figure 7. *Egfr*$^{\Delta Glepi}$ mice demonstrate no alterations in M1 macrophage activation during colon tumorigenesis. (a) Protein levels of M1 stimuli, IFN-γ and TNF-α, were assessed by Luminex Multiplex Array from colonic tissues 77 days post-AOM injection. *n* = 5 control tissues and 5-6 tumors with paired non-tumor area per genotype. (b) mRNA levels of M1 markers, *Nos2* and *Il1b*, were assessed by qRT-PCR from colonic tissues 77 d post-AOM injection. *n* = 5 control tissues and 5 tumors with paired non-tumor area per genotype. (c) Protein levels of M1 marker, IL-1β, were assessed by Luminex Multiplex Array from colonic tissues 77 days post-AOM injection. *n* = 5 control tissues and 5-6 tumors with paired non-tumor area per genotype. In all panels, **P* < 0.05, ***P* < 0.01 by one-way ANOVA with Kruskal-Wallis test, followed by Mann-Whitney *U* test.

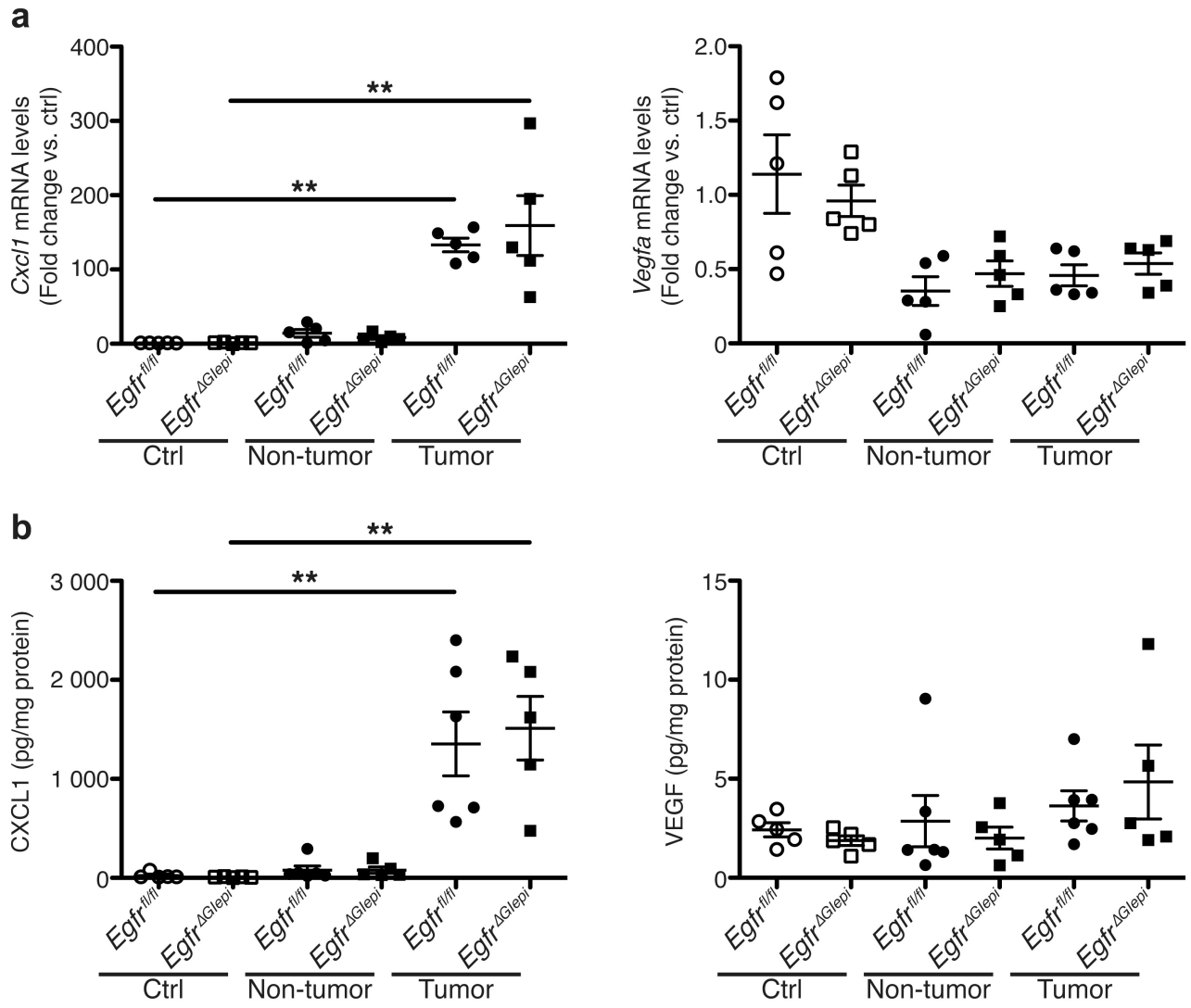

Appendix B, Figure 8. *Egfr*$^{\Delta Glepi}$ mice demonstrate no alterations in pro-angiogenic chemokine/cytokine production during colon tumorigenesis. (a) mRNA levels of the pro-angiogenic chemokine, *Cxcl1*, and the pro-angiogenic cytokine, *Vegfa*, were assessed by qRT-PCR from colonic tissues 77 days post-AOM injection. n = 5 control tissues and 5 tumors with paired non-tumor area per genotype. (b) Protein levels of CXCL1 and VEGF were assessed by Luminex Multiplex Array from colonic tissues 77 days post-AOM injection. n = 5 control tissues and 5-6 tumors with paired non-tumor area per genotype. In all panels, *P < 0.05, **P < 0.01 by one-way ANOVA with Kruskal-Wallis test, followed by Mann-Whitney U test.

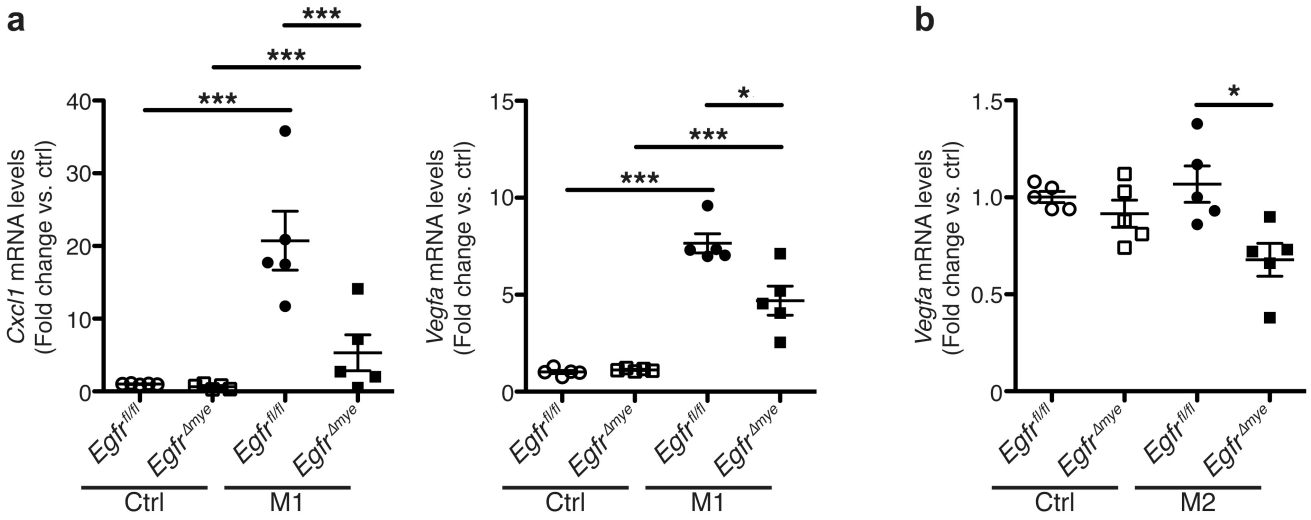

Appendix B, Figure 9. *Egfr*$^{\Delta mye}$ BMmacs demonstrate significant alterations in *Cxcl1* and *Vegfa* mRNA levels during M1 or M2 macrophage activation. (a) mRNA levels of the pro-angiogenic chemokine, *Cxcl1*, and the pro-angiogenic cytokine, *Vegfa*, were assessed by qRT-PCR in BMmacs 24 h post-stimulation with IFN-γ (200 U/mL) and LPS (10 ng/mL). *n* = 5 biological replicates per genotype. (b) mRNA levels of the pro-angiogenic cytokine, *Vegfa*, were assessed by qRT-PCR in BMmacs 24 h post-stimulation with IL-4 (10 ng/mL) and IL-10 (10 ng/mL). *n* = 5 biological replicates per genotype. In all panels, **P* < 0.05, ****P* < 0.001 by one-way ANOVA with Newman-Keuls post-test.

Analyte	Concentration of Analyte (pg/mg protein); Mean ± S.E.M.					
	***Egfr*$^{fl/fl}$**			***Egfr*$^{\Delta mye}$**		
	Control	**Non-tumor**	**AOM-DSS**	**Control**	**Non-tumor**	**AOM-DSS**
CCL2	3.87 ± 0.40	6.85 ± 1.55	113.5 ± 20.32***	4.03 ± 1.39	1.36 ± 0.88	83.90 ± 17.56##
CCL5	7.08 ± 1.43	8.15 ± 2.22	2.62 ± 0.45	5.04 ± 0.66	3.06 ± 0.61	0.80 ± 0.11
CCL11	109.6 ± 48.44	130.8 ± 27.15	145.2 ± 36.29	134.6 ± 27.05	84.97 ± 15.02	113.5 ± 44.59
CSF2	0.21 ± 0.88	0.36 ± 0.15	15.65 ± 4.24***	0.16 ± 0.68	0.20 ± 0.01	11.06 ± 2.81#
CSF3	2.71 ± 0.92	34.29 ± 23.53	277.1 ± 108.6**	4.45 ± 0.66	15.15 ± 3.15	366.2 ± 120.0##
CXCL2	4.66 ± 0.54	47.66 ± 13.03	2492 ± 507.3***	4.15 ± 0.94	58.25 ± 27.15	1478 ± 340.1###
CXCL5	0.04 ± 0.01	15.83 ± 14.49	117.7 ± 56.67**	0.04 ± 0.01	0.08 ± 0.01	10.38 ± 6.65
IL-2	1.15 ± 0.21	1.30 ± 0.31	1.85 ± 0.55	0.92 ± 0.15	1.94 ± 0.16	0.81 ± 0.16§
IL-5	0.95 ± 0.28	0.84 ± 0.35	0.80 ± 0.26	0.76 ± 0.27	0.42 ± 0.08	0.25 ± 0.07
IL-6	1.47 ± 0.68	3.77 ± 0.95	548.4 ± 234.2***	1.33 ± 0.48	5.94 ± 1.74	465.9 ± 119.7##
IL-7	2.14 ± 0.20	2.34 ± 0.33	4.19 ± 0.52*	2.20 ± 0.15	3.01 ± 0.41	1.22 ± 0.39§§§
IL-9	32.41 ± 8.75	41.05 ± 9.63	72.04 ± 19.40	22.84 ± 8.14	39.38 ± 4.70	24.90 ± 2.02§§
IL-12B	2.09 ± 0.30	1.59 ± 0.40	1.92 ± 0.44	1.19 ± 0.25	2.68 ± 0.15	1.77 ± 0.26
IL-15	7.60 ± 1.40	5.86 ± 2.03	3.97 ± 1.06	6.32 ± 0.72	3.55 ± 0.94	1.84 ± 0.51
IL-17	0.64 ± 0.16	1.79 ± 0.43	24.74 ± 5.71***	0.45 ± 0.06	1.29 ± 0.45	18.89 ± 3.26##
Not detected: IL-3, IL-12A						

Appendix B, Table 1. Luminex analytes that did not demonstrate significant differences in colonic tissues from *Egfr*$^{fl/fl}$ and *Egfr*$^{\Delta mye}$ mice. A total of 32 distinct analytes were assessed in colonic tissues from control mice and from tumor and adjacent non-tumor tissues from mice treated with AOM-DSS. Listed are the analytes that were not significantly induced during AOM-DSS treatment, were not relevant to subsequent analyses in the study or demonstrated no significant differences between genotypes. *n* = 5 control and 6-9 non-tumor/tumor pairs per genotype. **P*<0.05, ***P*<0.01, and ****P*< 0.001 versus *Egfr*$^{fl/fl}$ control. #*P*<0.05, ##*P*<0.01, and ###*P*< 0.001 versus *Egfr*$^{\Delta mye}$ control. §*P*<0.05, §§*P*<0.01, and §§§*P*< 0.001 versus *Egfr*$^{fl/fl}$ AOM-DSS by one-way ANOVA with Kruskal-Wallis test, followed by Mann-Whitney *U* test.

Analyte	Concentration of Analyte (pg/mg protein); Mean ± S.E.M.					
	***Egfr*$^{fl/fl}$**			***Egfr*$^{\Delta Glepi}$**		
	Control	**Non-tumor**	**AOM-DSS**	**Control**	**Non-tumor**	**AOM-DSS**
CCL2	9.67 ± 0.99	17.28 ± 2.81	110.7 ± 28.54**	4.705 ± 0.90	13.82 ± 4.94	144.2 ± 42.02##
CCL5	15.08 ± 1.27	6.39 ± 0.95	4.75 ± 1.86	9.68 ± 1.47	5.39 ± 1.33	4.57 ± 2.30
CCL11	136.9 ± 23.32	196.8 ± 22.02	202.4 ± 32.14	219.8 ± 26.30	360.5 ± 100.7	504.0 ± 125.3
CSF2	1.30 ± 0.13	0.95 ± 0.42	19.19 ± 7.13**	0.31 ± 0.11	0.45 ± 0.23	24.77 ± 8.90##
CSF3	6.86 ± 4.27	14.93 ± 3.66	254.3 ± 126.3**	1.98 ± 0.32	15.16 ± 5.50	262.8 ± 160.5##
CXCL2	26.10 ± 16.47	102.6 ± 87.36	1952 ± 727.4***	4.54 ± 0.92	77.22 ± 53.77	2186 ± 625.3##
CXCL5	2.39 ± 0.19	5.95 ± 2.06	155.3 ± 34.67**	2.28 ± 0.36	4.46 ± 1.14	116.9 ± 46.21##
IL-2	0.72 ± 0.07	2.99 ± 2.17	7.32 ± 5.58	0.71 ± 0.11	1.38 ± 0.68	12.13 ± 10.35
IL-5	0.62 ± 0.10	0.46 ± 0.06	1.01 ± 0.17	0.54 ± 0.15	0.47 ± 0.12	0.83 ± 0.19
IL-6	6.15 ± 5.10	4.81 ± 1.16	490.3 ± 275.2*	0.67 ± 0.09	8.56 ± 3.45	909.9 ± 517.9##
IL-7	2.27 ± 0.20	2.72 ± 0.39	3.06 ± 0.27	1.85 ± 0.13	3.62 ± 1.53	2.53 ± 0.28
IL-9	26.01 ± 3.37	43.58 ± 9.70	72.24 ± 13.17*	21.40 ± 4.24	29.28 ± 6.35	91.55 ± 25.81##
IL-12B	1.12 ± 0.41	0.16 ± 0.05	0.50 ± 0.31	0.39 ± 0.16	0.12 ± 0.03	0.62 ± 0.39
IL-13	0.25 ± 0.20	1.14 ± 0.46	1.07 ± 0.28	0.06 ± 0.02	1.22 ± 0.21	1.36 ± 0.14
IL-15	7.28 ± 0.27	2.58 ± 0.50	3.72 ± 0.67	5.67 ± 1.17	2.15 ± 0.75	2.56 ± 0.67
IL-17	0.85 ± 0.43	2.89 ± 0.51	18.02 ± 3.36**	0.35 ± 0.09	1.57 ± 0.66	11.70 ± 4.83##
Not detected: IL-3, IL-12A						

Appendix B, Table 2. Luminex analytes that did not demonstrate significant differences in colonic tissues from *Egfr*$^{fl/fl}$ and *Egfr*$^{\Delta Glepi}$ mice. A total of 32 distinct analytes were assessed in colonic tissues from control mice and from tumor and adjacent non-tumor tissue from mice treated with AOM-DSS. Listed are the analytes that were not significantly induced during AOM-DSS treatment or demonstrated few or no significant differences between genotypes. *n* = 5 control and 6-9 non-tumor/tumor pairs per genotype. **P*<0.05, ***P*<0.01, and ****P*< 0.001 versus *Egfr*$^{fl/fl}$ control. ##*P*<0.01 versus *Egfr*$^{\Delta mye}$ control by one-way ANOVA with Kruskal-Wallis test, followed by Mann-Whitney *U* test.

Species	Target	Sequence
Mouse	*β-actin*	F: CCAGAGCAAGAGAGGTATCC
		R: CTGTGGTGGTGAAGCTGTAG
Mouse	*Nos2*	F: CACCTTGGAGTTCACCCAGT
		R: ACCACTCGTACTTGGGATGC
Mouse	*Tnfa*	F: CTGTGAAGGGAATGGGTGTT
		R: GGTCACTGTCCCAGCATCTT
Mouse	*Il1b*	F: ACCTGCTGGTGTGTGACGTTCC
		R: GGGTCCGACAGCACGAGGCT
Mouse	*Arg1*	F: AAGAAAAGGCCGATTCACCT
		R: CACCTCCTCTGCTGTCTTCC
Mouse	*Chil3*	F: ACTTTGATGGCCTCAACCTG
		R: AATGATTCCTGCTCCTGTGG
Mouse	*Il10*	F: CCAAGCCTTATCGGAAATGA
		R: TCACTCTTCACCTGCTCCAC
Mouse	*Cxcl1*	F: GCTGGGATTCACCTCAAGAA
		R: CTTGGGGACACCTTTTAGCA
Mouse	*Vegfa*	F: GAGGATGTCCTCACTCGGATG
		R: GTCGTGTTTCTGGAAGTGAGCAA

Appendix B, Table 3. List of primers used for qRT-PCR.

Antibody	Dilution	Application	Source (Location)
Rabbit polyclonal anti-pEGFR Y1068	Pre-diluted	IHC-P IF	Biocare Medical (Concord, CA) Cat. No. API 300
Rabbit polyclonal anti-tEGFR	1:3,000 1:100	WB IF	Cell Signaling (Danvers, MA) Cat. No. 2232
Rat monoclonal anti-CD31	1:100	IHC-P	Dianova (Hamburg Germany) Cat. No. DIA 310
Mouse monoclonal anti-b-actin	1:10,000	WB	Sigma-Aldrich (St. Louis, MO) Cat. No. A1978
Goat anti-mouse IgG, HRP labeled	1:30,000	WB	Jackson ImmunoResearch (St. Louis, MO) Cat. No. 115-035-003
Goat anti-rabbit IgG, HRP labeled	1:3,000	WB	Jackson ImmunoResearch (St. Louis, MO) Cat. No. 115-035-003
Mouse monoclonal anti-CD68	Pre-diluted	IF	Biocare Medical (Concord, CA) Cat. No. PM033AA
Goat anti-mouse IgG, Alexa555	1:500	IF	Life Technologies (Carlsbad, CA) Cat. No. A31570
Goat anti-rabbit IgG, Alexa488	1:500	IF	Jackson ImmunoResearch (St. Louis, MO) Cat. No. 111-095-003
Rabbit HRP Polymer	Pre-diluted	IF/IHC-P*	Biocare Medical (Concord, CA) Cat. No. RHRP520
Donkey anti-HRP, FITC	1:400	IF	Jackson ImmunoResearch (St. Louis, MO) Cat. No. 123-545-021
Rabbit anti-rat IgG, biotinylated	1:200	IHC-P**	Vector Laboratories (Burlingame, CA) Cat. No. BA-4000
Goat anti-rabbit IgG, biotinylated	1:400	IHC-P***	Vector Laboratories (Burlingame, CA) Cat. No. BA-1000
Rabbit polyclonal anti-CD68	1:200	IHC-P	Boster Biological Technology (Pleasanton, CA) Cat. No. PA-1518
Rabbit polyclonal anti-MPO	Pre-diluted	IHC-P	Biocare Medical (Concord, CA) Cat. No. PP-023-AA
Rabbit monoclonal anti-CD3	1:250	IHC-P	Abcam (Cambridge, MA) Cat. No. ab16669
Rat monoclonal anti-CD45R	1:30,000	IHC-P	BD Pharmingen (San Jose, CA) Cat. No. 553084
Rabbit polyclonal anti-pSTAT6 Y941	1:100	IHC-P	Lifespan Biosciences, Inc. (Seattle, WA) Cat. No. LS-C117487

Appendix B, Table 4. List of all antibodies used for this study, including the dilution, application and company/catalog number from which the antibodies were purchased. WB = western blotting, IF = immunofluorescence, IHC-P = immunohistochemistry-immunoperoxidase. * = used for CD68, MPO, and pSTAT6 IHC-P. ** = used for CD45R and CD31 IHC-P. *** = used for CD3 IHC-P.

Figure	Panel	*P* value
1	b	= 0.002
1	c	= 0.008
2	a	< 0.0001
2	b	< 0.0001
2	d	< 0.0001
3	a	CCL3: = 0.0005 CCL4: = 0.0003 CXCL9: = 0.0003 CXCL10: = 0.0011
3	b	< 0.0001
3	c	CSF1: = 0.0003 IL-1a: = 0.0011
5	a	IFN-g: = 0.0079 TNF-a: < 0.0001
5	b	*Nos2*: < 0.0001 *Il1b*: < 0.0001
5	c	= 0.0004
6	a	IL-4: = 0.002 IL-10: = 0.04 IL-13: = 0.0049
6	b	*Arg1*: < 0.0001 *Il10*: = 0.0032
7	a	*Cxcl1*: < 0.0001 *Vegfa*: = 0.05
7	b	CXCL1: < 0.0001 VEGF: = 0.0095

Figure	Panel	*P* value
S5	a	CCL3: = 0.0005 CCL4: = 0.0003 CXCL9: = 0.0003 CXCL10: = 0.0011
S5	b	< 0.0001
S5	c	CSF1: = 0.0003 IL-1a: = 0.0011
S6	a	IL-4: = 0.0202 IL-10: = 0.05
S6	b	*Arg1*: 0.0012 *Il10*: = 0.0049
S7	a	< 0.0001
S7	b	*Nos2*: = 0.0002 *Il1b*: = 0.0002
S7	c	= 0.0004
S8	a	= 0.0002
S8	b	< 0.0001

Appendix B, Table 5. List of all *P* values derived from Kruskal-Wallis testing. S = Appendix B, figure.

Appendix C

Supplementary Figures for Chapter 5

Ornithine Decarboxylase Regulates M1 Macrophage Activation and Mucosal Inflammation via Chromatin Modifications

Dana M. Hardbower[a, b], Mohammad Asim[b], Paula B. Luis[c], Kshipra Singh[b], Daniel P. Barry[b], Chunying Yang[d,e], Meredith A. Steeves[e], John L. Cleveland[d,e], Claus Schneider[c], M. Blanca Piazuelo[b], Alain P. Gobert[b], and Keith T. Wilson[a, b, f, g, h]

[a]Department of Pathology, Microbiology and Immunology; Vanderbilt University Medical Center; Nashville, TN 37232

[b]Division of Gastroenterology, Hepatology and Nutrition, Department of Medicine; Vanderbilt University Medical Center; Nashville, TN 37232

[c]Department of Pharmacology; Vanderbilt University School of Medicine; Nashville, TN 37232

[d]Department of Tumor Biology; Moffitt Cancer Center and Research Institute; Tampa, FL 33612

[e]Department of Cancer Biology; The Scripps Research Institute; Jupiter, FL 33458

[f]Department of Cancer Biology; Vanderbilt University School of Medicine; Nashville, TN 37232

[g]Center for Mucosal Inflammation and Cancer, Vanderbilt University Medical Center; Nashville, TN 37232

[h]Veterans Affairs Tennessee Valley Healthcare System; Nashville, TN 37232

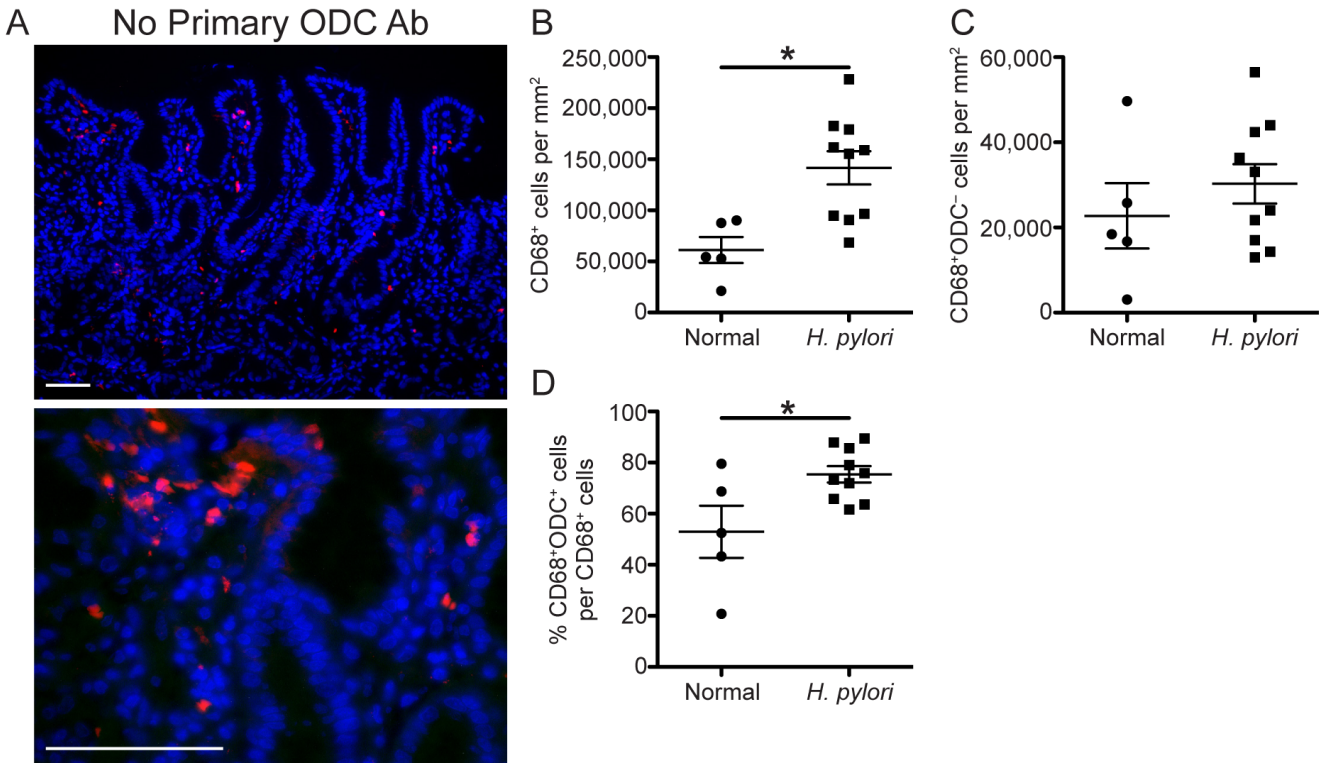

Appendix C, Figure 1. Immunofluorescence staining for CD68 and ODC in human gastric biopsies. (a) Representative images of staining where no primary anti-ODC antibody was utilized, in order to confirm specificity of the ODC antibody. Note that the case utilized is the same *H. pylori*$^{+}$ case as in Figure 1c. Scale bar = 50 μm. (b) Number of CD68^{+} macrophages per tissue area (mm^{2}) as determined by the average counts of 4 blinded observers. *$P < 0.05$ by Student's *t* test. $n = 5$ normal and 10 *H. pylori*$^{+}$ cases. (c) Number of CD68^{+}ODC^{-} macrophages per tissue area (mm^{2}) as determined in (b). $n = 5$ normal and 10 *H. pylori*$^{+}$ cases. (d) Percentage of CD68^{+}ODC^{+} macrophages per the total number of CD68^{+} macrophages as determined in (b). *$P < 0.05$ by Student's *t* test. $n = 5$ normal and 10 *H. pylori*$^{+}$ cases. Data displayed as mean ± S.E.M.

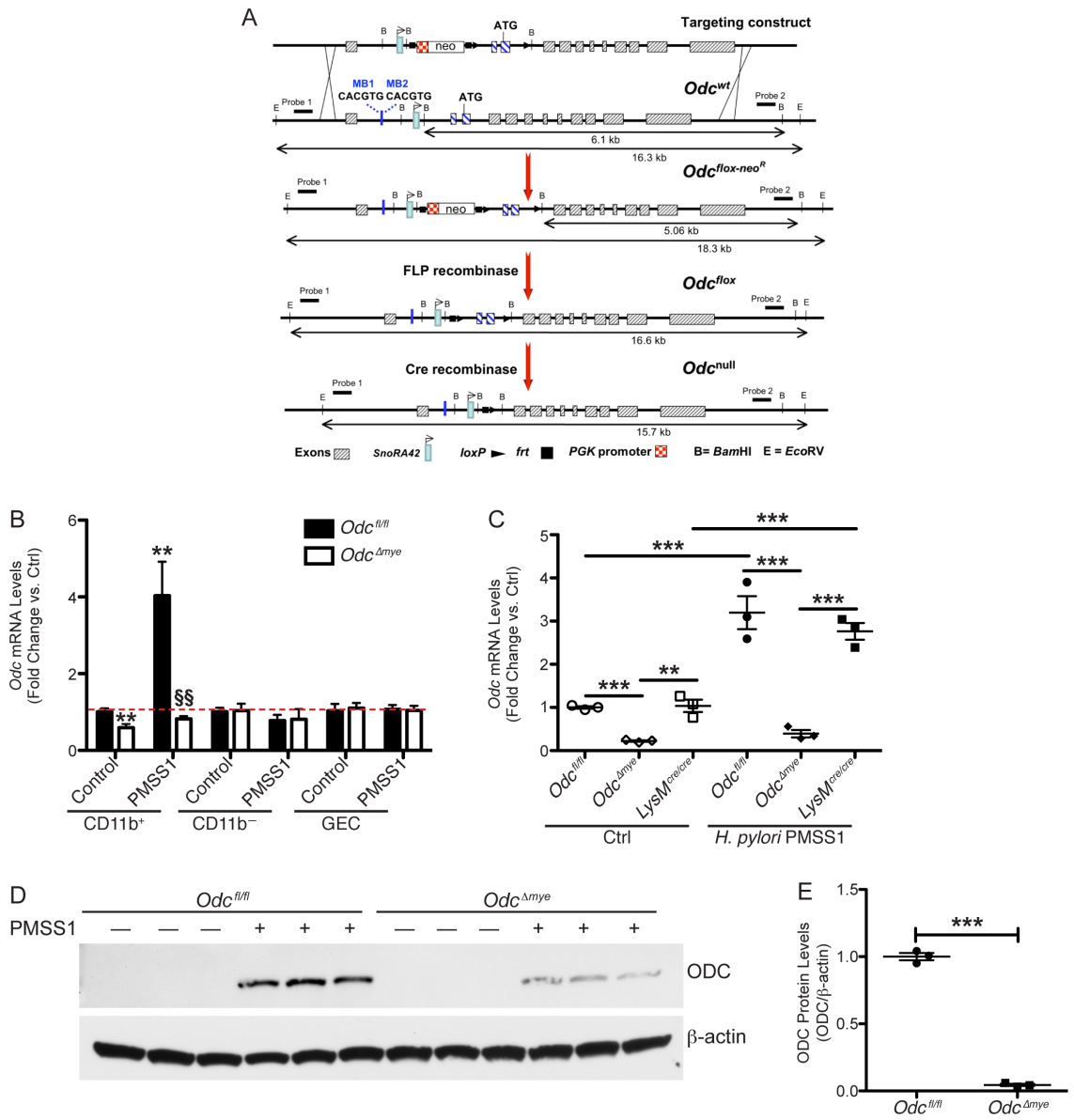

Appendix C, Figure 2. Creation of *Odc*$^{\Delta mye}$ mice and confirmation of *Odc* deletion in myeloid cells. (a) A schematic representation of the insertion of *loxP* sites within the *Odc* gene to generate *Odc*$^{fl/fl}$ mice and the creation of *Odc*$^{\Delta mye}$ mice by crossing with *LysM*$^{cre/cre}$ mice, to create a myeloid-specific knockout of *Odc*. (b) *Odc* mRNA levels were assessed by RT-PCR in isolated gastric lamina propria CD11b^{+} (myeloid cells), isolated gastric lamina propria CD11b^{-} (non-myeloid cells) and gastric epithelial cells from *Odc*$^{fl/fl}$ and *Odc*$^{\Delta mye}$ mice 48 h p.i. with *H. pylori* PMSS1. $^{**}P < 0.01$ versus *Odc*$^{fl/fl}$ control. §§$P < 0.01$ versus *Odc*$^{fl/fl}$ + *H. pylori* PMSS1. $n = 3$ uninfected and 5 infected mice per genotype. Dashed line indicates basal level of *Odc* mRNA in *Odc*$^{fl/fl}$ CD11b^{+} cells. (c) *Odc* mRNA levels were assessed by RT-PCR in *Odc*$^{fl/fl}$, *Odc*$^{\Delta mye}$, and *LysM*$^{cre/cre}$ bone marrow-derived macrophages (BMmacs) 6 h p.i. with *H. pylori* PMSS1. $^{**}P < 0.01$, $^{***}P < 0.001$. $n = 3$ biological replicates per genotype. Statistical significance in (b) and (c) was calculated by one-way ANOVA with Newman-Keuls post-test. (d) Representative western blot of ODC levels in *Odc*$^{fl/fl}$ and *Odc*$^{\Delta mye}$ BMmacs at 6 h p.i. with *H. pylori* PMSS1. (e) Quantification of ODC levels from (d). $^{***}P < 0.001$. $n = 3$ biological replicates per genotype. Statistical significance was calculated by two-tailed Student's *t* test. Data displayed as mean ± S.E.M.

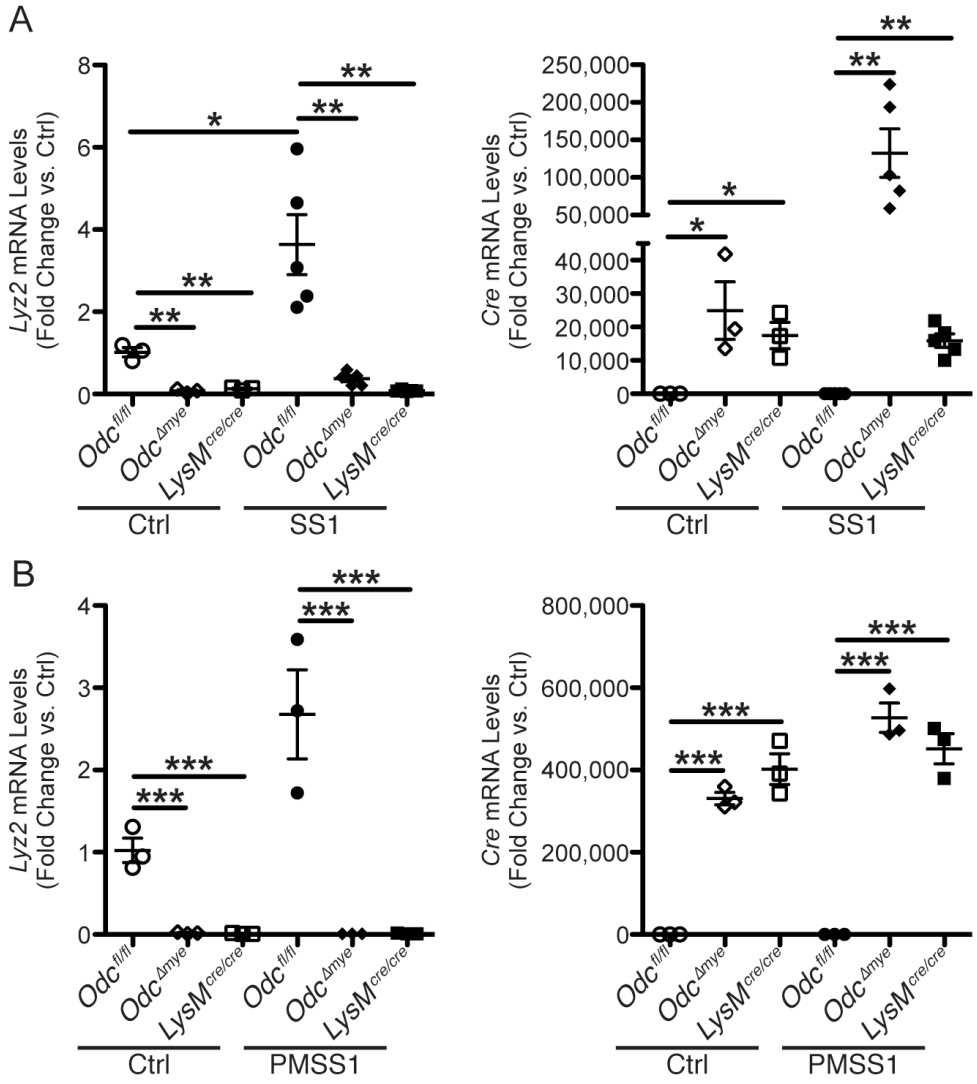

Appendix C, Figure 3. *Odc*$^{\Delta mye}$ gastric tissues and BMmacs have no detectable *Lyz2* expression and robust *Cre* expression. (A) *Lyz2* (also referred to as *LysM*) and *Cre* mRNA levels were assessed by RT-PCR in *Odc*$^{fl/fl}$, *Odc*$^{\Delta mye}$, and *LysM*$^{cre/cre}$ gastric tissues 4 mo p.i. with *H. pylori* SS1. **P* < 0.05, ***P* < 0.01. *n* = 3 uninfected and 5 infected mice per genotype. (B) *Lyz2* and *Cre* mRNA levels were assessed by RT-PCR in *Odc*$^{fl/fl}$, *Odc*$^{\Delta mye}$, and *LysM*$^{cre/cre}$ BMmacs 24 h p.i. with *H. pylori* PMSS1. ****P* < 0.001. *n* = 3 biological replicates per genotype. Statistical significance in all panels was calculated by one-way ANOVA with Newman-Keuls post-test. Data displayed as mean ± S.E.M.

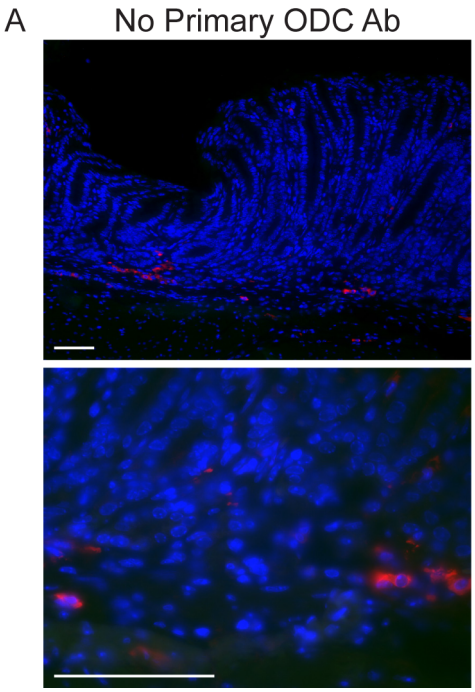

Appendix C, Figure 4. Immunofluorescence staining for CD68 and ODC in murine gastric tissues. (a) Representative images of staining where no primary anti-ODC antibody was utilized to confirm specificity of the ODC antibody. Note that the case utilized is the same *Odc*$^{fl/fl}$ case as in Figure 1i. Scale bar = 50 μm.

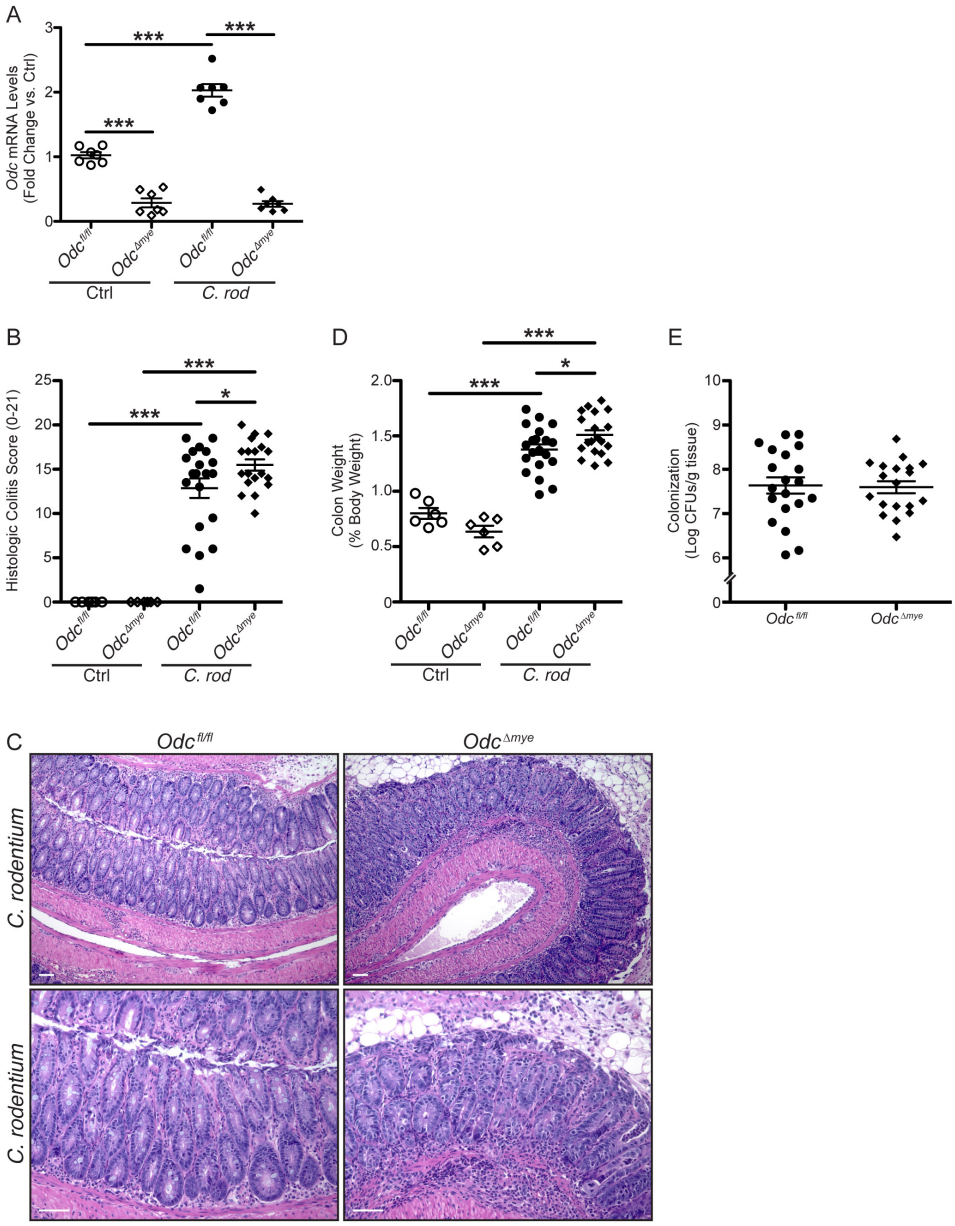

Appendix C, Figure 5. *Odc*$^{\Delta mye}$ mice exhibit significantly increased histologic colitis and increased disease severity during *Citrobacter rodentium* infection. (a) *Odc* mRNA levels were assessed by RT-PCR in *Odc*$^{fl/fl}$ and *Odc*$^{\Delta mye}$ BMmacs 6 h p.i. with *C. rodentium*. ***$P <$ 0.001. Statistical significance was calculated by one-way ANOVA with Newman-Keuls post-test. $n = 7$ biological replicates per genotype. (b) Histologic colitis scores were assessed 14 d p.i. with *C. rodentium* by a gastrointestinal pathologist in a blinded manner. *$P < 0.05$, ***$P <$ 0.001. $n = 6$ uninfected and 19-20 *C. rodentium*-infected mice per genotype. (c) Representative H&E images from infected mice in (b). Note the transmural inflammation, crypt abcesses, and loss of goblet cells in the *Odc*$^{\Delta mye}$ mouse that is not present in the *Odc*$^{fl/fl}$ mouse. Scale bars = 100 μm. (d) Colon weight as a percentage of body weight on the day of sacrifice. *$P < 0.05$, ***$P < 0.001$. $n = 6$ uninfected and 19-20 *C. rodentium*-infected mice per genotype. In (b), and (d), statistical significance was calculated by one-way ANOVA with Newman-Keuls post-test on square-root transformed data. (e) Colonization of *C. rodentium* was assessed by serial dilution and culture 14 d p.i. $n = 6$ uninfected and 19-20 *C. rodentium*-infected mice per genotype. Data displayed as mean ± S.E.M.

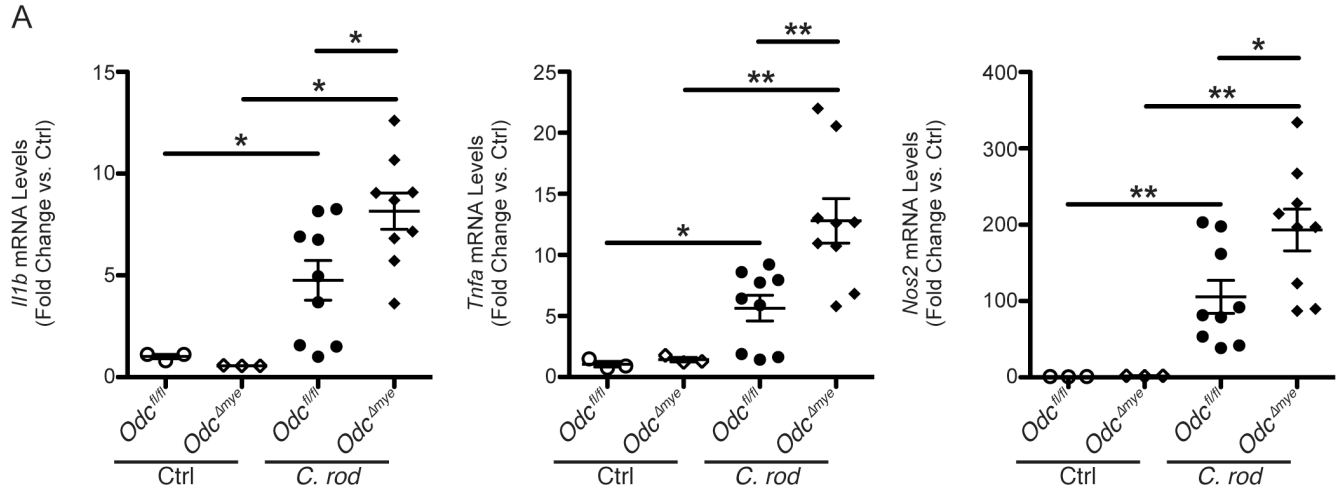

Appendix C, Figure 6. *Odc*$^{\Delta mye}$ colonic tissues express significantly increased levels of M1 macrophage markers during *C. rodentium* infection. (a) *Il1b*, *Tnfa*, and *Nos2* mRNA levels were assessed by RT-PCR in *Odc*$^{fl/fl}$, *Odc*$^{\Delta mye}$, and *LysM*$^{cre/cre}$ colonic tissues 14 d p.i. with *C. rodentium*. **P* < 0.05, ***P* < 0.01. *n* = 3 uninfected and 9 infected mice per genotype. Statistical significance was calculated by one-way ANOVA with Newman-Keuls post-test. Data displayed as mean ± S.E.M.

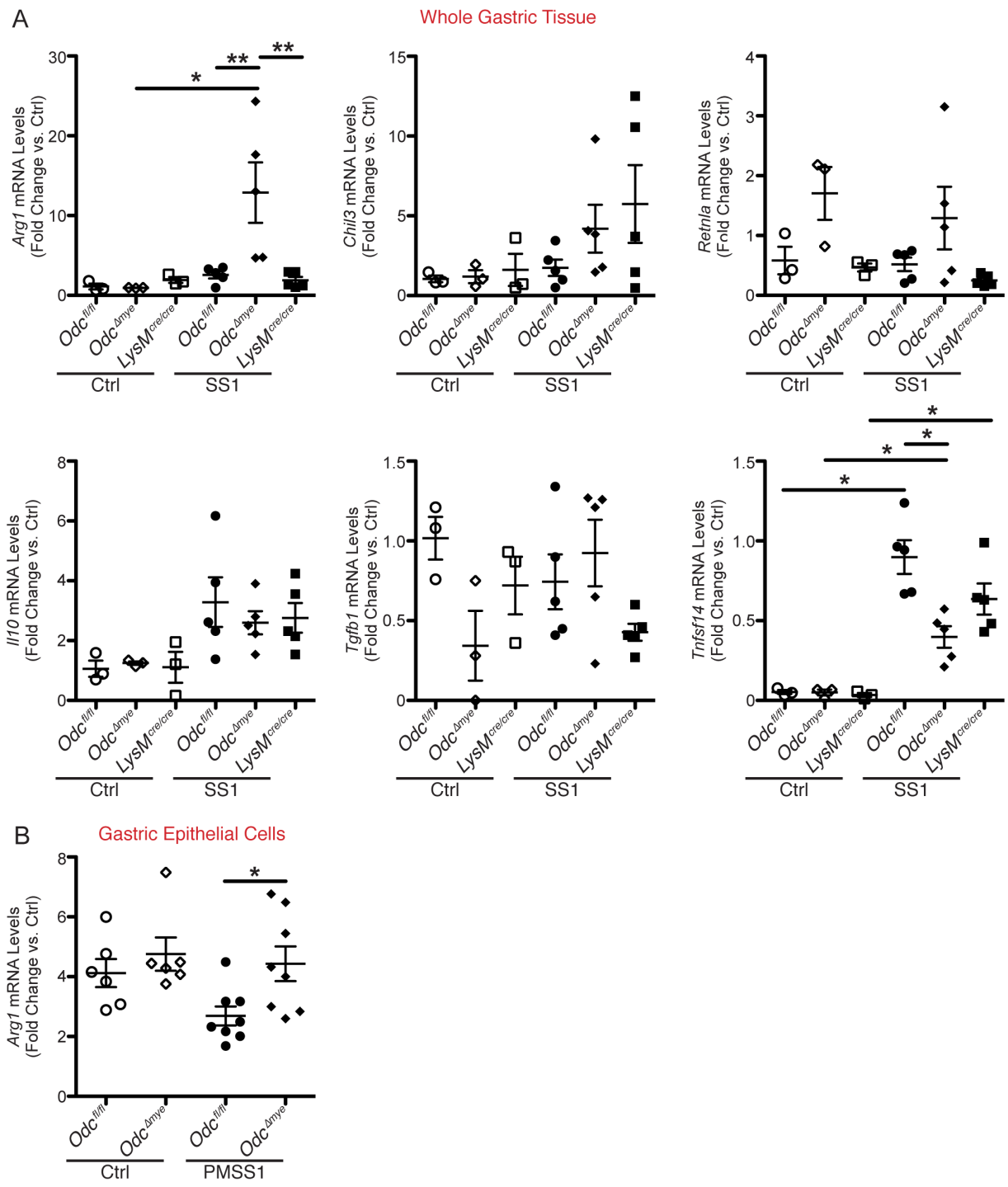

Appendix C, Figure 7. Markers of M2 macrophage activation are not substantially altered in *Odc*$^{\Delta mye}$ gastric tissues during *H. pylori* infection. (a) *Arg1*, *Chil3*, *Retnla*, *Il10*, *Tgfb1*, and *Tnfsf14* mRNA levels were assessed by RT-PCR in *Odc*$^{fl/fl}$, *Odc*$^{\Delta mye}$, and *LysM*$^{cre/cre}$ gastric tissues 4 mo p.i. with *H pylori* SS1. **P* < 0.05, ***P* < 0.01. *n* = 3 uninfected and 5 infected mice per genotype. (b) *Arg1* mRNA levels were assessed by RT-PCR *Odc*$^{fl/fl}$, and *Odc*$^{\Delta mye}$ gastric epithelial cells 48 h p.i. with *H. pylori* PMSS1. **P* < 0.05. *n* = 4 uninfected and 8 infected mice per genotype. In all panels, statistical significance was calculated by one-way ANOVA with Newman-Keuls post-test. Data displayed as mean ± S.E.M.

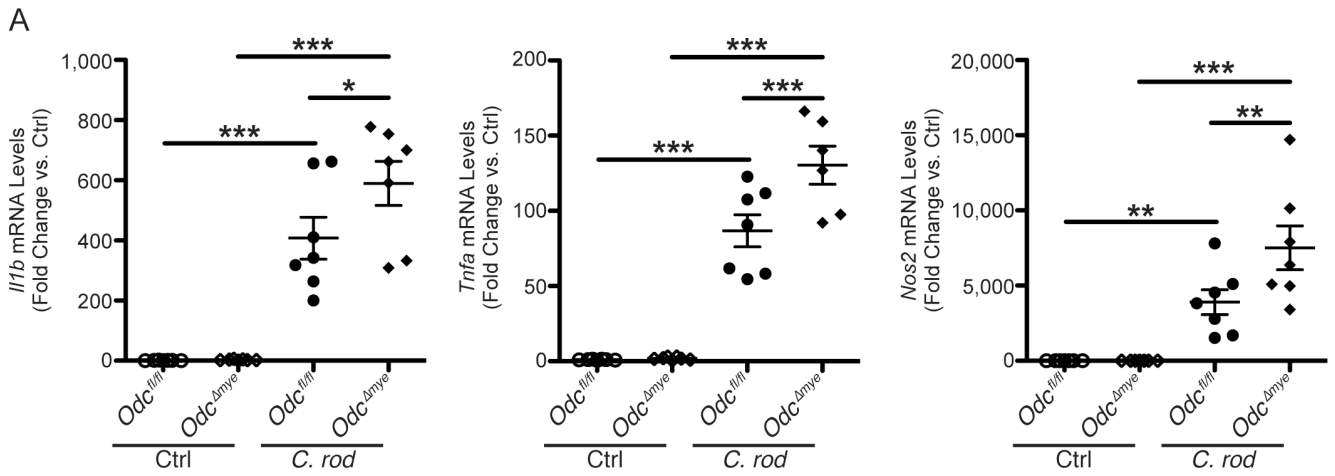

Appendix C, Figure 8. *Odc*$^{\Delta mye}$ BMmacs express significantly increased levels of M1 macrophage markers during *C. rodentium* infection. (a) *Il1b*, *Tnfa*, and *Nos2* mRNA levels were assessed by RT-PCR in BMmacs from *Odc*$^{fl/fl}$ and *Odc*$^{\Delta mye}$ mice 6 h p.i. with *C. rodentium*. **P* < 0.05, ***P* < 0.01, ****P* < 0.001. *n* = 7 biological replicates per genotype. Statistical significance was calculated by one-way ANOVA with Newman-Keuls post-test. Data displayed as mean ± S.E.M.

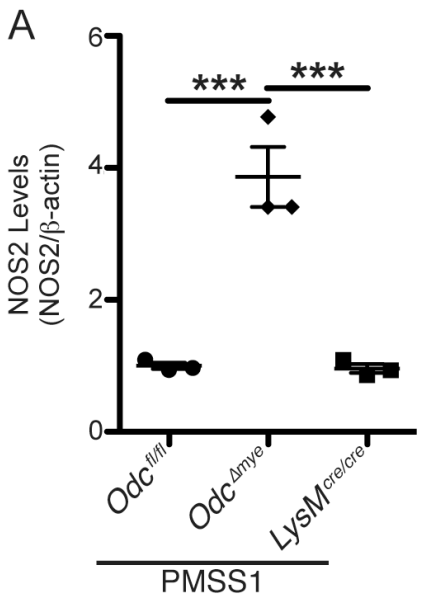

Appendix C, Figure 9. Densitometric analysis of NOS2 levels in *Odc*$^{fl/fl}$, *Odc*$^{\Delta mye}$, and *LysM*$^{cre/cre}$ BMmacs (a) Densitometric analysis of NOS2 protein levels from the representative western blot in Figure 3d. ***$P < 0.001$. $n = 3$ biological replicates per genotype. Statistical significance was calculated by one-way ANOVA with Newman-Keuls post-test. Data displayed as mean ± S.E.M.

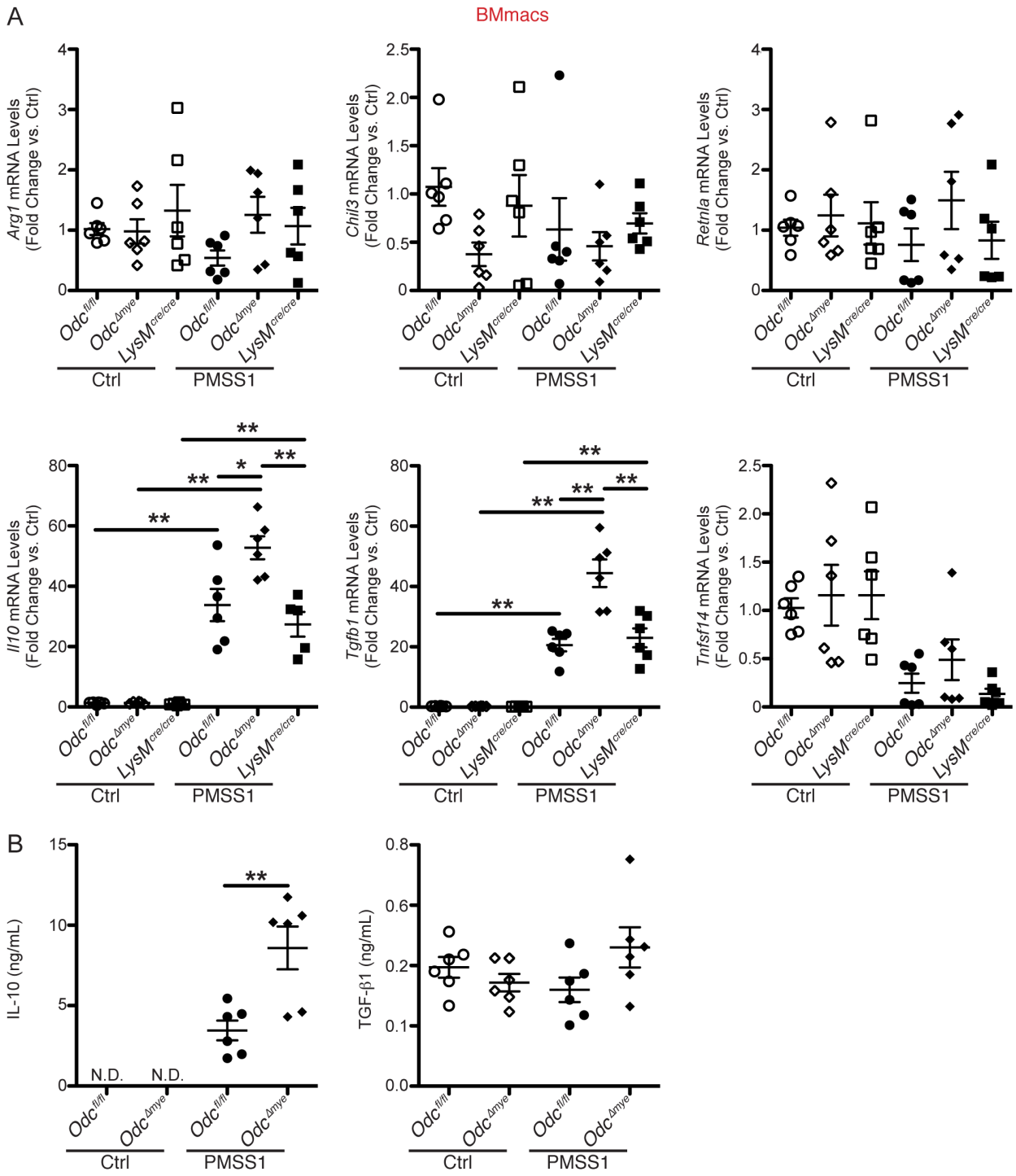

Appendix C, Figure 10. Markers of M2 macrophage activation are not substantially altered in *Odc*$^{\Delta mye}$ BMmacs during *H. pylori* infection. (a) *Arg1*, *Chil3*, *Retnla*, *Il10*, *Tgfb1*, and *Tnfsf14* mRNA levels were assessed by RT-PCR in BMmacs from *Odc*$^{fl/fl}$, *Odc*$^{\Delta mye}$, and *LysM*$^{cre/cre}$ mice 24 h p.i. with *H pylori* PMSS1. **P* < 0.05, ***P* < 0.01. *n* = 6 mice per genotype. (b) Secreted levels of IL-10 and TGF-β1 were measured by ELISA from supernatants of BMmacs 24 h p.i. with *H. pylori* PMSS1. ***P* < 0.01. *n* = 6 mice per genotype. In all panels, statistical significance was calculated by one-way ANOVA with Newman-Keuls post-test. Data displayed as mean ± S.E.M.

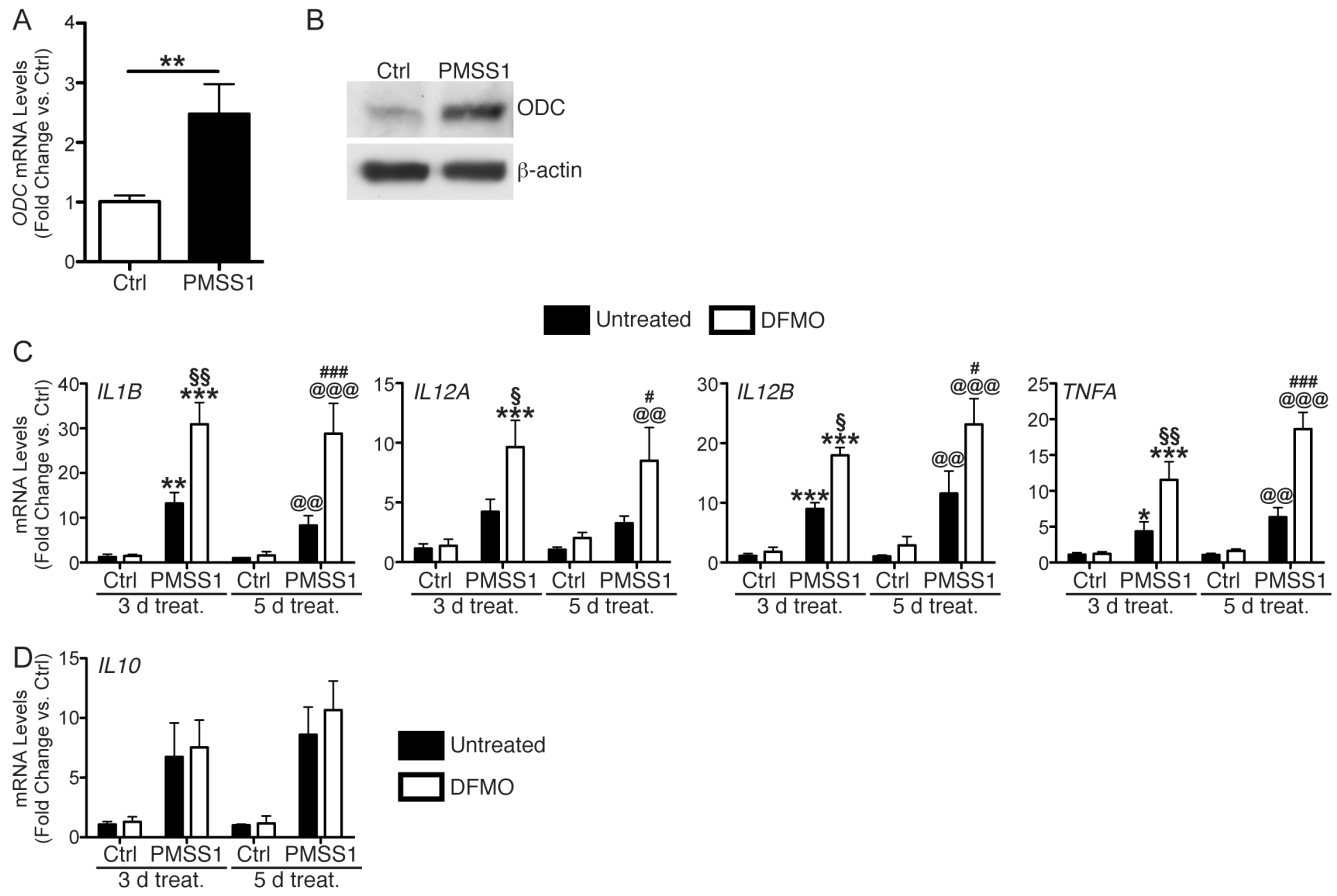

Appendix C, Figure 11. DFMO-mediated ODC inhibition leads to enhanced M1 macrophage activation in human THP1 cells during *H. pylori* infection. (a) *ODC* mRNA was assessed in THP1 cells that were differentiated into macrophages following 18 h treatment with PMA (10 ng/mL) and subsequent 6 h infection with *H. pylori* PMSS1. $^{**}P < 0.01$. $n = 3$ biological replicates. Statistical significance was determined by Student's t test. (b) Representative western blot of ODC protein levels in THP1 cells that were differentiated into macrophages following 18 h treatment with PMA (10 ng/mL) and subsequent 6 h infection with *H. pylori* PMSS1. $n = 3$ biological replicates. (c) *IL1B*, *IL12A*, *IL12B*, and *TNFA* mRNA levels were assessed by RT-PCR in THP1 cells ± DFMO (5 nM) for 3 or 5 d prior to 18 h treatment with PMA (10 ng/mL) and subsequent 6 h infection with *H. pylori* PMSS1. $^{*}P < 0.05$, $^{**}P < 0.01$, $^{***}P < 0.001$ versus 3 d ctrl. §$P < 0.05$, §§$P < 0.01$ vs. 3 d PMSS1. @@$P < 0.01$, @@@$P < 0.001$ vs. 5 d ctrl. #$P < 0.05$, ###$P < 0.001$ vs. 5 d PMSS1. $n = 3$ biological replicates. Statistical significance was determined by one-way ANOVA with Newman Keuls post-test on square-root transformed data. (d) *IL10* mRNA levels were assessed by RT-PCR in THP1 cells ± DFMO (5 nM) for 3 or 5 d prior to 18 h treatment with PMA (10 ng/mL) and subsequent 6 h infection with *H. pylori* PMSS1. n = 3 biological replicates. Data displayed as mean ± S.E.M.

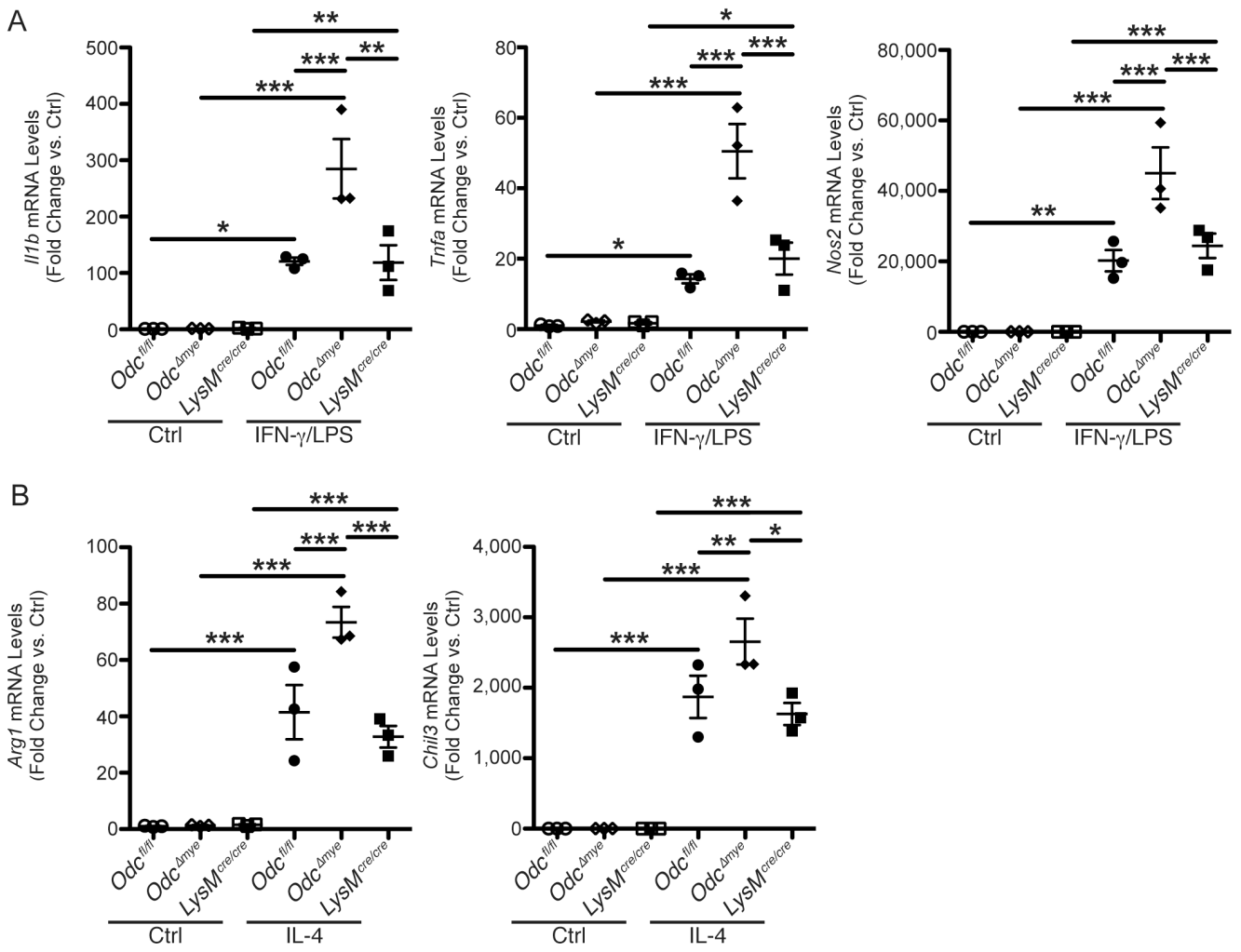

Appendix C, Figure 12. *Odc* deletion results in enhanced M1 and M2 macrophage activation during treatment with classical stimuli. (a) *Il1b*, *Tnfa*, and *Nos2* mRNA levels were assessed by RT-PCR in BMmacs from $Odc^{fl/fl}$, $Odc^{\Delta mye}$, and $LysM^{cre/cre}$ mice 24 h post-stimulation with IFN-γ (200 U/mL) and LPS (10 ng/mL). $^{*}P < 0.05$, $^{**}P < 0.01$, $^{***}P < 0.001$. n = 3 biological replicates per genotype. (b) *Arg1* and *Chil3* mRNA levels were assessed by RT-PCR in BMmacs from $Odc^{fl/fl}$, $Odc^{\Delta mye}$, and $LysM^{cre/cre}$ mice 24 h post-stimulation with IL-4 (10 ng/mL). $^{*}P < 0.05$, $^{**}P < 0.01$, $^{***}P < 0.001$. n = 3 biological replicates per genotype. Statistical significance in all panels was calculated by one-way ANOVA with Newman-Keuls post-test. Data displayed as mean ± S.E.M.

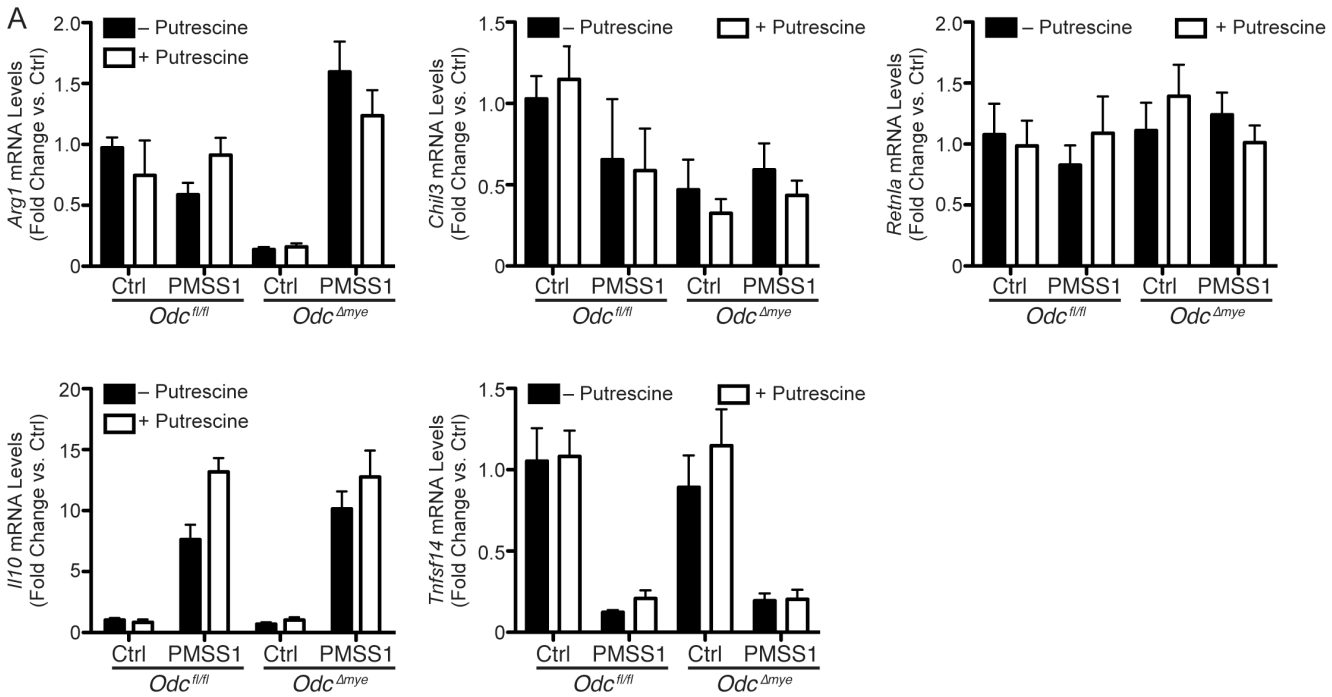

Appendix C, Figure 13. Addition of excess putrescine does not alter M2 macrophage activation marker expression during *H. pylori* infection. (a) *Arg1*, *Chil3*, *Retnla, Il10, and Tnfsf14* mRNA levels were assessed by RT-PCR in BMmacs from $Odc^{fl/fl}$, $Odc^{\Delta mye}$, and $LysM^{cre/cre}$ mice 24 h p.i. with *H. pylori* PMSS1 ± 25 μM putrescine added 60 min prior to infection. $n = 4$ biological replicates per genotype. Data displayed as mean ± S.E.M.

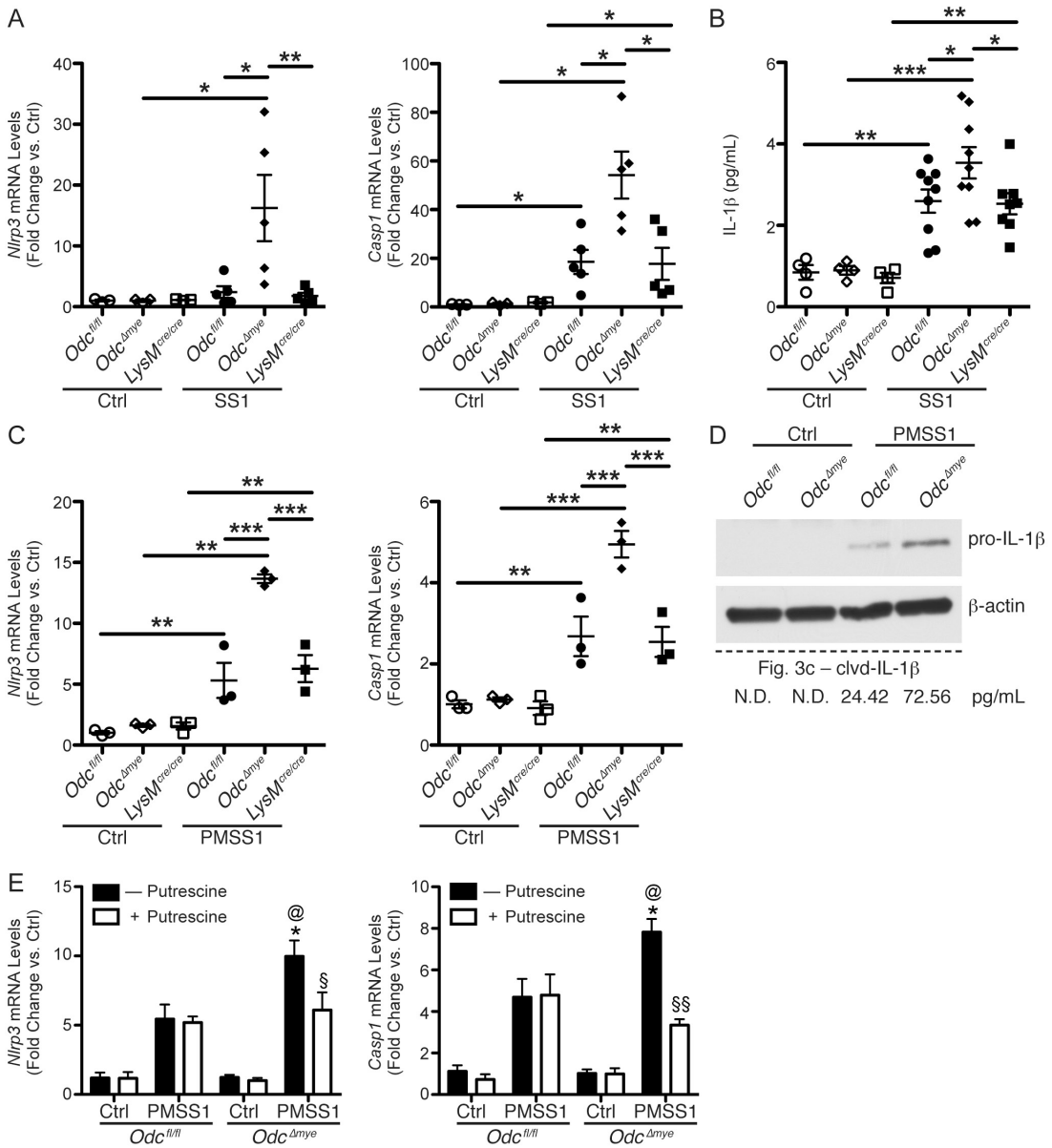

Appendix C, Figure 14. *Odc* deletion in macrophages enhances NLRP3-inflammasome activation during *H. pylori* infection. (a) mRNA levels of *Nlrp3* and *Casp1* were assessed by RT-PCR in gastric tissues 4 mo p.i. with *H. pylori* SS1. **P*<0.05, ***P*<0.01, ****P*<0.001 by one-way ANOVA with Kruskal-Wallis post-test, followed by Mann-Whitney *U* test. *n* = 3 uninfected and 5 *H. pylori* SS1 infected mice per genotype. (b) mRNA levels of *Nlrp3* and *Casp1* were assessed by RT-PCR in BMmacs 24 h p.i. with *H. pylori* PMSS1. ***P*<0.01, ****P*<0.001 by one-way ANOVA with Newman-Keuls post-test. *n* = 3 mice per genotype. (c) IL-1β protein levels were assessed by ELISA in gastric tissues 4 mo p.i. with *H. pylori* SS1. **P*<0.05, ***P*<0.01, ****P*<0.001 by one-way ANOVA with Kruskal-Wallis post-test, followed by Mann-Whitney *U* test. *n* = 4 uninfected and 8-9 *H. pylori* SS1-infected mice per genotype. (d) pro-IL-1β protein levels were assessed by western blotting in BMmacs 24 h p.i. with *H. pylori* PMSS1. *n* = 4 mice per genotype. (e) mRNA levels of *Nlrp3* and *Casp1* were assessed by RT-PCR in BMmacs 24 h p.i. with *H. pylori* PMSS1 ± 25 mM putrescine added 60 min prior to infection. **P*<0.05 vs. $Odc^{fl/fl}$ + PMSS1; @*P*<0.05, @@@*P*<0.001 vs. $Odc^{fl/fl}$ + PMSS1 + putrescine; §*P*<0.05, §§*P*<0.01 vs. $Odc^{\Delta mye}$ + PMSS1 by one-way ANOVA with Newman-Keuls post-test. *n* = 4 biological replicates. Data displayed as mean ± S.E.M.

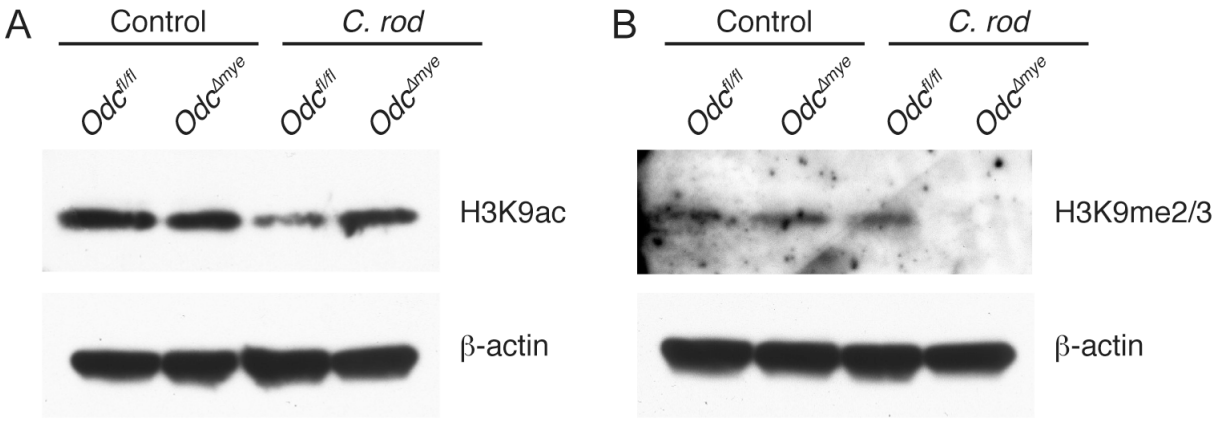

Appendix C, Figure 15. *Odc* deletion in macrophages alters acetylation and di/tri-methylation of histone 3, lysine 9 during *C. rodentium* infection. (a) Representative western blot of H3K9ac and levels in BMmacs 6 h p.i. with *C. rodentium*. *n* = 3 biological replicates. (b) Representative western blot of H3K9me2/3 levels in BMmacs 24 h p.i. with *C. rodentium*. *n* = 3 biological replicates.

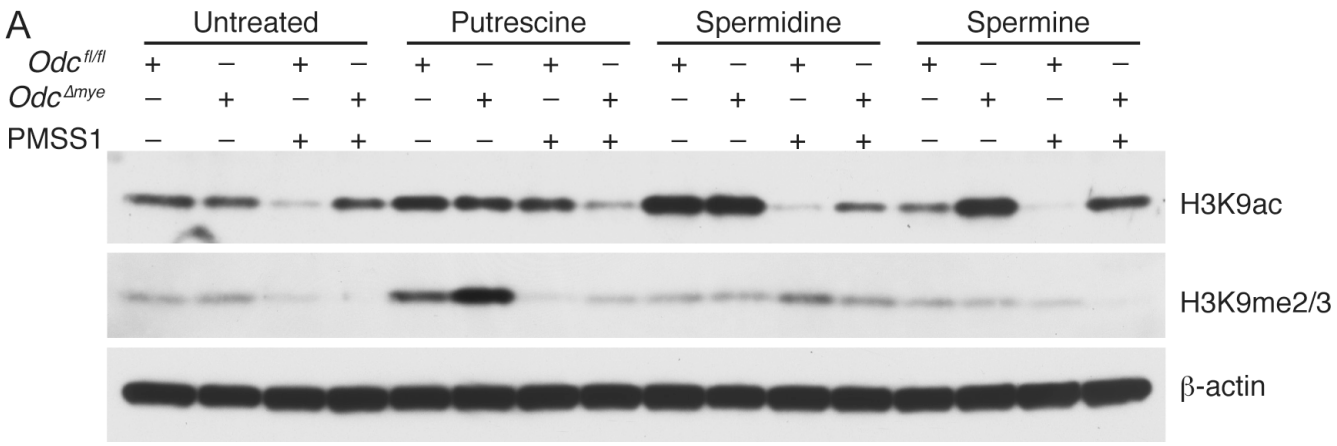

Appendix C, Figure 16. Putrescine add-back returns the H3K9ac and H3K9me2/3 levels in *Odc*$^{\Delta mye}$ BMmacs to those in *Odc*$^{fl/fl}$ BMmacs. (a) Representative western blot of H3K9ac and H3K9me2/3 levels in BMmacs 24 h p.i. with *H. pylori* PMSS1 ± 25 mM putrescine, 10 mM spermidine, or 10 mM spermine added 60 min prior to infection. *n* = 3 biological replicates.

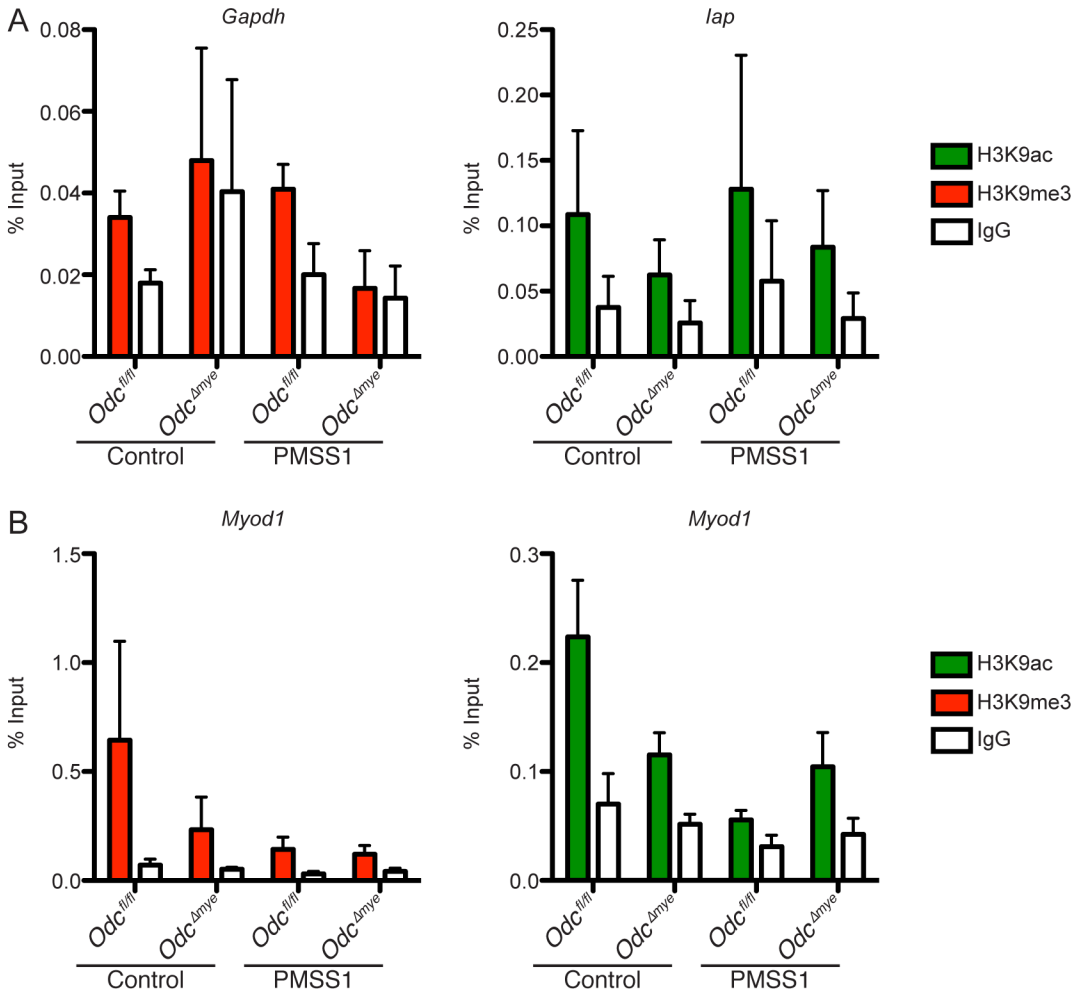

Appendix C, Figure 17. Gene expression of unchanged markers of general transcriptional levels following ChIP with anti-H3K9ac and anti-H3K9me3 antibodies in *Odc*-deficient BMmacs. (a) Expression of *Gapdh* and *Iap* was assessed by RT-PCR in BMmacs from $Odc^{fl/fl}$ and $Odc^{\Delta mye}$ mice 24 h p.i. with *H. pylori* PMSS1 with subsequent ChIP with the denoted antibodies. $n = 3$ biological replicates. (b) Expression of *Myod1* was assessed by RT-PCR in BMmacs from $Odc^{fl/fl}$ and $Odc^{\Delta mye}$ mice 24 h p.i. with *H. pylori* PMSS1 with subsequent ChIP with the denoted antibodies. Data displayed as mean ± S.E.M.

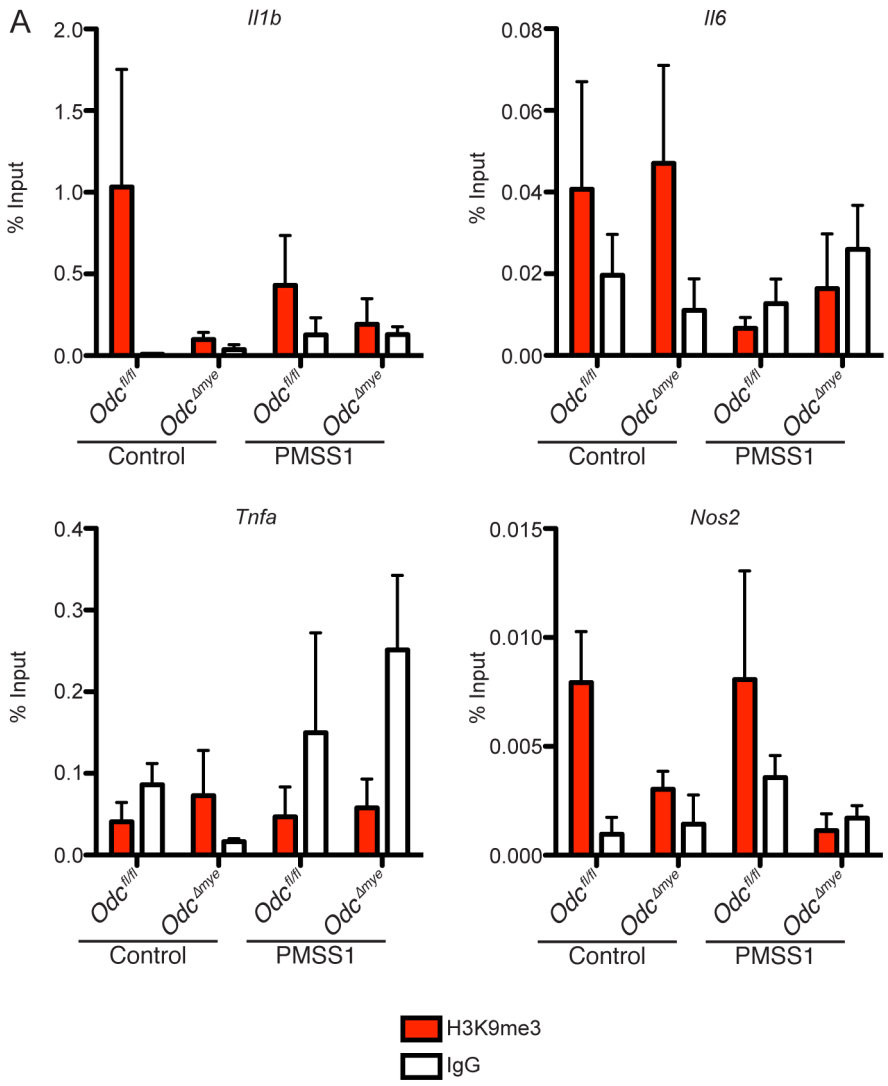

Appendix C, Figure 18. Gene expression of unchanged pro-inflammatory markers following ChIP with anti-H3K9ac and anti-H3K9me3 antibodies in *Odc*-deficient BMmacs. (a) Expression of *Il1b*, *Il6*, *Tnfa*, and *Nos2* promoter sequences was assessed by RT-PCR in BMmacs from $Odc^{fl/fl}$ and $Odc^{\Delta mye}$ mice 24 h p.i. with *H. pylori* PMSS1, followed by subsequent ChIP with the denoted antibodies. *n* = 3 biological replicates. Data displayed as mean ± S.E.M.

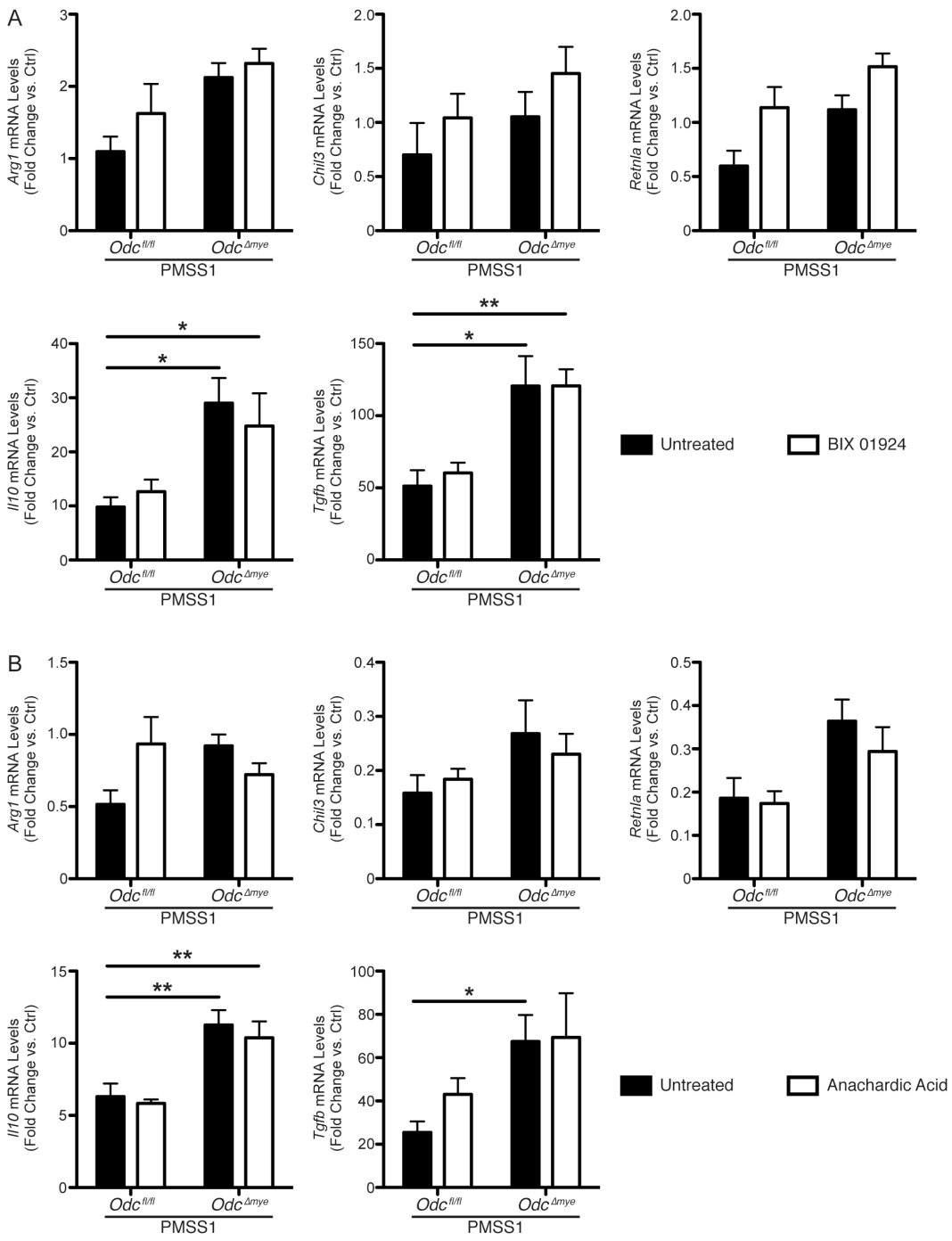

Appendix C, Figure 19. Alterations in histone modifications and chromatin structure in ODC-deficient macrophages does not alter M2 macrophage activation during *H. pylori* infection. (a) M2 markers, *Arg1*, *Chil3*, and *Retnla*, *Il10,* and *Tgfb* were assessed at the mRNA level by RT-PCR in BMmacs 24 h p.i. with *H. pylori* PMSS1 ± 5 μM BIX 01924 added 60 min prior to infection. **P*<0.05, ***P*<0.01, by one-way ANOVA with Kruskal-Wallis post-test, followed by Mann-Whitney *U* test. *n* = 5 mice per genotype. (b) M2 markers, *Arg1*, *Chil3*, and *Retnla*, *Il10,* and *Tgfb* were assessed at the mRNA level by RT-PCR in BMmacs 24 h p.i. with *H. pylori* PMSS1 ± 10 μM anacardic acid added 60 min prior to infection. ****P*<0.001 by one-way ANOVA with Kruskal-Wallis post-test, followed by Mann-Whitney *U* test. *n* = 5 mice per genotype. Data displayed as mean ± S.E.M.

Analyte	Concentration of Analyte (pg/mg protein); Mean ± S.E.M.					
	***Odc*$^{fl/fl}$**		***Odc*$^{\Delta mye}$**		***LysM*$^{cre/cre}$**	
	Uninfected	***H. pylori* SS1**	**Uninfected**	***H. pylori* SS1**	**Uninfected**	***H. pylori* SS1**
CSF2	3.70 ± 0.77	5.30 ± 0.53	3.42 ± 0.24	6.77 ± 0.86*	2.61 ± 0.56	4.09 ± 0.64
CSF3	0.79 ± 0.35	0.95 ± 0.20	0.30 ± 0.04	0.44 ± 0.11	0.38 ± 0.10	0.29 ± 0.07
IFN-γ	0.84 ± 0.11	1.33 ± 0.21	0.86 ± 0.20	2.02 ± 0.47***	0.67 ± 0.13	0.53 ± 0.07
IL-1α	24.01 ± 2.41	24.30 ± 4.01	31.80 ± 3.52	32.00 ± 2.97	31.01 ± 5.44	28.17 ± 2.44
IL-2	1.08 ± 0.08	0.65 ± 0.09	0.90 ± 0.20	0.53 ± 0.07	1.19 ± 0.26	0.74 ± 0.14
IL-4	0.22 ± 0.03	0.20 ± 0.03	0.18 ± 0.03	0.18 ± 0.04	0.20 ± 0.06	0.21 ± 0.05
IL-5	0.84 ± 0.24	0.70 ± 0.08	0.40 ± 0.04	0.56 ± 0.12	0.40 ± 0.07	0.58 ± 0.17
IL-6	1.30 ± 0.40	1.07 ± 0.12	1.23 ± 0.27	1.76 ± 0.64	2.15 ± 1.27	0.93 ± 0.10
IL-7	0.68 ± 0.14	1.31 ± 0.33	0.69 ± 0.06	0.96 ± 0.11	0.46 ± 0.09	0.60 ± 0.08
IL-9	10.84 ± 2.01	8.91 ± 1.40	10.73 ± 3.35	7.46 ± 1.63	10.81 ± 3.25	5.49 ± 1.28
IL-10	0.24 ± 0.09	0.26 ± 0.05	0.14 ± 0.02	0.24 ± 0.08	0.12 ± 0.01	0.10 ± 0.03
IL-12B	1.96 ± 0.54	1.01 ± 0.15	1.13 ± 0.28	0.49 ± 0.15	0.62 ± 0.53	0.69 ± 0.21
IL-12	0.56 ± 0.10	0.48 ± 0.09	0.47 ± 0.09	0.78 ± 0.22	0.46 ± 0.09	0.29 ± 0.04
IL-13	0.06 ± 0.04	0.57 ± 0.29	0.04 ± 0.02	0.99 ± 0.40	0.54 ± 0.52	0.37 ± 0.18
IL-15	0.51 ± 0.19	2.13 ± 0.41	1.59 ± 0.40	1.77 ± 0.29	1.11 ± 0.36	0.87 ± 0.10

Appendix C, Table 1. Luminex analytes that did not demonstrate significant differences in gastric tissues from uninfected and infected *Odc*$^{fl/fl}$, *Odc*$^{\Delta mye}$, and *LysM*$^{cre/cre}$ mice. A total of 25 distinct analytes were assessed in gastric tissue from uninfected and infected mice from each of the three genotypes. Listed are the analytes that were not significantly induced by infection, or demonstrated few or no significant differences between genotypes. Note that IL-1β is not shown, as this analyte was measured by ELISA. *n* = 4 uninfected and 8-9 *H. pylori SS1* infected mice per genotype. **P*<0.05 and ****P*< 0.001 versus *LysM*$^{cre/cre}$ + *H. pylori* SS1.

Antibody	Dilution	Application	Source (Location)
Rabbit polyclonal anti-NOS2	1:5,000	WB	EMD Millipore (Darmstadt, Germany) Cat. no. ABN26
Mouse monoclonal anti-IL-1β	1:1,000	WB	Cell Signaling Technology (Danvers, MA) Cat. no. 12242
Rabbit polyclonal anti-ODC	1:5,000 1:2,000 1:2,000	WB IF IHC-P	Lisa Shantz (Penn State College of Medicine) David Feith (University of Virginia)
Mouse monoclonal anti-H3K9me2/3	1:1,000	WB	Cell Signaling Technology (Danvers, MA) Cat. no. 5327
Rabbit polyclonal anti-H3K9ac	1:1,000 1:200	WB IF	Cell Signaling Technology (Danvers, MA) Cat. no. 9649
Rabbit polyclonal anti-H3K4me1	1:1,000	WB	Cell Signaling Technology (Danvers, MA) Cat. no. 9723
Mouse monoclonal anti-β-actin	1:10,000	WB	Sigma-Aldrich (St. Louis, MO) Cat. no. A1978
Goat anti-mouse IgG, HRP labeled	1:30,000	WB	Sigma-Aldrich (St. Louis, MO) Cat. no. 115-035-003
Goat anti-rabbit IgG, HRP labeled	1:3,000	WB	Sigma-Aldrich (St. Louis, MO) Cat. no. 111-035-003
Rabbit polyclonal anti-CD68	1:200	IF	Boster Biological Technology (Pleasanton, CA) Cat. no. PA1518
Goat anti-rabbit IgG, Alexa488	1:400	IF	ThermoFisher Scientific (Waltham, MA) Cat. no. A11078
Goat anti-rabbit IgG, Alexa555	1:500	IF	ThermoFisher Scientific (Waltham, MA) Cat. no. A21429

Appendix C, Table 2. List of all antibodies used for this study, including the dilution, application and company from which the antibodies were purchased. WB = western blotting, IF = immunofluorescence. IHC-P = immunoperoxidase.

Species	Target	Sequence
Mouse	*β-actin*	F: CCAGAGCAAGAGAGGTATCC
		R: CTGTGGTGGTGAAGCTGTAG
Mouse	*Nos2*	F: CACCTTGGAGTTCACCCAGT
		R: ACCACTCGTACTTGGGATGC
Mouse	*Tnfa*	F: CTGTGAAGGGAATGGGTGTT
		R: GGTCACTGTCCCAGCATCTT
Mouse	*Il1b*	F: ACCTGCTGGTGTGTGACGTTCC
		R: GGGTCCGACAGCACGAGGCT
Mouse	*Il6*	F: AGTTGCCTTCTTGGGACTGA
		R: TCCACGATTTCCCAGAGAAC
Mouse	*Il12a*	F: AAATGAAGCTCTGCATCCTGC
		R: TCACCCTGTTGATGGTCACG
Mouse	*Il12b*	F: GAAAGACCCTGACCATCACT
		R: CCTTCTCTGCAGACAGAGAC
Mouse	*Il23a*	F: CCAGCAGCTCTCTCGGAATC
		R: TCATAGTCCCGCTGGTGC
Mouse	*Arg1*	F: AAGAAAAGGCCGATTCACCT
		R: CACCTCCTCTGCTGTCTTCC
Mouse	*Chil3*	F: ACTTTGATGGCCTCAACCTG
		R: AATGATTCCTGCTCCTGTGG
Mouse	*Retnla*	F: GGGATGACTGCTACTGGGTG
		R: TCAACGAGTAAGCACAGGCA
Mouse	*Il10*	F: CCAAGCCTTATCGGAAATGA
		R: TCACTCTTCACCTGCTCCAC
Mouse	*Tgfb1*	F: TCCTTGCCTGCGGAAGTG
		R: GGAGAGCATTGAGCAGTTCGA
Mouse	*Tnfsf14*	F: CTGCATCAACGTCTTGGAGA
		R: GATACGTCAAGCCCCTCAAG
Mouse	*Odc*	F: CCTTGTGAGGAGCTGGTGATA
		R: GGTCCAGAATGTCCTTAGCAGT
Mouse	*Nlrp3*	F: ATGCTGGCTTCGACATCTCCT
		R: GTTTCTGGAGGTTGCAGAGC
Mouse	*Casp1*	F: AGATGCCCACTGCTGATAGG
		R: TTGGCACGATTCTCAGCATA
Mouse	*Nos2* (Promoter)	F: ATGGCCTTGCATGAGGATAC
		R: CACCAAGGTGGCTGAGAAGT
Mouse	*Il1b* (Promoter)	F: CCCCTAAGAATTCCCATCAAGC
		R: GAGCTGTGAAATTTTCCCTTGG
Mouse	*Tnfa* (Promoter)	F: CCCCAGATTGCCACAGAATC
		R: CCAGTGAGTAAAGGGACAG
Mouse	*Il6* (Promoter)	F: CCCACCCTCCAACAAAGATT
		R: GCTCCAGAGCAGAATGAGCTA
Human	*IL1B*	F: TGAACTGCACGCTCCGG
		R: GAACACCACTTGTTGCTC
Human	*TNFA*	F: ATGAGCACTGAAAGCATGATCC
		R: GAGGGCTGATTAGAGAGAGGTC

Human	*IL6*	F: GTAGCCGCCCCACACAGA
		R: CATGTCTCCTTTCTCAGGGCTG
Human	*IL12A*	F: CAAAACCTGCTGAGGGCCGTCA
		R: GGAGGCCAGGCAACTCCCATTAG
Human	*IL12B*	F: CCAAGAACTTGCAGCTGAAG
		R: TGGGTCTATTCCGTTGTGTC
Human	*IL10*	F: GCCTAACATGCTTCGAGATC
		R: TGATGTCTGGGTCTTGGTTC

Appendix C, Table 3. List of primers used for RT-PCR. (Promoter) = primers utilized for ChIP-PCR.

APPENDIX D

The original publication (listed below) is included as a PDF, as it relates to macrophage activation and function during *H. pylori* infection.

Hardbower, D.M., Verriere, T., Asim, M., Barry, D.P., Murray-Stewart, T., Lewis, N.D. Chaturvedi, R., Casero, R.A. Jr., Piazuelo, M.B., and Wilson, K.T. Arginase 2 deletion leads to enhanced M1 macrophage activation and upregulated polyamine metabolism in response to *Helicobacter pylori* infection. (2016) ***Amino Acids.*** 48(10): 2375-2388. PMID: 27074721

Amino Acids (2016) 48:2375–2388
DOI 10.1007/s00726-016-2231-2

ORIGINAL ARTICLE

Arginase 2 deletion leads to enhanced M1 macrophage activation and upregulated polyamine metabolism in response to *Helicobacter pylori* infection

Dana M. Hardbower[1,2] · Mohammad Asim[2] · Tracy Murray-Stewart[3] · Robert A. Casero Jr.[3] · Thomas Verriere[2] · Nuruddeen D. Lewis[2] · Rupesh Chaturvedi[2,4] · M. Blanca Piazuelo[2] · Keith T. Wilson[1,2,5,6,7]

Received: 28 January 2016 / Accepted: 5 April 2016 / Published online: 13 April 2016

Abstract We reported that arginase 2 (ARG2) deletion results in increased gastritis and decreased bacterial burden during *Helicobacter pylori* infection in mice. Our studies implicated a potential role for inducible nitric oxide (NO) synthase (NOS2), as $Arg2^{-/-}$ mice exhibited increased NOS2 levels in gastric macrophages, and NO can kill *H. pylori*. We now bred $Arg2^{-/-}$ to $Nos2^{-/-}$ mice, and infected them with *H. pylori*. Compared to wild-type mice, both $Arg2^{-/-}$ and $Arg2^{-/-}$;$Nos2^{-/-}$ mice exhibited increased gastritis and decreased colonization, the latter indicating that the effect of ARG2 deletion on bacterial burden was not mediated by NO. While $Arg2^{-/-}$ mice demonstrated enhanced M1 macrophage activation, $Nos2^{-/-}$ and $Arg2^{-/-}$;$Nos2^{-/-}$ mice did not demonstrate these changes, but exhibited increased CXCL1 and CXCL2 responses. There was an increased expression of the Th1/Th17 cytokines, interferon gamma and interleukin 17, in gastric tissues and splenic T-cells from $Arg2^{-/-}$, but not $Nos2^{-/-}$ or $Arg2^{-/-}$;$Nos2^{-/-}$ mice. Gastric tissues from infected $Arg2^{-/-}$ mice demonstrated increased expression of arginase 1, ornithine decarboxylase, adenosylmethionine decarboxylase 1, spermidine/spermine N^1-acetyltransferase 1, and spermine oxidase, along with increased spermine levels. These data indicate that ARG2 deletion results in compensatory upregulation of gastric polyamine synthesis and catabolism during *H. pylori* infection, which may contribute to increased gastric inflammation and associated decreased bacterial load. Overall, the finding of this study is that ARG2 contributes to the immune evasion of *H. pylori* by restricting M1 macrophage activation and polyamine metabolism.

Keywords *Helicobacter pylori* · Immune evasion · Polyamines · Macrophage activation

Abbreviations

AMD1	Adenosylmethionine decarboxylase 1
ARG1	Arginase 1; arginase, type I
ARG2	Arginase 2; arginase, type II

Handling Editor: E. Agostinelli.

Electronic supplementary material The online version of this article (doi:10.1007/s00726-016-2231-2) contains supplementary material, which is available to authorized users.

✉ Keith T. Wilson
keith.wilson@vanderbilt.edu

[1] Department of Pathology, Microbiology and Immunology, Vanderbilt University Medical Center, Vanderbilt University School of Medicine, 2215 Garland Avenue, 1030C Medical Research Building IV, Nashville, TN 37232, USA

[2] Division of Gastroenterology, Hepatology and Nutrition, Department of Medicine, Vanderbilt University Medical Center, Nashville, TN, USA

[3] The Sydney Kimmel Comprehensive Cancer Center, Johns Hopkins University School of Medicine, Baltimore, MD, USA

[4] School of Biotechnology, Jawaharlal Nehru University, New Delhi, India

[5] Department of Cancer Biology, Vanderbilt University Medical Center, Nashville, TN, USA

[6] Center for Mucosal Inflammation and Cancer, Vanderbilt University Medical Center, Nashville, TN, USA

[7] Veterans Affairs Tennessee Valley Healthcare System, Nashville, TN, USA

CCL	C–C chemokine ligand
CD	Cluster of differentiation
CHIA1	Chitinase, acidic 1
CXCL	C–X–C chemokine ligand
FPL	French-pressed lysate
IFN-γ	Interferon gamma
IL	Interleukin
M-CSF	Macrophage colony stimulating factor
MOI	Multiplicity of infection
NO	Nitric oxide
NOS2	Nitric oxide synthase 2; inducible nitric oxide synthase
ODC	Ornithine decarboxylase
PMSS1	Pre-mouse Sydney Strain 1
RT-PCR	Real-time polymerase chain reaction
RETNLA	Resistin like molecule alpha
SAT1	Spermidine/spermine N^1-acetyltransferase 1
SMOX	Spermine oxidase
SS1	Sydney Strain 1
TGF	Transforming growth factor
Th	T helper
TNF	Tumor necrosis factor
TNFSF14	Tumor necrosis factor superfamily member 14

Introduction

Helicobacter pylori is a Gram-negative, microaerophilic bacterium that selectively colonizes the gastric mucosa of humans (Cover and Blaser 2009; Hardbower et al. 2014; Sibony and Jones 2012). It is estimated that more than 50 % of the human population is infected with *H. pylori*, leading to chronic gastritis and peptic ulcer disease (Cover and Blaser 2009; Sibony and Jones 2012). Importantly, *H. pylori* is the greatest risk factor for the development of gastric adenocarcinoma, the third leading cause of cancer deaths worldwide (Bonequi et al. 2013; Hardbower et al. 2013, 2014; Nomura et al. 1991; Parsonnet et al. 1991; Peek and Blaser 2002; Ferlay et al. 2015). The global prevalence of infection and the high degree of gastric cancer mortality clearly indicate that *H. pylori* is a significant public health issue.

H. pylori infection induces both innate and adaptive immune responses, but these responses are inadequate to clear the infection and result in pro-carcinogenic, chronic inflammation (Hardbower et al. 2013, 2014; Peek et al. 2010; Robinson et al. 2007; Wilson and Crabtree 2007). Macrophages represent a dynamic subset of innate immune cells and serve to coordinate the immune response to *H. pylori* (Murray and Wynn 2011; Peek et al. 2010; Robinson et al. 2007; Wilson and Crabtree 2007). Macrophage activation is a critical component in the response to bacterial pathogens (Benoit et al. 2008). There are three classes of activated macrophages—M1, M2, and Mreg (Martinez and Gordon 2014; Mosser 2003; Mosser and Edwards 2008). M1 macrophages are highly pro-inflammatory: expressing high levels of inducible nitric oxide synthase (NOS2), interleukin (IL)-1β, and tumor necrosis factor (TNF)-α; they are aimed at the clearance of pathogens (Benoit et al. 2008; Martinez and Gordon 2014; Mosser 2003; Mosser and Edwards 2008; Murray and Wynn 2011; Strauss-Ayali et al. 2007). Alternatively activated M2 macrophages are specialized for wound healing and responses to parasites, with enhanced expression of arginase 1 (ARG1), chitinase 1 (CHIA1) and resistin-like molecule alpha (RETNLA) (Anderson and Mosser 2002; Martinez and Gordon 2014; Mosser and Edwards 2008). M2 macrophages are also referred to as tumor-associated macrophages, given their pro-angiogenic and pro-tumorigenic properties (Ostuni et al. 2015; Pander et al. 2011). Regulatory macrophages, Mreg, are anti-inflammatory and secrete high levels of IL-10 and transforming growth factor (TGF)-β (Fleming and Mosser 2011; Mosser and Edwards 2008; Murray and Wynn 2011). *H. pylori* infection most commonly results in M1 and Mreg macrophage activation (Gobert et al. 2014).

H. pylori has developed effective mechanisms to thwart the macrophage response, which appears to be centralizing around the roles of NOS2 and arginase 2 (ARG2) in macrophage function. Infection with a bacterial pathogen, including *H. pylori*, leads to induction of NOS2 and production of nitric oxide (NO), a potent anti-microbial molecule, from L-arginine (L-Arg) (Shapiro and Hotchkiss 1996; Wilson et al. 1996; Gobert et al. 2002b). *H. pylori* diminishes the efficacy of the NO response via production of the bacterial arginase, RocF, leading to depletion of L-Arg that is available to the host (Gobert et al. 2001, 2011; Chaturvedi et al. 2007). Additionally, *H. pylori* infection leads to induction of ARG2, which also utilizes L-Arg as a substrate (Lewis et al. 2010, 2011). Induction of ARG2 further reduces L-Arg availability to NOS2, and also leads to macrophage apoptosis (Gobert et al. 2002a; Gogoi et al. 2015; Lewis et al. 2010, 2011). By modulating L-Arg levels, the efficacy of both NOS2 and ARG2, and macrophage viability, *H. pylori* effectively hinders the macrophage response, allowing for the establishment of a pro-tolerogenic environment in which to survive over the lifetime of the host (Chaturvedi et al. 2010, 2012; Wilson and Crabtree 2007). The purpose of the current study was to determine the role of NO or other mechanisms in the altered immunity to *H. pylori* attributable to ARG2.

Results

The role of ARG2 in *H. pylori* immunopathogenesis is not NOS2-dependent

We have previously reported that *Arg2*$^{-/-}$ mice had significantly increased *H. pylori*-induced gastritis, with a concomitant decrease in bacterial burden (Lewis et al. 2011). We determined that ARG2 attenuated NOS2 translation, and thus, we hypothesized that the augmented gastritis in the Arg2$^{-/-}$ mice was due to enhanced NOS2 translation and NO production (Lewis et al. 2010, 2011). To determine if the ARG2 phenotype was dependent on NOS2, we crossed *Nos2*$^{-/-}$ mice and *Arg2*$^{-/-}$ mice, creating *Arg2*$^{-/-}$*;Nos2*$^{-/-}$ mice. ARG2 and NOS2 are both highly inducible in macrophages during *H. pylori* infection (Gobert et al. 2002a; Shapiro and Hotchkiss 1996; Wilson et al. 1996). Thus, we took advantage of this fact and utilized macrophages to confirm *Arg2* and *Nos2* knockout in bone marrow-derived macrophages (BMmacs) infected ex vivo with *H. pylori* (Supp. Fig. 1a, b), as differences in ARG2 and NOS2 levels would be most apparent in macrophages. Wild type (WT), *Arg2*$^{-/-}$, *Nos2*$^{-/-}$ and *Arg2*$^{-/-}$*;Nos2*$^{-/-}$ mice were infected with *H. pylori* SS1 for 4 months, after which the mice were killed and their stomachs isolated for analysis. Consistent with our previous studies (Lewis et al. 2011), *Arg2*$^{-/-}$ mice had significantly increased gastritis versus WT mice (Fig. 1a). *Arg2*$^{-/-}$*;Nos2*$^{-/-}$ mice also had significantly increased gastritis when compared to WT mice (Fig. 1a). *Nos2*$^{-/-}$ mice had similar gastritis as WT mice (Fig. 1a). The representative images of the gastritis further demonstrate the increased inflammation in *Arg2*$^{-/-}$ and *Arg2*$^{-/-}$*;Nos2*$^{-/-}$ mice, as compared to WT and *Nos2*$^{-/-}$ mice (Fig. 1b). Consistent with the increase in gastritis, *Arg2*$^{-/-}$ and *Arg2*$^{-/-}$*;Nos2*$^{-/-}$ mice both showed significantly decreased bacterial burden when compared to WT mice (Fig. 1c). These data, especially the finding that *Arg2*$^{-/-}$*;Nos2*$^{-/-}$ mice did not lose the reduced colonization of *Arg2*$^{-/-}$ mice, indicate that the role of ARG2 in *H. pylori* pathogenesis is not dependent on NOS2, but rather some other aspect of the immune response to the pathogen. Additionally, *Nos2*$^{-/-}$ mice exhibited a modest decrease in colonization compared to WT mice (Fig. 1c), further suggesting that NOS2-derived NO is not the primary effector that controls colonization in this infection model.

ARG2 reduces pro-inflammatory cytokine expression and immune cell-derived chemokine production in response to *H. pylori*

To begin to address how ARG2 alters the immune response to *H. pylori*, we performed Luminex analysis on gastric tissues from WT, *Arg2*$^{-/-}$, *Nos2*$^{-/-}$ and *Arg2*$^{-/-}$*;Nos2*$^{-/-}$ mice after chronic infection to assess differences in cytokine and chemokine levels in tissues. We found that *Arg2*$^{-/-}$ and *Arg2*$^{-/-}$*;Nos2*$^{-/-}$ mice had significantly increased protein levels of C–C chemokine ligand (CCL) 3 (MIP-1α), CCL4 (MIP-1β), and CCL5 (RANTES), as compared to WT and *Nos2*$^{-/-}$ mice (Fig. 2a). CCL3, CCL4, and CCL5 are typically produced by immune cells, such as macrophages, in response to pathogens (Algood et al. 2004). These data indicate that ARG2 regulates the innate immune response to *H. pylori*. Specifically, ARG2 deletion may affect M1 macrophage activation, as M1 macrophages are pro-inflammatory drivers of the innate immune response to many pathogens (Benoit et al. 2008; Martinez and Gordon 2014; Mosser and Edwards 2008; Murray and Wynn 2011). Thus, we assessed mRNA expression levels of the M1 macrophage markers, *Nos2*, *Il-1β*, and *Tnf-α* (Mosser and Edwards 2008) in gastric tissues from WT, *Arg2*$^{-/-}$, *Nos2*$^{-/-}$, and *Arg2*$^{-/-}$*;Nos2*$^{-/-}$ mice. *Nos2*$^{-/-}$ and *Arg2*$^{-/-}$*;Nos2*$^{-/-}$ mice did not express *Nos2*, further confirming knockout of the gene (Fig. 2b). *Arg2*$^{-/-}$ mice had significantly enhanced mRNA levels of the M1 markers, compared to the other three genotypes (Fig. 2b). Markers of M2 and Mreg macrophage activation were also assessed in these gastric tissues. M2 markers, *Chia1* (also known as *Ym1)* and *Retnla* (also known as *Fizz1/Relm-α*) (Anderson and Mosser 2002; Mosser and Edwards 2008), were not induced by *H. pylori* infection (data not shown). Moreover, Mreg markers, *Il-10* and *Tgf-β* (Anderson and Mosser 2002; Mosser and Edwards 2008; Murray and Wynn 2011), were not significantly altered between the four genotypes (data not shown), indicating that the effect of ARG2 knockout is specifically on M1 activation.

Interestingly, as shown in Fig. 3, NOS2 knockout, in both *Nos2*$^{-/-}$ and *Arg2*$^{-/-}$*;Nos2*$^{-/-}$ mice, resulted in significantly increased levels of the chemokines, C–X–C chemokine ligand (CXCL) 1 (KC) and CXCL2 (MIP2), which have been shown to be primarily produced by epithelial cells (Schleimer et al. 2007). These data indicate that the effects of the *Nos2* deletion may be more significant in epithelial cell function than in immune cell function.

ARG2 diminishes Th1/Th17 T-cell differentiation in response to chronic *H. pylori* infection

A second essential component to *H. pylori*-driven gastritis is the adaptive T-cell response (Robinson et al. 2007). To evaluate the T helper (Th) cell response to *H. pylori* infection, gastric tissues from WT, *Arg2*$^{-/-}$, *Nos2*$^{-/-}$, and *Arg2*$^{-/-}$*;Nos2*$^{-/-}$ mice were assessed for gene expression of Th1-, Th17-, Th2-, and Treg-specific markers. The mRNA levels of Th1 marker, *Ifn-γ*, and Th17 marker, *Il-17*, were significantly increased in *Arg2*$^{-/-}$ mice, when compared to WT mice (Fig. 4a). This correlates with the significantly

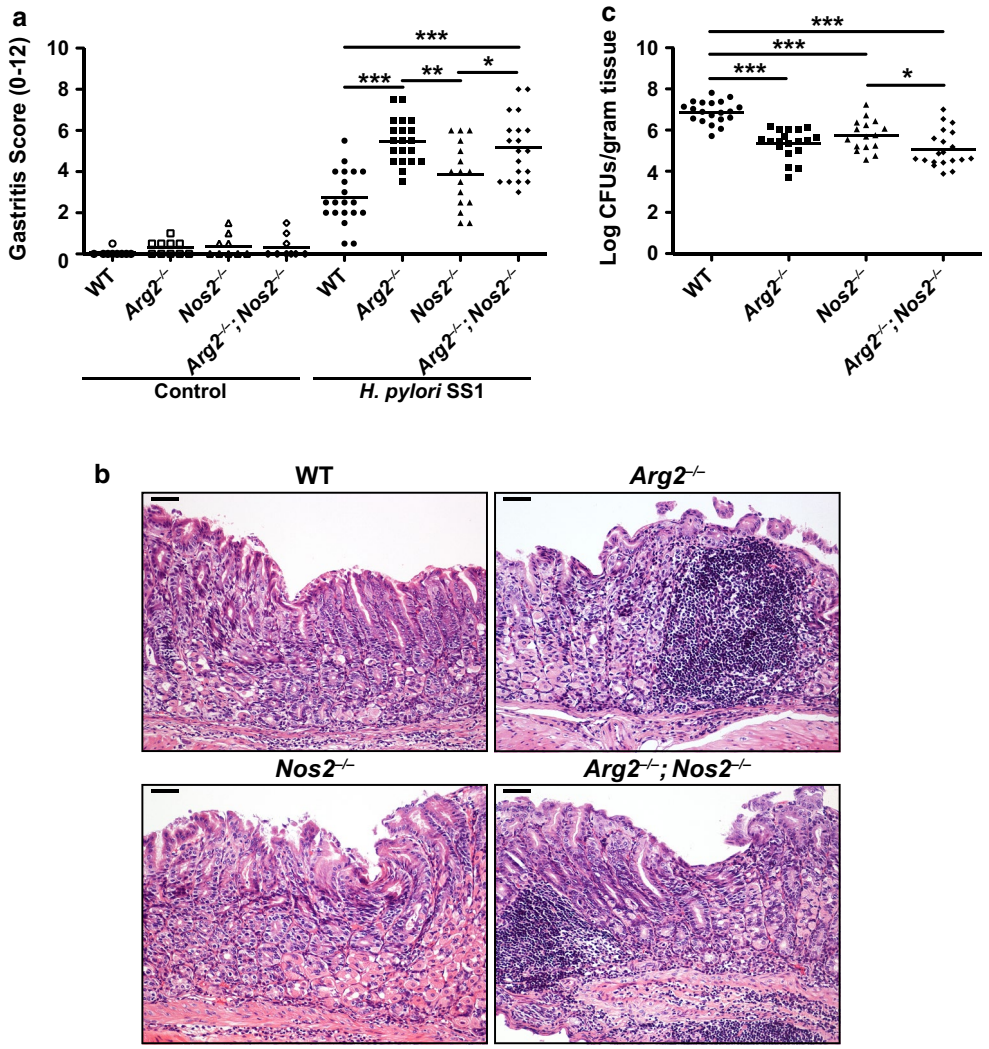

Fig. 1 Effect of *Arg2* and/or *Nos2* knockout on *H. pylori* pathogenesis after chronic infection. WT, $Arg2^{-/-}$, $Nos2^{-/-}$, and $Arg2^{-/-}$;$Nos2^{-/-}$ mice were infected with *H. pylori* Sydney Strain 1 (SS1) for 4 months. Mice were killed and their stomachs were isolated for analysis. **a** Histologic gastritis was assessed in a blinded manner according to the Sydney System by a gastrointestinal pathologist. $n = 9$–10 uninfected and 16–20 *H. pylori* SS1-infected mice per genotype. Statistical significance was determined by one-way ANOVA with Kruskal–Wallis test, followed by Mann–Whitney *U* test. **b** Representative images of hematoxylin and eosin-stained tissues, from *H. pylori*-infected mice of each genotype. *Scale bars* 100 μM. **c** *H. pylori* colonization was assessed by serial dilution and culture. $n = 16$–20 *H. pylori* SS1-infected mice per genotype. Statistical significance was determined by one-way ANOVA with NewmanKeuls post-test. In **a** and **c**, $*p < 0.05$, $**p < 0.01$, $***p < 0.001$

increased histologic gastritis observed in these mice (Fig. 1a). However, WT, $Nos2^{-/-}$, and $Arg2^{-/-}$;$Nos2^{-/-}$ mice demonstrated similar levels of *Ifn-γ* and *Il-17a* expression in gastric tissues, and each had significantly lower expression than in $Arg2^{-/-}$ mice (Fig. 4a). These data suggest that the increase in the Th1/Th17 response to *H. pylori* in $Arg2^{-/-}$ mice is dependent on NOS2, as $Arg2^{-/-}$;$Nos2^{-/-}$ mice demonstrated the same Th1/Th17 phenotype as $Nos2^{-/-}$ mice. mRNA expression of Th2 marker, *Il-4*, and expression of Treg marker, *Foxp3*, were also measured in gastric tissues from these mice and no significant differences were found between genotypes (data not shown).

To confirm the enhanced Th1/Th17 findings in $Arg2^{-/-}$ mice, splenocytes were isolated from *H. pylori*-infected WT and $Arg2^{-/-}$ mice, and cultured in the presence of CD3 and CD28 to promote T-cell proliferation. The splenic T-cells were then treated with *H. pylori* SS1 French-pressed lysate (FPL) to allow *H. pylori*-specific T-cells to proliferate, and levels of secreted IFN-γ and IL-17 were assessed. Consistent with the mRNA findings in gastric tissue, $Arg2^{-/-}$ mice had significantly increased IFN-γ and IL-17 secretion from splenic T-cells (Fig. 4b). Additionally, the Th1 population within the *H. pylori*-stimulated splenic T-cells was assessed by flow cytometry for CD4, a T helper

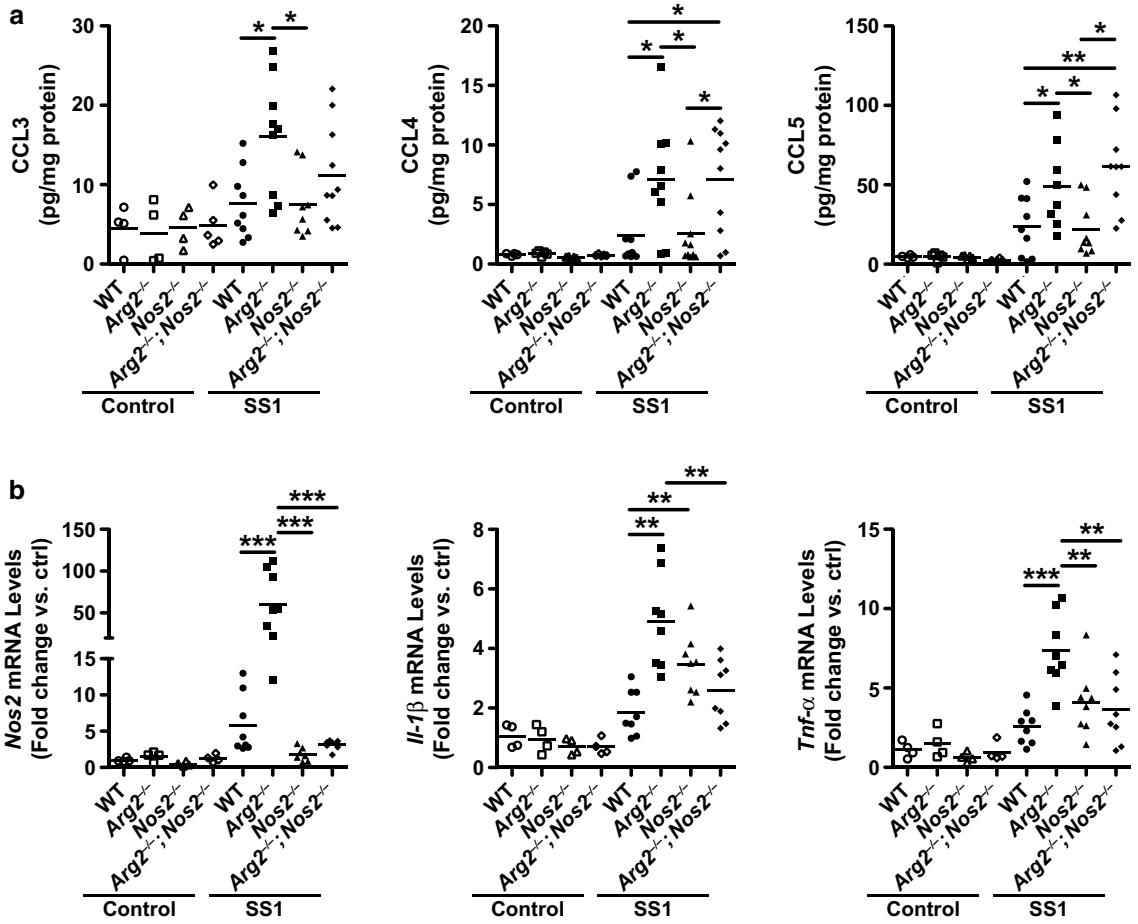

Fig. 2 Loss of ARG2 leads to enhanced pro-inflammatory innate immune responses to *H. pylori*. **a** Protein was isolated from gastric tissues from WT, $Arg2^{-/-}$, $Nos2^{-/-}$, and $Arg2^{-/-};Nos2^{-/-}$ mice 4 months post-inoculation (p.i.). with *H. pylori* SS1. Protein levels of the immune cell-derived chemokines, CCL3 (MIP-1α), CCL4 (MIP-1β), and CCL5 (RANTES) were assessed by Luminex assay. $n = 4$–5 uninfected and 8–10 *H. pylori* SS1-infected mice per genotype. Statistical significance was determined by one-way ANOVA with Kruskal–Wallis test, followed by Mann–Whitney *U* test. **b** RNA was isolated from gastric tissues from WT, $Arg2^{-/-}$, $Nos2^{-/-}$, and $Arg2^{-/-};Nos2^{-/-}$ mice 4 months p.i. with *H. pylori* SS1. The pro-inflammatory markers, *Nos2*, *Il-1β*, and *Tnf-α*, were assessed by RT-PCR. $n = 4$ uninfected and 7–8 *H. pylori* SS1-infected mice per genotype. Statistical significance was determined by one-way ANOVA with Kruskal–Wallis test, followed by Mann–Whitney *U* test. In **a** and **b**, $*p < 0.05$, $**p < 0.01$, $***p < 0.001$

cell marker, and intracellular IFN-γ. Again, $Arg2^{-/-}$ mice had a significantly increased $CD4^{+}$/IFN-γ^{+} Th1 population, as compared to *H. pylori*-stimulated WT splenic T-cells (Fig. 4c).

ARG2 mediates M1 macrophage activation and function, but not M2 or Mreg activation, in response to *H. pylori*

As previously reported, ARG2 and NOS2 are highly inducible in macrophages during *H. pylori* infection (Gobert et al. 2002a, b; Lewis et al. 2010). Bone marrow-derived macrophages (BMmacs) were isolated from WT, $Arg2^{-/-}$, $Nos2^{-/-}$ and $Arg2^{-/-};Nos2^{-/-}$ mice to specifically evaluate the affect of ARG2 and NOS2 knockout on macrophage activation and function. BMmacs from each of the four genotypes in this study were co-cultured with *H. pylori* for 24 h, followed by assessment of M1, M2, and Mreg activation markers by real-time polymerase chain reaction (RT-PCR). Gene expression levels of *Nos2*, *Il-1β*, and *Tnf-α* were utilized as representative M1 markers, *Chia1* and *Retnla* as M2 markers, and *Il-10*, *Tgf-β*, and *Tnfsf14* as Mreg markers. As expected, $Nos2^{-/-}$ and $Arg2^{-/-};Nos2^{-/-}$ BMmacs did not expresses *Nos2* (Fig. 5a). $Arg2^{-/-}$ BMmacs demonstrated enhanced M1 activation, as evidenced by significantly increased *Nos2*, *Il-1β*, and *Tnf-α*, as compared to WT and $Nos2^{-/-}$ BMmacs (Fig. 5a). Interestingly, $Arg2^{-/-};Nos2^{-/-}$ BMmacs demonstrated increased *Il-1β* expression to a similar level as $Arg2^{-/-}$ BMmacs, while *Tnf-α* expression remained similar to WT and $Nos2^{-/-}$ BMmacs, rather than increasing as in $Arg2^{-/-}$ BMmacs (Fig. 5a). The effects of ARG2 and NOS2 on

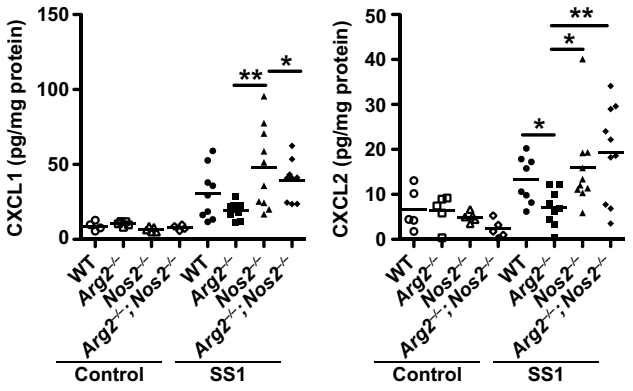

Fig. 3 Loss of NOS2 leads to enhanced epithelial cell-derived chemokine production. Protein was isolated from gastric tissues from WT, *Arg2*$^{-/-}$, *Nos2*$^{-/-}$, and *Arg2*$^{-/-}$*;Nos2*$^{-/-}$ mice 4 months p.i. with *H. pylori* SS1. Levels of the epithelial cell-derived chemokines, CXCL1 (KC) and CXCL2 (MIP-2), were assessed by Luminex assay. $n = 4$–5 uninfected and 9–10 *H. pylori* SS1-infected mice per genotype. Statistical significance was determined by one-way ANOVA with Kruskal–Wallis test, followed by Mann–Whitney *U* test. *$p < 0.05$, **$p < 0.01$, ***$p < 0.001$

macrophage activation were also studied in BMmacs from each genotype, utilizing IFN-γ/LPS activation as a classical M1 stimulus. Under these conditions, both *Arg2*$^{-/-}$ and *Arg2*$^{-/-}$*;Nos2*$^{-/-}$ BMmacs had enhanced M1 activation, when compared with WT and *Nos2*$^{-/-}$ BMmacs (Supp. Fig. 2a). *Arg2*$^{-/-}$*;Nos2*$^{-/-}$ BMmacs had the highest expression of *Il-1β*, even when compared to *Arg2*$^{-/-}$ BMmacs (Supp. Fig. 2a).

M2 and Mreg markers were also assessed in BMmacs from all four genotypes. Consistent with the gastric tissue mRNA data, *H. pylori* infection did not induce expression of *Arg1*, *Chia1,* or *Retnla* in BMmacs, from any of the genotypes (data not shown). As *H. pylori* did not induce an M2 response, BMmacs from each of the four genotypes were stimulated with IL-4, the canonical M2 stimulus. Stimulation with IL-4 induced an M2 response in these mice, but there were no significant differences between the genotypes (Supp. Fig. 2b). Moreover, *H. pylori* infection had a very modest effect on Mreg activation between the four genotypes. *Arg2*$^{-/-}$ BMmacs had significantly increased *Il-10* expression, when compared to each of the other genotypes (data not shown). Additionally, there was no difference in *Tgf-β* or *Tnfsf14* expression between each of the genotypes (data not shown).

To confirm the effect of ARG2 on M1 macrophage activation in vivo, splenic macrophages were isolated from chronically infected WT and *Arg2*$^{-/-}$ mice, and stimulated with *H. pylori* SS1 FPL. As expected, splenic macrophages from *Arg2*$^{-/-}$ mice had significantly increased levels of secreted IL-1β and TNF-α (Fig. 5b). Moreover, *Arg2*$^{-/-}$ BMmacs produced significantly increased levels of NO, in response to *H. pylori* infection ex vivo (Fig. 5c). Taken together, these data demonstrate that ARG2 can modulate M1 macrophage responses to *H. pylori* and other stimuli, but ARG2 does not have a role in regulating M2 and Mreg activation.

ARG2 deletion results in a compensatory upregulation in polyamine metabolism in response to *H. pylori*

ARG1 and ARG2 are redundant enzymes responsible for the conversion of L-Arg to L-ornithine, which is the substrate for ornithine decarboxylase (ODC) (Chaturvedi et al. 2010, 2012). ARG1 is essential for life, and can be induced by certain stimuli; ARG2 is also inducible under conditions of stress, such as bacterial infections (Chaturvedi et al. 2012; Gobert et al. 2002a; Gogoi et al. 2015; Lewis et al. 2010, 2011). *Arg2*$^{-/-}$ and *Arg2*$^{-/-}$*;Nos2*$^{-/-}$ mice are lacking this inducible form of the enzyme, potentially altering both the response to pathogens and polyamine metabolism. We hypothesized that the loss of *Arg2* could lead to an upregulation of *Arg1* expression, and an increase in gene expression related to polyamine metabolism. We assessed a panel of genes involved in polyamine metabolism, including *Arg1,* which generates substrates for polyamine metabolism, polyamine synthetic enzymes, *Odc* and adenosylmethionine decarboxylase 1 (*Amd1)*, and polyamine catabolic enzymes, spermidine/spermine N^1-acetyltransferase 1 (*Sat1)* and spermine oxidase (*Smox)*. Expression of each of these genes was examined in chronically infected gastric tissues from WT, *Nos2*$^{-/-}$, and *Arg2*$^{-/-}$*;Nos2*$^{-/-}$ mice by RT-PCR. *Arg2*$^{-/-}$ mice had significantly increased *Arg1* and *Sat1* levels compared to each of the other genotypes (Fig. 6a). Both *Arg2*$^{-/-}$ and *Arg2*$^{-/-}$*;Nos2*$^{-/-}$ mice had significantly enhanced *Odc*, *Amd1*, and *Smox* expression, as compared to WT and *Nos2*$^{-/-}$ mice (Fig. 6a). Thus, ARG2 knockout enhanced the expression of polyamine metabolism genes, while NOS2 deletion had no effect on expression of these genes.

Additionally, *Arg1* and *Odc* gene expression was increased in BMmacs from both *Arg2*$^{-/-}$ and *Arg2*$^{-/-}$*;Nos2*$^{-/-}$ mice (Fig. 6b). However, *Amd1*, *Sat1*, and *Smox* were not significantly induced by *H. pylori* infection in BMmacs, nor were differences between the genotypes detected (data not shown). These data suggest that ARG2 in macrophages has a role in polyamine synthesis, but not in polyamine catabolism.

Furthermore, the levels of putrescine, spermidine, and spermine were measured in gastric tissues by high-performance liquid chromatography. *Arg2*$^{-/-}$ and *Arg2*$^{-/-}$*;Nos2*$^{-/-}$ mice demonstrated significantly increased spermine levels (Fig. 7a), and higher spermidine and total polyamine levels as compared to WT and *Nos2*$^{-/-}$ mice, although the latter differences did not reach

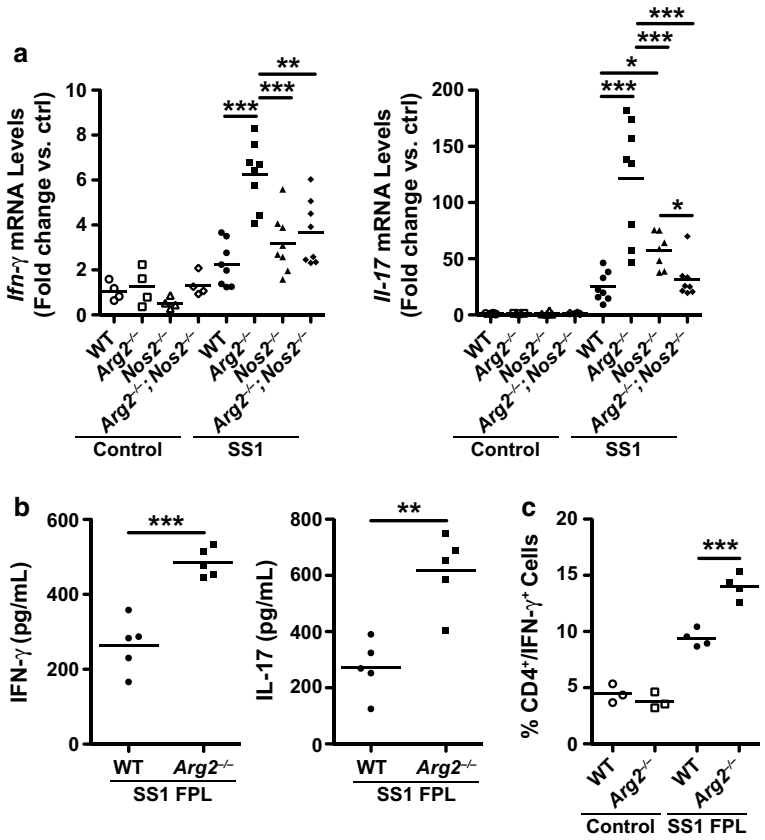

Fig. 4 Loss of ARG2 results in diminished Th1/Th17 T-cell differentiation in response to *H. pylori*. **a** RNA was isolated from gastric tissues from WT, $Arg2^{-/-}$, $Nos2^{-/-}$, and $Arg2^{-/-};Nos2^{-/-}$ mice 4 months p.i. Expression of the Th1 marker, *Ifn-γ*, and the Th17 marker, *Il-17a*, was assessed by RT-PCR. $n = 4$ uninfected and 8 *H. pylori* SS1-infected mice per genotype. Statistical significance was determined by one-way ANOVA with Kruskal–Wallis test, followed by Mann–Whitney *U* test. **b** Splenocytes were isolated from WT and $Arg2^{-/-}$ mice 4 months p.i. and cultured in the presence of CD3 and CD28. The splenic T-cells were then stimulated with *H. pylori* SS1 French-pressed lysate (FPL) for 24 h. Protein levels of secreted IFN-γ (Th1) and IL-17 (Th17) were assessed by Luminex assay on the splenic T-cell supernatants. $n = 5$ mice per genotype. Statistical significance was determined by Student's *t* test. **c** Splenic T-cells were generated as in **b**. The $CD4^{+}IFN\text{-}\gamma^{+}$ population of Th1 cells was assessed by flow cytometry. $n = 3$ uninfected and 4 *H. pylori* SS1-infected mice per genotype. Statistical significance was determined by one-way ANOVA with NewmanKeuls post-test. In **a**–**c**, $*p < 0.05$, $**p < 0.01$, $***p < 0.001$

significance (Fig. 7a, b). Further, the significant decrease in putrescine (Fig. 7a) in the $Arg2^{-/-}$ and $Arg2^{-/-};Nos2^{-/-}$ mice suggests an increased conversion to spermidine and spermine. These data indicate that the loss of ARG2 drives enhanced polyamine metabolism in $Arg2^{-/-}$ and $Arg2^{-/-};Nos2^{-/-}$ mice. Taken together, these data indicate that the loss of ARG2 enhances polyamine metabolism.

Discussion

In this study, we show that ARG2 deletion leads to increased gastritis following chronic *H. pylori* infection. This is similar to previously published data from our laboratory (Lewis et al. 2011), which implied that effects of ARG2 deletion were mediated by enhanced NOS2 expression and NO production (Lewis et al. 2010, 2011). However, the present study demonstrated that the role of ARG2 in *H. pylori* infection is more complex. ARG2 knockout leads to enhanced overall M1 macrophage activation, and upregulated polyamine metabolism. There appeared to be a partial role for NOS2 in regulation of M1 activation, as some changes observed in $Arg2^{-/-}$ mice were observed in $Arg2^{-/-};Nos2^{-/-}$ mice, and others were not.

Our previous studies led us to hypothesize that deletion of both ARG2 and NOS2 in $Arg2^{-/-};Nos2^{-/-}$ mice would restore WT colonization levels, such that reduced colonization in $Arg2^{-/-}$ mice would be lost when the *Nos2* gene was also deleted. However, $Arg2^{-/-};Nos2^{-/-}$ mice demonstrated similar colonization and gastritis levels as $Arg2^{-/-}$ mice, indicating that the role of ARG2 is NOS2-independent. While $Nos2^{-/-}$ mice demonstrated a similar level of gastritis as WT mice, colonization was decreased, and statistically similar to the $Arg2^{-/-}$ and $Arg2^{-/-};Nos2^{-/-}$ mice.

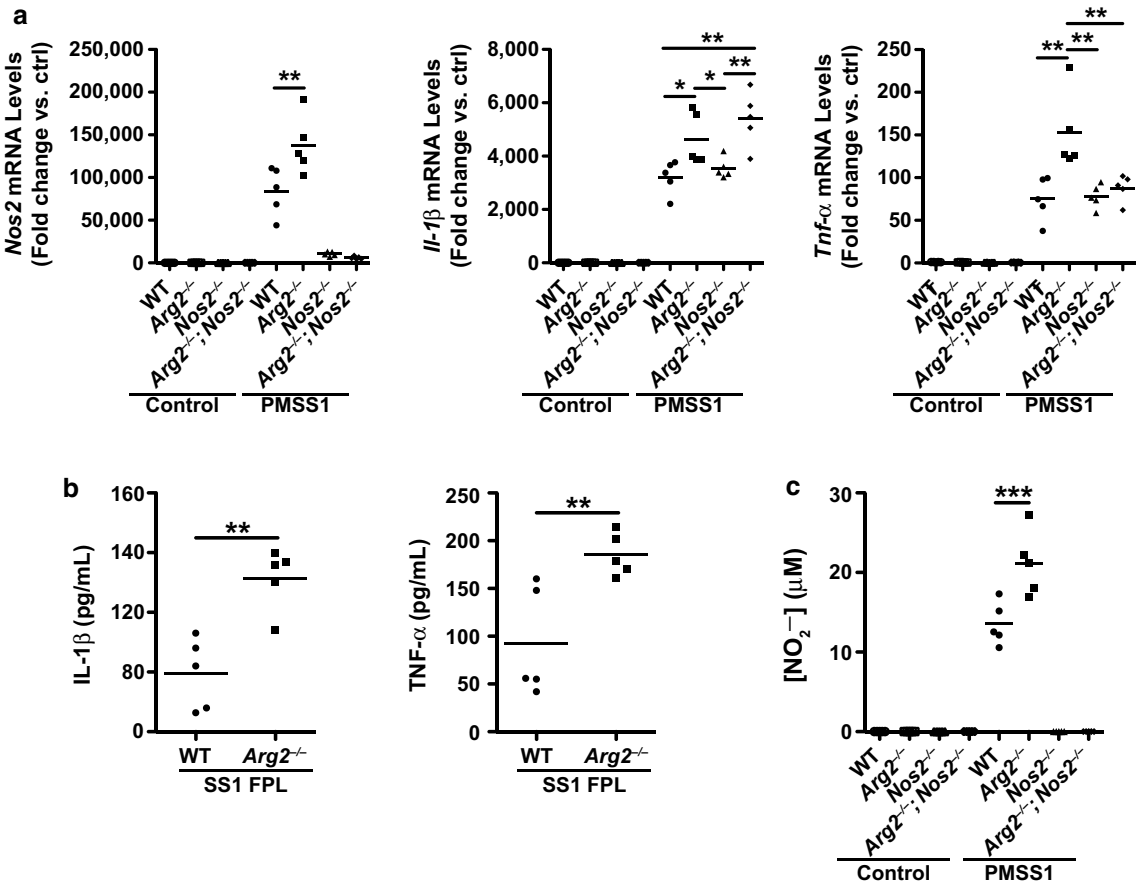

Fig. 5 *Arg2* knockout leads to super-induction of M1 macrophage activation in response to *H. pylori*. **a** Bone marrow-derived macrophages (BMmacs) were isolated from WT, $Arg2^{-/-}$, $Nos2^{-/-}$, and $Arg2^{-/-}$;$Nos2^{-/-}$ mice and stimulated with *H. pylori* Pre-Mouse Sydney Strain 1 (PMSS1) ex vivo for 24 h. Markers of M1 macrophage activation, *Nos2*, *Il-1β*, and *Tnf-α*, were assessed by RT-PCR. $n = 5$ biological replicates per genotype. Statistical significance was determined by one-way ANOVA with NewmanKeuls post-test. **b** Splenic macrophages were isolated from WT and $Arg2^{-/-}$ mice 4 months p.i. and stimulated ex vivo with SS1 FPL. Protein levels of secreted IL-1β and TNF-α, M1 macrophage effector proteins, were assessed by Luminex assay on the splenic macrophage supernatants. $n = 5$ mice per genotype. Statistical significance was determined by Student's *t* test. **c** BMmacs were isolated as in **a**. Levels of the oxidized NO metabolite, NO_2^-, was assessed by the Griess reaction. $n = 5$ biological replicates per genotype. Statistical significance was determined by one-way ANOVA with NewmanKeuls post-test. In **a**–**c**, $*p < 0.05$, $**p < 0.01$, $***p < 0.001$

This may be explained by an increased production of epithelial-derived chemokines, which activate inflammatory cells, in $Nos2^{-/-}$ and $Arg2^{-/-}$;$Nos2^{-/-}$ mice, indicating that NOS2 has an important role in modulating responses in epithelial cells. This is unexpected given that the major source of NOS2 during infection has been reported to be macrophages and neutrophils (Goto et al. 1999; Mannick et al. 1996; Sakaguchi et al. 1999; Lewis et al. 2011). Future studies are required to determine the role of NOS2 in epithelial cells during *H. pylori* infection.

We focused on the role that ARG2 plays in innate and adaptive immune response to *H. pylori* infection. Consistent with the increase in gastritis, ARG2 knockout led to increased M1 macrophage activation in tissues and macrophages. *Il-1β* expression was increased in $Arg2^{-/-}$ and $Arg2^{-/-}$;$Nos2^{-/-}$ BMmacs with either *H. pylori* infection or the classical M1 stimuli, IFN-γ and LPS. These findings were limited to mice carrying the ARG2 deletion and not found in WT or $Nos2^{-/-}$ mice, indicating that these findings are NOS2/NO-independent. The overall increase in *Il-1β* gene expression, despite the stimulus, could indicate that ARG2 plays a role in inflammasome function within macrophages, as pro-IL-1β cleavage into mature IL-1β is the primary pro-inflammatory function of the inflammasome (Latz et al. 2013). This may contribute to the enhanced inflammation observed in $Arg2^{-/-}$;$Nos2^{-/-}$ mice after chronic *H. pylori* infection.

ARG2 does not appear to play a global role in macrophage activation. While loss of ARG2 enhanced M1 macrophage activation, M2 macrophage activation was not affected by ARG2. Our laboratory reported that *H. pylori* does not induce a significant M2 response (Gobert et al.

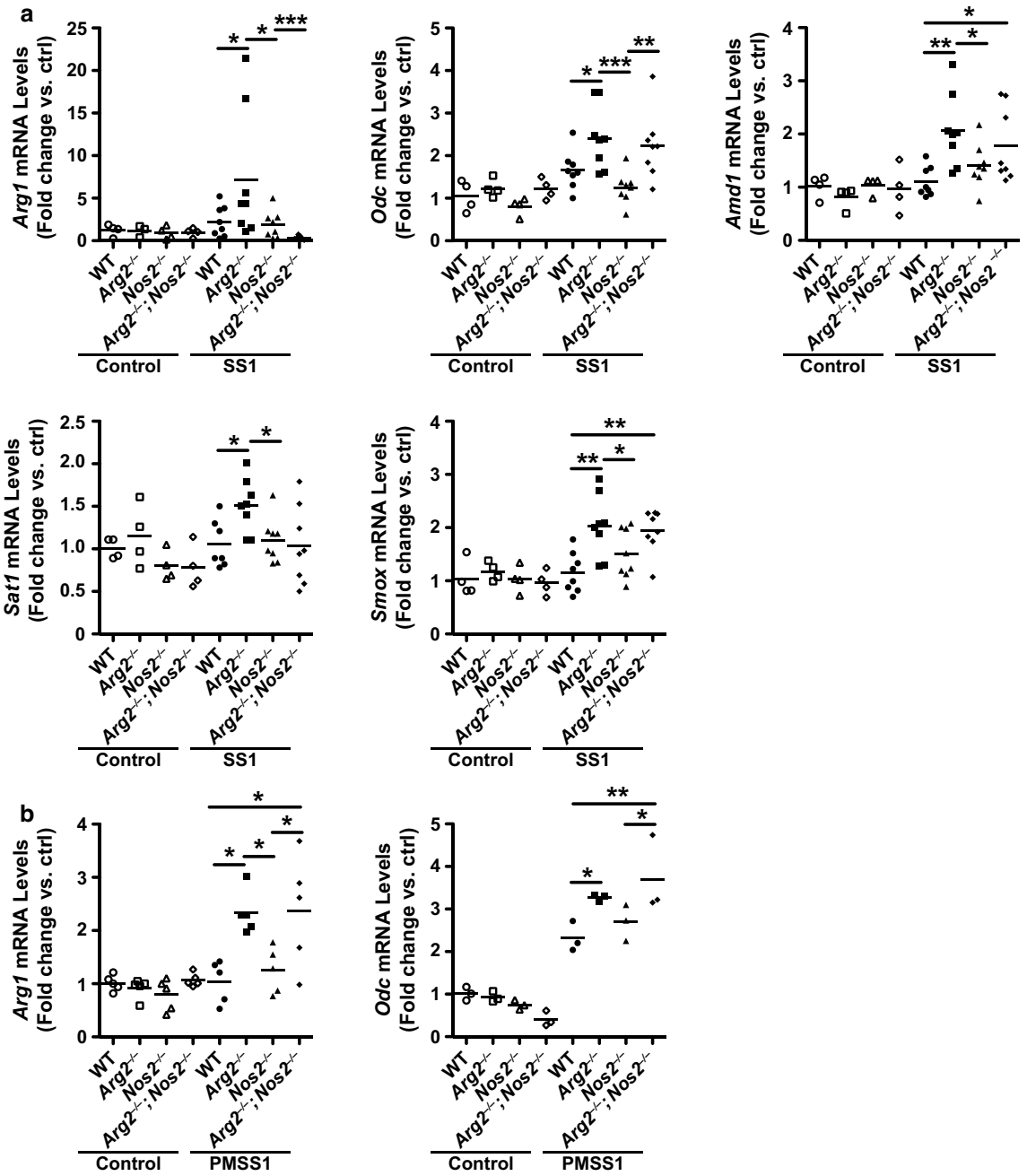

Fig. 6 Loss of ARG2 leads to a compensatory upregulation in polyamine metabolic enzyme expression in response to *H. pylori*. **a** RNA was isolated from gastric tissues from WT, $Arg2^{-/-}$, $Nos2^{-/-}$, and $Arg2^{-/-};Nos2^{-/-}$ mice 4 months p.i. mRNA levels of *Arg1, Odc*, *Amd1*, *Sat1*, and *Smox* were assessed by RT-PCR. $n = 3$–4 uninfected and 7–8 *H. pylori* SS1-infected mice per genotype. Statistical significance was determined by one-way ANOVA with Kruskal–Wallis test, followed by Mann–Whitney *U* test. **b** RNA was isolated from BMmacs from WT, $Arg2^{-/-}$, $Nos2^{-/-}$, and $Arg2^{-/-};Nos2^{-/-}$ mice 24 h (*Arg1*) and 6 h (*Odc*) p.i. mRNA levels of *Arg1* and *Odc* were assessed by RT-PCR. $n = 3$–5 biological replicates per genotype. Statistical significance was determined by one-way ANOVA with NewmanKeuls post-test. In **a** and **b**, $*p < 0.05$, $**p < 0.01$, $***p < 0.001$

2014). However, we now show that IL-4 stimulation produced an M2 response in BMmacs, but there were no differences between the genotypes. Moreover, ARG2 knockout did not have a profound effect on Mreg macrophage activation. There was a modest increase in *Il-10* expression in $Arg2^{-/-}$ mice that was not found in $Arg2^{-/-};Nos2^{-/-}$ mice. The lack of *Il-10* expression in $Arg2^{-/-};Nos2^{-/-}$ BMmacs may partially explain why histologic gastritis in $Arg2^{-/-};Nos2^{-/-}$ mice is statistically similar to that in $Arg2^{-/-}$ mice; lack of an anti-inflammatory response may

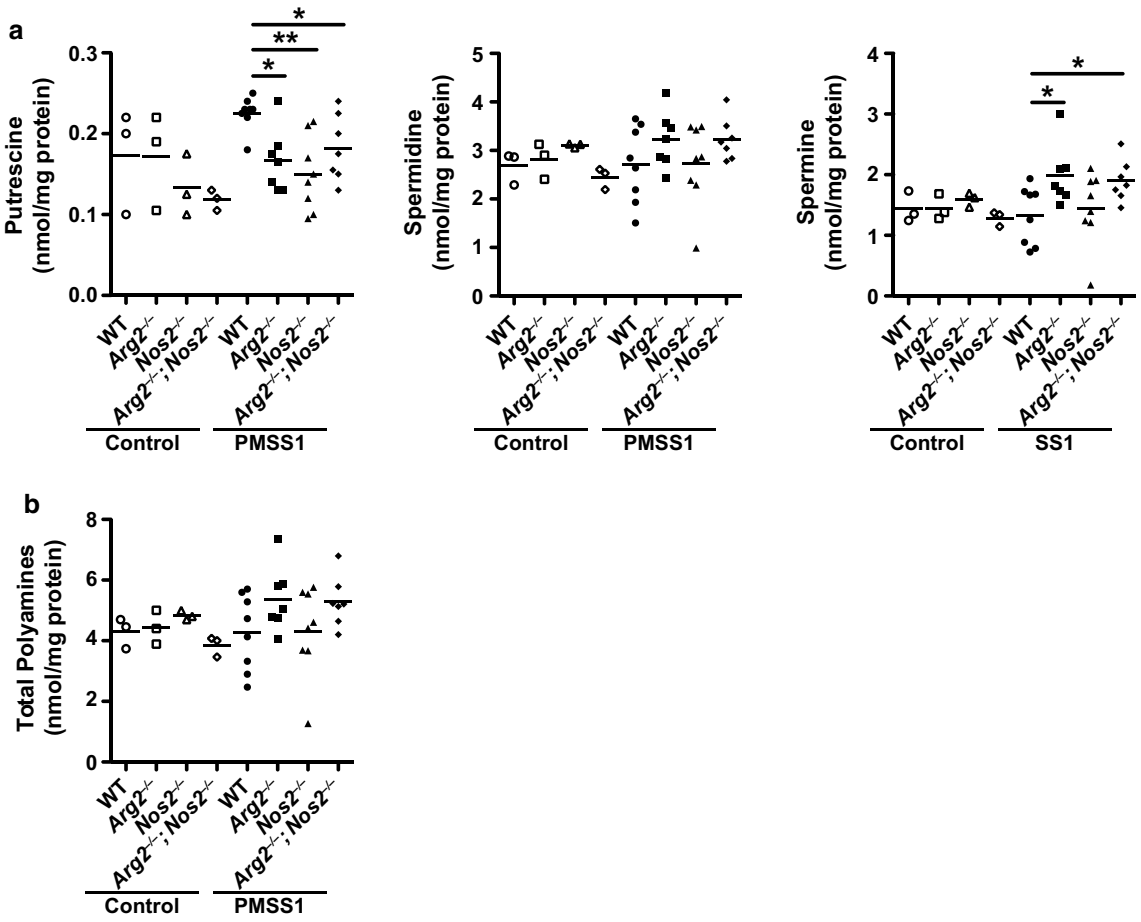

Fig. 7 Loss of ARG2 increases polyamine levels in response to *H. pylori*. **a** Levels of putrescine, spermidine, and spermine were assessed by high-performance liquid chromatography in gastric tissues 4 months p.i. from WT, *Arg2*$^{-/-}$, *Nos2*$^{-/-}$, and *Arg2*$^{-/-}$;*Nos2*$^{-/-}$ mice. $n = 3$ uninfected and 7–8 *H. pylori* SS1-infected mice per genotype. Statistical significance was determined by one-way ANOVA with Kruskal–Wallis test, followed by Mann–Whitney *U* test. *$p < 0.05$, **$p < 0.01$. **b** Total polyamine levels were calculated from the sum of putrescine, spermidine, and spermine in **a**

allow for pro-inflammatory M1 macrophage response to go unchecked. Together, these data reinforce that the role of ARG2 is specifically important in M1 macrophage activation. The T-cell phenotypes herein provide partial support for our initial hypothesis that effects of ARG2 deletion were dependent on NOS2. There is a significant Th1/Th17 response in *Arg2*$^{-/-}$ mice, that is ablated in *Arg2*$^{-/-}$;*Nos2*$^{-/-}$ mice. These data indicate that either expression of Th1/Th17 markers and/or that recruitment and differentiation of Th1/Th17 cells is directly dependent on NOS2.

Our most novel finding was the dramatic effect of ARG2 deletion on the polyamine pathway. Both *Arg2*$^{-/-}$ and *Arg2*$^{-/-}$;*Nos2*$^{-/-}$ mice demonstrated upregulated expression of various polyamine metabolism enzymes, as well as significantly increased spermine levels within gastric tissue. These data suggest that ARG2 has an important role in regulation of polyamine synthesis and catabolism, which would have broad effects on polyamine flux within tissues. *Arg1* and *Odc* expression was similarly increased in primary macrophages as well, indicating an important role for ARG2 in polyamine synthesis within macrophages. Our laboratory has demonstrated that polyamines and the enzymes involved in their metabolism are important in macrophage function, specifically in response to *H. pylori* infection (Barry et al. 2011; Chaturvedi et al. 2004, 2007, 2010, 2012, 2014; Gobert et al. 2002a, b, 2001, 2011; Lewis et al. 2010, 2011). The current study specifically highlights the importance of ARG2 as a regulator of polyamine metabolism in gastric tissues and in macrophage function and thus, the immune response to chronic *H. pylori* infection. Potential explanations for how upregulation of polyamine metabolism within *Arg2*$^{-/-}$ and *Arg2*$^{-/-}$;*Nos2*$^{-/-}$ mice could contribute to increased gastritis in a NOS2-independent manner, include alterations in macrophage viability allowing for enhanced function

(Gobert et al. 2002a; Chaturvedi et al. 2004) or direct alteration of macrophage phenotypes (Van den Bossche et al. 2012).

Polyamine metabolism has been implicated in the regulation of immune responses to various pathogens, in addition to *H. pylori* (Bansal and Ochoa 2003; Bronte and Zanovello 2005; Chaturvedi et al. 2010). We have now identified ARG2 as a critical player in polyamine metabolism in response to a major human pathogen. Future studies investigating the role of ARG2 in polyamine metabolism during other bacterial infections, particularly in the gastrointestinal system, could provide additional insights into their immunopathogenesis. ARG2 could potentially serve as a target for intervention in mucosal infections, allowing for an enhanced immune response to prevent bacterial survival within the host.

Methods

Materials

All chemicals were purchased from Sigma-Aldrich (St. Louis, MO, USA) unless otherwise stated. All reagents used for cell culture were from Invitrogen (Carlsbad, CA, USA). RNA extraction reagents were from Qiagen (Valencia, CA, USA), and reagents utilized for cDNA synthesis and RT-PCR were from Bio-Rad (Hercules, CA, USA). Recombinant macrophage colony stimulating factor (M-CSF) was purchased from Peprotech (Rocky Hill, NJ, USA). Protease Inhibitor Cocktail, Set III and Phosphatase Inhibitor Cocktail, Set I were purchased from Calbiochem (Darmstadt, Germany). BCA protein assay was from Pierce Biotechnology (Rockford, IL, USA).

Bacteria, cells, cell culture conditions and infections

Helicobacter pylori strains PMSS1 and SS1 were grown as previously described (Chaturvedi et al. 2010; Lewis et al. 2011). French-pressed lysates were prepared as described (Asim et al. 2010).

Bone marrow-derived macrophages (BMmacs) were isolated from all mouse genotypes utilized in this study. BMmacs were differentiated as previously described (Weischenfeldt and Porse 2008), but with the following exceptions: red blood cells were lysed with ammonium-chloride-potassium (ACK) lysing buffer for 3–5 min, and recombinant murine M-CSF was utilized at a concentration of 20 ng/mL over the course of 7 days.

All co-culture experiments were performed in an antibiotic-free Dulbecco's modified Eagle's medium (DMEM), supplemented with 10 % fetal bovine serum (FBS), 2 mM L-glutamine, 25 mM HEPES, and 10 mM sodium pyruvate. BMmacs were infected at a multiplicity of infection (MOI) of 100, for all *H. pylori* experiments in vitro.

Animal studies

WT and $Arg2^{-/-}$ mice were utilized as previously described (Lewis et al. 2011). $Nos2^{-/-}$ mice were initially purchased from Jackson Laboratories (Farmington, CT, USA) and then bred in-house for all animal experiments. $Arg2^{-/-}$;$Nos2^{-/-}$ mice were generated by crossing the $Arg2^{-/-}$ and $Nos2^{-/-}$ mice. See Supplemental Table 1 for primers used for genotyping. Male mice between the ages of 6–12 weeks at the time of infection were used for all studies, regardless of genotype, and mice were not moved from the cages into which they were weaned. Male mice were selected based on previous data indicating that female mice were protected from *H. pylori*-induced histologic gastritis (Sheh et al. 2011). Sample sizes were based on previous studies from our laboratory (Chaturvedi et al. 2010; Gobert et al. 2014; Lewis et al. 2011). All mice were randomly selected for control and experimental groups.

Mice were orogastrically infected with 5×10^8 CFUs of *H. pylori* SS1, every other day for a total of three inoculations. Mice were killed 4 months post-inoculation and their stomachs divided longitudinally into four sections for additional studies. Colonization was assessed by serial dilution and culture. Histologic gastritis was assessed by a gastrointestinal pathologist (M.B.P.), using the Sydney System (Gobert et al. 2014). All scoring was performed in a blinded manner.

Real-time polymerase chain reaction

RNA was isolated from tissue and BMmacs using the RNeasy kit. cDNA was prepared using the iScript cDNA synthesis kit with 1 μg of RNA. RT-PCR was performed as described (Gobert et al. 2014). See Supplemental Table 1 for all primers utilized in this study.

Western blot analysis

Tissue and BMmacs were lysed in CellLytic MT Reagent supplemented with Protease Inhibitor Cocktail (Set III) and Phosphatase Inhibitor Cocktail (Set I). Protein concentration was determined by BCA protein assay. The following antibodies were utilized in this study: Rabbit polyclonal anti-NOS2 (1:5000; EMD Millipore), Rabbit polyclonal anti-ARG2 (1:1000; Santa Cruz Biotechnology), Mouse monoclonal anti-β-actin (1:10,000; Sigma-Aldrich), Goat anti-mouse IgG, HRP labeled (1:30,000; Sigma-Aldrich), and Goat anti-rabbit IgG, HRP labeled (1:3000–1:6000; Sigma-Aldrich).

Luminex assay

A 25-plex assay (EMD Millipore, Cat. MCYTOMAG-70K-PMX, Billerica, MA, USA) was performed on gastric tissues from control and *H. pylori* SS1-infected mice from all genotypes. A 25-plex assay was also performed on supernatants from splenic T-cell cultures. Protein isolation, quantification and Luminex assay were performed as previously described (Coburn et al. 2013).

Measurement of nitric oxide

The concentration of nitrite (NO_2^-), the oxidized metabolite of NO, was assessed by the Griess reaction as previously described (Chaturvedi et al. 2010).

Flow cytometry

Flow cytometry was performed as previously described (Lewis et al. 2011). The following antibodies were utilized in this study: Anti-mouse CD4-PerCp-Cy5.5 (1:200; Biolegend), and Anti-mouse IFN-γ-FITC (1:100; BD Biosciences).

Measurement of polyamines

Polyamines were measured from gastric tissue lysates by high-performance liquid chromatography as previously described (Chaturvedi et al. 2010).

Splenocyte isolation

Splenocytes were isolated from the spleens of control and infected WT and *Arg2*$^{-/-}$ mice. Red blood cells were lysed with ACK for 3–5 min. Splenocytes utilized for T-cell studies were plated in 96-well plates coated with anti-CD3 antibody and stimulated with anti-CD28 for 24 h. Cells were then stimulated with *H. pylori* SS1 French-pressed lysate for 4 days. Luminex assay and flow cytometry were then performed. Splenocytes utilized for macrophage studies were plated in 96-well plates without anti-CD3. Adherent cells were then stimulated with *H. pylori* French-pressed lysate for 24 h.

Statistical analysis

All data shown in this study represent the mean. The *n* for each experiment is listed in the figure legends. Where data were normally distributed, Student's *t* test was used to determine significance in studies with only two groups, and one-way ANOVA with a NewmanKeuls post-test was used to determine significance in studies with multiple groups. Where data were not normally distributed, one-way ANOVA with a Kruskal–Wallis test, followed by a Mann–Whitney *U* test was performed. All statistical tests for each experiment are listed in the figure legends. All statistical analyses were performed using GraphPad Prism 5.0 (GraphPad Software, San Diego, CA, USA). A p value of <0.05 was considered to be significant.

Acknowledgments We thank Alain P. Gobert (Vanderbilt University) for intellectual input and for his review of the manuscript. We thank Daniel P. Barry (Vanderbilt University) for his assistance with the breeding and maintenance of the mouse colonies utilized in this study. We thank Margaret Allaman (Vanderbilt University) for her assistance with the Luminex assays.

Compliance with ethical standards

Funding This work was funded by NIH Grants R01DK053620, R01AT004821, R01CA190612, P01CA116087, and P01CA028842 (K.T.W.), Merit Review Grant I01BX001453 from the United States Department of Veterans Affairs Biomedical Laboratory R&D (BLRD) Service (K.T.W.), the Vanderbilt Digestive Disease Research Center, supported by NIH Grant P30DK058404, the Thomas F. Frist Sr. Endowment (K.T.W.), and the Vanderbilt Center for Mucosal Inflammation and Cancer (K.T.W.). D.M.H. was supported by NIH Grants T32GM008554 and F31DK10715.

Conflict of interest The authors declare that no conflict of interest exists.

References

Algood HMS, Lin PL, Yankura D, Jones A, Chan J, Flynn JL (2004) Tnf influences chemokine expression of macrophages in vitro and that of CD11b+ cells in vivo during *Mycobacterium tuberculosis* infection. J Immunol 172(11):6846–6857

Anderson CF, Mosser DM (2002) A novel phenotype for an activated macrophage: the type 2 activated macrophage. J Leukoc Biol 72(1):101–106

Asim M, Chaturvedi R, Hoge S, Lewis ND, Singh K, Barry DP, Algood HS, de Sablet T, Gobert AP, Wilson KT (2010) *Helicobacter pylori* induces erk-dependent formation of a phospho-c-fos c-jun activator protein-1 complex that causes apoptosis in macrophages. J Biol Chem 285(26):20343–20357

Bansal V, Ochoa JB (2003) Arginine availability, arginase, and the immune response. Curr Opin Clin Nutr Metab Care 6(2):223–228

Barry DP, Asim M, Scull BP, Piazuelo MB, de Sablet T, Lewis ND, Coburn LA, Singh K, Ellies LG, Gobert AP, Chaturvedi R, Wilson KT (2011) Cationic amino acid transporter 2 enhances innate immunity during *Helicobacter pylori* infection. PLoS One 6(12):e29046

Benoit M, Desnues B, Mege J-L (2008) Macrophage polarization in bacterial infections. J Immunol 181(6):3733–3739

Bonequi P, Meneses-Gonzalez F, Correa P, Rabkin CS, Camargo MC (2013) Risk factors for gastric cancer in latin america: a meta-analysis. Cancer Causes Control 24(2):217–231

Bronte V, Zanovello P (2005) Regulation of immune responses by L-arginine metabolism. Nat Rev Immunol 5(8):641–654

Chaturvedi R, Cheng Y, Asim M, Bussière FI, Xu H, Gobert AP, Hacker A, Casero RA, Wilson KT (2004) Induction of polyamine oxidase 1 by *Helicobacter pylori* causes macrophage apoptosis by hydrogen peroxide release and mitochondrial membrane depolarization. J Biol Chem 279(38):40161–40173

Chaturvedi R, Asim M, Lewis ND, Algood HMS, Cover TL, Kim PY, Wilson KT (2007) L-arginine availability regulates inducible nitric oxide synthase-dependent host defense against *Helicobacter pylori*. Infect Immun 75(9):4305–4315

Chaturvedi R, Asim M, Hoge S, Lewis ND, Singh K, Barry DP, de Sablet T, Piazuelo MB, Sarvaria AR, Cheng Y, Closs EI, Casero RA Jr, Gobert AP, Wilson KT (2010) Polyamines impair immunity to *Helicobacter pylori* by inhibiting L-arginine uptake required for nitric oxide production. Gastroenterology 139(5):1686–1698 **(e1686)**

Chaturvedi R, de Sablet T, Coburn LA, Gobert AP, Wilson KT (2012) Arginine and polyamines in *Helicobacter pylori*-induced immune dysregulation and gastric carcinogenesis. Amino Acids 42(2–3):627–640

Chaturvedi R, Asim M, Barry DP, Frye JW, Casero RA Jr, Wilson KT (2014) Spermine oxidase is a regulator of macrophage host response to *Helicobacter pylori*: enhancement of antimicrobial nitric oxide generation by depletion of spermine. Amino Acids 46(3):531–542

Coburn LA, Horst SN, Chaturvedi R, Brown CT, Allaman MM, Scull BP, Singh K, Piazuelo MB, Chitnavis MV, Hodges ME, Rosen MJ, Williams CS, Slaughter JC, Beaulieu DB, Schwartz DA, Wilson KT (2013) High-throughput multi-analyte luminex profiling implicates eotaxin-1 in ulcerative colitis. PLoS One 8(12):e82300

Cover TL, Blaser MJ (2009) *Helicobacter pylori* in health and disease. Gastroenterology 136(6):1863–1873

Ferlay J, Soerjomataram I, Dikshit R, Eser S, Mathers C, Rebelo M, Parkin DM, Forman D, Bray F (2015) Cancer incidence and mortality worldwide: sources, methods and major patterns in Globocan 2012. Int J Cancer 136(5):E359–E386

Fleming BD, Mosser DM (2011) Regulatory macrophages: setting the threshold for therapy. Eur J Immunol 41(9):2498–2502

Gobert AP, McGee DJ, Akhtar M, Mendz GL, Newton JC, Cheng Y, Mobley HL, Wilson KT (2001) *Helicobacter pylori* arginase inhibits nitric oxide production by eukaryotic cells: a strategy for bacterial survival. Proc Natl Acad Sci USA 98(24):13844–13849

Gobert AP, Cheng Y, Wang J-Y, Boucher J-L, Iyer RK, Cederbaum SD, Casero RA, Newton JC, Wilson KT (2002a) *Helicobacter pylori* induces macrophage apoptosis by activation of arginase II. J Immunol 168(9):4692–4700

Gobert AP, Mersey BD, Cheng Y, Blumberg DR, Newton JC, Wilson KT (2002b) Cutting edge: urease release by *Helicobacter pylori* stimulates macrophage inducible nitric oxide synthase. J Immunol 168(12):6002–6006

Gobert AP, Asim M, Piazuelo MB, Verriere T, Scull BP, de Sablet T, Glumac A, Lewis ND, Correa P, Peek RM, Chaturvedi R, Wilson KT (2011) Disruption of nitric oxide signaling by *Helicobacter pylori* results in enhanced inflammation by inhibition of heme oxygenase-1. J Immunol 187(10):5370–5379

Gobert AP, Verriere T, Asim M, Barry DP, Piazuelo MB, de Sablet T, Delgado AG, Bravo LE, Correa P, Peek RM Jr, Chaturvedi R, Wilson KT (2014) Heme oxygenase-1 dysregulates macrophage polarization and the immune response to *Helicobacter pylori*. J Immunol 193(6):3013–3022

Gogoi M, Datey A, Wilson KT, Chakravortty D (2015) Dual role of arginine metabolism in establishing pathogenesis. Curr Opin Microbiol 29:43–48

Goto T, Haruma K, Kitadai Y, Ito M, Yoshihara M, Sumii K, Hayakawa N, Kajiyama G (1999) Enhanced expression of inducible nitric oxide synthase and nitrotyrosine in gastric mucosa of gastric cancer patients. Clin Cancer Res 5(6):1411–1415

Hardbower DM, de Sablet T, Chaturvedi R, Wilson KT (2013) Chronic inflammation and oxidative stress: the smoking gun for *Helicobacter pylori*-induced gastric cancer? Gut Microbes 4(6):475–481

Hardbower DM, Peek RM Jr, Wilson KT (2014) At the bench: *Helicobacter pylori*, dysregulated host responses, DNA damage, and gastric cancer. J Leukoc Biol 96(2):201–212

Latz E, Xiao TS, Stutz A (2013) Activation and regulation of the inflammasomes. Nat Rev Immunol 13(6):397–411

Lewis ND, Asim M, Barry DP, Singh K, de Sablet T, Boucher JL, Gobert AP, Chaturvedi R, Wilson KT (2010) Arginase II restricts host defense to *Helicobacter pylori* by attenuating inducible nitric oxide synthase translation in macrophages. J Immunol 184(5):2572–2582

Lewis ND, Asim M, Barry DP, de Sablet T, Singh K, Piazuelo MB, Gobert AP, Chaturvedi R, Wilson KT (2011) Immune evasion by *Helicobacter pylori* is mediated by induction of macrophage arginase II. J Immunol 186(6):3632–3641

Mannick EE, Bravo LE, Zarama G, Realpe JL, Zhang XJ, Ruiz B, Fontham ET, Mera R, Miller MJ, Correa P (1996) Inducible nitric oxide synthase, nitrotyrosine, and apoptosis in *Helicobacter pylori* gastritis: effect of antibiotics and antioxidants. Cancer Res 56(14):3238–3243

Martinez FO, Gordon S (2014) The M1 and M2 paradigm of macrophage activation: time for reassessment. F1000Prime Rep 6:13

Mosser DM (2003) The many faces of macrophage activation. J Leukoc Biol 73(2):209–212

Mosser DM, Edwards JP (2008) Exploring the full spectrum of macrophage activation. Nat Rev Immunol 8(12):958–969

Murray PJ, Wynn TA (2011) Protective and pathogenic functions of macrophage subsets. Nat Rev Immunol 11(11):723–737

Nomura A, Stemmermann G, Chyou P, Kato I, Perez-Perez G, Blaser M (1991) *Helicobacter pylori* infection and gastric carcinoma among Japanese Americans in Hawaii. N Engl J Med 325:1132–1136

Ostuni R, Kratochvill F, Murray PJ, Natoli G (2015) Macrophages and cancer: from mechanisms to therapeutic implications. Trends Immunol 36(4):229–239

Pander J, Heusinkveld M, van der Straaten T, Jordanova ES, Baak-Pablo R, Gelderblom H, Morreau H, van der Burg SH, Guchelaar HJ, van Hall T (2011) Activation of tumor-promoting type 2 macrophages by EGFR-targeting antibody cetuximab. Clin Cancer Res 17(17):5668–5673

Parsonnet J, Friedman GD, Vandersteen DP, Chang Y, Vogelman JH, Orentreich N, Sibley RK (1991) *Helicobacter pylori* infection and the risk of gastric carcinoma. N Engl J Med 325(16):1127–1131

Peek RM, Blaser MJ (2002) *Helicobacter pylori* and gastrointestinal tract adenocarcinomas. Nat Rev Cancer 2(1):28–37

Peek RM, Fiske C, Wilson KT (2010) Role of innate immunity in *Helicobacter pylori*-induced gastric malignancy. Physiol Rev 90(3):831–858

Robinson K, Argent RH, Atherton JC (2007) The inflammatory and immune response to *Helicobacter pylori* infection. Best Pract Res Clin Gastroenterol 21(2):237–259

Sakaguchi AA, Miura S, Takeuchi T, Hokari R, Mizumori M, Yoshida H, Higuchi H, Mori M, Kimura H, Suzuki H, Ishii H (1999) Increased expression of inducible nitric oxide synthase and peroxynitrite in *Helicobacter pylori* gastric ulcer. Free Radical Biol Med 27(7–8):781–789

Schleimer RP, Kato A, Kern R, Kuperman D, Avila PC (2007) Epithelium: at the interface of innate and adaptive immune responses. J Allergy Clin Immunol 120(6):1279–1284

Shapiro KB, Hotchkiss JH (1996) Induction of nitric oxide synthesis in murine macrophages by *Helicobacter pylori*. Cancer Lett 102(1, A2):49–56

Sheh A, Ge Z, Parry NM, Muthupalani S, Rager JE, Raczynski AR, Mobley MW, McCabe AF, Fry RC, Wang TC, Fox JG (2011) 17-beta-estradiol and tamoxifen prevent gastric cancer by modulating leukocyte recruitment and oncogenic pathways in

Helicobacter pylori-infected ins-gas male mice. Cancer Prev Res 4(9):1426–1435

Sibony M, Jones NL (2012) Recent advances in *Helicobacter pylori* pathogenesis. Curr Opin Gastroenterol 28(1):30–35

Strauss-Ayali D, Conrad SM, Mosser DM (2007) Monocyte subpopulations and their differentiation patterns during infection. J Leukoc Biol 82(2):244–252

Van den Bossche J, Lamers WH, Koehler ES, Geuns JM, Alhonen L, Uimari A, Pirnes-Karhu S, Van Overmeire E, Morias Y, Brys L, Vereecke L, De Baetselier P, Van Ginderachter JA (2012) Pivotal advance: arginase-1-independent polyamine production stimulates the expression of IL-4-induced alternatively activated macrophage markers while inhibiting LPS-induced expression of inflammatory genes. J Leukoc Biol 91(5):685–699

Weischenfeldt J, Porse B (2008) Bone marrow-derived macrophages (BMM): isolation and applications. Cold Spring Harb Prot 12:1–6

Wilson KT, Crabtree JE (2007) Immunology of *Helicobacter pylori*: insights into the failure of the immune response and perspectives on vaccine studies. Gastroenterology 133(1):288–308

Wilson KT, Ramanujam KS, Mobley HL, Musselman RF, James SP, Meltzer SJ (1996) *Helicobacter pylori* stimulates inducible nitric oxide synthase expression and activity in a murine macrophage cell line. Gastroenterology 111(6):1524–1533